STUDIES ON SOME BIPHENYL BENZOATE BASED CHIRAL LIQUID CRYSTAL COMPOUNDS

Thesis submitted to the University of North Bengal for the award of the degree of
Doctor of Philosophy (Science) in Physics

By

Debarghya Goswami

Supervisor

Prof. Pradip Kumar Mandal

Department of Physics
University of North Bengal
Siliguri 734013, West Bengal, India

February 2020

DECLARATION

I declare that the thesis entitled "STUDIES ON SOME BIPHENYL BENZOATE BASED CHIRAL LIQUID CRYSTAL COMPOUNDS" has been prepared by me under the guidance of Dr. Pradip Kumar Mandal, Professor, Department of Physics, University of North Bengal. No part of this thesis has formed the basis for the award of any degree or fellowship previously.

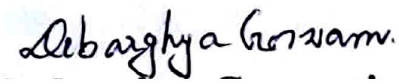

Debarghya Goswami
Department of Physics
University of North Bengal
P.O.: North Bengal University
Siliguri, Dist: Darjeeling
Date:10.02.2020

UNIVERSITY OF NORTH BENGAL
Accredited by NAAC with Grade A

DEPARTMENT OF PHYSICS
P.O. NORTH BENGAL UNIVERSITY
RAJA RAMMOHUNPUR, DIST. DARJEELING,
WEST BENGAL, PIN 734013,
INDIA

ENLIGHTENMENT TO PERFECTION

Railway Station: New Jalpaiguri
Nearest Airport: Bagdogra
Phone: +91-(0) 353-2776338
Fax: +91-(0) 353-2699001
Website:www.nbu.ac.in

Ref. No. .....

Date : .....

CERTIFICATE

I certify that Mr. Debarghya Goswami has prepared the thesis entitled "STUDIES ON SOME BIPHENYL BENZOATE BASED CHIRAL LIQUID CRYSTAL COMPOUNDS" for the award of Ph. D degree (science) in Physics of University of North Bengal under my guidance and supervision. He has carried out the work at the Department of Physics, University of North Bengal.

Date: 10.02.2020
Place: NBU

PROF. PRADIP KUMAR MANDAL
Department of Physics
University of North Bengal
Raja Rammohunpur
P.O: North Nengal University Campus
Dist: Darjeeling, pin 734013, West Bengal

URKUND

Urkund Analysis Result

Analysed Document:	Debarghya Goswami_Physics.pdf (D63078381)
Submitted:	1/28/2020 7:02:00 AM
Submitted By:	nbuplg@nbu.ac.in
Significance:	4 %

Sources included in the report:

https://www.scirp.org/xml/19089.xml
https://www.researchgate.net/publication/233319014_Direct_transition_from_the_SmA_phase_to_the_tilted_hexatic_phase_in_liquid_crystals_with_several_lactate_units
https://www.researchgate.net/publication/257307116_Antiferroelectric_Liquid_Crystals_Smart_Materials_for_Future_Displays
https://www.researchgate.net/profile/Ravindra_Dhar/publication/232873686_Dielectric_Spectroscopy_of_a_Newly_Synthesized_Chlorinated_Analogue_of_MHPOBC_Antiferroelectric_Liquid_Crystals/links/02e7e527bc17febf7f000000.pdf?inViewer=true&disableCoverPage=true&origin=publication_detail
https://www.researchgate.net/publication/233475132_Ferroelectric_behaviour_of_hexatic_phases
https://www.researchgate.net/publication/312080349_Synthesis_and_characterization_of_new_homologous_series_of_unsymmetrical_liquid_crystalline_compounds_based_on_chalcones_and_3_5-disubstituted_isoxazoles
https://www.researchgate.net/profile/Praveen_Malik_Assistant_Professor/publication/216294747_Dielectric_spectroscopy_of_a_high-polarization_ferroelectric_liquid_crystal/links/066b0dcde018586fa48bb0aa.pdf?origin=publication_detail
https://www.researchgate.net/profile/Asim_Debnath2/publication/303514367_Maxwell_Wagner_and_Goldstone_mode_relaxations_in_a_oligomethylene_spacer_based_ferroelectric_liquid_crystal/links/57480a3008ae2301b0b852cc.pdf?origin=publication_detail
de53e032-cdba-4cb7-b03e-ef54d00cf547
ff306de3-3b41-4b6a-ae56-18864dd66a36
57886672-939a-493d-b99d-08a8624f9704
2c94b87a-4719-45cb-93f5-1d3fc491d416
https://www.researchgate.net/publication/303782738_Wide_range_room_temperature_ferroelectric_liquid_crystal_mixture_with_microsecond_order_switching
https://pubs.rsc.org/en/content/articlehtml/2016/ra/c6ra11238b

URKUND

https://www.researchgate.net/publication/307550724_Induction_of_a_room_temperature_ferroelectric_SmC_phase_in_binary_mixtures_with_moderate_spontaneous_polarization_and_sub-millisecond_switching_time
https://www.researchgate.net/figure/Temperature-variation-of-relaxation-frequency-f-C-of-a-MIX0-b-MIX1-c-MIX2-and_fig2_326168305
https://www.researchgate.net/publication/280528661_Formulation_Of_A_Room_Temperature_Ferroelectric_Liquid_Crystal_Mixture_With_Sub-millisecond_Switching_Time

Instances where selected sources appear:

61

Abarghya Goswami
10.02.2020

10.02.2020

ACKNOWLEDGEMENT

I would like to express my sincere thanks and deepest gratitude to my supervisor Prof. Pradip Kumar Mandal for his supervision and constant help all through the period of my research work. I am much indebted for his valuable guidance and suggestions in each aspect of my experimental works and in the interpretation of the results.

A large debt of gratitude is owed to Prof. R. Dabrowski, Military University of Technology, Warsaw, Poland for supplying the good quality liquid crystal samples studied in this dissertation.

I would also like to thank Department of Science and Technology, Government of India for providing financial support to perform experiment at Deutsches Elektronen-Synchrotron (DESY), Hamburg, Germany. Technical support by Olof Gutowski and Abhisek Sharma of DESY is thankfully acknowledged.

I am thankful to my lab mates Dr. Debashis Sinha, Dr. Asim Debnath and Mr. Kartick Ch. Dey for their fruitful discussions and encouragement.

I am thankful to Mr. Subrata Hazra for his support in preparing the experimental set up in the laboratory.

I would like to thank Fr Dr. Donatus Kujur, S.J, Principal, St. Joseph's College, where I am working for last nine years. I like to thank my colleagues and students for their unfailing support.

I am thankful to my parents, family and friends for their endless encouragements.

I extend my sincere thanks to Dr. Sripad Halder, Head, Department of Physics, NBU and all teaching and non-teaching staffs and research scholars of my department for their support.

Place: N. B. U

Date: 10.02.2020

Debarghya Goswami

Debarghy Goswami

Abstract

Due to the coexistence of liquid-like fluidity with conventional solid like anisotropy, liquid crystals exhibit unique optical, dielectric or elastic properties which make them suitable for a variety of technical and scientific applications, especially in display devices. The dielectric and electro-optic properties of these materials, along with their phase behaviour, are of immense importance from application perspective. It's essential to know the said parameters, to decide whether a LC compound is fit to be used in display devices or not. Moreover, the study of the phase behaviour of liquid crystal materials, which can typically have various mesophases with different structures within a short temperature range, may help us to comprehend the physics behind the different kind of phase transitions in such compounds.

Though traditionally nematic liquid crystals are used in the most LCDs but they have higher response time and thus are unsuitable for fast display applications. Chiral liquid crystals may have ferroelectric or antiferroelectric mesophases for which the response time is sharper. Thus chiral liquid crystals are of current interest for display technology.

Keeping these in mind we have chosen eight chiral liquid crystal compounds (**1F3R, 2F3R, 3F3R, 5F3R, 6F3R, 4F4R, 4F5R** and **7F3R**) to study their phase behaviour and dielectric, electro-optic characteristics. For a few of them synchrotron X-ray diffraction study has also been performed to explore their structural behaviour. All the selected compounds have biphenyl benzoate core and fluorinated chains. The biphenyl benzoate core normally ensures higher thermal stability often with wide range low temperature ferroelectric and antiferroelectric

phases and chiral liquid crystals with fluorinated chain usually exhibit enhanced spontaneous polarization, higher dielectric anisotropy, lower optical anisotropy which are beneficial for display applications.

Since all the compounds, selected for investigation, have the same back bone differing only by the number of carbons and the number of oligomethylene spacers in the fluorinated chain, efforts have been made to explore a relationship of their phase behaviour and dielectric, electro-optic, structural properties with change in their molecular structures. Also to see the efficacy of the compounds in formulating mixtures suitable for display applications, one multi-component mixture has been prepared using 7F3R as dopant and its various properties have been investigated.

The compound 1F3R, with least number of carbon atoms in the chain, has only orthogonal phases. Tilted phases are induced when one extra carbon is added in the fluorinated chain (2F3R) and sustained in all other compounds. Hexagonal phases are observed only in 1F3R (orthogonal), 2F3R (tilted) and 3F3R (tilted), but not in higher homologous. SmA* phase is observed in 1F3R and 2F3R but is found to disappear in higher homologous and re-entered in the phase sequence of the longest compound 7F3R. A new smectic *subphase*, termed as SmX* phase, has been observed in 4F4R. All compounds except 1F3R have SmC* phase and the temperature span of that phase (ΔT_{SmC}^{*}) increases with chain length except in 4F4R which might be due to the presence of the *subphase* SmX*.

In the Frequency dependent dielectric relaxation study non-collective mode of relaxation is observed only in the SmE*, $SmB_{hex}^{*\,mo}$ and, $SmB_{hex}^{*\,lo}$ phases of 1F3R which exhibited short axis rotation mode in those phases. In SmF* phase of 2F3R and 3F3R both bond orientation

order phason and tilt phason relaxations are observed, to the best of our knowledge for the first time in a single compound. In all compounds having only SmC* phase, Goldstone mode relaxation is observed in that phase but no soft mode. In nF3R compounds the Goldstone mode critical frequencies are found to increase with chain length. However, after addition of extra oligomethylene spacers it decreases. Soft mode relaxation is observed only in 2F3R and 7F3R throughout the SmA* phase and also in SmC* phase in the vicinity of SmC* to SmA* transition. From the absence of soft mode relaxation in all compounds having only SmC* phase it is concluded that in absence of any orthogonal to tilted phase transition soft mode relaxation cannot be observed.

The shortest three compounds (1F3R, 2F3R, 3F3R) and the longest one (7F3R) have also been investigated by synchrotron X-ray diffraction technique. Existence of two variants of SmB* phase has been confirmed in 1F3R along with SmE* and SmA* phases. Cell parameters of 1F3R in SmE*, $SmB_{he}^{*\,mo}$ and $SmB_{hex}^{*\,lo}$ phases are determined and a hexagonal lattice with herringbone structure has been confirmed in these phases. All the phases of 1F3R are found to be partially bilayer type, which has been observed for the first time in a chiral system. Tilted hexagonal phases - SmJ* and SmF* - in 2F3R while SmG* and SmF* in 3F3R have been identified and cell parameters of these phases have also been determined. A coexistence phase of (SmC*+SmF*) has also been observed. The SmA* phase of 2F3R and 7F3R is found to have de Vries type characteristics.

All the compounds have moderate value of spontaneous polarisation (P_S). In nF3R series of compounds the spontaneous polarisation (P_S) is found to increase with the molecular length. However, P_S in SmC* phase

is observed to increase significantly after addition of oligomethylene spacer and possesses the highest in 4F5R.

Micro second range response time (τ) is observed in all the compounds, however, in 2F3R the response is found to be the fastest. In nF3R compounds, the response times exhibit an inverse correlation with the molecular dipole moment, except in 7F3R. However, addition of oligomethylene spacers results in slower response, being the slowest in 4F4R.

Rotational viscosity (γ_φ) is found to be lowest in 2F3R which also showed smallest response time. Among the compounds nF3R, rotational viscosity (γ_φ) initially increases with chain fluorination and reaches the highest value in 5F3R then it decreases again. γ_φ is found to be highest in 4F5R.

Finally a ferroelectric liquid crystal mixture has been formulated by doping 7F3R in an achiral pyrimidine based host mixture. The mixture is found to exhibit ferroelectric SmC* phase over a wide temperature range from below room temperature and then shows SmA* phase before melting into isotropic phase. The SmA* phase is found to have partial de Vries type property as well as electroclinic effect. It is found to possess moderate spontaneous polarization. Optical tilt of around 20° at room temperature and a response time of a few hundred microseconds make the mixture suitable to use in SSFLCDs.

Most of the results have been published in journals of repute.

PREFACE

The present dissertation entitled "STUDIES ON SOME BIPHENYL BENZOATE BASED CHIRAL LIQUID CRYSTAL COMPOUNDS" is submitted to fulfill the requirements for the degree of Doctor of Philosophy (Science) of the University of North Bengal. This thesis includes a detailed investigation of the properties of eight chiral liquid crystal compounds having biphenyl benzoate core and formulation of one room temperature ferroelectric liquid crystal mixture. The work presented here is expected to be helpful in realizing a relationship between the changes in physical properties of the selected compounds with change in their molecular structures and also to recognize the efficacy of the compounds in formulating mixtures suitable for display applications. Most of the studies presented here have been carried out in Liquid Crystal Research Laboratory, Department of Physics, University of North Bengal under the supervision of Prof. Pradip Kumar Mandal, Department of Physics, University of North Bengal. However, the synchrotron X-ray diffraction experiments were carried out at Deutsches Elektronen-Synchrotron (DESY), Hamburg, Germany.

The thesis contains eight chapters.

A brief introduction to liquid crystals and list of investigated compounds are given in **Chapter 1**.

In **Chapter 2** the theoretical backgrounds and the experimental techniques used for characterizing the liquid crystal materials have been discussed in detail.

Chapter 3 describes the characterization of 1F3R, with least number of carbon atoms in the chain and the only compound having no tilted phase

phases, by polarizing optical microscopy, synchrotron X-ray diffraction and dielectric spectroscopy.

Chapter 4 presents the phase behavior, structural, dielectric and electro-optic properties of 2F3R and 3F3R.The molecular structures of 2F3R and 3F3R differ from that of 1F3R only by one and two number of carbon atoms in the fluorinated chain respectively, resulting in the induction of tilted phases.

In **Chapter 5** phase sequence, dielectric and electro-optic properties of the compounds 5F3R and 6F3R, which show only ferroelectric phase throughout its liquid crystalline state, have been discussed.

In **Chapter 6** properties of 4F4R and 4F5R, the only two compounds in this series for which number of oligomethylene spacers differ from other compounds, have been presented.

In **Chapter 7**, 7F3R**,** the longest among the selected compound has been characterized. Using this compound as dopant, the formulation and characterization of one room temperature ferroelectric liquid crystal mixture has also been discussed in this chapter.

Summery and conclusions and of all the experimental results have been presented in **Chapter 8**.

A list of selected books and monographs on liquid crystals has been put in **Appendix A**. Most of the results incorporated in this dissertation have already been published in different international scientific journals and also been presented in conferences and seminars, a list of which is given in **Appendix B**.

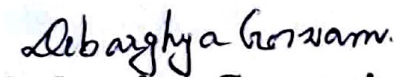

Debarghya Goswami
Department of Physics
University of North Bengal
Date:10.02.2020

'It is the city of mirrors, the city of mirages, at once solid and liquid at once air and stone'

Erica Jong.

Table of Contents

Chapters

Chapter 1

Introduction

Chapter 2

Experimental techniques and relevant theory

Chapter 3

Structural and dielectric properties of orthogonal smectic phases in a chiral mesogen having biphenyl benzoate core

List of tables

List of figures

Chapter 1

Chapter 2

Chapter 3

Chapter 4

Chapter 5

Chapter 6

Chapter 7

Chapter 8

List of Appendices

CHAPTER-1

Introduction

1.1 Liquid Crystal

Substances often encountered in everyday experiences typically pass through a direct transition from three dimensionally ordered crystalline solids to isotropic liquids. The solid state possesses long range positional and orientational ordering whereas none of these ordering sustains in liquid phase. However, there are many organic materials for which there exist one or more intermediate phases between solid and liquid states, known as 'mesophases': a word originated from the Greek word 'meso', meaning 'in between'[1]. These mesophases are characterized by certain properties of both of a conventional liquid like fluidity and of a conventional solid crystal like dielectric anisotropy and are known as Liquid Crystals (LC) [2,3]. This intermediate phase was first discovered by the Austrian botanist, Friedrich Reinitzer in 1888 [4]. In liquid crystalline phase the substances exhibit orientational order and in addition to it sometimes even partial positional order. A number of books and monograohs on liquid crystals, constituent molecules, structures of various liquid crystalline phases, their numerous interesting properties and applications are now available[1–3,5–9], only the salient features, relevant to the present dissertation, will be discussed below in brief.

Liquid crystals can be classified in two categories on the basis of their mode of phase transition. Liquid crystals whose mesophase formation is temperature dependent are called thermotropic liquid crystals and those whose phase formation depends on the concentration of a suitable solvent are called lyotropic liquid crystals. As this dissertation has focused only on thermotropic liquid crystals, any farther discussions on lyotropic liquid crystals will be beyond the scope of this work.

Liquid crystals are also classified in three main groups, namely nematic, cholesteric, and smectic, on the basis of their structure as proposed by Friedel in 1922 [1,2,10].

Nematic phase arises just below the isotropic phase. It has only orientational ordering around the long molecular axis but the centres of masses of the molecules are isotropically distributed in three dimensions.

Cholesteric phase is very similar to nematic phase in local scale, but on a larger scale the cholesteric director follows a helix. This phase is observed only in chiral compounds or in mixture of achiral and chiral compounds.

The smectic phase, which often arises on cooling from nematic phase, has partial positional order in addition to orientational order, as the centre of mass of the molecules are arranged in layers. Depending on the nature of orientation and extent of translational order within the layers, smectic phase can be divided in several sub-groups as follows:

1.1.1 Smectic A phase

In Smectic A (SmA) phase the director of the molecules are perpendicular to the smectic layer. There can be different types of smectic layer arrangements in this phase. When the smectic layer spacing (d) is approximately equal to the molecular length (l), it's called monolayer smectic A phase (SmA_1). If the layer spacing is approximately double of the molecular length, it is called bilayer phase (SmA_2) and when there are intermediate molecular arrangements i.e. for which $l < d < 2l$, the phase is known as partially bilayer smectic (SmA_d) [1]. Sometimes even in SmA phase the molecules are found to be tilted but tilted directions in this case are randomly oriented in azimuthal angles

along a diffused cone.This type of SmA phase are called de Vries type SmA phase, for which d is found to be less than *l* [11].

1.1.2 Smectic C Phase

In Smectic C (SmC) phase the director of the molecules are tilted with respect to the smectic layer normal. As the molecules are tilted in this phase, so the smectic layer spacing is always less than the molecular length and it increase with increasing temperature.

A schematic diagram of the molecular distributions in nematic, smectic A and smectic C phases is given in **figure 1.1**.

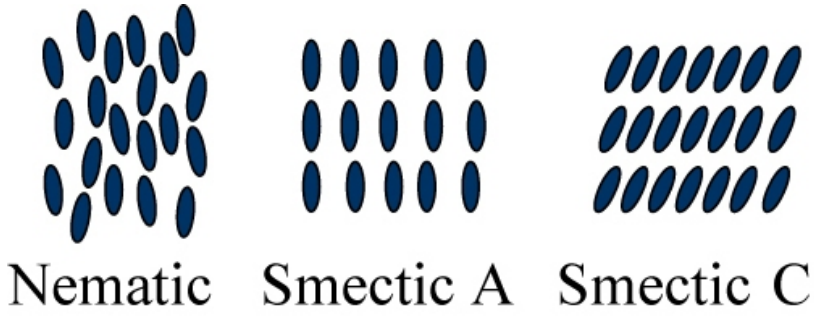

Figure 1.1: Molecular configuration of nematic, smectic A and smectic C phases. Adapted after ref [12]

1.1.3 Hexatic smectic phases

In some smectic phases the centre of mass of the molecules are arranged in a hexagonal manner within the smectic layers. However, this type of positional ordering within the layer, called bond orientation ordering, are short ranged because of insertion of defects. If the molecular director of the hexatic phase is orthogonal to the smectic layer, it is called Smectic B (SmB) phase. There can also be two kind of tilted hexatic phase. If the molecules are tilted towards the apex of the hexagon, it's called smectic I

(SmI) phase and if they are tilted towards the sides of the hexagon, they are called Smectic F (SmF) phase.

Apart from these, there can be soft crystal phases like soft crystal B, J, G, F, K, H phases. B, J and G soft crystal phases are similar to SmB, SmI and SmF phases, only with additional long range positional order. E phase is another orthogonal hexatic soft crystal phase with herringbone structure. The corresponding tilted phase is called K phase. H phase is yet another tilted soft crystal phase corresponding to SmG phase but with additional herringbone structure. The structural relationship of these phase are show in **table 1.1**.

Table 1.1: Structural relationship of smectic phases [This table is adapted from ref [5]]

Fluid smectic	**Stacked hexatic**	**3-D ordered smectic (pseudo hexagonal)**	**3-D ordered smectic (herringbone)**	**Tilt**
SmA	SmB	B	E	Orthogonal
SmC	SmF	G	H	Tilted towards face of hexagon
	SmI	J	K	Tilted towards apex of hexagon

From the existing knowledge, the phase sequence of the liquid crystalline phases in a hypothetical liquid crystal with an increase of temperature is shown below [1]:

Crystal→H→K→E→G→J→B→SmF→SmI→SmB→SmC→SmA→N → Isotropic.

No liquid crystalline substance is found to exhibit all the above phases.

1.2 Chirality in liquid crystal

Any structure that lacks mirror symmetry is called chiral in nature. Chirality may be induced in liquid crystals by incorporating chirality within the molecules by inserting one or more carbon atoms asymmetrically bounded with four distinct groups or by doping chiral mesogenic or nonmesogenic compounds in some non chiral liquid crystal [6,7,9,13–16].

Usually the chiral phases are distinguished by an asterisk "*" followed by the phase symbol.

1.2.1 Chiral nematic phase

The chiral version of nematic phase, also called cholesteric phase (N*), possesses only orientational ordering just like achiral counterpart. But, in addition it shows a spontaneous macroscopic helical structure about an axis perpendicular to the local director.

1.2.2 Chiral smectic phases

Introduction of chirality in smectic compounds have far reaching effects on their phase behaviour and physical properties. It made possible to integrate novel properties of solid polar dielectric materials, like ferroelectricity, antiferroeletricity, pyroelectricity etc. with the flow characteristics of liquids.

1.2.2.1 Ferroelectric liquid crystal (FLC)

Materials which may reveal spontaneous polarization (P_S) even in the absence of external electric field and whose polarity can easily be reversed by application of an electric field are called ferroelectric materials. It is well known that ferroelectric materials must possess non-centro symmetric structure. Though it is easy to realise non- centro symmetric space groups in solids, it's difficult to imagine the same in fluid like materials. It was quite certain that isotropic liquids could not be ferroelectric. As a matter of fact most liquid crystals also fail to exhibit ferroelectricity as they possess inversion symmetry. However, way back in 1974, Robert Mayer established by symmetry arguments that chiral smectic C phase (SmC*) can display ferroelectric properties. Though SmC phase has inversion symmetry, situation changes radically for SmC* phase. It is evident from **figure 1.2** SmC phase has the following symmetries:

i) A two-fold rotational symmetry around an axis perpendicular to the tilt, within the smectic layer.

ii) An inversion symmetry about a mirror plane normal to the tilt and smectic layer.

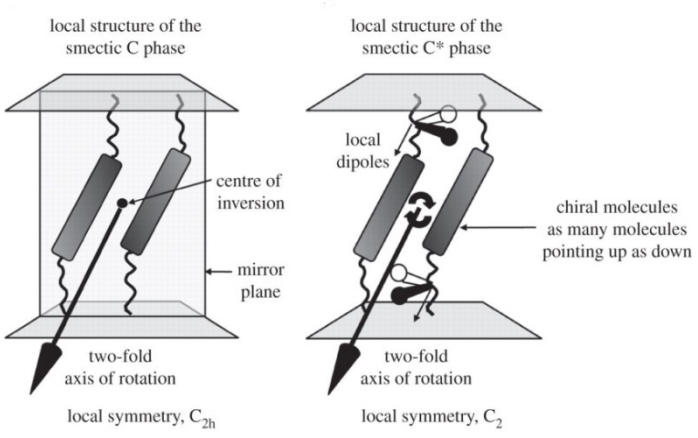

Figure 1.2: Symmetries in SmC and SmC* phases. Adapted after ref [14]

Thus SmC phase exhibits C_{2h} symmetry operation. But the mirror symmetry is removed in SmC* phase due to the chirality of the molecules and the symmetry reduces to C_2 in this phase. Thus due to the non-centrosymmetric structure, SmC* phase may possess spontaneous polarization along the two-fold axis of rotation, in absence of external electric field. If an external electric field is applied then molecules rotate around a virtual cone with an angle twice of the tilt angle of the molecules and the direction of the spontaneous polarization and that of the molecular tilt are inverted as shown in **figure 1.3**.

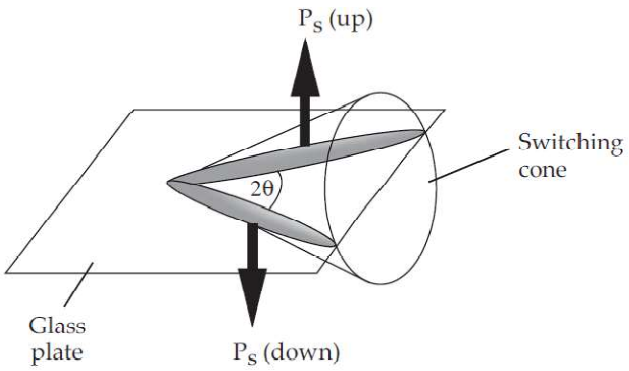

Figure 1.3:Bistable rotation of molecule in SmC* phase. Adapted after ref [6].

The corresponding response time for this molecular reorientation is in the range of sub-millisecond to microsecond, much faster than nematic materials. Moreover, it is necessary to apply an external field to change one switched state of polarization, which makes SmC* phase to be bistable [14,17,18] . Hence SmC* phase exhibits ferroelectric properties. Being optically active, the switching of molecules from one state to other under external electric field in SmC* phase is associated with a change in

the transmitted intensity of light. This specific electro-optic effect is the fundamental principle for the liquid crystal based display.

However, the bulk material in SmC* phase doesn't show any spontaneous polarization as a consequence of the helical molecular arrangement in this phase. In SmC* phase, though a constant molecular tilt angle is maintained throughout the sample, the directors rotates slowly from layer to layer forming a helical structure around the layer normal, as shown in **figure 1.4**. P_S, being perpendicular to both layer normal and molecule, rotates similarly and cancels to zero over the distance of the pitch. The SmC* phase is therefore more correctly called helielectric.

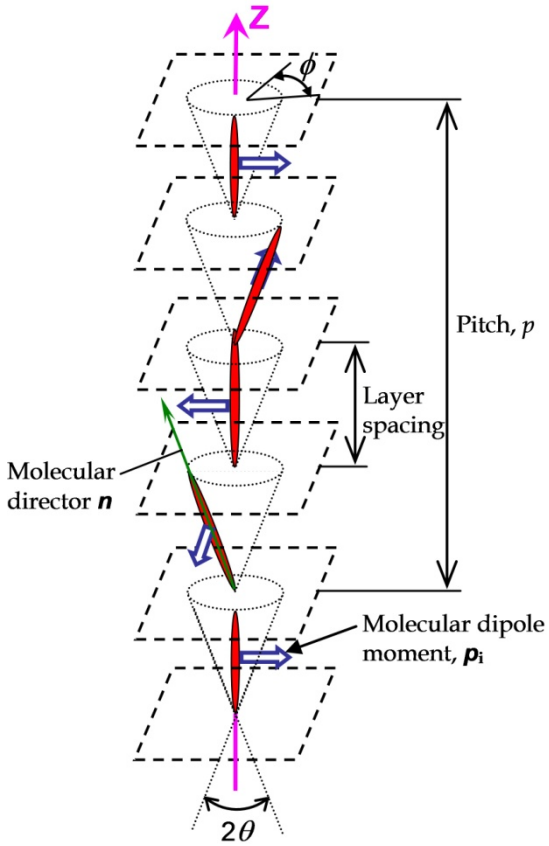

Figure 1.4: Helical structure in SmC* phase. Adapted after ref [19]

Thus to exploit the ferroelectric property in bulk SmC* phase the helix has to be broken. In 1980 Clark and Lagerwall presented the idea of unwinding the helix by pinning the molecules via surface interaction[18].

The first FLC display device reported by them is known as surface stabilized ferroelectric liquid crystal (SSFLC) display.

Apart from this, the chiral tilted hexatic phases SmI* and SmF* also show ferroelectric properties like SmC*. These phases also exhibit macroscopic spontaneous polarization in sufficiently thin cell [1,20,21].

1.2.2.2 Antiferroelectric liquid crystal (SmC*$_A$)

Like SmC* phase, in antiferroelectric SmC*$_A$ phase also the molecules are arranged in layers with a finite tilt with the layer normal, but the tilt director changes sign from one layer to the adjacent layer. Thus SmC*$_A$ has anticlinic structure (**figure 1.5**) unlike SmC* phase, which has synclinic structure. Therefore in the helical superstructure of antiferroelectric SmC*$_A$ phase, P_S points in opposite directions in adjacent layers, making P_S zero even in microscopic level. The antiferroelectric liquid crystal phase has ‘ tristable switching’ under an applied electric field: (a) the anticlinic antiferroelectric state (b) the synclinic ferroelectric state with +ve P_S and (c) the synclinic ferroelectric state with -ve P_S. Antiferroelectric liquid crystals can be utilised to design high resolution displays, for its inherent natural grey scale.

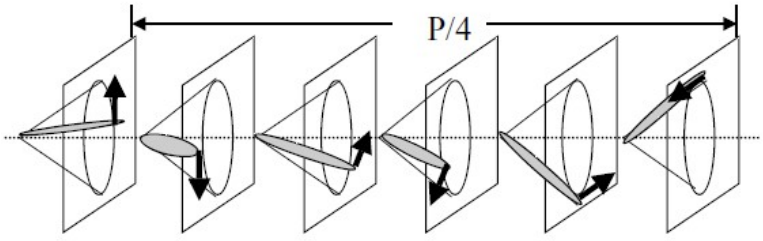

Figure 1.5: Helical structure in SmC*$_A$ phase. Adapted after ref [1]

1.2.2.3 SmC* *subphases* (SmC*$_\alpha$, SmC*$_\beta$, SmC*$_\gamma$)

Apart from SmC*$_A$ phase, several *subphases* have also been reported. These sub phases can be distinguished by the number of layers and their orientations in unit cell. For example, the SmC*$_\beta$ and SmC*$_\gamma$ phases have four and three layers in their unit cells respectively, as can be seen in **figure 1.6.** They may appear in between SmC* and SmC*$_A$ phase within a small temperature range (1-2K). SmC*$_\alpha$ possess an incommensurate structure and may appear in between SmA* and SmC* phase.

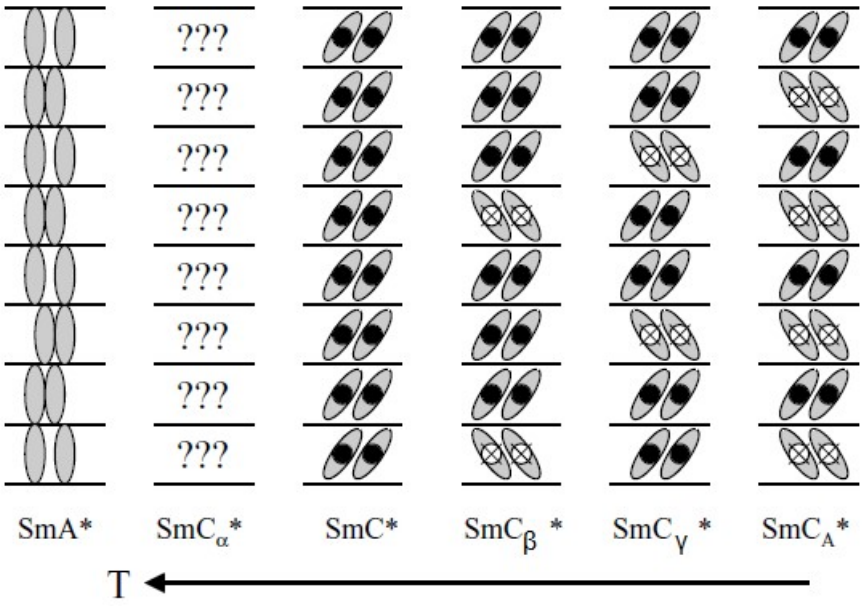

Figure 1.6: Nonhelical local model of chiral smectic phases Adapted after ref [1]

1.2.2.4 Paraelectric liquid crystal (SmA*)

SmA* phase is an orthogonal phase where the molecules are parallel to the smectic layer normal. There is no helical superstructure in this phase

and the spontaneous polarization is zero in this phase. Without any presence of external electric field it's difficult to distinguish between the chiral SmA* and nonchiral SmA phase. However, in some compounds having SmA* phase, an electric field, applied in a direction parallel to the layer of SmA* phase, may induce a tilt of the molecular axis perpendicular to the field. This is known as electroclinic effect [22–25].

In classical SmA* phases, due to the emergence of finite molecular tilt at SmA* to SmC* transition, a layer shrinkage can be observed in the said transition under cooling. This layer contraction along with the surface anchoring effects leads to 'zig-zag' defect in the optical texture, degrading the quality of the device. To avoid such defect, materials with minimum or zero layer contractions are required. There are few such materials known as de Vries type materials. In these type of material the molecules are tilted even in SmA* phase but the tilted directors are randomly oriented in azimuthal angles along a diffused cone. After entering in SmC* phase the tilt director become ordered, azimuthal degeneracy is lifted and macroscopic tilt can be observed without any layer shrinkage [11,26,27].

1.3 Applications of liquid crystals

Due to their unique optical, dielectric or elastic behaviour, liquid crystals have a variety of technical and scientific applications like spatial light modulator, tuneable colour filters, telecommunication switching, optical computing etc [28–34]. Liquid crystals can also potentially be used as new functional materials for electron, ion, molecular transporting, sensory, catalytic, optical and bio-active materials [35]. However, owing

to their strong sensitivity towards electric and magnetic field along with their fluid nature and optical activity liquid crystals have dominantly been used for display applications. Liquid crystal displays (LCD) have almost completely replaced cathode ray display (CRD) for their higher energy efficiency, low volume, wider range of screen size, safe disposability etc.[36–39]. Though most of the liquid crystal devices discussed above are based on achiral nematic liquid crystals, but after the introduction of chirality in liquid crystals, chiral liquid crystals have drawn the attention of most researchers not only for the induction of various new phases with distinctive structures (N*, SmA*, SmC*, SmC_A* etc, as discussed before) but also for their superior and exclusive electro-optic properties which are promising for advanced display applications.

SmC* phase which exhibits ferroelectric properties like spontaneous polarization can be used for very fast display devices as it shows much sharper (in μs range) response to electric field compared to achiral nematics (ms range). Because of inherent bistability of SmC* phase, as discussed before, nearly no power is needed to maintain an image in ferroelectric liquid crystal device (FLCD). In fact, because of fast response time, wide viewing angle and V-shape switching characteristics, the FLC based displays are potentially much more advantageous compared to nematic based displays. High resolution fast FLCD may also be used for field sequential colour (FSC) microdisplays, which are one of the most superior technology for pico-projectors now a days. The switchable goggles and lenses based on FLCs can very effectively be used for modern switchable 2D/3D TVs. Apart from displays, liquid crystals having SmC* phase can also be utilised to design memory devices, for its bistability [9,15,40].

SmC^*_A phase which shows anti ferroelectric characteristics are attractive for their trisatable switching behaviour and can also be used to design anti ferroelectric liquid crystal display (AFLCD). For their easy dc compensation, sharp response time in microsecond range, hemispherical viewing angle (in-plane switching geometry), intrinsic analog gray-scale capability, and lack of ghost effect AFLCD can also be a superior replacement of NLCDs [41]. Orthoconic AFLC with 45° tilt, can be used to design display devices to get rid of the problem of poor alignment and leakage of light in dark state [42]. de Vries type SmA* phase with almost zero layer contraction and high electronilic effect can be used to design fast display devices free from 'zig-zag' defects which arise due to bulking of layers [27,43].

1.4 Importance of chiral systems with Biphenyl Benzoate core

The immense possibility of using chiral liquid crystals in different useful applications has already been discussed. However, still they have some issues at various levels. For example, display operation requires a chemically and photo-chemically stable liquid crystal with wide temperature range around room temperature. Along with that various characteristics like response time, tilt angle, rotational viscosity, spontaneous polarization etc. are needed to be optimised in accordance to the requirements of the device. Keeping those in mind there is a constant strive to design and study new liquid crystal materials, which can be suitable for application purpose.

Molecules of liquid crystals generally have two or more benzene groups linked by intermediate groups. This builds the rigid core of the molecule. Usually long chain end groups (mostly alkyl groups) are

attached with the core. They can be directly linked with the benzene ring, or by an intermediate ether or ester [5].

In application level, the inferior chemical and photochemical stabilities and natural strong colours of liquid crystals have been a difficulty. The origin of the problem is related with the intermediate linking groups between benzene rings of the core, which is the weakest part of the molecule as a whole. The poor chemical stability and colouration of liquid crystals can be overcome by removing the linking group, which results a stable and colourless biphenyl based liquid crystal [5]. So currently, different LCs having biphenyl based mesogenic core have been widely investigated. LCs lacking a linkage group between two benzene units in their core exhibit the following distinctive characteristics, which can potentially be handy from application perspective.

- Liquid crystals having biphenyl core have very high thermal, chemical, and UV stability [44].
- They have appropriately low viscosity, fast response, and low driving voltage[45–48].
- Their alkoxy derivates can potentially have an large birefringence which will be beneficial to their optical performances [49].

Besides there are existing nematic esters which are widely recognized for its stability and colourlessness. So it was tried to fit in ester based structure with the biphenyl core. The introduction of a third benzene ring, linked with the biphenyl core with an ester group results a biphenyl benzoate core. Chiral liquid crystals having biphenyl benzoate core are found to have higher thermal stability, often with wide range low temperature ferroelectric and antiferroelectric phases. Besides, due to inherent angle in ester group, the biphenyl benzoate core results in highly tilted ferroelectric and antiferroelectric liquid crystals with high spontaneous polarization, which qualities are otherwise rare in chiral

liquid crystals. Quite a few biphenyl benzoate cored ferroelectric and antiferroelectric liquid crystals were reported to have tilt angle as high as ~45° which can be utilized to design displays with perfect dark state, excellent contrast ratio and wide viewing angle. [50–54].

Apart from that due to their the smaller size and higher strength of C-F bonds, chiral liquid crystals with fluorinated chain exhibit enhanced spontaneous polarization, higher dielectric anisotropy, lower optical anisotropy etc. which can again be useful from application perspective[55–57].

Keeping all these in mind eight ferroelectric liquid crystal compounds (**1F3R, 2F3R, 3F3R, 5F3R, 6F3R, 4F4R, 4F5R** and **7F3R**) with biphenyl benzoate core and fluorinated chains have been selected for investigation in the present dissertation employing various experimental techniques.

1.5 List of the compounds selected for investigation

The code names, molecular structures and chemical names of the compounds studied in this dissertation are listed below. These compounds were synthesized by Ziobro et. al [50] and obtained from them and used without any further purification.

1. Code name 1F3R

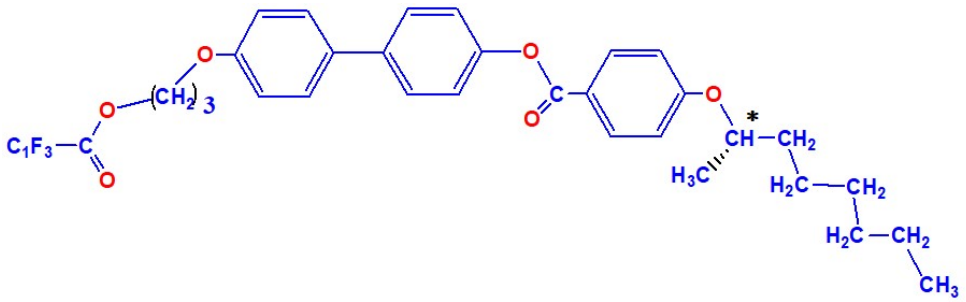

(*S*)-(+)-4′-[(3-trifluoroetanoyloxy)prop-1-oxy] biphenyl-4-yl 4-(1-methyl- heptyloxy)benzoate.

2. Code name 2F3R

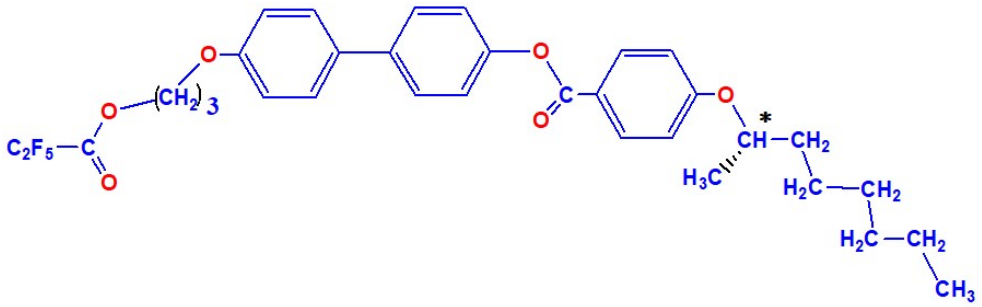

(*S*)-(+)-4′-[(3-pentafluoropropanoyloxy)prop-1-oxy]biphenyl-4-yl4-(1-ethylheptyloxy) - benzoate.

3. Code name 3F3R

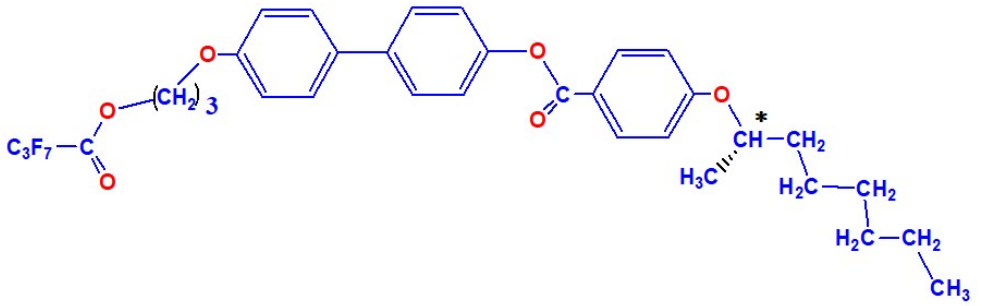

(*S*)-(+)-4′-[(3-heptafluorobutanoyloxy) prop-1-oxy] biphenyl-4-yl 4-(1-methylheptyloxy) benzoate.

4. Code name 4F4R

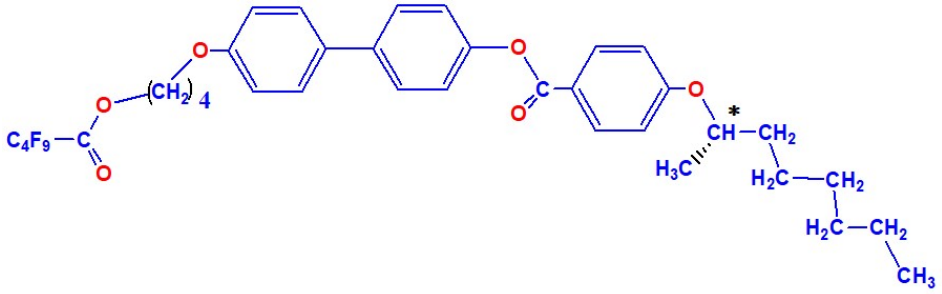

(*S***)**-(+)- 4′ - [(4 - nonafluoropentanoyloxy)but-1-oxy] biphenyl-4-yl 4-(1-methylheptyloxy)-benzoate.

5. Code name 4F5R

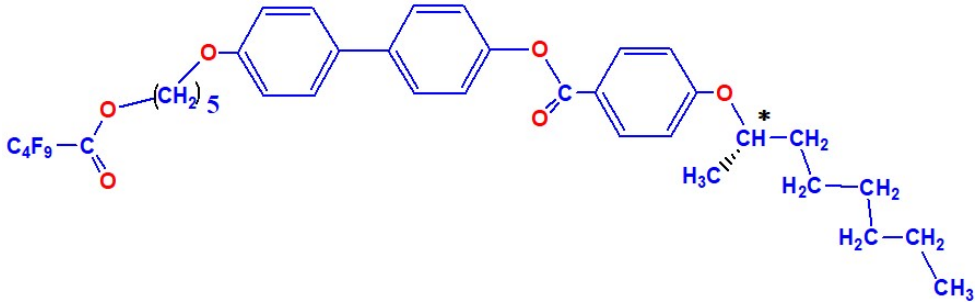

(*S***)**-(+)-4′-[(5-nonafluoro-pentanoyloxy)pent-1-oxy]biphenyl-4-yl4-(1-methylheptyloxy)benzoate.

6. Code name 5F3R

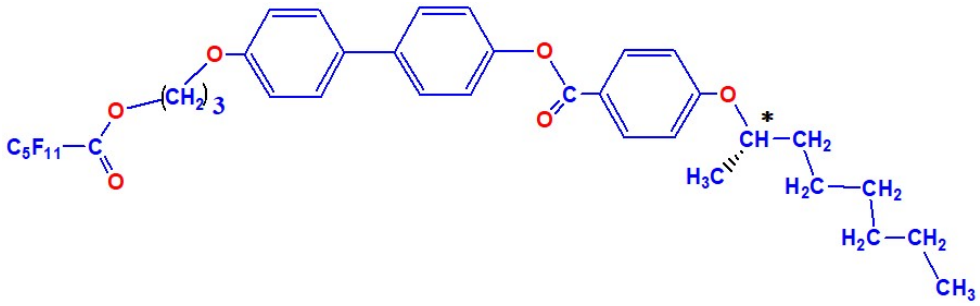

(*S*)-(+)-4′-[(3-undecafluorohexanoyloxy)prop-1-oxy]biphenyl-4-yl 4-(1-methylheptyloxy)- benzoate.

7. Code name 6F3R

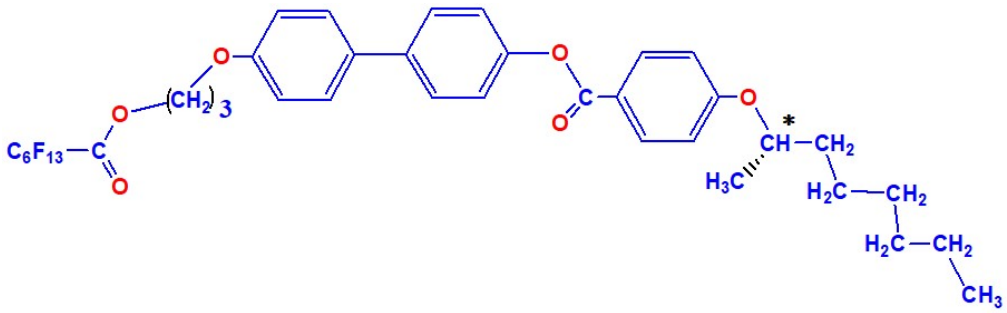

(*S*)-(+)-4′-[(3-tridecafluoroheptanoyloxy)prop-1-oxy]biphenyl-4-yl 4-(1-methylheptyloxy) benzoate.

8. Code name 7F3R

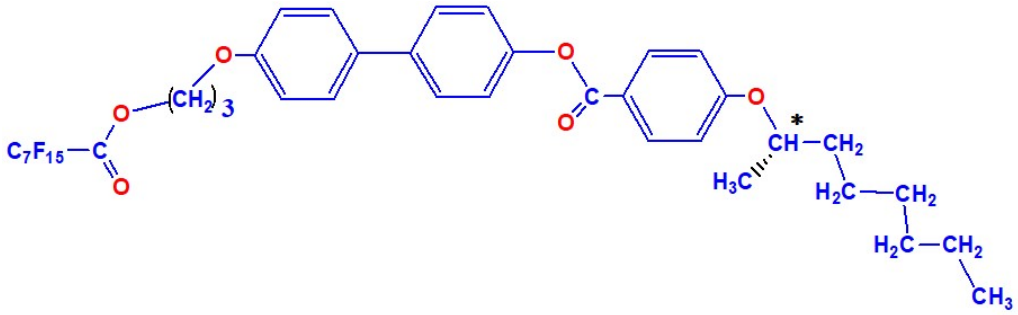

(*S*) - (+) -4′-[(3-pentadecafluorooctanoyloxy) prop-1-oxy]biphenyl-4-yl 4-(1-methylheptyl oxy)benzoate.

In the code name nFmR , n and m respectively stand for the number of C atoms in the perfluorinated chain and in the oligomethylene spacer.
All compounds have same biphenyl benzoate core, one fluorinated and one protonated chain, chiral centre being at the protonated chain. Since in the synthesis paper the authors have used the term biphenyl-yl benzoate in the chemical names of the compounds, we have also used the term biphenyl-yl benzoate core molecules in the published papers. However, we used 'biphenyl benzoate' throughout this dissertation.

Apart from these pure compounds a room temperature ferroelectric liquid crystal mixture has been formulated using one of the compounds (7F3R) as a chiral dopant.

1.6 Motivations and Objectives of the dissertation

The study of the phase behaviour of liquid crystal materials, which can typically have various mesophases within a short temperature range, may help us to comprehend the physics behind the different kind of phase transitions in such compounds. The dielectric and electro-optic properties of these materials are of immense importance from application perspective. It's essential to know the said parameters, to decide whether a LC compound is fit to be used in display devices or whether it can be used as a chiral dopant to formulate any chiral liquid crystal mixture or not. As described before, different LC phases have diverse structures which change with temperature. The structures also have great influence on their electro-optic properties. Thus the knowledge about the structural properties of LCs is also vital both from fundamental knowledge and utilitarian perspective [58].

Keeping these in mind the main objective of this dissertation is set to characterize the selected liquid crystal compounds using different experimental techniques, mainly focusing on the identification of various mesophases, exploration of their dielectric and electro-optic behaviour. Structural investigation of the phases, by synchrotron X-ray diffraction, is also planned only for some of these compounds due to limited availability of synchrotron beam time.

Since all the compounds, selected for investigation, have same back bone differing only by the number of carbons and the number of oligomethylene spacers in the fluorinated chain, efforts will be made to

inculcate a relationship of their phase behaviour and dielectric, electro-optic, structural properties with change in their molecular structures. Also to see the efficacy of the compounds in formulating mixtures suitable for display applications, various properties of one multi-component mixture will be investigated.

Reference

[1] Dierking I. Textures of Liquid Crystals. wiley-vch. Weinheim: WILEY-VCH; 2003.

[2] Priestley E., Wojtowicz PJ, Sheng P. INTRODUCTION TO LIQUID CRYSTALS. London: Plenum Press; 1974.

[3] Collings P, Hird M. Introduction to liquid crystals Chemistry and Physics. Gray G, Goodby J, Fakuda A, editors. London: Taylor & Francis; 1997.

[4] Reinitzer F. Beitr ge zur Kenntniss des Gholesterins. Monatshefte fur Chemie. 1888;9:421–441.

[5] Demus D, Goodby J, Gray GW, et al. Handbook of Liquid Crystals. New y: WILEY-VCH; 1998.

[6] Lagerwall ST. Ferroelectric and antiferroelectric liquid crystals. Newyork: WILEY-VCH; 1999.

[7] Oswald P, Pieranski P. SMECTIC AND COLUMNAR LIQUID CRYSTALS. London: Taylor & Francis; 2006.

[8] Chandrasekhar S. Liquid crystals. 2nd ed. New York: Cambridge University Press; 1977.

[9] Dierking I. Chiral liquid crystals: Structures, phases, effects. Symmetry (Basel). 2014;6:444–472.

[10] Sluckin T, Dunmur D, Stegemeyer H. Crystals That Flow : Classic Papers From the History of Liquid Crystals Liquid Crystals Book Series. London: Taylor & Francis; 2004.

[11] Gorkunov M V, Giesselmann F, Lagerwall JPF, et al. Molecular model for de Vries type smectic A - smectic C phase transition in liquid crystals. Phys. Rev. E. 2007;75:060701.

[12] Larsen T, Bjarklev A, Hermann D, et al. Optical devices based on liquid crystal photonic bandgap fibres. Opt. Express. 2003;11:2589.

[13] Meyer RB, Liebert L, Strzelecki L, et al. Ferroelectric liquid crystals . le J. Phys. 1975;36:69–71.

[14] Goodby JW. Twisted and frustrated states of matter. Proc. R. socity A. 2012;468:1521–1542.

[15] Collings P. Ferroelectric liquid crystals : The 2004 Benjamin Franklin Medal in Physics presented to Robert B . Meyer of Brandeis University. J. Franklin Inst. 2005;342:599–608.

[16] Ghosh S. DIELECTRIC RELAXATION SPECTROSCOPY AND ELECTRO-OPTICAL STUDIES OF ANTIFERROELECTRIC AND FERROELECTRIC LIQUID CRYSTALS AND. Indian Association for the cultivation of science, Jadavpur University; 2012.

[17] Hird M. Ferroelectricity in Liquid Crystals and Its Applications. Liq. Cryst. 2011;38:1467–1493.

[18] Clark NA, Lagerwall ST. Submicrosecond bistable electro-optic switching in liquid crystals. Appl. Phys. Lett. 1980;36:899–901.

[19] Pirkl S, Glogarova M. Ferroelectric Liquid Crystals with High Spontaneous Polarization. In: Lallart M, editor. Ferroelectr. Phys. Eff. London: intech open; 2011.

[20] Wróbel S, Mikułko A, Douali R, et al. Ferroelectric behaviour of hexatic phases. Phase Transitions. 2005;78:905–913.

[21] Sinha D, Debnath A, Mandal PK. Hexatic and blue phases in a chiral liquid crystal: Optical polarizing microscopy, synchrotron radiation and dielectric study. Mater. Res. Express. 2014;1:035101.

[22] Blinov L, Chigrinov VG. Electrooptic Effects in Liquid Crystal Materials. Newyork: Springer-Verlag; 1996.

[23] Garoff S, Meyer R. Electroclinic Effect at the A-C Phase Change in a Chiral Smectic Liquid Crystal. Phys. Rev. Lett. 1977;38:848–851.

[24] Garoff S, Meyer RB. Electroclinic effect at the A-C phase change

in a chirai smectic liquid crystal. Phys. Rev. A. 1979;19:338–347.

[25] Andersson G, Dahl I, Kuczynski W, et al. The soft-mode ferroelectric effect. Ferroelectrics. 1988;84:285–315.

[26] Takashishi Y, Ouchi Y, Takezoe H, et al. Spontaneous Formation of Quasi-Bookshelf Layer Structure in New Ferroelectric Liquid Crystals Derived from a Naphthalene Ring. Jpn. J. Appl. Phys. 1990;29:L984–L986.

[27] Sreenilayam SP, Rodriguez-Lojo D, Agra-Kooijiman D, et al. De Vries liquid crystals based on a chiral 5-phenylpyrimidine benzoate core with a tri- and tetra-carbosilane backbone tetra-carbosilane backbone. Phys. Rev. Mater. 2018;2:025603-1-025603–025612.

[28] Lagerwall S, Andersson G, Dahl I. Device for submicrosecond electro-optic modulationin the liquid crystal smectic-A phase using orthogonal bookshelf geometry. U.S; 1989.

[29] Kondoh S, Kawada S. Ferroelectrics 2 . 7inch QVGA type FLC-device for SLM. Ferroelectrics. 2000;246:121–129.

[30] Beresnev L, Haase W. Ferroelectric liquid crystals : development of materials and fast electrooptical elements for non-display applications. Opt. Mater. (Amst). 1998;9:201–211.

[31] Ratna BR, Crawford GP, Prasad SK, et al. Ferroelectrics Electroclinic materials with large induced tilt angles. Ferroelectrics. 1993;148:425–434.

[32] Williams PA, Clark NA, Ros MB, et al. Large electroclinic effect in new liquid crystal material. Ferroelectrics. 1991;121:143–146.

[33] Abdulhalim I, Moddel G, Johnson KM. Highspeed analog spatial light modulator using a hydrogenated amorphous silicon photosensor and an electroclinic liquid crystal. Appl. Phys. Lett. 1989;55:1603.

[34] Andersson G, Dahl I, Komitov L, et al. Device physics of the

softmode electrooptic effect. J. Appl. Phys. 1989;66:4983.

[35] Bisoyi HK. Synthesis and Characterization of Novel Mesogenic Materials. Jawaharlal Nehru University; 2009.

[36] Bureau F. Frost & Sullivan Flat Panel Display (FPD) TV Market in India Estimated to Grow to USD 6.39 billion by 2015 at a CAGR of 21.7 Percent. Free Press J. 2013 Aug 23;

[37] Tarumi K, Finkenzeller U, Schuler B. Dynamic Behaviour of Twisted Nematic Liquid Crystals. Jpn. J. Appl. Phys. 1992;31:2829–2836.

[38] Huh I, Kim Y. New low viscosity liquid crystal compounds containing the 2 , 3 , 4-trifluorophenyl moiety for active matrix displays. Liq. Cryst. 2002;29:1265–1273.

[39] Sprokel GJ, editor. The Physics and Chemistry of Liquid Crystal Devices. Newyotk: Springer Science and Buisness Meadia; 1980.

[40] Prakash J, Chandran A, Biradar AM. Scientific developments of liquid crystal-based optical memory: a review. Reports Prog. Phys. 2017;80:016601.

[41] Otón JM, Quintana X, Castillo PL, et al. Antiferroelectric Liquid Crystal Displays. OPTO−ELECTRONICS Rev. 2004;12:263–269.

[42] D'have K, Rudquist P, Lagerwall ST, et al. Solution of the dark state problem in antiferroelectric liquid crystal displays. Applied Physics Letters. 2000;76:3528.

[43] Debnath A, Sinha D, Mandal PK. Wide range room temperature electroclinic liquid crystal mixture with large induced tilt and very small layer contraction. J. Appl. Phys. 2016;119:124103-1-124103–124121.

[44] Luo S-H, Wang Q-F, Wang Z-Y, et al. Synthesis and characterization of biphenyl liquid crystal based on natural molecules and 2(5H)-furanone moiety. Res Chem Intermed.

2013;39:2513–2526.

[45] Hsu S, Wu M, Chen S, et al. Synthesis , morphology and physical properties of multi-walled carbon nanotube / biphenyl liquid crystalline epoxy composites. Carbon. 2012;50:896–905.

[46] López-velázquez D, Hernández-sosa AR, Castillo-rojas S. Molecular Crystals and Liquid Crystals Dihydroxypropoxy) Diphenyl 4-n-Alcoxy Acids. Mol. Cryst. Liq. Cryst. 2012;553:175–184.

[47] Milette J, Relaix S, Lavigne C, et al. Reversible long-range patterning of gold nanoparticles by smectic liquid crystals. Soft Matter. 2012;8:6593–6598.

[48] Zhang J, Su J, Ma Y, et al. Coarse-Grained Molecular Dynamics Simulations of the Phase Behavior of the 4-Cyano-4 ′ -pentylbiphenyl Liquid Crystal System. J. Phys. Chem. B. 2012;116:2075–2089.

[49] Arakawa Y, Nakajima S, Ishige R, et al. Synthesis of diphenyl-diacetylene-based nematic liquid crystals and their high birefringence properties. J. Mater. Chem. 2012;22:8394–8398.

[50] Ziobro D, Dąbrowski R, Tykarska M, et al. Synthesis and properties of new ferroelectric and antiferroelectric liquid crystals with a biphenylyl benzoate rigid core. Liq. Cryst. 2012;39:1011–1032.

[51] Ahmed S, Rahman M, Rabbi AR, et al. Synthesis, characterization and liquid crystalline properties of a series of hydroxybiphenyl benzoate and biphenyl bis(benzoate). J. Mol. Liq. 2016;224:265–273.

[52] Morawiak P, Piecek W, Żurowska M, et al. Effect of fluorination of molecular rigid core in liquid crystal biphenyl benzoate based homologous series. Opto- Electron. revies. 2009;17:40–44.

[53] Węgłowska D, Dabrowski R. Highly tilted ferroelectric liquid crystals with biphenylyl benzoate rigid core. Liq. Cryst. 2014;41:1116–1129.

[54] Dabrowski R, Gasowska J, Oton J, et al. High tilted antiferroelectric liquid crystalline materials. Displays. 2004;25:9–19.

[55] Potukuchi DM, George AK, Carboni C, et al. Low Frequency Dielectric Relaxation , Spontaneous Polarization , Optical Tilt Angle and Response Time Investigations in a Flourinated Ferroelectric Liquid Crystal , N125F2 (R *). 2004;300:79–93.

[56] NGUYEN H, ROUILLON J, BABEAU A, et al. Synthesis , properties and crystal structure of chiral semiper ¯ uorinated liquid crystals with ferro and anticlinic smectic phases. Liq. Cryst. 1999;26:1007–1019.

[57] Dabrowski R. Ferroelectrics Liquid crystals with fluorinated terminal chains and antiferroelectric properties. Ferroelectricd. 2000;243:1–18.

[58] An J, Hina S, Yang Y, et al. CHARACTERIZATION OF LIQUID CRYSTALS : A LITERATURE REVIEW. Rev .adv. mater. sci. 2016;44:398–406.

CHAPTER-2

Experimental techniques and relevant theory

2.1 Introduction

The compounds selected for study in this dissertation were characterized by measuring various material constants using different experimental techniques. Phases present in the compounds were identified and the specific transition temperatures were measured by polarizing optical microscopy (POM) method. The dielectric properties of the compounds were studied in details using relaxation spectroscopy. The response time (τ), optical tilt angle (θ), spontaneous polarization (P_S), rotational viscosity (γ_φ) were measured with the help of electro-optic method. The structural properties of the compounds were investigated by synchrotron X-ray diffraction techniques. Details of the above experimental techniques and the theoretical background needed to comprehend the data are discussed briefly in this chapter.

2.2 The theory of liquid crystals

With the aspiration to explain the phase behaviour and the phase transitions in liquid crystals, people had tried to develop suitable molecular statistical theory from the middle of the twentieth century. However, this has been a challenging effort, due to the presence of diverse phases in those compounds and for their complex intermolecular interactions. In 1949 Onsager offered his theory for liquid crystals by investigating the influence of anisotropy in hardcore repulsion under excluded volume approximation [1]. Though his theory could match up with the qualitative description of the characteristics of liquid crystals, but it failed to do so with quantitative accuracy. Maier and Saupe came

up with a better theory in 1958-60 for nematics [2,3]. They developed the theory on the anisotropy of soft dispersion interaction with the mean field approximation. This theory was found to be more accurate than that of their predecessors. A molecular statistical theory for Smectic A phase was developed by McMIllan [4]. But to comprehend the behaviour of smectic liquid crystals especially the chiral ones, the well-known theory of phase transition of Landau [5], modified by different scientists has been used most conveniently till date. As the present dissertation is focused only on the chiral smectic compounds, only the Landau theory will be discussed in brief, many books and monographs are available on theoretical exposition of liquid crystals[6–17].

2.2.1 The Landau-de Gennes theory of liquid crystal

Any theory that deals with a system undergoing a phase transition usually utilizes the 'order parameter', which changes from a finite value in low temperature phase to zero in the high-temperature phase, with a continuous or discrete change at the transition point. The free energy of the system can be calculated as a function of the order parameter and it can be minimized to obtain the equilibrium condition. According to the hypothesis proposed by Landau, the free energy of the system near a second order phase transition can be written as a power series of the order parameter and its special derivatives with suitable temperature dependent coefficients.

For ferroelectric SmC* to paraelectric SmA* phase transition the order parameters are two component tilt vector $\vec{\boldsymbol{\xi}}$ and in plane polarization $\vec{\boldsymbol{P}}$. The projections of the molecules in the smectic plane (xy plane) can be expressed in terms of the tilt order parameter as $\vec{\boldsymbol{\xi}} = \boldsymbol{\xi_1}\hat{\boldsymbol{x}} + \boldsymbol{\xi_2}\hat{\boldsymbol{y}}$ and the

transverse in-plane polarization can also be written in its component form as $\vec{P} = P_x\hat{x} + P_y\hat{y}$ [12,13,18].

Following the Landau's expansion it was attempted to express the free energy density of in the vicinity of SmC* to SmA* transition in terms of their order parameters [19] as follows :

$$F(z) = \frac{1}{2}a\left(\xi_1^2 + \xi_2^2\right) + \frac{1}{4}b\left(\xi_1^2 + \xi_2^2\right)^2 - \Lambda\left(\xi_1\frac{d\xi_2}{dz} - \xi_2\frac{d\xi_1}{dz}\right) + \frac{1}{2}k_{33}\left[\left(\frac{d\xi_1}{dz}\right)^2 + \left(\frac{d\xi_2}{dz}\right)^2\right] + \frac{1}{2\varepsilon}\left(P_x^2 + P_Y^2\right) - \mu\left(P_x\frac{d\xi_1}{dz} + P_y\frac{d\xi_2}{dz}\right) + C(P_x\xi_2 - P_y\xi_1) \quad \textbf{[2.1]}$$

Here, 'a' is a temperature dependent term, b is a positive parameter, K_{33} is the elastic modulus, Λ the coefficient of the Lifshitz term responsible for the modulation, ε is the dielectric permittivity, μ and C are the coefficients of the "flexo" and "piezo" electric coupling between the tilt and polarization and director gradient and polarization respectively.

By minimizing this free energy the equilibrium values of different parameters were predicted in the said phase transition. However few discrepancies were observed between the experimental data and the theoretically predicted values. In 1984 Zeks [20] added a biquadratic coupling term between the tilt and polarization, in the expression of free energy. This generalised model fitted better with the static dielectric experimental data. It was modified later by Carlsson et al.[21] for the dynamic studies. Finally the expression of free energy for C* to A* transition was written as:

$$F(z) = \frac{1}{2}a\left(\xi_1^2 + \xi_2^2\right) + \frac{1}{4}b\left(\xi_1^2 + \xi_2^2\right)^2 + \frac{1}{6}c\left(\xi_1^2 + \xi_2^2\right)^3 - \Lambda\left(\xi_1\frac{d\xi_2}{dz} - \xi_2\frac{d\xi_1}{dz}\right) + \frac{1}{2}k_{33}\left[\left(\frac{d\xi_1}{dz}\right)^2 + \left(\frac{d\xi_2}{dz}\right)^2\right] + \frac{1}{2\varepsilon}\left(P_x^2 + P_Y^2\right) - \mu\left(P_x\frac{d\xi_1}{dz} + P_y\frac{d\xi_2}{dz}\right) + C\left(P_x\xi_2 - P_y\xi_1\right) - \frac{1}{2}\Omega\left(P_x\xi_2 - P_y\xi_1\right)^2 + \frac{1}{4}\eta\left(P_x^2 + P_Y^2\right)^2 - d\left(\xi_1^2 + \xi_2^2\right)\left(\xi_1\frac{d\xi_2}{dz} - \xi_2\frac{d\xi_1}{dz}\right) \quad [2.2]$$

Where Ω is the coefficient of biquadratic coupling and η was added to stabilise the system.

The nature of temperature variation of different dielectric and electro-optic parameters of chiral liquid crystals, having C* to A* transition can be predicted theoretically by minimizing the free energy given by **equation 2.2** as will be discussed in next few sections.

2.3 Preparation of liquid crystal cells

For most of the applications of liquid crystals, it is required to align them in particular orientations. There can be mainly two types of orientations of liquid crystal molecules. When the direction of the molecular directors are parallel with the direction of measuring electric field, it's called homeotropic alignment (HT) and if the molecular directors are perpendicular to the direction of measuring field, it's called homogeneous alignment (HG). There can be other kinds of alignments also like twisted alignment, pre-tilt alignment etc. In practice, these kinds of alignments are usually achieved by inserting the compounds inside specially designed glass cells. Thus to investigate different properties of liquid crystals under actual LCD conditions, it's important to prepare the liquid crystal cells on which experiments can be carried out. These cells consist of two glass plates, separated by spacers, with a coat of

transparent and conducting Indium tin oxide layer at the inner surface. ITO layer serves the purpose of a transparent electrode. On top of the ITO coat, there is a coating of transparent polymer designed to align the liquid crystal molecules by surface interaction. [22–24]. A schematic diagram of liquid crystal cell is shown in **figure 2.1**.

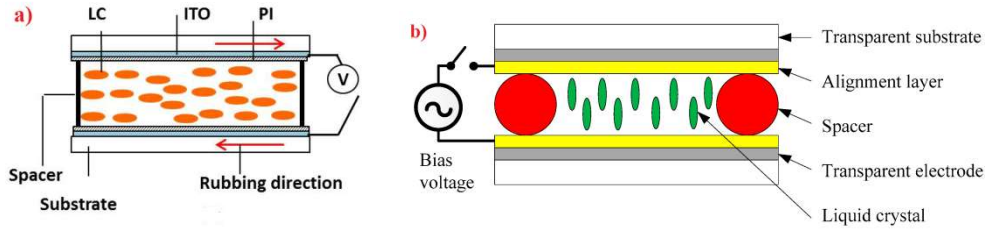

Figure 2.1 Schematic diagram of a) homogeneously and b) homeotropically aligned cell. Adapted after ref [25,26].

In the present work polymer coated homogeneous commercial cells (EHC, Japan), with transparent ITO electrodes were used. The sheet resistance was about 20Ω/□. The cell area was 1 cm^2 and thickness ranged from 5-10μm. The desired alignment was achieved by slowly cooling the sample from the isotropic phase to the required temperature, often accompanied by an ac voltage. Polarized optical microscopy, dielectric, electro-optic measurements and for few compounds small angle X-ray scattering study were done using these cells.

2.4 Surface stabilized ferroelectric liquid crystal (SSFLC)

As discussed in chapter I, the bulk material in SmC* phase forms a helical molecular arrangement. Thus macroscopic value of spontaneous polarization becomes zero, neither the bulk material exhibits bistability even in SmC* phase. However, Clark and Lagerwall came up with an artifice [27] which can turn on these characteristics in SmC* phase even in bulk. As described in the above paragraph, when the FLC compound

is fed into cell, molecules get aligned due to strong surface anchoring. If the thickness of the cell is small enough, the helix of the FLC gets unwind by the surface forces. Thus inside such cells an uniaxial plane of the compound is formed where only two possible orientation of the molecular director (where the surface cuts the smectic cone) is allowed, depending on the direction of external field. It leads to bistability and macroscopic polarization of the compounds in SmC* phase [14]. This structure is called surface stabilized ferroelectric liquid crystal (SSFLC). In most of our experiments we have used this structure. A schematic diagram of SSFLC cell is shown in **figure 2.2.**

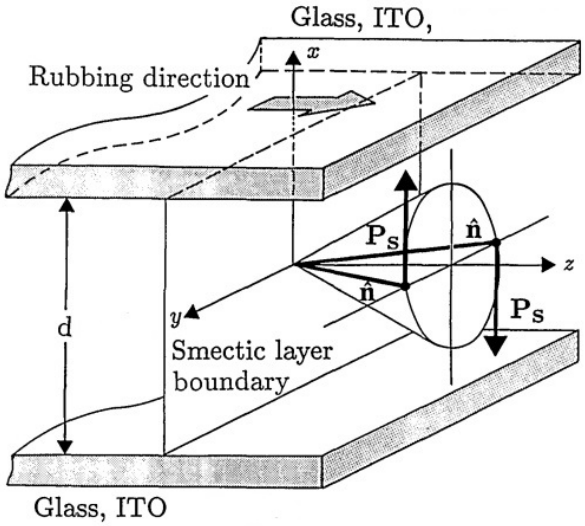

Figure 2.2: Schematic diagram of ideal SSFLC cell. Adapted after ref [28].

2.5 Polarized optical microscopy (POM)

Polarized optical microscopy (POM) is a powerful and easy technique to determine the phase transition temperatures and to identify different phases of liquid crystal compounds. Between crossed polarizers, liquid crystal compounds exhibit optical patterns of different types and of

diverse colours, which are called textures. This arises due to the topological defects of the compounds. Different phases have different types of topological defects and thus have distinguishable textures. Thus temperature dependent texture observation can reveal the phase sequence and transition temperatures of the compounds. The detailed account of different types of textures associated with different phases can be found in the reference [15,29–31]. It should be noted that a particular phase may also display different types of textures depending on thickness, surface treatment and thermal history.

To observe the textures, the compounds were fed into the liquid crystal cell by capillary action. Then the cells were placed inside Mettler FP82HT hot stage for thermal insulation and temperature variation. The temperature was controlled with an accuracy of ±0.1°C with the help of a Mettler FP90 temperature controller. The textures of the compounds were observed in between crossed polarizer with the help of a high-resolution Olympus BX41 polarizing microscope (magnification 10x and 20x) equipped with a 5MP CCD camera. The detail setup is shown in **figure 2.3**.

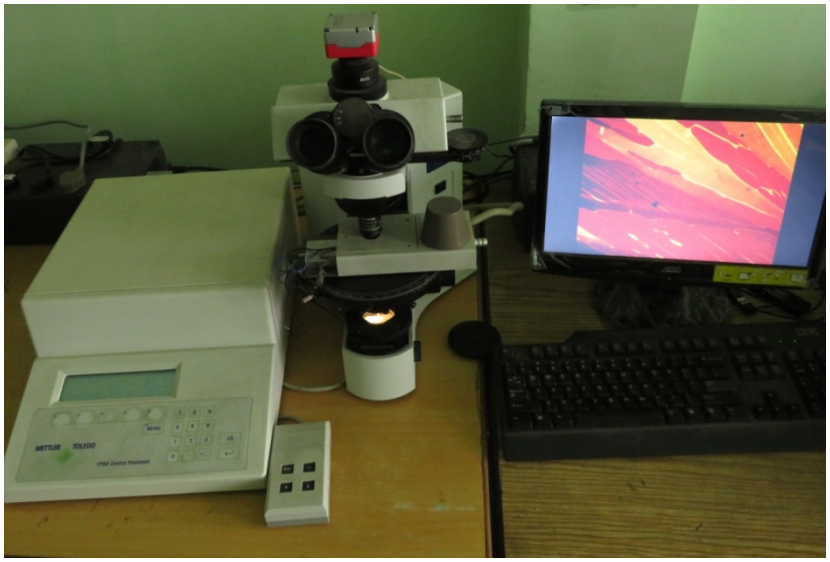

Figure 2.3: The experimental setup for polarizing microscopy

2.6 Dielectric study

Liquid crystals behave as dielectric medium. Because of different kinds of charge distribution inside the dielectric materials, there can be field induced dipole moments inside them, constituent molecules may also possess permanent dipole moments. However, due to the symmetries in their structure, often no macroscopic polarization is observed in absence of any external field (with few exceptions). For example, for SmC* liquid crystals, as discussed in the previous chapter, because of their chirality the component of their dipole moment perpendicular to the long molecular axis doesn't cancel out and they form a polar smectic layer. Nevertheless, the chirality itself generates the helical structure which makes the macroscopic dipole density to be zero. But when a dielectric material, say for example SmC* liquid crystal, is placed inside an external electric field, the field distorts and breaks the symmetry and induces macroscopic polarization. The distortions may be in different atomic or collective level. The real part of the dielectric constant of any dielectric material measures the magnitude of deformability corresponding to different distortion process in the presence of an external electric field.

When a time-dependent electric field is applied to a dielectric material, the induced dipoles take some finite time to get into equilibrium with the applied field. If the frequency of the measuring voltage is high enough, the slower relaxation processes cannot keep pace with the applied field and the system becomes dissipative. The phase difference between the applied field and the induced polarization can be expressed in terms of the imaginary part of the dielectric permittivity [10,18,32,33].

To study different types of dielectric relaxations, frequency domain dielectric spectroscopy with temperature as a parameter is a powerful

method to explore the molecular dynamics or the intermolecular interactions of the material.

2.6.1 Debye Model

One of the standard models of dielectric relaxation was given by Debye assuming a simple exponential decay of the relaxation function with a single characteristic time. According to this model, the complex dielectric permittivity (ε*) can be written as:

$$\boldsymbol{\varepsilon^*(\omega) = \varepsilon'(\omega) - i\varepsilon''(\omega) = \varepsilon_\infty + \frac{\varepsilon_0 - \varepsilon_\infty}{1 + i\omega\tau}} \qquad \textbf{[2.3]}$$

This is called the Debye equation [34,35]. Here, $\varepsilon'(\omega)$ and $\varepsilon''(\omega)$ are respectively the real and imaginary parts of the complex dielectric permittivity at frequency ω, ε_0 and ε_∞ are the low (static) and the high-frequency limit of the real part of dielectric permittivity. The difference $\varepsilon_0 - \varepsilon_\infty$ is also called the dielectric increment ($\Delta\varepsilon$). τ is the relaxation time of the relaxation process which is related to the corresponding relaxation frequency (f) with the relation $\tau = 1/2\pi f$.

By separating the real and imaginary parts of the complex dielectric permittivity from **equation 2.3** it can be written as:

$$\boldsymbol{\varepsilon'(\omega) = \varepsilon_\infty + \frac{\varepsilon_0 - \varepsilon_\infty}{1 + (\omega\tau)^2}} \qquad \textbf{[2.4]}$$

$$\boldsymbol{\varepsilon''(\omega) = \frac{\varepsilon_0 - \varepsilon_\infty}{1 + (\omega\tau)^2}\,\omega\tau} \qquad \textbf{[2.5]}$$

The highest value of $\varepsilon''(\omega)$ is observed when $\omega\tau = 2\pi f_C \tau_C = 1$, that means when the frequency of the measuring field matches with the natural frequency of the relaxation process. The corresponding frequency (f_C) is called the critical frequency.

The highest value of $\varepsilon^{//}(\omega)$ at the critical frequency, as can be obtained from **equation 2.5**, is

$$\boldsymbol{\varepsilon^{//}(\omega) = \varepsilon^{//}_{max}\ \frac{\varepsilon_0 - \varepsilon_\infty}{2}} \qquad \textbf{[2.6]}$$

A representative curve showing the variation of the components of dielectric constants as a function of frequency, in logarithmic scale is shown in **figure 2.4**.

The frequency curve of the real and imaginary part of dielectric constants are usually called the dispersion curve and the absorption curve respectively.

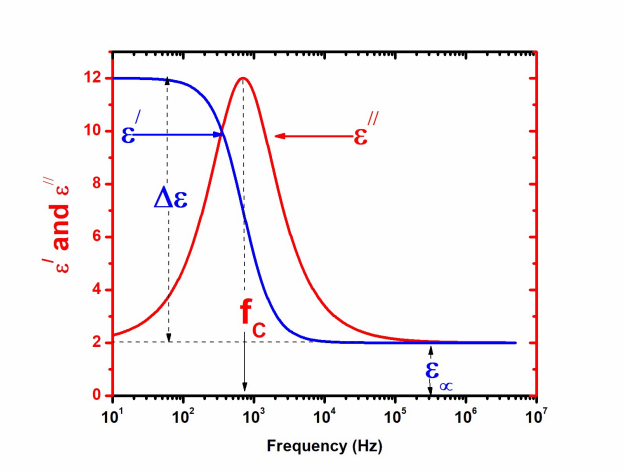

Figure 2.4: Typical dielectric spectra of Debye type dielectric material

Dielectric spectra can also be represented by plotting $\varepsilon^{//}$ as a function of $\varepsilon^{/}$ for different frequencies as shown in **figure 2.5**. This is known as the Cole-Cole plot. For ideal Debye type material Cole- Cole curve should be an exact semicircle with centre at $((\varepsilon_0+\varepsilon_\infty)/2, 0)$ and radius $(\varepsilon_0-\varepsilon_\infty)/2$.

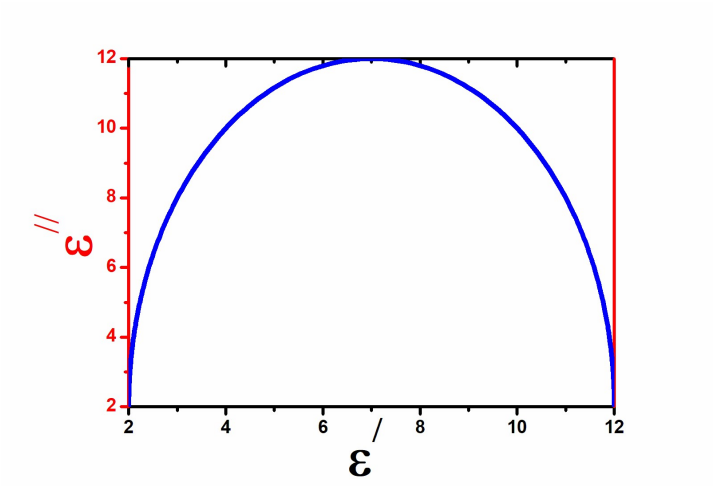

Figure 2.5: Cole-Cole plot for Debye type spectra.

2.6.2 Cole-Cole model

In 1941 K. S. Cole and R. H. Cole pointed out that the dielectric relaxations of many systems particularly molecules with long chains, polymers etc. deviate considerably from Debye's model. They exhibit a broader dispersion curve and lower the maximum loss than what was predicted by Debye's model. Hence the Cole-Cole plots of those compounds reduce inside the Debye's semicircle. [31,27,28,30,32]

To describe the dielectric behaviour of such materials Cole and Cole hypothesized that the idea of single relaxation time of Debye, doesn't fit well for them. Rather the relaxation times of such long molecules are distributed statistically around a most probable value. They had modified the Debye's formula and suggested the following equation:

$$\boldsymbol{\varepsilon^* = \varepsilon^{/} - i\varepsilon^{//} = \varepsilon_\infty + \frac{\Delta\varepsilon}{1+(i\omega\tau)^{1-\alpha}}} \qquad \textbf{[2.7]}$$

Here α is a parameter responsible for the symmetric distribution of the relaxation times and other parameters are already defined before [37].

Separating the real and imaginary part, it can be shown that the maximum value of $\varepsilon''(\omega)$ is given by:

$$\varepsilon''(\omega_C) = \varepsilon''_{max} = \frac{\varepsilon_0 - \varepsilon_\infty}{2} \frac{\cos\frac{\pi\alpha}{2}}{1+\sin\frac{\pi\alpha}{2}} \qquad [2.8]$$

For small values of the α, one can write

$$\varepsilon''_{max} \cong \frac{\varepsilon_0 - \varepsilon_\infty}{2+\alpha\pi} \qquad [2.9]$$

Thus it is clear that for non-Debye material the absorption peak is lowered and broadened.

To consider the low-frequency parasitic effect **equation 2.7** can further be modified and the final expression for the modified Cole-Cole function can be written as [10]

$$\varepsilon^* = \varepsilon' - i\varepsilon'' = \varepsilon_\infty + \frac{\Delta\varepsilon}{1+(i\omega\tau_0)^{1-\alpha}} - i\frac{\sigma}{\omega\epsilon_0} \qquad [2.10]$$

Where τ_0 is the most probable relaxation time related to the critical frequency, σ is the conductivity related to the motion of charge carriers which contributes mainly in the low frequency regime and ϵ_0 is the free space dielectric permittivity. The real and imaginary parts can easily be separated and the following expressions are found:

$$\varepsilon'(\omega) = \varepsilon_\infty + \Delta\varepsilon \frac{1+(\omega\tau_0)^{1-\alpha}\sin(\frac{1}{2}\pi\alpha)}{1+2(\omega\tau_0)^{1-\alpha}\sin(\frac{1}{2}\pi\alpha)+(\omega\tau_0)^{2(1-\alpha)}} \qquad [2.11]$$

$$\varepsilon''(\omega) = \Delta\varepsilon \frac{(\omega\tau_0)^{1-\alpha}\cos\left(\frac{1}{2}\pi\alpha\right)}{1+2(\omega\tau_0)^{1-\alpha}\sin\left(\frac{1}{2}\pi\alpha\right)+(\omega\tau_0)^{2(1-\alpha)}} + \frac{\sigma}{\omega\epsilon_0} \qquad [2.12]$$

If the material shows multiple relaxations with different relaxation times, then **equation 2.10** can be rewritten as:

$$\varepsilon^* = \varepsilon^{/} - i\varepsilon^{//} = \varepsilon_\infty + \sum \frac{\Delta\varepsilon_k}{1+(i\omega\tau_k)^{1-\alpha_k}} - i\frac{\sigma}{\omega\epsilon_0} \qquad [2.13]$$

Here, the subscript 'k' represents the parameters for k^{th} mode of relaxation.

In this dissertation modified Cole- Cole function was used to fit the observed dielectric spectra. In some cases we had to fit more than one relaxation processes as shown in **figure 2.6**. Further, it is worth mentioning that to accommodate the contribution of free charges and ITO layer sometimes in the conductivity part "ω" is taken as $2\pi f^n$ instead of $2\pi f$ [38], where n is a fitting parameter. However, in all compounds studied in this dissertation the behaviour of the cell in low frequency is ohmic and thus the value of "n" reduces to "1". In the third chapter the fitted value of n has been shown for the compound 1F3R. In rest of the thesis n has been taken to be 1.

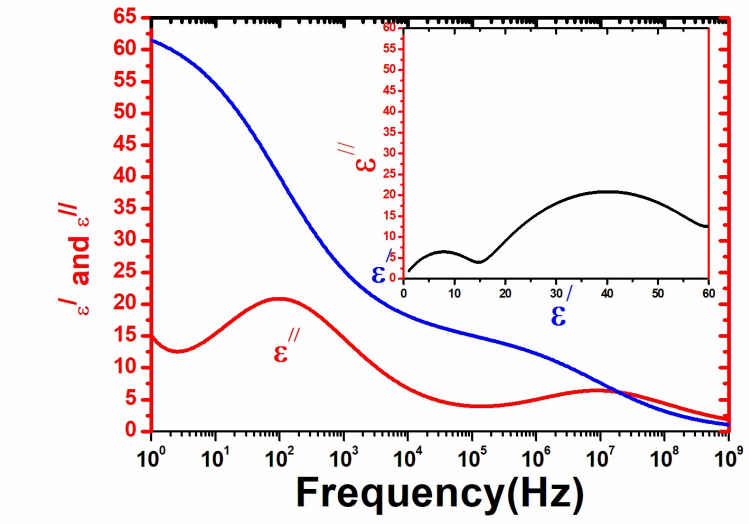

Figure 2.6: Cole -Cole type spectra

2.6.3 Modes of dielectric relaxations in chiral liquid crystals

Mainly two types of dielectric relaxations are observed in chiral liquid crystals: non-collective and collective modes of relaxations.

2.6.3.1 Non –collective relaxation

In this category also two kinds of relaxation behaviour are observed. The first one is related to the rotation of the molecules about its short axis, it is usually observed in ~10^{10} Hz range. The second type of non-collective relaxation is related to the rotation of molecules about its long axis. The characteristic frequency of this relaxation is in 10^7-10^9 Hz region. For most of the compounds these non-collective relaxations fall beyond our observed frequency window. Thus, this thesis dealt with mostly the collective modes of relaxations [10,18,39].

2.6.3.2 Collective modes of relaxation

Only one collective mode of relaxation is observed in SmA* phase which is known as soft mode relaxation (SM), also known as amplitudon mode. This mode is connected with the tilt fluctuation of the molecular directors. This mode can also be observed even in SmC* phase, in the vicinity of SmA* to SmC* transition in some compounds. It is a strongly temperature dependent mode which is usually observed in the region of few hundred kHz. The dielectric increment of SM ($\Delta\varepsilon_{SM}$) is another temperature dependent quantity, whose magnitude is much smaller as compared to the dielectric increment of other collective modes.

But the most commonly observed collective mode of relaxation in the SmC* phase is called the Goldstone mode relaxation (also known as phason mode), that originates due to the phase fluctuations of the molecular directors. The critical frequency of GM relaxation is in the order of lower kHz. But the dielectric increment ($\Delta\varepsilon_{GM}$) of this mode is much higher than that of SM. So often the soft mode is masked by the goldstone mode in SmC* phase. However, under sufficient DC bias, GM relaxation can be suppressed as a result of unwinding of the SmC* helix, but SM remains as it is. By this method even a weak SM can be observed in SmC* phase in a substance whose GM is much stronger than SM. These two relaxation modes are schematically shown in **figure 2.7**.

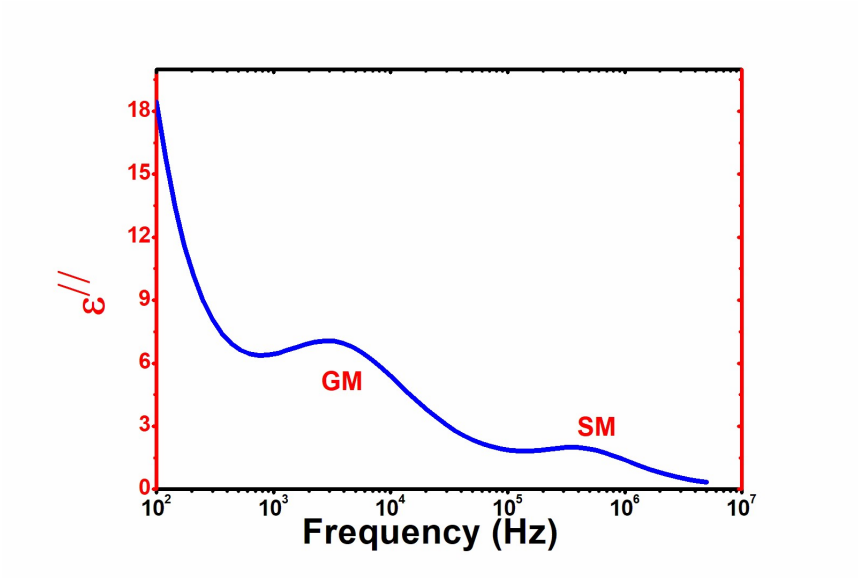

Figure 2.7 : A schematic diagram of both GM and SM relaxation observed together.

In the second order SmA* to SmC* phase transition, the continuous symmetry group of SmA* (D_∞) spontaneously breaks into C_2, the symmetry group of SmC*. Thus soft mode is a symmetry breaking mode which slows down while approaching the transition from above but the

GM relaxation tries to restore the broken symmetry. That is why the SM splits into the amplitude mode (SM) and the phase mode (GM) in SmC* near the C* -A* transition. [10,14,18,40,41].

The nature of temperature variation of critical frequency and dielectric increment of SM and GM can be predicted using modified Landau expression of free energy (**equation 2.2**). To elucidate their temperature dependency Carlsson et al.[21] had defined a parameter $\boldsymbol{\beta} = \frac{\tilde{\eta}^{\frac{1}{2}}\tilde{C}\varepsilon_0\tilde{\varepsilon}}{\tilde{\Omega}^{\frac{1}{2}}}$ where, the tilde denotes normalised forms of the parameters. It is a measure of the ratio of bilinear and biquadratic coupling between the tilt and polarization in **equation 2.2**. The theoretically predicted temperature dependence of critical frequency and dielectric increment of the collective modes, depend strongly on the relative strength of bilinear and biquadratic coupling of the tilt and polarization in the expression of Landau free energy as shown in **figure 2.8**.

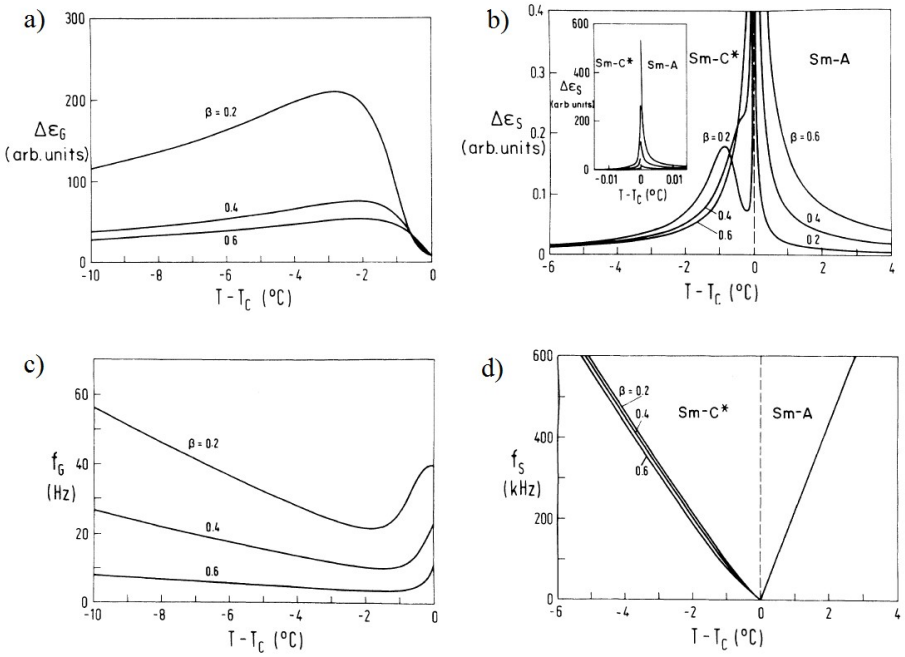

Figure 2.8: Theoretically predicted temperature variation for different β of a) dielectric increment of GM b) dielectric increment of SM C) critical frequency of GM d) critical frequency of SM. Adapted after ref [12]

In the tilted hexagonal chiral phases (SmI* and SmF*) the collective relaxations are mainly dominated by two mechanisms. As described in the first chapter, these phases have long-range bond orientation order (BOO) along with the molecular tilt. Depending on the coupling of tilt and BOO the phason mode of relaxation splits into two distinct relaxations in these phases: tilt angle phason and BOO phason [42–45]. As suggested by Rychetsky´ and Glogarova [43], a stronger BOO phason results in the softening of the frequency near SmC* to SmF*/SmI* transition following an increase in permittivity and decrease in critical frequency. Conversely, the tilt angle phason mode causes a decrease in permittivity and an increase in critical frequency.

2.6.3.3 Maxwell Wagner relaxation

Sometimes a low-frequency relaxation is observed in a heterogeneous structure if at least one of the materials has non-zero electrical conductivity. Polarization may occur due to the accumulation of charges in the interface, which can cause relaxation. This is called Maxwell Wagner (MW) relaxation [10]. If the liquid crystal sample, taken inside a dielectric cell, have high conductivity, at times charges may accumulate in between the liquid crystal material and the polymer coating of the cell. This may contribute a MW relaxation in the dielectric spectrum. MW relaxation can be suppressed by a sufficient DC bias. It can be distinguished from the other characteristics relaxations of LCs by looking at the frequency range and also by the fact that MW sustains even in the isotropic phase. [10,46]

To perform the dielectric measurements, impedance analyzers Hioki 3532-50 (for frequency range 40Hz- 5 MHz) and Hioki IM3533 (for frequency range 0.1 MHz- 270 KHz), equipped with data acquisition system through RS232 interface to a computer, were used. The temperature was controlled within an accuracy of ±0.1°C with the help of FP82HT hot stage and Mettler FP90 temperature controller. The experimental setup is shown in **figure 2.9**.

Figure 2.9: Experimental setup for dielectric measurement.

The maximum error involved in the measurement of dielectric permittivities by this process was calculated to be less than 1%.

2.7 Synchrotron X-ray Diffraction Study

X-ray diffraction study is extremely useful to identify and classify the mesophases of liquid crystals and to elucidate their structural properties. Due to their intrinsic structural arrangements different mesophases have distinguishable X-ray diffraction patterns [13,47–52]. The major traits of

the X-ray diffraction pattern of two smectic phases, which are oriented normal to the incident X-ray beam, are shown in **figure 2.10**. To compare, the actual diffraction photographs are also shown in **figure 2.11**. The diffraction photographs consist of one low angle meridional and one high angle equatorial diffraction maxima. The lower and higher angle features correspond to the correlation of molecules along the molecular director and ordering within the layers respectively from which one can calculate the layer spacing (d) and the intermolecular distance (D).

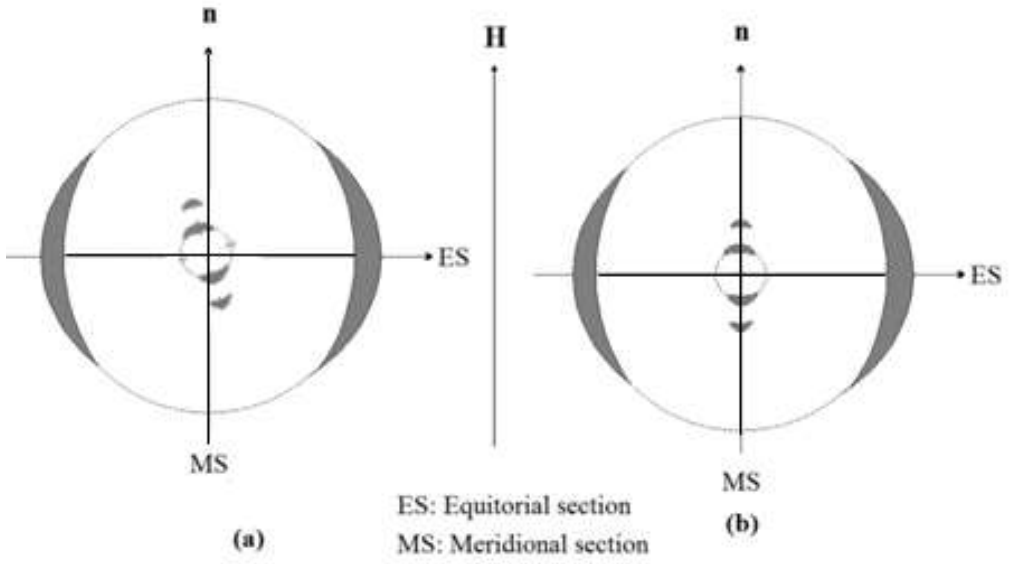

Figure 2.10: Schematic diagram of X-ray diffraction photographs of a) SmC phase and b) SmA phase.

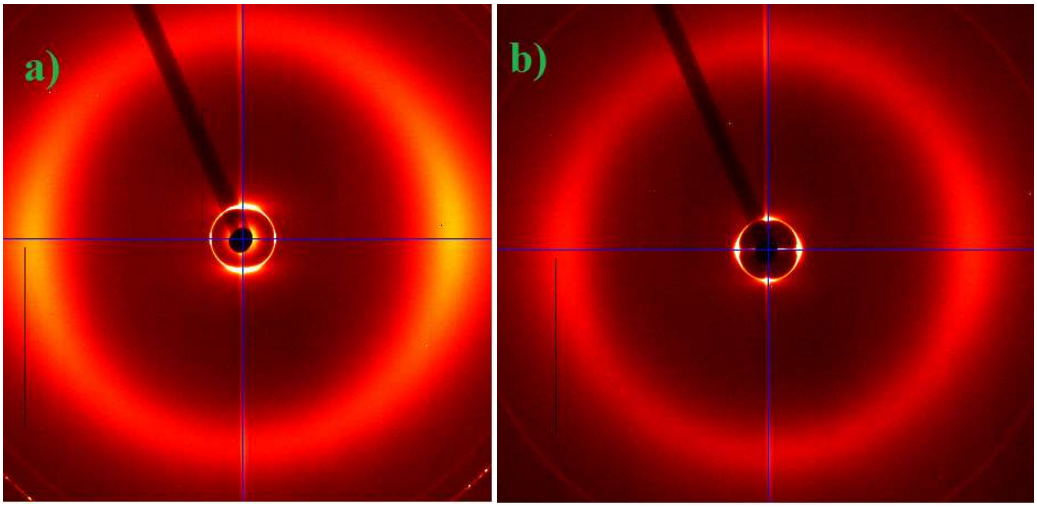

Figure 2.11: Observed X-ray diffraction photograph of a) SmC* and b) SmA* phase of a chiral liquid crystal mixture.

It may be mentioned here that by conventional X-ray diffraction technique it is possible to distinguish only those liquid crystal phases, which differ in their packing, but not those which differ just by orientation of molecules in successive layer. For example ordinary X-ray scattering cannot differentiate between SmC* and SmC*$_A$ phases or smectic phases of chiral and achiral compounds. These phases can be distinguished by resonant X-ray scattering experiment which was not performed in this dissertation [53].

The average lateral distance between the molecules (D) was calculated from the higher angle equatorial maxima using **equation 2.14** [54].

$$2D\,sin\theta = k\lambda \qquad [2.14]$$

Here, θ is the Bragg's angle for the higher angle diffraction, λ is the wavelength of the X-ray beam and k is a constant which arises due to cylindrical symmetry and whose value is 1.17 for the perfectly ordered state.

Similarly, the layer thickness (d) can be calculated using **equation 2.15**.

$$2d\,sin\theta = \lambda \qquad [2.15]$$

Here, θ is the Bragg angle of the meridional maxima.

The Bragg angles were determined by fitting the corresponding intensity profile to a Lorentzian of the form:

$$L(x) = y_0 + \frac{2A}{\pi}\frac{\omega}{4(x-x_0)^2+\omega^2} \qquad [2.16]$$

Where, y_0 is the minimum value of y (here minimum value of intensity), A is the area under the curve, ω is the full width at half maxima and x_0 is the value of x (here value of angle) for which y is maximum.

As a representative example, the fitted intensity profile at low and high angle of one compound is shown in **figure 2.12**.

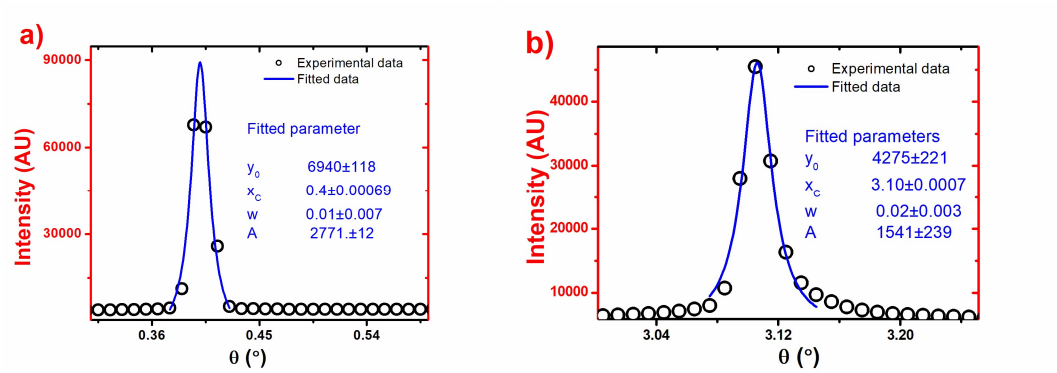

Figure 2.12: Fitted intensity profile of SAXS data a) at low and b) high angle.

For tilted phases like SmC* phase, the tilt of the molecule is usually calculated, using **equation 2.17**.

$$\theta_{xray} = cos^{-1}\frac{d}{d_A} \qquad [2.17]$$

Here d_A is the maximum layer spacing in SmA* phase. However most of the compounds selected in this study melt directly to isotropic phase from SmC* phase. Thus the tilts of the molecules in these compounds were calculated idealizing the molecules as rigid rods, using **equation 2.18**.

$$\theta_{xray} = cos^{-1}\frac{d}{l} \qquad [2.18]$$

Here *l* is the optimised molecular length of the molecule.

Even in compounds where SmA* phase is present above SmC* phase, **equation 2.18** was used to calculate the tilt to make comparison with other compounds on equal footing. Only in case of the formulated mixture and its dopant **equation 2.12** was used, as it was not possible to find the effective optimised length of mixing molecules.

The length scale over which the correlation between the molecules exist, both within and across the smectic planes, can be calculated by estimating the correlation length (ξ). It was calculated using **equation 2.19** [55].

$$\xi = \frac{2\pi}{FWHM} \qquad [2.19]$$

where FWHM is the full width at half maxima at the scattering vector Q in the relevant Bragg's peak which was determined by fitting the intensity profile to a Lorentzian function as stated before.

For hexagonal mesophases and soft crystal phases, additional peaks can be observed due to their long-range bond orientation order. By indexing the peaks, the cell parameters of such phases can be calculated from the diffraction photographs [56,57].

X-ray scattering experiments were performed using PETRA III synchrotron beamline at P07 Physics Hutch station at Deutsches Elektronen-Synchrotron (DESY), Hamburg, Germany within an angular range 2θ = 0 - 5°. For some compounds Lindeman glass capillary of diameter 1.0 mm was used as sample holder, other compounds were taken inside a dielectric cell. In both cases, samples were filled by capillary action in the isotropic phase and alignment was achieved by slow cooling. For the samples taken inside the dielectric cell, the X-ray beam was directed through the cell gap to avoid absorption from the glass. It was done by mounting the liquid crystal cell on a stage whose

orientation could be controlled very precisely and remotely when the beam was on. Ten images of exposure time 0.1 s were taken and averaged to get one diffraction image. For capturing the image, a Perkin Elmer 2D detector of total size 400 × 400 mm^2 and with individual pixel size 200 × 200 μm^2 was used. The detector was placed at a distance of 3.3 m from the sample. To control the temperature a Lakeshore 340 temperature controller was used. While studying the mixture, SAXS was also done applying a voltage across the cell (12V/μm) from a Delta Electronica power supply ES030-10. QXRD program (PE Area Detectors; G Jennings, version 0.9.8, 64 bit) was used for data acquisition. To get intensity versus Bragg angle (2θ) distribution, images were integrated using a step size of 0.001. The experimental set up used for the scattering experiment at DESY is shown in **figure 2.13**.

The errors in the measurement of layer spacing, intermolecular distance and tilt angle never found to exceed 0.5%, however, in case of correlation lengths the maximum error was higher, about ~3.5%.

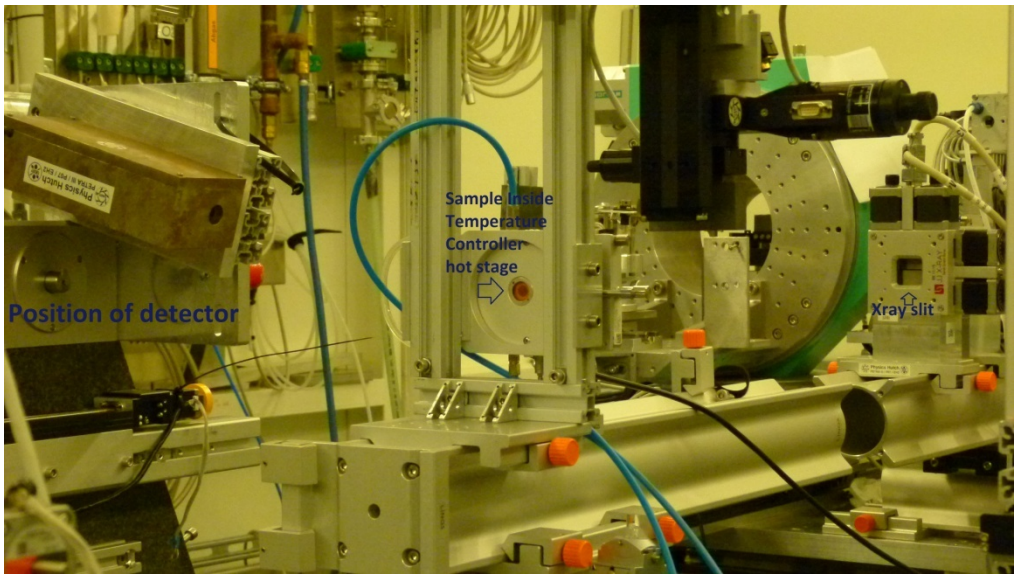

Figure 2.13: Experimental set up for X-ray scattering experiment.

2.8 Electro-Optic Measurements

By electro-optic methods spontaneous polarization, response time and tilt angle of the compounds have been measured. Details of these measuring techniques are discussed below.

2.8.1 Spontaneous Polarization (P_S)

As discussed in chapter 1 spontaneous polarization is a secondary order parameter for the ferroelectric SmC* phase. The value of P_S is important from an application point of view and also from the theoretical perspective. It is possible to determine the type of phase transition by looking at the temperature variation of P_S in the vicinity of SmC* to SmA* transition. By minimizing the expression of Landau free energy (**equation 2.2**) one can find out the expression for P_S as a function of temperature T as given by **equation 2.20** [14].

$$P_S = P_0\left(1 - \frac{T}{T_C}\right)^{\beta} \qquad [2.20]$$

Here, P_0 is the value of P_S at T=0, T_C is the SmC* to SmA* transition temperature, and β is the critical exponent associated with the order parameter P_S, which for an ideal second-order phase transition should be 0.5 [5,18,21].

It is possible to measure P_S by different techniques like (i) Sawyer-Tower method [58] , (ii) reverse field method[59] and (iii) reversal current method [60]. In this dissertation, the reversal current method using a triangular signal was used to measure P_S. A schematic diagram of the experimental setup is given in **figure 2.14**.

Ferroelectric liquid crystals have finite conductivity. So, a dielectric cell filled with FLCs can be considered as a parallel combination of a capacitor (C) and a resistance (R). Thus the current induced in a ferroelectric liquid crystal cell, under the application of an alternating voltage, has mainly three contributions in it [60], namely (i) ionic flow current I_i, (ii) current I_c due to charge accumulation in the capacitor and (iii) the polarization realignment current I_p as given by **equation 2.21**.

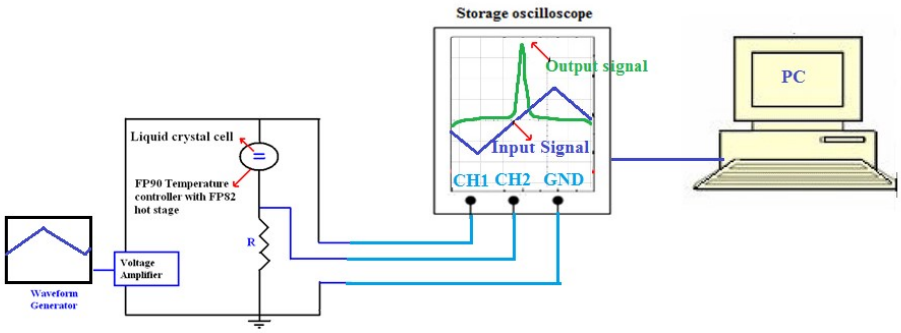

Figure 2.14: Schematic diagram of the experimental setup to measure spontaneous polarization and response time.

$$\boldsymbol{I(t) = I_i + I_c + I_p = \frac{V}{R} + C\left(\frac{dV}{dt}\right) + \frac{dp}{dt}} \qquad \textbf{[2.21]}$$

Here P is the charge induced by polarization reversal. Under a triangular wave in reversal current method the capacitive contribution of current (I_C) cannot interfere with the current due to polarization reversal (I_P) and a characteristic bump appears in the output wavefront due to the reversal of spontaneous polarization which can be subtracted from the contributions of the ionic and capacitive current drawing an appropriate baseline from the overall current profile. From the area, under the polarization bump the value of P_S can be calculated using **equation 2.22**.

$$\boldsymbol{P_S = \int \frac{Vdt}{2AR}} \qquad \textbf{[2.22]}$$

where A is the effective area of the cell and R is the series resistance across which the voltage drop is measured.

For anti-ferroelectric SmC^*_A phase in suitable frequency range, double polarization bump can be observed under triangular current reversal method. In fact, SmC*, SmC^*_A and other ferroelectric *subphases* can be easily distinguished by a hysteresis study of the spontaneous polarization. SmC* being a bistable phase shows a single hysteresis loop, SmC^*_A for being tristable state exhibits a double hysteresis loop and SmC^*_γ shows a triple hysteresis curve as shown in **figure 2.15** [15].

However, practically SmC^*_γ phase along with the plateau at $1/3P_S$ shows zero polarization at zero field, unlike **figure 2.15** which indicates helielectric behaviour of the phase [15].

The spontaneous polarization (P_S) was measured with the help of an Agilent 33220A function generator which was used to apply an ac triangular signal of voltage 0.1-50V and frequency 10-60 Hz as the input signal. An amplifier (FLC Electronics, Sweden) was used to amplify the signal. The voltage drop across a 100kΩ resistor in series with the sample cell was stored in a digital oscilloscope (Tektronix TDS 2012B) as a function of time. The peak area under the V-t curve of the stored image was calculated after creating an appropriate baseline using a commercial software package Origin 7.0 [61].

The maximum error related with the measurement of spontaneous polarization was found to be about 2.5%.

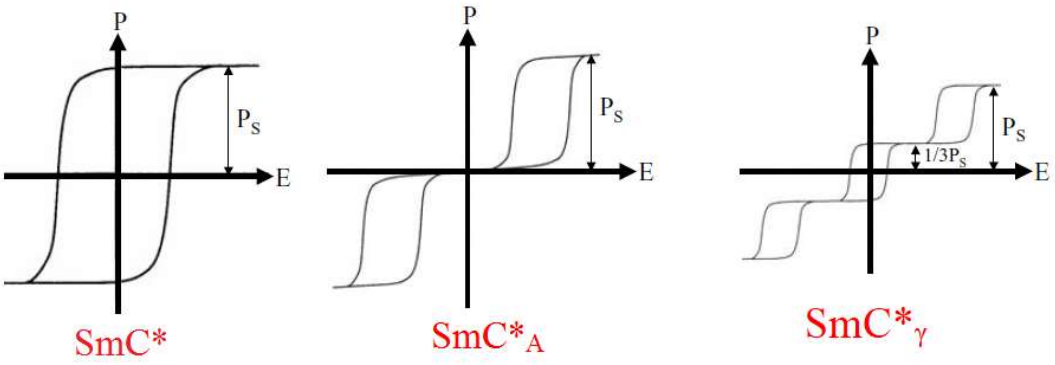

Figure 2.15: Hysteresis loop of P_S at different phases. Adapted after ref [15]

2.8.2 Response Time (τ)

The response time (τ) is yet another important parameter of ferroelectric liquid crystals from an application perspective. The smaller is the response time, the more suitable is the FLC for using in fast display devices.

τ can be measured with the same experimental setup as used for the measurement of P_S. However, here a square pulse has to be used as the input signal, rather than a triangular wave. The response time can be measured by measuring the time delay of the occurrence of polarization bump from the applied square pulse edge while monitoring the voltage across the resistor R in series with the cell [62,63]. A typical polarization bump observed in SmC* phase under a square pulse is shown in **figure 2.16**. The input square wave signal of voltage range 0.1-50V and frequency range 10-60Hz was used to measure τ. The images of the wavefronts stored in the storage oscilloscope were analyzed using Origin 7.0 software [61].

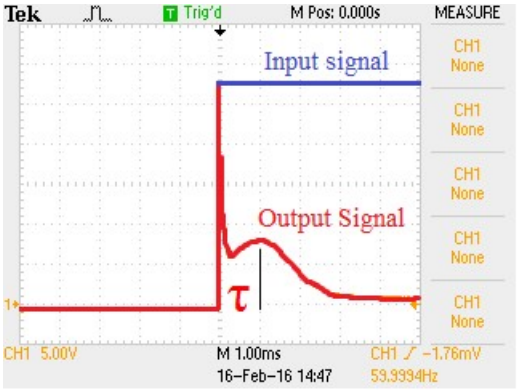

Figure 2.16: Polarization bump in SmC* phase under square pulse.

The maximum error involved in the measurement of response time was calculated to be about 3%.

2.8.3 Optical Tilt Angle (θ_{OPT})

As described before, the angle which the molecular long axis makes with the smectic layer normal the tilt angle and it is the primary order parameter of ferroelectric SmC* phase. Under the application of an ac signal, the molecules of liquid crystals in ferroelectric or anti-ferroelectric phase rotate around an imaginary cone by twice the tilt angle. Thus the optical tilt of molecules in smectic layers can be determined by electrically switching the sample under a low-frequency square wave and simultaneously observing the texture under a polarizing microscope. The angle of rotation of the sample between two dark states is a measure of double the tilt angle.

To perform this measurement, the liquid crystal samples were first fed into a homogeneous cell and the cell was mounted in between the crossed polarizers of the optical microscope. An ac field of magnitude 5-70 V was applied across the cell which was sufficient to unwind the helix and to align the molecules uniformly at a tilt angle θ with the layer normal. The frequency of the square wave pulses was kept in the range 1-10Hz.

The sample stage was rotated to a position of minimum optical transmission. When the field was reversed the molecules tilt in the opposite direction with an angle –θ with the layer normal and again another dark state was achieved by rotating the sample stage. Thus the angle of rotation of the sample between two consecutive dark states gives a direct measure of $2\theta_{OPT}$.

Another method of measuring the tilt using X-ray diffraction (θ_{xray}) was discussed before. The main difference between the tilt angles measured by these different techniques is that the θ_{xray} measures the tilt of the special period of the molecular arrangement (whole molecule) while θ_{OPT} measures the tilt made by the polarisable aromatic core of the molecules. Thus depending on whether the terminal chains are in *cis* or in *trans* configuration the θ_{xray} can be greater or smaller than θ_{OPT} respectively [64].

The error related with the measurement of optical tilt was found to be ~0.6%.

2.8.4 Rotational Viscosity (γ_φ)

The rotational viscosity related to the Goldstone Mode relaxation is another important parameter for ferroelectric liquid crystals. It greatly influences the response time of FLCs. The lower is the value of γ_φ, the lesser is the hindrances faced by the molecules to rotate around the tilt cone and the smaller will be the response time. The expression for rotational viscosity (**equation 2.23**) can be derived from the generalized Landau model [21].

$$\gamma_\varphi = \frac{1}{4\pi\varepsilon_0}\frac{1}{\Delta\varepsilon f_C}\left(\frac{P_S}{\theta}\right)^2 \qquad [2.23]$$

Using the values of Goldstone mode dielectric strength ($\Delta\varepsilon$) and relaxation frequency (f_C) obtained from the dielectric relaxation study and of spontaneous polarization (P_S) and tilt angle (θ) measured by electro-optic study the value of rotational viscosity was calculated by **equation 2.23**.

The maximum error related to the calculation of rotational viscosity was found to be ~2%.

Reference

[1] Onsager L. THE EFFECTS OF SHAPE ON THE INTERACTION OF COLLOIDAL PARTICLES. Ann. N. Y. Acad. Sci. 1949;51:627–659.

[2] Maier VW, Saupe A. Eine einfache molekulare Theorie des nematischen kristallinflüssigen Zustandes. Z. Naturforschg. A. 1958;13:564–566.

[3] Maier W, Saupe A. Eine einfache molekular-statistische Theorie der nematischen kristallinflüssigen Phase. Teil I. Zeitschrift für Naturforsch. A. 1959;14:882–889.

[4] McMillan WL. Simple Molecular Model for the Smectic A Phase of Liquid Crystals. Phys. Rev. A 1971;4:1238–1246.

[5] Landau LD, Lifshitz EM. Statistical Physics. New York: Pergamon Press; 1980.

[6] Muševic I, Blinc R, Zekš B, et al. The Physics of Ferroelectric and Antiferroelectric Liquid Crystals. 2nd ed. Goodby J, Blinc R, Clark N, et al., editors. Phil. Trans. R. Soc. Lond. A. New York: The Authors; 1993.

[7] Goodby J, Blinc R, Clark N, et al., editors. Ferroelectric Liquid Crystals: Principles, Properties and applications. Philadelphia: Gordon & Breach; 1991.

[8] Tarazona P. Theroies of phase behaviour and phase transition in liquid crystals. Phil. Trans. R. Soc. Lond. A. 1993;344:307–322.

[9] Oswald P, Pieranski P. SMECTIC AND COLUMNAR LIQUID CRYSTALS. London: Taylor & Francis; 2006.

[10] Hasse W, Wróbel S. Relaxation Phenomena: Liquid Crystals, Magnetic Systems, Polymers, High-Tc Superconductors, Metallic Glasses Berlin: Springer; 2003.

[11] Collings P, Hird M. Introduction to liquid crystals Chemistry and

Physics. Gray G, Goodby J, Fakuda A, editors. London: Taylor & Francis; 1997.

[12] Priestley E., Wojtowicz PJ, Sheng P. INTRODUCTION TO LIQUID CRYSTALS. London: Plenum Press; 1974.

[13] Demus D, Goodby J, Gray GW, et al. Handbook of Liquid Crystals. New y: WILEY-VCH; 1998.

[14] Lagerwall ST. Ferroelectric and antiferroelectric liquid crystals. Newyork: WILEY-VCH; 1999.

[15] Dierking I. Textures of Liquid Crystals. wiley-vch. Weinheim: WILEY-VCH; 2003.

[16] Chandrasekhar S. Liquid crystals. 2nd ed. New York: Cambridge University Press; 1977.

[17] Gennes P, Prost J. The Physics of liquid crystal. New York: Oxford university press; 1993.

[18] Gouda F. Dielectric relaxation spectroscopy of chiral smectic liquid crystals. Chalmers University of Technology,Goteberg; 1992.

[19] Blinc R, Zekes B. Dynamics of helicoidal ferroelectric smectic-C liquid crystals. Phys. Rev. A. 1978;18:740–745.

[20] Žekš B. Landau Free Energy Expansion for Chiral Ferroelectric Smectic Liquid Crystals. Mol. Cryst. Liq. Cryst. 1984;114:259–270.

[21] Carlsson T, Žekš B, Filipič C, et al. Theoretical model of the frequency and temperature dependence of the complex dielectric constant of ferroelectric liquid crystals near the smectic-C* — smectic- A phase transition. Phys. Rev. A 1990;42:877–889.

[22] Berreman DW. Solid surface shape and the alignment of an adjacent nematic liquid crystal. Phys. Rev. Lett. 1972;28:1683–1686.

[23] Barbero G, Evangelista LR. Adsorption phenomena and anchoring

energy in nematic liquid crystals. New York: Taylor & Francis; 2006.

[24] Bahadur B. Liquid Crystals: Applications and Uses. Singapore: World Scientific; 1993.

[25] Torres JC, García-Cámara B, Pérez I, et al. Wireless temperature sensor based on a nematic liquid crystal cell as variable capacitance. Sensors. 2018;18:3436-1-3436-9.

[26] Xu S, Li Y, Liu Y, et al. Fast-Response Liquid Crystal Microlens. Micromachines 2014;5:300–324.

[27] Clark NA, Lagerwall ST. Submicrosecond bistable electro-optic switching in liquid crystals. Appl. Phys. Lett. 1980;36:899–901.

[28] MacGregor AR. Method for computing the optical properties of a smectic C* liquid-crystal cell. J. Opt. Soc. Am. A 1989;6:1493–1503.

[29] Demus D. Textures of liquid crystals. New York: Verlag Chemie Weinheim; 1978.

[30] Slaney A, Takatohi K, Goodby J. Defect textures in liquid crystals. In: Elston S, Sambles R, editors. The Optics of Thermotropic Liq. Cryst. New York: Taylor & Francis; 1998.

[31] Bouligand Y. Defects and textures. In: . D. Demus, J. Goodby, G.W Gray, H.-W. Spiess VV, editor. Handbook of Liq. Cryst. vol I. Weinheim: WILEY-VCH, Verlag GmbH; 1998.

[32] Minkin V, Osipov O, Zhdanov Y. Dipole Moments in Organic Chemistry. New York- London: Springer; 1970.

[33] Böttcher C, Belle O, Rip A, et al. Theory of Electric Polarization, Vol II. Amsterdam, New York: Elsevier, Scientific Publishing Co; 1973.

[34] Blinov L, Chigrinov VG. Electrooptic Effects in Liquid Crystal Materials. Newyork: Springer-Verlag; 1996.

[35] Debye P. Polar molecules. Newyork: Dover publications, Inc.; 1945.

[36] Daniel V. Dielectric Relaxation. London and New York: Academic Press; 1967.

[37] Cole KS, Cole RH. Dispersion and absorption in dielectrics I. Alternating current characteristics. J. Chem. Phys. 1941;9:341–351.

[38] BUIVYDAS M, GOUDA F, ANDERSSON G, et al. Collective and non-collective excitations in antiferroelectric and ferrielectric liquid crystals studied by dielectric relaxation spectroscopy and electro-optic measurements. Liq. Cryst. 1997;23:723–739.

[39] Clark MG. Macroscopic Properties of Liquid Crystals. Mol. Cryst. Liq. Cryst. 1985;127:1–41.

[40] Durand G, Martinot-lagarde P. Physical properties of ferroelectric liquid crystals. Ferroelectrics. 1980;24:89–97.

[41] Delaye M, Keller P. Critical angular fluctuations of molecules above a second-order smectic-A to smectic-C phase transition. Phys. Rev. Lett. 1976;37:1065–1068.

[42] Glogarová M, Pociecha D, Gorecka E, et al. Dielectric spectroscopy study of the transition into the hexatic phase in chiral smectics. Ferroelectrics. 2000;245:43–50.

[43] I. Rychetsky′, M. Glogarova′ VN. Competition between the chiral smectic-C* and hexatic phases . Phys. Rev. E. 2003;67:021704-1-021704-12.

[44] Schacht J, GieBelmann F, Zugenmaier P, et al. Collective director modes at the transitions to hexatic ferroelectric liquid crystalline phases. Phys. Rev. E. 1997;55:5633–5640.

[45] Rychetský I, Pociecha D, Dvořák V, et al. Dielectric behavior of ferroelectric liquid crystals in the vicinity of the transition into the hexatic phase. J. Chem. Phys. 1999;111:1541–1550.

[46] Aliev F. Liquid crystals and polymers in Pores. In: Crawford G, Zumer S, editors. Liq. Cryst. complex Geom. Form. by Polym. porous Netw. London: Taylor & Francis; 1996.

[47] Pershan PS. Structure of Liquid Crystal Phases. World Scientific Publishing Co. Pte. Ltd.; 1998.

[48] Richardson RM, Leadbetter AJ, Frost JC. A comparative study of the molecular motions in the three smectic phases of isobutyl 4(4′ phenylbenzylideneamino) cinnamate using incoherent neutron scattering. Mol. Phys. 1982;45:1163–1191.

[49] Hardouin F, Levelut AM, Benattar JJ, et al. X-rays investigations of the smectic A1 - smectic A2 transition. Solid State Commun. 1980;33:337–340.

[50] Hardouin F, Sigaud G, Nguyen Huu Tinh, et al. A fluid smectic A antiphase in a pure nitro rod-like compound. J. Phys. Lettres 1981;42:63–66.

[51] Prost J. The smectic state. Adv. Phys. 1984;33:1–46.

[52] Gane PAC, Leadbetter AJ, Wrighton PG. Structure and Correlations in Smectic B, F and I Phases. Mol. Cryst. Liq. Cryst. 1981;66:247–266.

[53] Gleeson HF, Hirst LS. Resonant X-ray scattering: A tool for structure elucidation in liquid CRYSTALS. ChemPhysChem. 2006;7:321–328.

[54] Vries A De. X-ray Photographic Studies of Liquid Crystals I. A Cybotactic Nematic Phase. Mol. Cryst. Liq. Cryst. 1970;10:219–236.

[55] Sirota EB, Pershan PS, Sorensen LB, et al. X-Ray Studies of Tilted Hexatic Phases in Thin Liquid-Crystal Films. Phys. Rev. Lett. 1985;55:2039–2042.

[56] Urban S, Czub J, Przedmojski J, et al. Dielectric and X-ray Studies

of Substances with the Smectic B phase. Mol. Cryst. Liq. Cryst. 2007;477:87–100.

[57] Osiecka N, Budziak A, Galewski Z, et al. X-ray studies of the smectic B phase of the 4-bromobenzylidene-4′-alkoxyanilines. Phase Transitions 2012;85:314–321.

[58] Sawyer C, Tower C. ROCHELLE SALT AS A DIELECTRIC. Phys. Rev. 1930;35:269–273.

[59] Skarp K, Dahl I, Lagerwal ST, et al. Polarization and Viscosity Measurements in a Ferroelectric Liquid Crystal by the Field Reversal Method. Mol. Cryst. Liq. Cryst. 1984;114:283–297.

[60] Miyasato K, Abe S, Takezoe H, et al. Direct Method with Triangular Waves for Measuring Spontaneous Polarization in Ferroelectric Liquid Crystals. Jpn. J. Appl. Phys. 1983;22:L661–L663.

[61] Origin, Version 07. OriginLab Corporation, Northampton, MA, USA.

[62] Debnath A, Mandal PK, Węglowska D, et al. Induction of a room temperature ferroelectric SmC* phase in binary mixtures with moderate spontaneous polarization and sub-millisecond switching time. RSC Adv. 2016;6:84369–84378.

[63] Xue J-Z, Handschy MA, Clark NA. Electrooptic response during switching of a ferroelectric liquid crystal cell with uniform director orientation. Ferroelectrics 1987;73:305–314.

[64] Ziobro D, Dąbrowski R, Tykarska M, et al. Synthesis and properties of new ferroelectric and antiferroelectric liquid crystals with a biphenylyl benzoate rigid core. Liq. Cryst. 2012;39:1011–1032.

CHAPTER 3

Structural and dielectric properties of orthogonal smectic phases in a chiral mesogen having biphenyl benzoate core

Part of this work has been published in Journal of Molecular Liquids, Vol:256, pp29-38,2018.

3.1 Introduction

In the chiral orthogonal smectic phases of liquid crystals, the molecular directors are oriented in a direction parallel to the layer normal like their achiral counterpart. Depending on the symmetries of the in-plane molecular arrangements they are classified in different mesophases like SmE*, SmB* (SmB*$_{Cryst}$, SmB*$_{hex}$), SmA* etc. In SmE* phase, the molecules are arranged in an orthorhombic unit cell with herringbone structure. SmB* is an orthogonal hexatic phase and in SmA* there is no structural order within the layer. The detail structure of each of these phases have been discussed in many books [1–3]. From the perspective of fundamental research, it's always appealing to inculcate the structural properties of orthogonal smectic liquid crystals for their diverse structures and in-plane symmetries. The knowledge about their structure can also be handy to identify and categorise the different orthogonal phases. Besides, the inter-molecular interactions, which are intimately related with the structural parameters, play a crucial role on the dielectric and electro-optic properties of the phase. Moreover, the orthogonal smectic mesogens have drawn the attention of various research groups also for their possible applicability. For their self assembly and two dimensional structures they are likely to be functional materials. For example, an orthogonal smectic liquid crystal Ph-BTBT-10 shows SmE phase with highest mobility and can be used to build an organic field effect transistor (OFET) [4–6]. Other smectic liquid crystals have also been used designing OFET [7]. Smectic liquid crystals have also been used in sensing applications [8].

Molecular structures of liquid crystals have profound effect on their physical properties and also on their phase behaviour. This can be observed even in the compounds selected for investigation in this

dissertation. Out of these compounds, the compound having the smallest chain (only one carbon in its fluorinated chain) i.e. 1F3R [(*S*)-(+)-4′-[(3-trifluoroetanoyloxy)prop-1-oxy] biphenyl-4-yl 4-(1-methylheptyloxy) benzoate.], shows four different types of chiral orthogonal smectic phases within a span of ~71°C and then melts into isotropic phase, with no tilted phase in between as observed in higher homologues [9]. This is one of the rare chiral compounds, showing large numbers of temperature induced orthogonal smectic phases within such small temperature range, with no tilted phase in between. To the best of our knowledge four orthogonal smectic phases were observed before only in an achiral bent-core system [10]. Thus, this can serve as an ideal candidate to investigate the structural and dielectric properties of chiral orthogonal smectic phases. Keeping this in mind we are reporting in this chapter, the phase behaviour as well as structural and dielectric relaxation properties of the compound 1F3R, whose molecular structure is shown in **figure 3.1**.

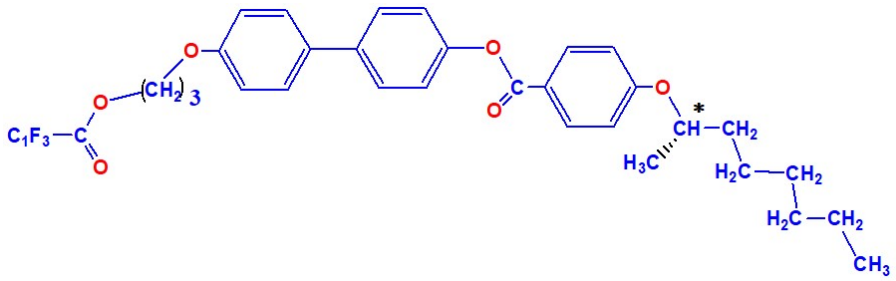

Figure 3.1: Molecular structure of 1F3R.

3.2 Experimental procedure

The transition temperatures of the compound were identified using polarising optical microscopy (POM) and differential scanning calorimetric (DSC) study. Olympus BX41 polarizing microscope equipped with a CCD camera was used for POM study. Metller FP90 temperature controller with FP82 hot-stage was used to control the

temperature with an accuracy of ±0.1°C. DSC was done with the same temperature controller, along with FP84HT hot stage and FP99A software.

The structural properties of different mesophases were investigated by small angle X-ray scattering (SAXS) experiments using PETRA III synchrotron beam line at P07 Physics Hutch station at Deutsches Elektronen-Synchrotron (DESY), Hamburg, Germany, within an angular range of 2θ = 0 - 5°. Lindeman glass capillary of diameter 0.1 mm was used as sample holder. A beam of wavelength 0.2483 Å was used for this experiment.

To perform the dielectric study the sample was fed into a homogeneous commercial cell (EHC, Japan) of thickness 8μm. The alignment of the sample within the cell was achieved by a slow controlled cooling from isotropic phase to the desired temperature. The dielectric permittivity was measured using a Hioki 3532 50 Impedance analyzer in the frequency range from 100 Hz to 5 MHz while in the frequency range of 0.1mHz to 270 kHz a HIOKI IM3533 analyzer was used. The dielectric spectra at each temperature were fitted to the Cole-Cole function [11], modified to take into account the low frequency parasitic effect (**equation 1**).

$$\varepsilon^* = \varepsilon^{/} - i\varepsilon^{//} = \varepsilon_\infty + \sum \frac{\Delta\varepsilon_k}{1+(i\omega\tau_k)^{1-\alpha_k}} - i\frac{\sigma}{2\pi f^n \epsilon_0} \qquad [3.1]$$

Here, $\Delta\varepsilon_k$ is the dielectric increment, ε_∞ is the real part of high frequency limit dielectric permittivity, τ_k is the relaxation time and α_k is the symmetry parameter of k-th mode relaxation, σ is the conductivity of the cell due to charge impurities, angular frequency $\omega = 2\pi f$ is the angular frequency of the measuring field and ϵ_0 is the free space dielectric permittivity.

As mentioned in chapter 2 to accommodate the contribution of free charges and ITO layer, in the conductivity part (third term) "ω" has been taken as $2\pi f^n$, where n is a fitting parameter [12]. The fitted value of "n" is found to be ~1 in all spectra of 1F3R. Hence in subsequent chapters we assumed that the behaviour of the cell in low frequency is ohmic and considered n=1.

Details of all these experiments have been presented in chapter 2.

3.3 Results and discussions

3.3.1 Observed phases

A phase sequence of this compound, based only on the POM study, was outlined in a prior publication, where the synthesis of this compound was reported [9]. With rising temperature, the compound was stated to exhibit SmE*, SmB* and SmA* phases before going to the isotropic phase. However, except POM results, no further substantive evidence was provided to identify the phases and the nature of SmB* phase was not confirmed. In our study, we have identified the structures of all the phases by SAXS and combining the results of POM, DSC, SAXS and dielectric study confirmed that the SmB* phase was actually SmB^*_{hex} phase. Moreover, a new phase was identified in between SmB* and SmA* phases which we initially designated as SmX* phase but finally had been established to be a variant of SmB^*_{hex} phase. The phase sequence of 1F3R, as observed in our study is listed in **table 3.1**.

Table 3.1: Phase sequence with transition temperatures of 1F3R

From Texture:	Cr 80°C SmE* 99°C SmB* 119°C SmX* 127.5°C SmA* 151°C Iso
From dielectric and XRD:	Cr 80°C SmE* 103°C $SmB_{hex}^{*\,mo}$ 121°C $SmB_{hex}^{*\,lo}$ 127.5°C SmA* 151°C Iso

mo: more ordered; lo: less ordered

3.3.2 Differential scanning calorimetry (DSC)

DSC thermograms, both for heating and cooling cycles, are shown in **figure 3. 2**. In both thermal cycles the thermograms show almost same transition temperatures.

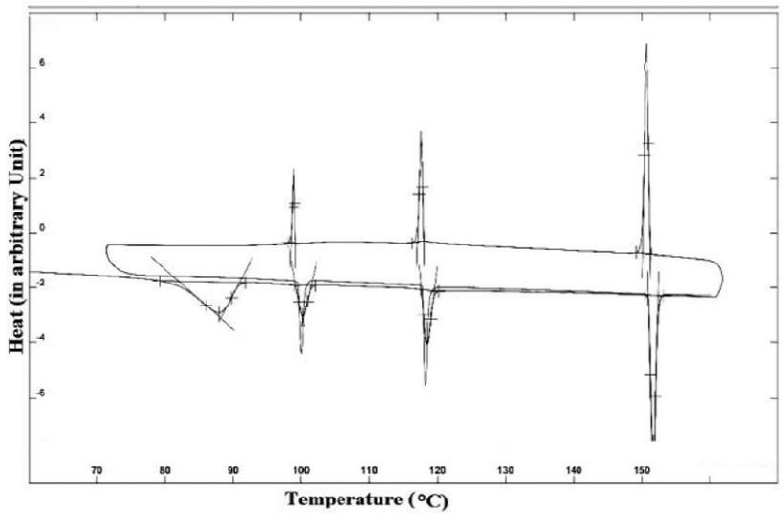

Figure 3.2: DSC thermogram of 1F3R in heating and cooling cycle.

However, SmX* phase could not be identified in DSC data probably due to very small change of enthalpy at this transition. Lack of such thermal signature at transitions involving higher ordered smectic phases is quite frequent as discussed by Budai *et al.* [13].

3.3.3 Polarized optical microscopy (POM) studies

Optical textures, observed during cooling (except **figure 3.3 (b)**), at selected temperatures are shown in **figure 3.3**. In all the phases fan

shaped textures were observed. Transition bars (parallel lines) appeared in the texture at the SmA* to SmX* transition temperature (127°C) while cooling (**figure 3.3 (c)**). The lines vanished quickly after entering into SmX* phase, leaving a clear fan shaped texture once again. Though no such line appeared during heating, but the fan shaped textures exhibited parabolic focal conic defects in SmA* phase (**figure 3.3 (b)**). This typical observation was reported before for SmA to hexatic B or crystal B transition in an achiral system [14]. Thus from POM study it could be deduced that the SmX* phase must be some kind of SmB* phase. For both SmB* and SmE* phases parallel lines appeared across the fan shaped texture, however, in SmE* phase these lines were slightly stronger than in SmB* phase.

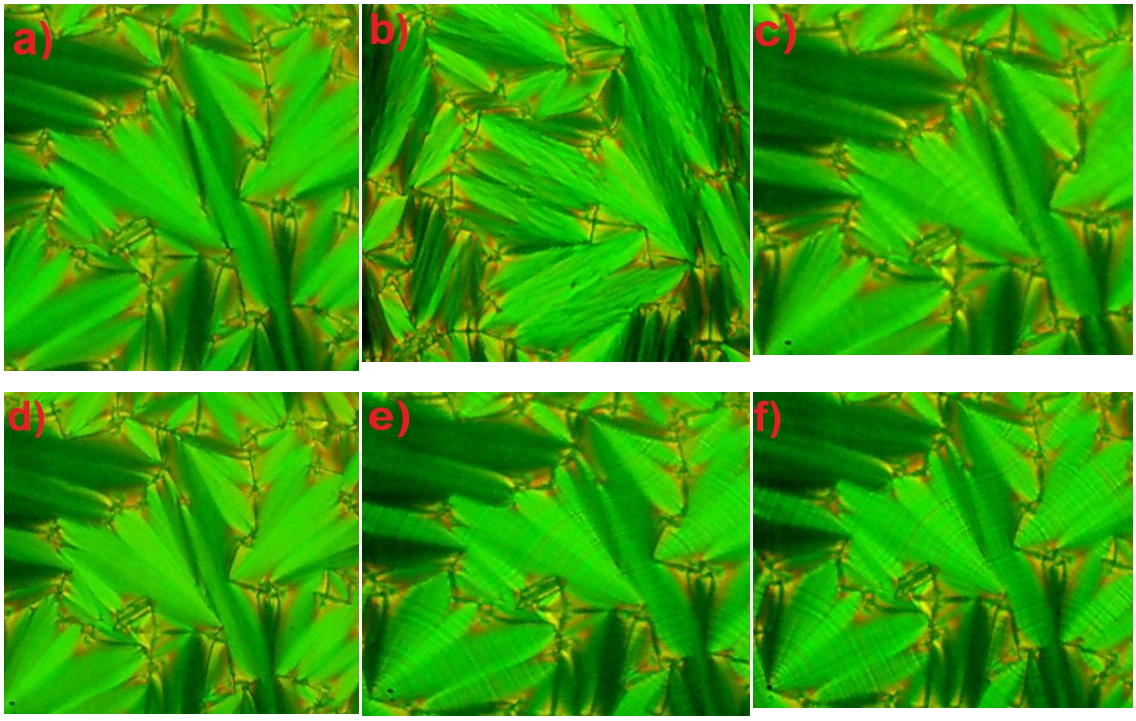

Figure 3.3: Observed textures of 1F3R at a) SmA* (143ºC) b) SmA* during heating (130ºC) c) SmA* to SmX* transition (127ºC), d) SmX* (125ºC), e) SmB* (112ºC) and e) SmE* (91ºC).

3.3.4 Optimised geometry

To elucidate the effect of molecular structure on the various properties of the material, the molecular structure of the compound was optimised applying Hartee Fock method and using 3-21G basis set in a commercial package [15]. The optimised structure of the molecule, the direction of principal inertial axes and the molecular dipole moment are shown in **figure 3.4**. The optimised length was measured to be 32.58Å and the dipole moment was found to be 6.60D with components of 4.93, 4.37 and 0.11 D along the three inertial axes, respectively. Such strong dipole moment might be attributed to the presence of the fluorine atoms in the chain of the molecule. It should be noted here that the initial structures of all the compounds taken for optimisation, that we are going to report in this dissertation, were build up from one single core of the molecule. Different compounds were built by modifying only the chain. This process differs from the process of optimisation that was reported in the published paper. Hence the optimised parameters reported here differ marginally from the values quoted in the paper.

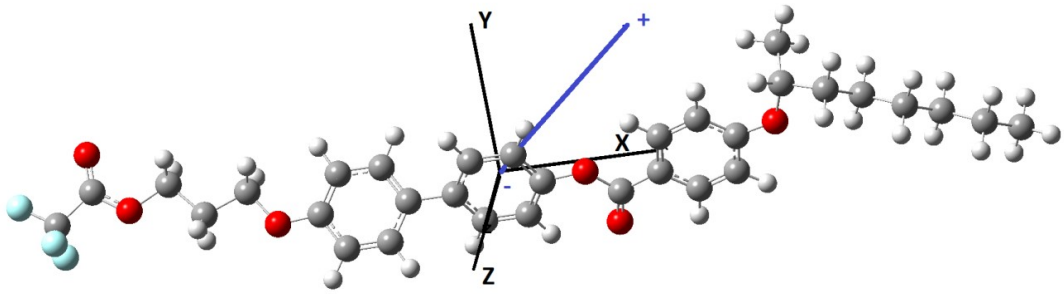

Figure 3.4: Optimised geometry of 1F3R.

3.3.5 Synchrotron X-ray diffraction study

The structural properties and temperature evolution of each phase were studied by synchrotron X-ray diffraction method. The transition temperature observed by SAXS was found to be shifted towards higher temperatures by a few degrees, than what were observed in dielectric, DSC and texture studies. This may be due to the fact that the compound was in different temperature bath in those cases and had different thermal history as well. By slow cooling and surface interaction the sample got aligned in the capillary, with molecular axis perpendicular to the beam direction even without any electric or magnetic field. In all the higher order smectic phases strong low angle maxima, corresponding to smectic layer spacing and high angle maxima corresponding to in-layer ordering were observed. Few representative diffraction photographs for each smectic phase are shown in **figure 3.5** while their intensity profiles are shown in **figure 3.6** and **3.7**.

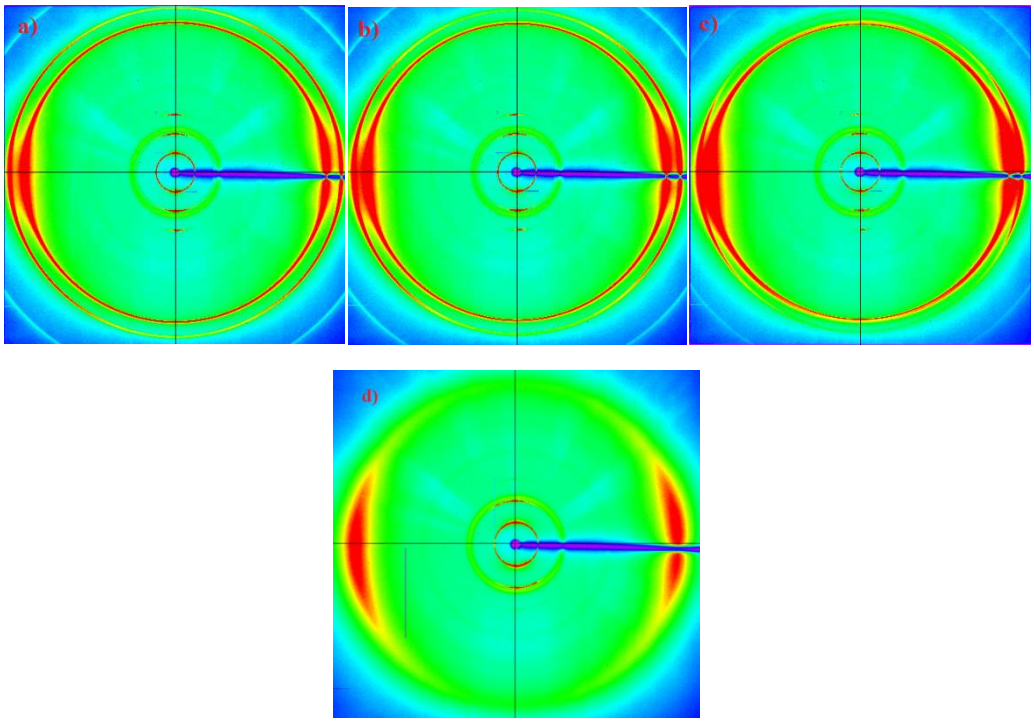

Figure 3.5: Diffraction photographs of (a) SmE* (89.5°C) (b) $SmB_{hex}^{*\,mo}$ (107°C) (c) $SmB_{hex}^{*\,lo}$ (SmX*) (125°C) (d) SmA*(140°C) phases.

It is evident from **figure 3.5** that the maxima of the low and high angle diffraction features are at 90° apart which signifies explicitly that all the phases are orthogonal in nature. Occurrence of pretty strong second order diffraction maxima at low angles also implies long range ordering across the smectic layers in all the phases. However, the intensity of the second order feature reduces with temperature as expected. It is also seen from **figure 3.5** that two sharp outer rings at higher angles are present in higher order smectic phases, whereas in SmA only one diffused high angle maxima is visible. It signifies the presence of positional ordering or bond orientational ordering within the layers in higher order smectic phases and absence of any such ordering in SmA* phase. The SmX* phase can also be distinguished by the emergence of satellite feature in higher angle outer ring, clearly visible in **figure 3.7**.

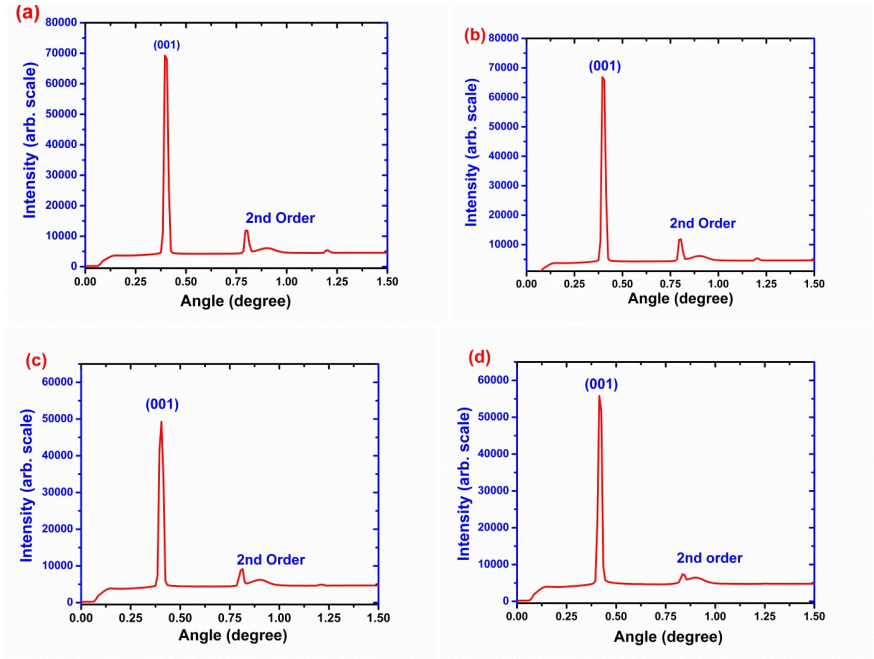

Figure 3.6: Intensity profile of inner ring: (a) SmE*(89.5°C), (b) $SmB_{hex}^{*\,mo}$ (107°C) (c) $SmB_{hex}^{*\,lo}$ (125°C) and (d) SmA*(140°C).

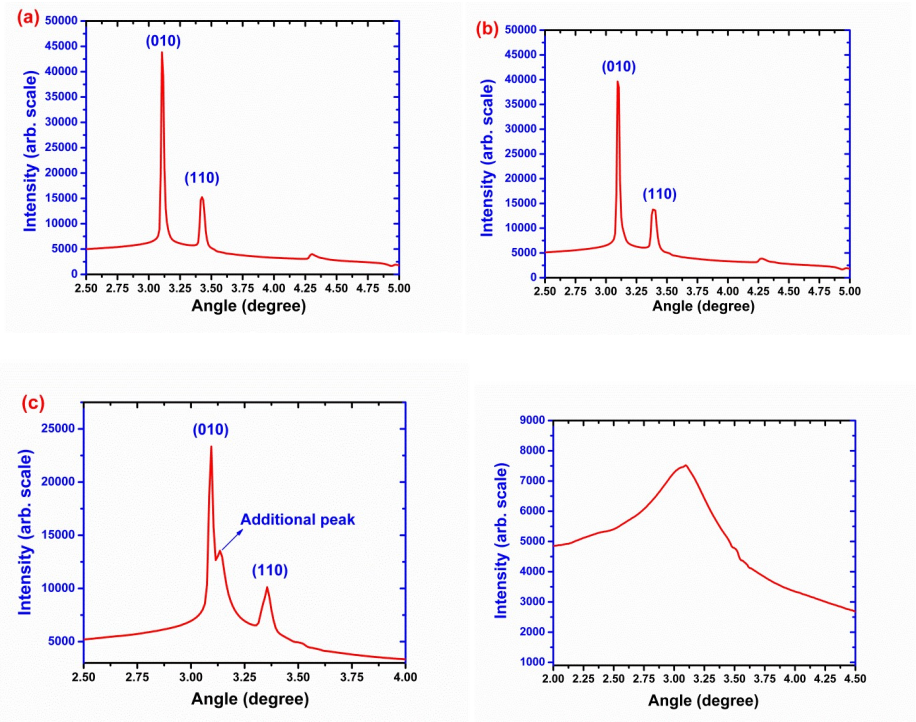

Figure 3.7: Intensity profile of outer ring: (a) SmE*(89.5°C), (b) $SmB_{hex}^{*\,mo}$ (107°C) (c) $SmB_{hex}^{*\,lo}$ (125°C) and (d) SmA*(140°C).

The inner ring (001) profiles of SmE*, SmB* and SmX*, more or less remain same, a broadening of the profile can, however, be observed in SmA*. Broadening of outer ring is also evident when we move from lower temperature phase towards higher temperature phase. Broadening of outer or inner ring profiles signify lowering of in-plane and across the plane ordering respectively. Satellite peak observed in the outer profile of SmX* phase may come up from a local herringbone packing structure as reported in hexatic B phase by Pindak et al. [16]. Thus the SmX* phase seems to fulfil the criteria of hexatic B phase. However, this kind of double peak were also reported to arise because of chain packing or partial ordering of the long alkyl tail of the LC molecule [17]. To affirm the presence of the new phase, the intensity of the Bragg scattering, both small angle and wide angle, is plotted as a function of temperature in

figure 3.8. This has been suggested by Chandrasekhar as a direct method of studying the translational order parameter of a phase [18].

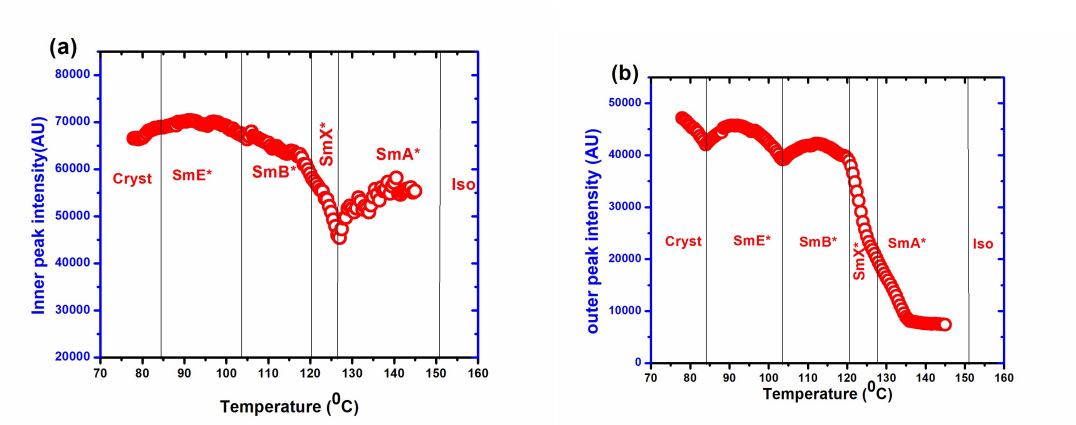

Figure 3.8: Intensity of the first order (a) inner and (b) outer diffraction peaks with temperature.

Change in slope or slight discontinuity of inner ring intensity is evident near each phase transitions. Different phases, including SmX*, are more distinctly distinguishable from the intensity plot of the outer maxima. Thus the temperature variation of Bragg diffraction intensity asserts once again the presence of the SmX* phase within the temperature range 121°C to 127°C which is in conformity with the POM result, with a deviation of ~2°C temperature range, because of different temperature bath of the sample as discussed above.

From (001) peak, the smectic layer spacing (d) of each phase was calculated and was found to be more than the optimised molecular length (32.58 Å) in all phases, which again confirms the absence of tilt and orthogonality of all phases. The temperature variation of layer spacing (d) is shown in **figure 3.9**.

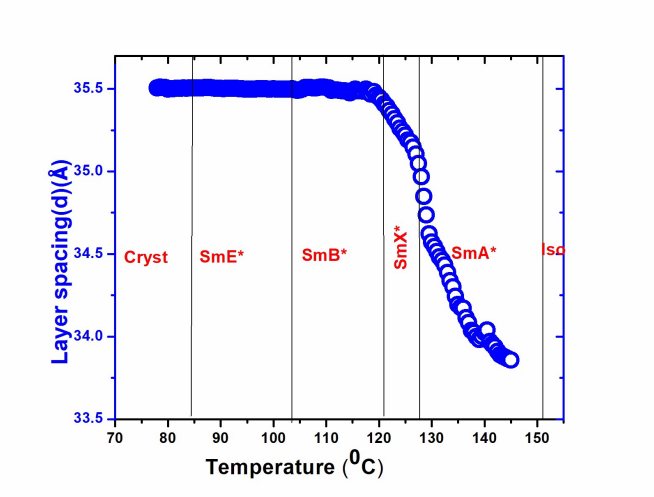

Figure 3.9: Layer spacing of all phases as a function of temperature.

Layer spacing 'd' remains almost constant throughout the crystal, SmE* and SmB* phases but starts to decrease with temperature from SmX* phase. The rate of decrease increases after entering into SmA* phase. Nevertheless, even in SmA* phase the 'd/*l*' ratio remains more than 1, which varies from 1.07 to 1.03, *l* being the most extended molecular length obtained from geometry optimisation. In few other members of the same homologues series 5F6R, 4F6R and 1F4R, this ratio was reported to be ~ 0.5, 0.76 and 0.97 respectively [9]. It is observed that the ratio increases with decreased fluorination and chain length. Similar observation was reported before in SmA* and SmB* phases of a Schiff base compound containing azomethin [19]. As discussed in chapter 1, a layer spacing larger than molecular length (*l*) but less than 2*l* suggests the orthogonal smectic phase to be partially bilayer. Thus all the smectic phases of 1F3R having $l \leq d \leq 2l$ are partial bilayer type, to the best of our knowledge there is no such report so far in any chiral compound. Madhusudan et al. in [20] proposed that achiral SmA liquid crystals with high longitudinal dipole moment (~ 4 D), should favour anti parallel arrangement to minimize the interaction energy which lead to polymorphism of SmA phase. The present 1F3R

system possesses strong longitudinal component of dipole moment (5.51 D), which is in conformity of the observed partial bilayer smectics, although other chiral systems, even higher homologues of this series, did not show such behaviour.

In **figure 3.10** we have presented the temperature variation of average intermolecular spacing (D) which, in all the phases, was calculated from the (010) peak. 'D' is found to increase with temperature in SmE* and SmB* phases but it decreases in SmX* phase. Anomalies are observed at the transition points of the phases. Near clearing point the peak become too defused to measure D accurately.

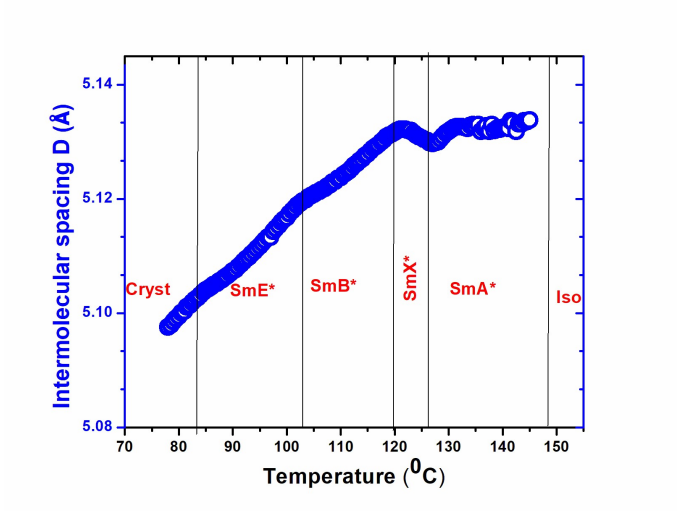

Figure 3.10: Variation of average intermolecular spacing (D) with temperature.

Although in smectic phases molecules are arranged in layers but the positional correlations of the layers do not have true long range order as observed in perfectly crystalline state rather exhibit algebraic decay with a temperature dependent exponent signifying quasi long range order. To estimate the extent of correlation of the molecular order, across and within the smectic layers, the correlation length (ξ) was calculated as,

$\xi = \frac{2\pi}{FWHM}$, where FWHM is the full width at half maxima in the scattering vector (Q) of the relevant Bragg's peak[21]. The temperature variation of correlation length is depicted in **figure 3.11**.

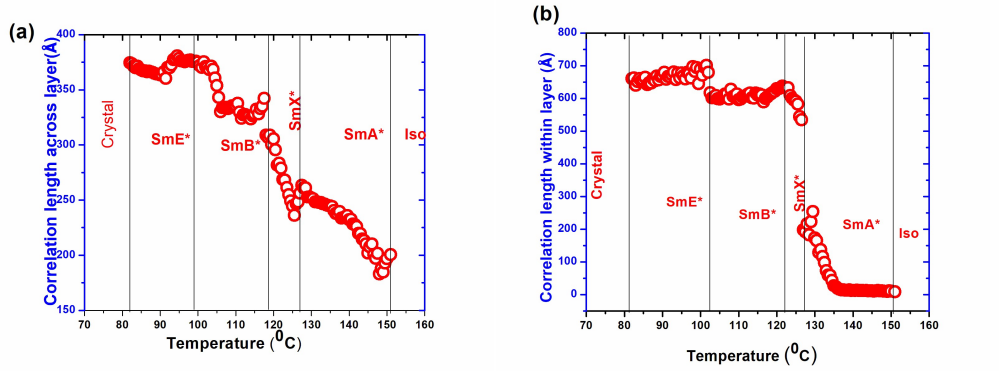

Figure 3.11: Temperature variation of correlation length (a) across the layer and (b) within the layer.

The correlation length across the layer varies with temperature differently at different phases. In the SmE* phase it increases from ~ 371 Å to ~ 375 Å and ultimately drops down sharply to ~ 333Å in SmB* phase. In SmX* phase it decreases strongly with temperature and reaches a minimum value of 236 Å. It continues to decrease in SmA* phase and reaches a lowest value of 180Å. The correlation length across the layer is found to be 11.4 times of the optimised molecular length in SmE* phase which implies that across the layer the correlation is extended upto nearly 11 molecular lengths in this phase. The same is found to be approximately 10, 7 and 5 molecular lengths in SmB*, SmX* and SmA* phases, respectively.

As far as the correlation within the layer is concerned, it shows quite high values in higher order smectic phases. It is found to be 656Å, 600Å and 534Å in SmE*, SmB* and SmX* phases respectively, much higher than those for across the plane correlation. During the phase transition

from HexB to CryB phase this kind of discontinuity in the correlation length had been reported before [22]. The lowest value of in-plane correlation is recorded to be ~11Å in SmA* phase. The anomalies observed at SmB* to SmX* and SmX* to SmA* transitions, in both types of correlation lengths, once again confirms the existence of SmX* phase. It had been explained before theoretically that smectic structure with dislocation type imperfections might lead to local displacements of the layers resulting in a much larger broadening of Bragg peaks in the direction $Q_{||}$, which is related with interlayer correlation, than in $Q_{\perp}$, which is related with the in plane correlation [23], as observed in our compound.

The cell parameters 'a', 'b' and 'c' in SmE*, SmB* and SmX* phases were estimated by a method used for indexing SmB* diffraction photographs, as discussed in reference [19,24]. Here the parameters a, b and c represent the distance between the centre of mass of the adjacent molecules, the molecular diameter and smectic layer thickness 'd' respectively. 'c' and 'b' can be directly calculated from d_{001} and d_{010} and 'a' is calculated from the relation a=2bcos30° which can be derived for a c-base centred orthorhombic unit cell resulting from a hexagonal lattice with herringbone structure as shown in **figure 3.12**.

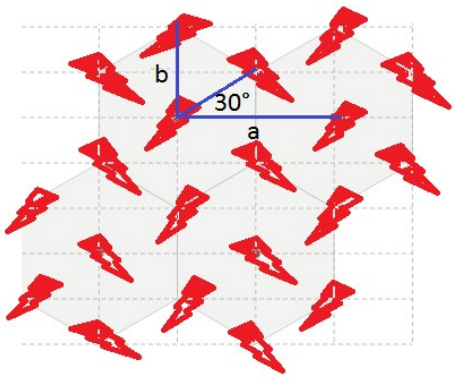

Figure 3.12: Hexagonal lattice with herringbone structure.

Values of d_{110} spacing were calculated using the values of the cell parameters and were compared with the observed values. It had never deviated more than 0.3Å signifying that the estimated cell parameters were quite good. Both the SmE* and SmB* phases are believed to exhibit herringbone crystal structure, though in SmB* phase herringbone structure is observed locally [1,3,16]. This is in conformity with our observation. No change in the structure of unit cell was observed even in SmX* phase. However, the values of the cell parameters are found to change at different phases. It implies that both the SmB* and SmX* phases are hexagonal type and displacive kind of phase transition is involved rather than reconstitutive type [25,26]. After calculating the volume of the optimised molecular geometry, the packing fraction (p) was calculated in each phase which was found to be ~ 0.65. It signifies a close packed hexagonal structure. Packing fraction of this order for hexatic B phase has been reported earlier [19]. It is worth mentioning here that in some earlier report it was suggested that the molecular flip flop rotation around short axis is possible for $p \leq 0.65$ [19,27], which have indeed been observed in dielectric spectroscopic study, as will be described in the next section. The values of the cell parameters, observed and calculated values of d_{110} spacing and packing fraction at different phases are summarised in **table 3.2**.

Table 3.2: X-ray data in SmE*(90°C), SmB*(110°C) and SmX*(123°C) phases

Phase	a (Å) [calc]	b (Å) [d_{010} obs]	c (Å) [d_{001} obs]	d_{110} (Å) [calc]	d_{110} (Å) [obs]	p
SmE*	8.85±0.02	5.11±0.002	35.50±0.15	4.43±0.008	4.63±0.010	0.65±0.006
SmB*	8.87±0.03	5.12±0.009	35.50±0.15	4.44±0.02	4.69±0.004	0.65±0.010
SmX*	8.88±0.01	5.13±0.0035	35.31±0.2	4.44±0.01	4.73±0.003	0.65±0.010

calc: calculated data obs: observed data

3.3.6 Dielectric spectroscopy study

Frequency dependent dielectric relaxation study was done in cooling cycle. To confirm the existence of different phases by dielectric method, the transverse component of the real part of the dielectric permittivity (ε') at 100 Hz is plotted against temperature and shown in **figure 3.13**.

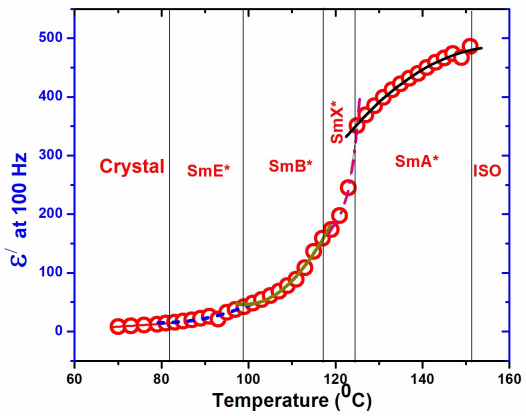

Figure 3.13: Temperature dependence of real part of dielectric permittivity $\varepsilon'_{\perp}$ at 100 Hz.

The real part of the dielectric permittivity (ε') was found to increase with temperature as expected. The minimum value of ε' in SmE* phase was observed to be 2 and finally it reached to 486 in SmA* phase. The

data in each phase are fitted with polynomial equation of order 2. It is evident from **figure 3.13** that the curvature of the fitted data changes in each phase transition, including the transitions associated with the newly identified SmX* phase. Hence, the occurrence of SmX* phase can be confirmed even by dielectric measurements. Such changes at transition points were also observed in higher members of the series 4F4R [discussed in chapter 6].

All the dielectric spectra were fitted to the modified Cole-Cole function. Two representative fitted spectra, showing Maxwell Wagner (MW) mode and short axis relaxation (SA) mode, discussed below, are shown in **figure 3.14**. Corresponding Cole-Cole plots are shown in **figure 3.15**. No collective mode relaxation is observed in this compound.

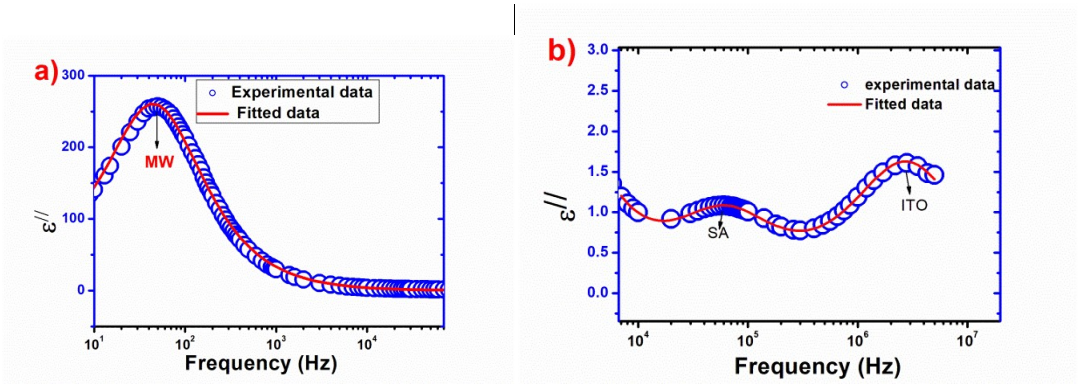

Figure 3.14: Fitted spectra of (a) MW mode in SmB* phase at 105^{0}C and of (b) SA mode in SmE* phase at 81^{0}C. fitted parameters for a) $\Delta\varepsilon_{MW}$ 585± 4.7, fc $_{MW}$ 45 ±0.5, α_{MW} 0.08± 0.006, σ 8.21E-9± 3.0E-10, n=0.98±0.04 and for b) $\Delta\varepsilon_{SA}$ 1.8± 0.03, fc $_{SA}$ 62000 ±27, α_{SA} 0.01± 0.002, $\Delta\varepsilon_{ITO}$ 3.4± 0.07, fc_{ITO} 2800000 ±654, α_{ITO} 0.04± 0.03, σ 3.8E-7± 2.624E-9, n=0.99±0.05

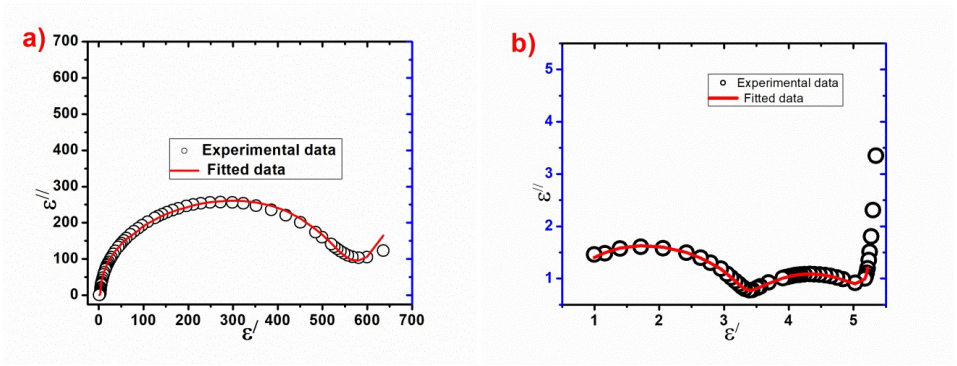

Figure 3.15: Fitted Cole-Cole plot of (a) MW mode in SmB* phase at 105^0C and (b) SA mode in SmE* phase at 81^0C.

In SmA* phase only one low frequency relaxation mode was observed. The critical frequency of this mode was found to increase from 100Hz to 950Hz with temperature. The dielectric increment (Δε) of this mode was very high and also found to increase with temperature (696-809) and it could be suppressed by applying adequate DC bias. This particular mode was observed in all other phases including the crystal and isotropic phase. Usually the dielectric relaxation in SmA* phase is dominated by only one collective mode that is the soft mode (SM) which arises due to the softening of polar part of the tilt fluctuations. The detail mechanism of this mode was discussed in chapter 2. But the critical frequency of the relaxation mode observed for this compound in SmA* phase is 2 order less than the expected soft mode frequency. The dielectric increment is also much higher than the values reported for soft mode relaxation. Moreover, soft mode is not suppressed by DC bias. These facts suggest that the observed peak is not due to soft mode relaxation. Looking into the frequency range, the values of Δε and its bias dependence and also considering the fact that this relaxation sustains even in the crystal and isotropic phase, this mode has been identified as Maxwell Wagner (MW) mode of relaxation which arises due to accumulation of charge in the interface of heterogeneous materials having non-zero electrical

conductivity [28]. Distinct MW mode was also observed in all phases in the higher homologue 6F3R, discussed in chapter 5. For a few other homologues (2F6R, 4F6R, 6F6R) of the present series MW mode was also reported earlier. But in those cases the mode was not observed as distinctly, since MW mode was overlapped by the conductivity contribution [29].

As described in chapter 2, soft mode is usually observed throughout SmA* phase and also in SmC* phase in the vicinity of SmA* to SmC* transition. When a liquid crystal compound is cooled down from orthogonal SmA* phase to the tilted SmC* phase, the elastic constant, responsible for keeping the molecules perpendicular to the smectic layer, vanishes. Due to softening of the restoring force, when an AC signal is applied, the molecules vibrate with fluctuations in their tilt angle. This gives rise to the soft mode relaxation. Thus, it can be argued that since in 1F3R there is no tilted phase below SmA* phase, no soft mode relaxation is expected. Absence of soft mode in SmC^* phase had also been reported earlier for the members 4F3R, [30] 4F4R, 4F5R, 5F3R and 6F3R (discussed in chapters 5 and 6), which directly melts to isotropic phase from SmC^* phase. Thus it can be inferred that SM is possible to observe only when orthogonal to tilted phase transition is present in a material.

In all other phases (SmX*, SmB* and SmE*) a high frequency second relaxation was observed. The critical frequency of this mode increases with temperature in SmX* (85 kHz- 86.5 kHz) and SmB* (70 kHz-85 kHz) phases, while the dielectric increment decreases in both the phases (SmX*: 1.3-1.1, SmB*: 1.6-1.3). Looking at the temperature dependence and range of the typical values of critical frequency (f_C) and dielectric increment ($\Delta\varepsilon$) it can be concluded that, this mode is due to fluctuation of molecules about their short axis (SA) [31]. It is in conformity with the

value of packing fraction of the unit cell, calculated from SAXS data, which ensured that the molecules had enough space inside the unit cell to have molecular flip-flop rotation around its short axis. When the compound is cooled down to SmE* phase from SmB*, the relaxation frequency of this mode drops discontinuously to 50 kHz from 71 kHz. Within SmE* phase, however, f_C increases slightly with decreasing temperature. A similar discontinuous decrease in $\Delta\varepsilon$ is also observed.

Critical frequency and dielectric increment of all the modes in all phases have been shown in **figure 3.16** for comparison which again confirms presence of the SmX* phase.

The high frequency SA mode of relaxation, however, was not observed in SmA* phase, probably because of the well planar alignment of the molecules in this phase. Besides, the value of dielectric increment of this mode decreased sharply with temperature, becoming very small in SmA* phase. Evolution of the real and imaginary parts of the dielectric permittivity in different phases (**figure 3.17** and **3.18** respectively) clearly depicts how the short axis mode became absent in SmA* phase.

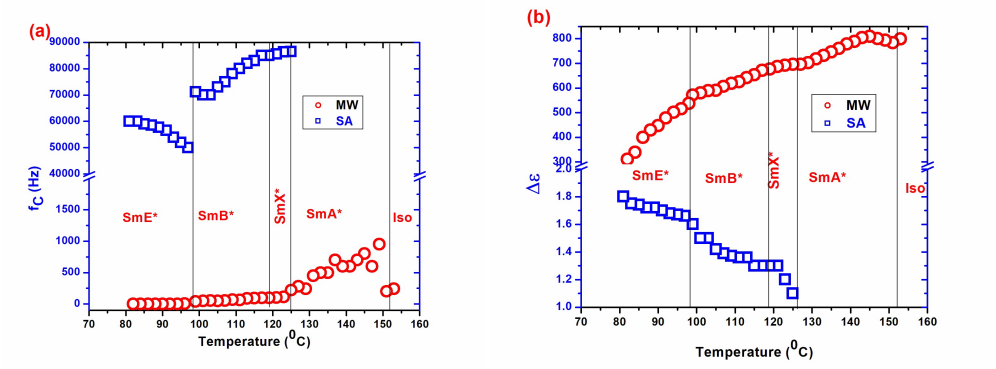

Figure 3.16: Temperature variation of (a) critical frequency and (b) dielectric increment.

Temperature dependence of critical frequencies of the SA mode obeys Arrhenius law in SmB* and SmX* phases but not in SmE* phase (**figure 3.19**). It was reported before that in some compounds both the long and short axis rotation modes in the SmE* phase did not follow Arrhenius law [32]. Activation energy in SmB* phase is found to be 14.2 kJ mol^{-1} which substantially decreased to a value of 3.78 kJ mol^{-1} in SmX* phase. Change in the activation energy again confirms the presence of the new phase. It was also reported earlier that in the crystal B phase the short axis relaxation is frozen whereas the long axis relaxation sustains [24,32,33]. Therefore SmB* and SmX* phases cannot be of crystal SmB* type.

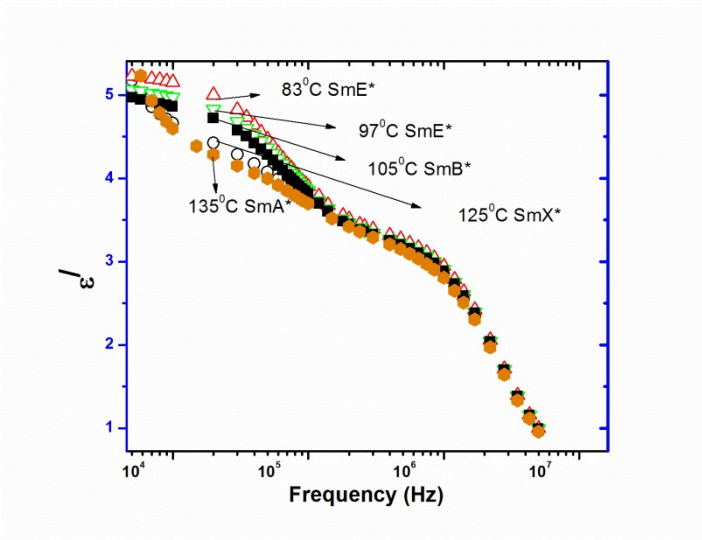

Figure 3.17: Real parts of the dielectric spectra in different phases.

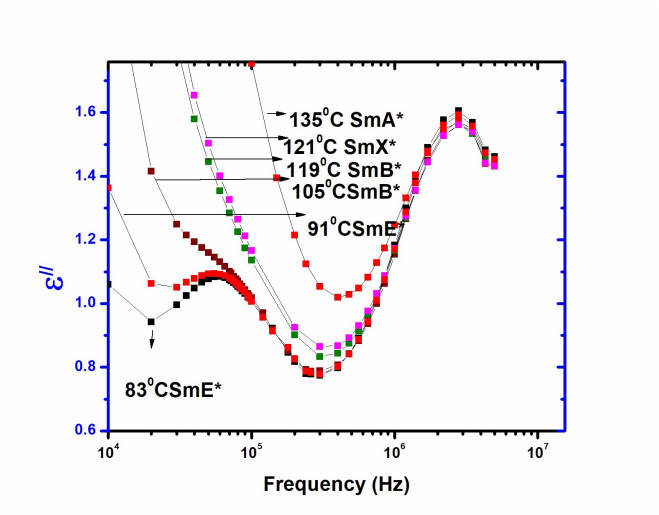

Figure 3.18: Imaginary parts of the dielectric spectra in different phases.

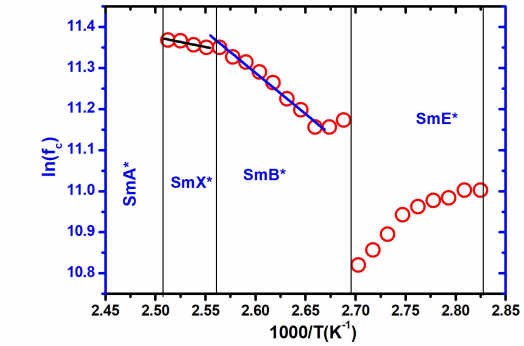

Figure 3.19: Arrhenius plot for 1F3R.

Besides, two variants of hexatic B phases -one more ordered and another less ordered- was reported before to persist together in some compounds and those were differentiated on the basis of the change in activation energy [24]. Thus it is concluded that the phase which was simply identified as SmB* in the synthesis paper [9] is a more ordered hexatic SmB* phase while the new phase, which initially we designated as SmX* phase, is a low ordered hexatic SmB* phase.

3.4 Conclusion

From different features observed in polarising optical microscopy, synchrotron X-ray diffraction and frequency domain dielectric spectroscopy studies it is concluded that three orthogonal smectic phases – SmE*, SmB*$_{hex}$ and SmA* – are present in the biphenyl benzoate chiral compound 1F3R and the SmB*$_{hex}$ phase exhibits two variants – the lower temperature phase is more ordered. The proper phase sequence of 1F3R is, therefore, finally taken as: Crystal – SmE* – $SmB^{*\,mo}_{hex}$ – $SmB^{*\,lo}_{hex}$ – SmA* – Isotropic. All higher homologues are reported to have at least one tilted phase. All the phases are partially bilayer type, observed first time in a chiral system. Transition from SmE* to SmB*$_{hex}$ and within the two SmB*$_{hex}$ variants are of displacive type. No collective mode relaxation is observed. Low frequency Maxwell Wagner mode has been observed in all phases with high dielectric increment. Short axis flip flop mode relaxation is present in both the SmB$_{hex}$ phases as well as in SmE* phase but only in the hexatic phases it shows Arrhenius behaviour. Absence of SA mode in SmA* phase is explained. No soft mode relaxation is also observed in SmA* phase. Comparing relaxation results observed in other homologues it is inferred that SM is possible to observe only when orthogonal to tilted phase transition is present in a material.

Reference

[1] Demus D, Goodby J, Gray GW, et al. Handbook of Liquid Crystals. New york: WILEY-VCH; 1998.

[2] Pershan PS. Structure of Liquid Crystal Phases. World Scientific Publishing Co. Pte. Ltd.; 1998.

[3] Dierking I. Textures of Liquid Crystals. wiley-vch. Weinheim: WILEY-VCH; 2003.

[4] Yamamura Y, Murakoshi T, Hishida M, et al. Examination of molecular packing in orthogonal smectic liquid crystal phases: A guide for molecular design of functional smectic phases. Phys. Chem. Chem. Phys. 2017;19:25518–25526.

[5] Coropceanu V, Cornil J, Silva D, et al. Charge transport in organic semiconductors. Chem. Rev. 2017;107:926–952.

[6] Iino H, Usui T, Hanna JI. Liquid crystals for organic thin-film transistors. Nat. Commun. 2015;6:1–8.

[7] Zou C, Yanahashi N, Wu Y, et al. Patterning Smectic Liquid Crystals for OFETs at Low Temperature. Adv. Funct. Mater. 2019;29:1804838.

[8] Khan M, Park S-Y. Liquid Crystal-Based Proton Sensitive Glucose Biosensor. Anal. Chem. 2014;86:1493–1501.

[9] Ziobro D, Dąbrowski R, Tykarska M, et al. Synthesis and properties of new ferroelectric and antiferroelectric liquid crystals with a biphenylyl benzoate rigid core. Liq. Cryst. 2012;39:1011–1032.

[10] Panarin YP, Nagaraj M, Sreenilayam S, et al. Sequence of Four

Orthogonal Smectic Phases in an Achiral Bent-Core Liquid Crystal: Evidence for the SmAPα Phase. Phys. Rev. Lett. 2011;107:247801.

[11] CJF B, P B. Theory of electric polarization. Vol 1. Amsterdam: Elsevier; 1978.

[12] BUIVYDAS M, GOUDA F, ANDERSSON G, et al. Collective and non-collective excitations in antiferroelectric and ferrielectric liquid crystals studied by dielectric relaxation spectroscopy and electro-optic measurements. Liq. Cryst. 1997;23:723–739.

[13] Budai J, Pindak R, Davey SC, et al. A structural investigation of the liquid crystal phases of 4-(2'-methylbutyl)phenyl 4'-n-octylbiphenyl-4-carboxylate. J. Phys. Lettres 1984;45:1053–1062.

[14] Goodby JW, Pindak R. Characterization of the Hexatic B and Crystal B phases by Optical Microscopy. Mol. Cryst. Liq. Cryst. 1981;75:233–247.

[15] Gaussian 09, Revision D.01, M. J. Frisch *et al.* Gaussian, Inc., Wallingford CT, 2013.

[16] Pindak R, Moncton DE, Davey SC, et al. X-ray observation of a stacked hexatic liquid-crystal B phase. Phys. Rev. Lett. 1981;46:1135–1138.

[17] Schenkel MR, Hooper JB, Moran MJ, et al. Effect of counter-ion on the thermotropic liquid crystal behaviour of bis(alkyl)-tris(imidazolium salt) compounds. Liq. Cryst. 2014;41:1668–1685.

[18] Chandrasekhar S. Liquid crystals. 2nd ed. New York: Cambridge University Press; 1977.

[19] Osiecka N, Budziak A, Galewski Z, et al. X-ray studies of the smectic B phase of the 4-bromobenzylidene-4′-alkoxyanilines. Phase Transitions. 2012;85:314–321.

[20] Madhusudana N. On the polymorphism of the smectic A phases of highly polar compounds. Proc. Indian Acad Sci (Chem Sci). 1983;92:509–525.

[21] Sirota EB, Pershan PS, Sorensen LB, et al. X-Ray Studies of Tilted Hexatic Phases in Thin Liquid-Crystal Films. Phys. Rev. Lett. 1985;55:2039–2042.

[22] Górecka E, Chen L, Pyżuk W, et al. X-ray studies of the hexatic phase in liquid crystals with a crystal- B –hexatic- B –smectic- A phase sequence. Phys. Rev. E. 1994;50:2863–2867.

[23] Kaganer VM, Ostrovskii BI, de Jeu WH. X-ray scattering in smectic liquid crystals: From ideal- to real-structure effects. Phys. Rev. A. 1991;44:8158–8166.

[24] Urban S, Czub J, Przedmojski J, et al. Dielectric and X-ray Studies of Substances with the Smectic B phase. Mol. Cryst. Liq. Cryst. 2007;477:87–100.

[25] Bryan RF, Forcier PG. Contrasting Solid-State Structures for Two Nematogenic Benzylideneanilines. Crystal Structures of p [(p ’-Ethoxybenzylidene)amino] -benzonitrile and p - [(p ’-Methoxybenzylidene)amino] -phenyl Acetate. Mol. Cryst. Liq. Cryst. 1980;60:133–152.

[26] Jaishi BR, Mandal PK, Goubitz K, et al. The molecular and crystal structure of a polar mesogen 4-cyanobiphenyl-4′-hexylbiphenyl carboxylate. Liq. Cryst. 2003;30:1327–1333.

[27] Urban S, Przedmojski J, Czub J. X-ray studies of the layer thickness in smectic phases. Liq. Cryst. 2005;32:619–624.

[28] Hasse W, Wróbel S. Relaxation Phenomena: Liquid Crystals, Magnetic Systems, Polymers, High-Tc Superconductors, Metallic Glasses Berlin: Springer; 2003.

[29] Czerwiec JM, Dąbrowski R, Żurowska M, et al. Dielectric Properties of Ferroelectric Liquid Crystals with Diversified Molecular Structure - ERRATUM. Acta Phys. Pol. A 2010;117:553–556.

[30] Goswami D, Sinha D, Debnath A, et al. Molecular and dynamical properties of a perfluorinated liquid crystal with direct transition from ferroelectric SmC* phase to isotropic phase. J. Mol. Liq. 2013;182:95–101.

[31] Mishra A, Węgłowska D, Dabrowski R, et al. Relaxation phenomena of a highly tilted ferroelectric liquid crystalline material (S)-(+)-4′-(3-pentanoyloxy prop-1-oxy)biphenyl-4-yl-4-(1-methylheptyloxy)benzoates. Liq. Cryst. 2015;42:1543–1549.

[32] Schacht J, Buivydas M, Gouda F, et al. Broad band dielectric relaxation spectroscopy of molecular reorientation in smectic liquid crystalline phases (SmA, SmB, and CrE). Liq. Cryst. 1999;26:835–

847.

[33] Gouda F, Lagerwall ST, Skarp K, et al. Broad band dielectric relaxation spectroscopy of a chiral smectic b-crystal phase. Liq. Cryst. 1994;17:367–379.

CHAPTER-4

Structural, dielectric and electro-optic properties of two biphenyl benzoate cored chiral liquid crystals having tilted hexagonal phases

---

- *Part of this work has been published in Liq cryst. Vol:46,pp2115-2126,2019.and Liq cryst. 2019 published online ; doi: https://doi.org/10.1080/02678292.2019.1686776*

4.1 Introduction

The phase behaviour, structural, dielectric and electro-optic properties of two chiral liquid crystals with biphenyl benzoate core, viz. (S)-(+)-4/-[(3-pentafluoropropanoyloxy)prop-1-oxy]biphenyl-4-yl 4-(1-methyl heptyloxy)- benzoate (2F3R) and (S)-(+)-4/-[(3-heptafluoro butanoyloxy)prop-1-oxy] biphenyl-4-yl 4-(1-methylheptyloxy)benzoate (3F3R) [1], [explanation of code name nFmR, is given in chapter one], have been discussed in this chapter. The molecular structures of the compounds (2F3R and 3F3R), differ from 1F3R (discussed in chapter 3) only by one and two number of additional carbons in the fluorinated chain respectively. As discussed in the previous chapter, the lower homologue 1F3R exhibit only orthogonal smectic phases - higher order hexatic phases (SmE* and SmB*) along with lower order SmA* phase. As a result of the addition of fluorine atoms in the chain, tilted phases are induced in 2F3R and 3F3R. Both the compounds are found to exhibit tilted hexagonal phases and a wide ranged SmC* phase. The molecular structures of the compounds are shown in **figure 4.1**.

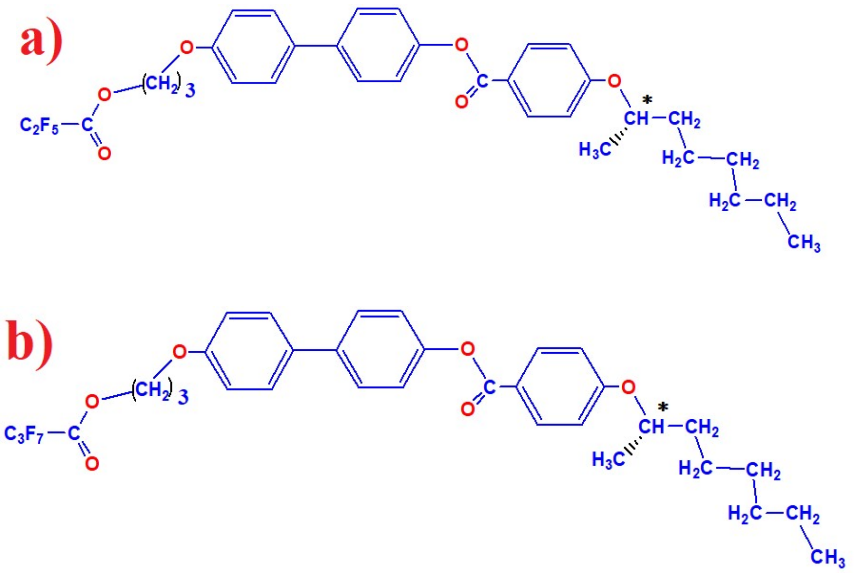

Figure 4.1: Molecular structures of (a) 2F3R and (b) 3F3R.

From the time when Mayer [2] discovered the 'ferroelectric' properties of SmC* phase in chiral liquid crystals (LC), there had been an extensive study on the dielectric and electro-optic properties of ferroelectric liquid crystals (FLCs), mainly focussing on their potential applications on advanced electro-optic devices. Thus the characterisation of 2F3R and 3F3R which display ferroelectric SmC* phase for a wide range of temperature, may contribute significantly to this stream of research. Besides, the compounds also exhibit tilted hexagonal phases (SmF* and SmG*/SmJ*). SmF* phase had also been identified as a ferroelectric phase. However, ferroelectricity of SmF* has not yet been explored well compared to SmC* phase, mostly because of their small temperature range, higher viscosity and instability [3,4]. Hence, structural, dielectric and electro-optic studies of the tilted hexagonal phases may be proved to be handy in exploring their fundamental properties and probable practical utilities.

4.2 Experimental methods

The sample was fed into an 8μm dielectric cell (EHC) with homogeneous polyimide alignment layer and the bookshelf alignment was achieved by slow regulated cooling of the samples from the isotropic phase to the desired temperatures often in presence of an ac electric field. The polarising optical microscopy (POM) was done using Olympus BX41 polarizing microscope equipped with a CCD camera. X-ray scattering experiments were performed using PETRA III synchrotron beamline at P07 Physics Hutch station at Deutsches Elektronen-Synchrotron (DESY), Hamburg, Germany to investigate their structural properties. A beam of wave length 0.164 Å was used to explore an angular range of Bragg angle (2θ) of nearly 5°. The complex permittivity was measured using a Hioki 3532-50 impedance analyzer in the

frequency range of 100 Hz to 5 MHz while Hioki IM3533 analyzer was used in the range of 0.1 mHz to 270 kHz. The Cole-Cole function [5] modified to consider the low frequency parasitic effect was used to fit the observed dielectric spectra. The spontaneous polarization (P_S) was measured by reversal current method [6]. Agilent 33220A function Generator was used to apply an ac triangular signal of voltage 20V and frequency 60 Hz as the input signal. The helical pitches of the compounds were measured from the optical textures by measuring the distances between the parallel lines in the chiral phases after proper length calibration of the captured textures [7].

A Lakeshore 340 temperature controller was used to control the temperature during SAXS study and a Mettller FP90 temperature controller along with FP82 hot stage was used to regulate temperature in all other experiments.

Detail procedures of all the experiments are discussed in chapter 2.

4.3 Results and discussion

4.3.1 Observed phases

Unifying the outcome of polarising optical microscopy, synchrotron diffraction, dielectric and electro-optic studies it is observed that while cooling down from isotropic phase, the lower member 2F3R formed SmA* and SmC* phases followed by tilted hexatic SmF* phase and finally settle into soft crystal SmJ* phase. On the other hand, the higher member 3F3R is found to form directly SmC* phase on cooling from the isotropic phase, giving rise to SmF* phase followed by soft crystal SmG* phase on further cooling. The phase sequences and transition temperatures are summarized in **table 4.1**.

Table 4.1: Phase sequence and transition temperatures of the compounds

2F3R:	Crystal 68ºC SmJ* 83°C SmF* 85°C (SmF*+SmC*) 100°C SmC* 129°C SmA*135ºC Iso
3F3R:	Crystal 65ºC SmG* 73.5°C SmF* 75°C (SmF*+SmC*) 83°C SmC* 131°C Iso

Both the compounds showed quite wide range of SmC* phase (ΔT_{SmC*}). It is observed from **table 4.1**, as a consequence of addition of extra fluorine in the chain, the SmA* phase was eliminated in 3F3R and the stability of SmC* phase (ΔT_{SmC*}) in that compound (48ºC) was also increased significantly than that of 2F3R (29ºC). In both the compounds a coexistence phase of SmC* and SmF* phases was observed in between the two phases.

4.3.2 Optimised geometry

To explore the structural dependency of the properties of the compounds the molecular structures were optimised, applying Hartree-Fock method and using 3-21G basis set in a commercial package[8]. The energy optimised structures are shown in **figure 4.2**.

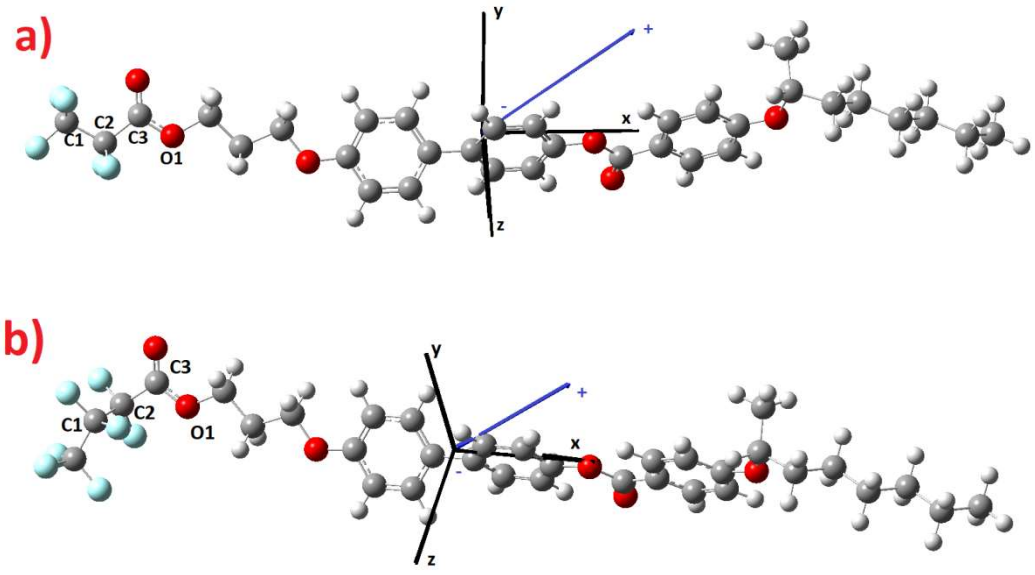

Figure 4.2: Optimised geometry of a) 2F3R and b) 3F3R.

It is worth mentioning here that, for the purpose of comparison, the initial structures of the compounds taken for optimisation, that we are going to report in this dissertation, were build up from one single core of the molecules. Different compounds were built by modifying the chain only. This process differs from the process of optimisation that was reported in the published paper. Hence the optimised parameters also changed a bit. Optimised molecular lengths (*l*) were found to be 33.75Å and 33.48Å for 2F3R and 3F3R respectively. Dipole moments (μ) of 2F3R and 3F3R molecules were respectively found to be 6.75 D (5.1, 4.35, 0.21) and 6.48D (5.0059, 4.12, 0.07) where the components of dipole moments along the three coordinate axes are shown within parentheses. The molecular length and dipole moment of 3F3R were found to be less than 2F3R, even after having one extra carbon and fluorine atoms in the chain, owing to the change in conformation of the fluorinated chain. After the addition of the third carbon in the fluorinated chain the optimised structure got twisted in the z direction (**figure 4.2b**). It can be quantitatively described by the value of the torsion angle between C1, C2, C3 and O1 atoms as shown in **figure 4.2**. The torsion angle for 2F3R was found to be -179.85º, exposing almost relatively linear positions of the said atoms. But the same torsion angle of 3F3R was found to be 92.35º, revealing a twist of almost ~87º of the chain. It is concluded that these changes in dipole moment and the molecular conformation give rise to subtle change in the intermolecular interaction and playing important role in the appearance of different phases in the two compounds.

4.3.3 Polarized optical microscopy (POM) study

The POM study was done in the cooling cycle. The optical textures of 2F3R and 3F3R at different phases in planar geometry are shown in

figure 4.3 and **4.4** respectively. A clear fan shaped texture was observed in SmA* phase of 2F3R. In the SmC* phase of same compound, broken fan shaped textures and small change in birefringence were observed with an equidistant line pattern due to the helical structure. On further cooling, at 85^0C a new phase was observed in a small temperature range which was denoted as $SmB^*_{Crystal}$ in a previous report [1].

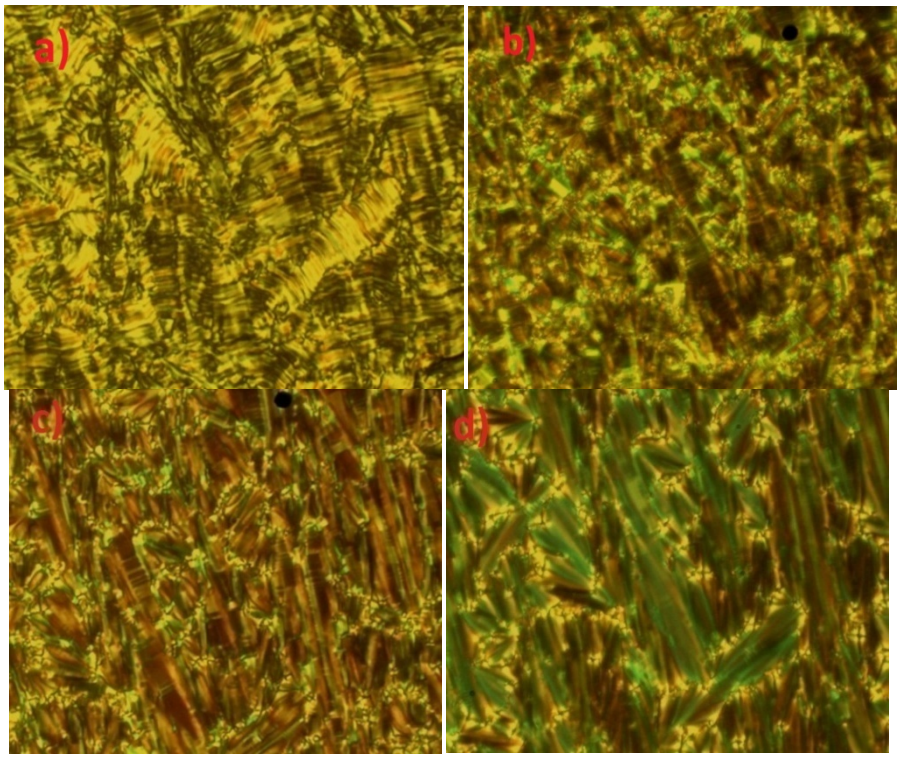

Figure 4.3: Textures of 2F3R at a) SmJ* (80°C) b) SmF* (84°C) c) SmC* (125°C) and d) SmA* (132°C).

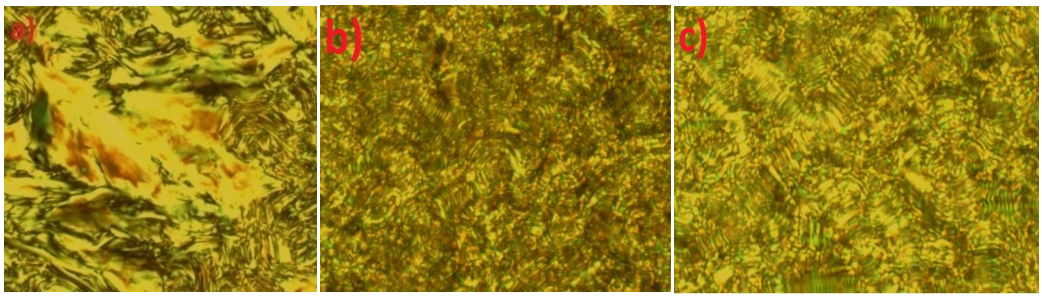

Figure 4.4: Textures of 3F3R at a) SmG* (70°C) b) SmF* (74°C) and c) SmC* (130°C).

However, the texture in this phase was observed to have even more pronounced broken fan texture with some change in the birefringence. Remnants of the parallel lines were also seen which indicated the persistence of helical structure even in this new phase. Thus this phase below SmC* phase must be a tilted phase, SmI* or SmF*, not an orthogonal $SmB^*_{Crystal}$ phase. This kind of texture has been reported before for SmI* and SmF* phases [9]. Finally a SmG*/SmJ* like mosaic texture [7,9] was observed under 83°C in 2F3R. On the other hand, in 3F3R directly SmC* phase was formed from the isotropic state. Though parallel chiral lines were seen in the texture with few defects but no significant domain was visible. In other members of the same series and with a direct transition from isotropic to SmC* phase similar textures were reported before in SmC* phase [1]. On further cooling at 75^0C, a small change in birefringence was observed with more defects but helicoidal lines were still visible. Hence this must also be a tilted phase viz. SmI*/SmF*, presence of this phase was not reported in [1]. Finally, at further lower temperature, SmG*/SmJ* mosaic like texture could be observed. No such soft crystalline phases were reported before in both the compounds [1]. Although from the POM study we could not differentiate SmI*/SmF* and SmG*/SmJ* phases but they were ascertained from the synchrotron diffraction study discussed in the next section.

4.3.4 Synchrotron X-ray diffraction study

The sharp lower and the diffuse higher angle features were observed in the diffraction photographs corresponding to the smectic layer spacing and ordering within the layers respectively. In SmJ*/SmG* phases higher angle features were also sharp. The presence of strong diffraction

maxima up to 4th order at low angles, in higher order smectic phases, signified the long range ordering across the smectic layers in those phases.

As mentioned in chapter 1, both the SmF* and SmI* phases have tilted pseudo-hexagonal packing within the layers with tilt of the molecules towards an edge or towards an apex of the hexagon respectively. In these phases, the in-plane bond orientational order (BOO) and the interlayer correlations are found to be quasi long range in nature. The other two low temperature phases - SmG* and SmJ* - are soft crystal-like tilted phases with pseudo-hexagonal packing within the smectic layers. In SmG* the tilt direction is similar to that of SmF* on the other hand in SmJ* it is similar to that of SmI*. But these phases have long range in plane bond orientational order as well as long range interlayer correlation and do not have any helical arrangement of tilt [7,10–12]. A schematic diagram of the structures of SmF* and SmI* phases and expected X-ray pattern are shown in **figure 4.5**.

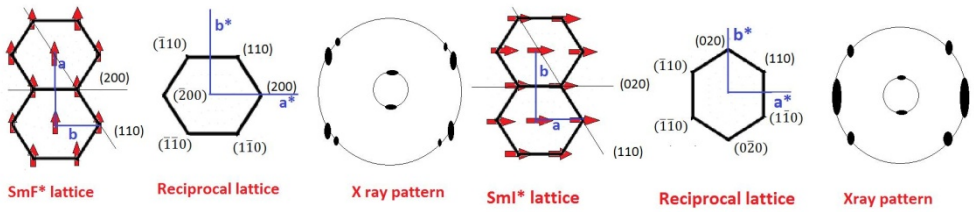

Figure 4.5: Schematic diagram of the structures and X-ray diffraction patterns of SmF* and SmI* phases.

SmF* and SmI* phases can be distinguished by the wide angle X-ray diffraction features of the two phases. At the outer diffraction maxima of a perfectly mono-domained sample, in SmF* phase, the (200) and (110) reflections can be observed at angles **θ** and $\sin^{-1}$ (±(1/2) sin **θ)** to the equator respectively, but in SmI* phase (020) and (110) reflections will

appear respectively at angles zero and $\sin^{-1}(\pm\frac{\sqrt{3}}{2}\theta)$ to the equator, θ being the tilt angle [10–12].

Though no field was applied to align the samples, but due to slow regulated cooling from isotropic phase to the desired temperature, the compounds got aligned only partially inside the cell. Some representative diffraction photographs of the compounds, at different phases are shown in **figure 4.6** and **4.7**.

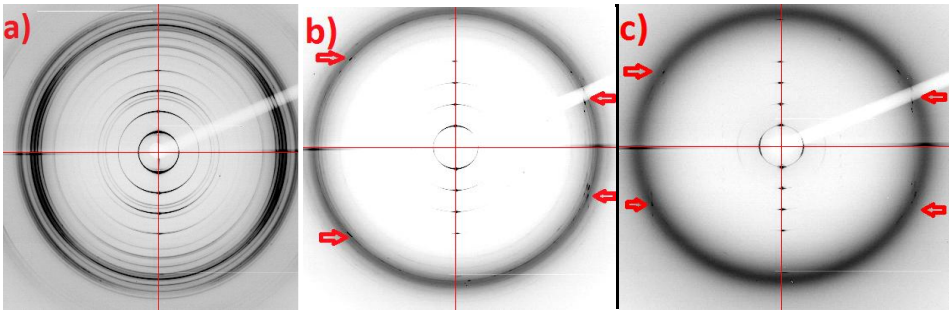

Figure 4.6: Diffraction pattern of 2F3R at a) SmJ* (80°C), b) SmF* (84°C) and c) mixed phase (100°C).

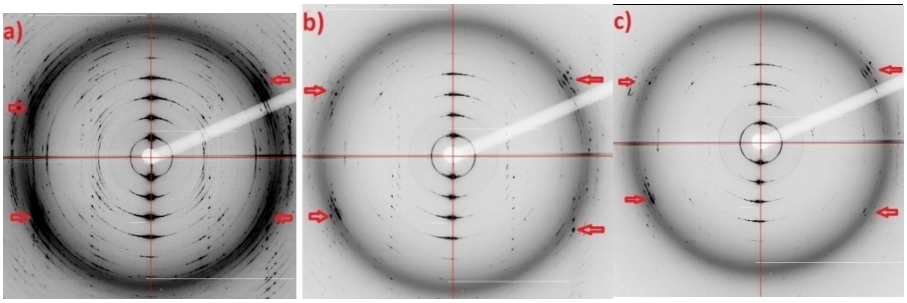

Figure 4.7: Diffraction pattern of 3F3R at a) SmG* (70°C), b) SmF* (75°C) and c) mixed phase (83°C).

The intensity profiles of the outer maxima of both the compounds are shown in **figure 4.8**.

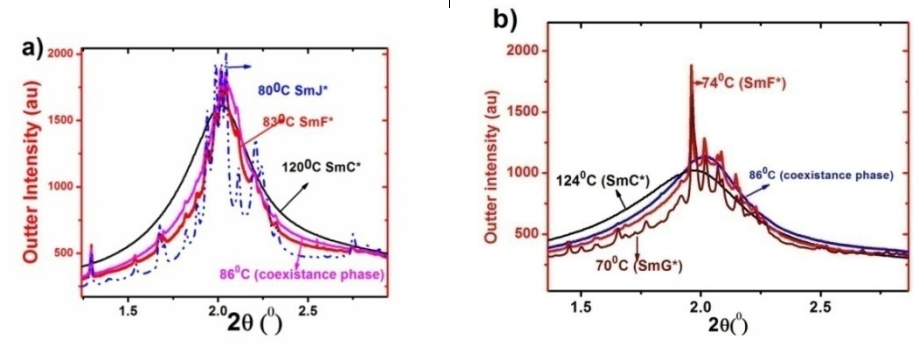

Figure 4.8: Intensity profiles of outer maxima in different phases of a) 2F3R and b) 3F3R.

A diffuse ring was observed at higher angle in SmC* phase, as expected. After entering in to the SmI*/SmF* phase the shape of the intensity profile at wider angle changed considerably, the width decreased significantly and a few satellites were seen. It is evident from **figure 4.6** and **4.7** that the diffraction features of SmF*/SmI* phase actually resembles that of SmF* phase. In both the compounds four maxima at wider angle diffraction pattern, visible more in 3F3R, can be observed at an angle of about 30° from the equator. This feature is more prominently displayed in the integrated intensity profiles of the outer maxima presented in **figure 4.8**. The diffraction pattern changed drastically but differently in the two compounds, after entering into the soft crystalline phase. In 2F3R the tilt direction changes, the features resemble to that of SmI* i.e. maximum can be observed at 0° from the equator (**figure 4.6a**) implying that this must be SmJ* phase while in 3F3R the tilt direction remains same, wide angle maximum at ~ 30° from the equator persists and become more prominent (**figure 4.7a**) confirming the soft crystalline phase of 3F3R to be SmG*. Similar intensity profiles had been reported for SmF*, SmG* and SmJ* phases in another chiral compound with the same core structure but with protonated end chain [9].

To explore the structural features of the hexagonal phases in more detail, their cell dimensions were estimated. SmF* phase can be realised considering a C-centred monoclinic unit cell with axis $\boldsymbol{a} > b$ where b is the axis around which tilting takes place and the angle between 'a' and 'c' is considered as β which equals to (90^o+θ) [11–13]. Considering the molecules as rigid rods, the tilt of the molecules (θ) was calculated from the smectic layer spacing (d) using the relation $\boldsymbol{\theta = cos^{-1}\frac{d}{l}}$ where the molecular length (*l*) was obtained from the optimised geometry. Values of 'c' and 'a' axes were calculated from d_{001} and d_{200} respectively using the standard expression for the interplanar spacings and then 'b' was calculated from the relation $a=2b\cos 30^o$ assuming an ideal hexagonal packing [13–15]. Cell parameters of SmG* phase were calculated in a similar way. For SmJ* phase, values of 'c' and 'b' were calculated from the peaks identified as (001) and (020) and 'a' was calculated using 'b' as before. Calculated lattice parameters are listed in **table 4.2**. As expected 'a' was found to be greater than 'b' in SmF* and SmG* phases, opposite behaviour was observed in case of SmJ* phase [13]. Among the satellites in the intensity profile of outer maxima (**figure 4.9**), only one additional peak could be identified as (110) and the observed values of d_{110} in the hexagonal phases never deviated more than 0.3 Å from the calculated values. Packing fractions (p) in each phase, shown in **table 4.2**, were also calculated employing the volumes of the molecules in the optimised geometry. Change of packing fraction is found to be much higher when the tilt direction changes. It is to be noted here that due to minute change in the optimised length (*l*), as mentioned in section 3.2, the crystal parameters reported here has changed by 1-2% of what was reported in the published paper. As a matter of fact, after this correction the calculated value of d_{110} was found to be closer to the observed value.

Table 4.2: Lattice parameters of 2F3R and 3F3R in SmF*, SmG* and SmJ* phases.

Compound	Phase	a (Å)	b (Å)	c (Å)	β (°)	d_{110}(Å) (calculated)	d_{110}(Å) (observed)	p
2F3R	SmF*(83°C)	11.91±0.02	6.87±0.01	33.68±0.52	120.38±1.7	5.7±0.08	5.4±0.005	0.45±0.03
	SmJ*(79°C)	6.09±0.001	10.56±0.002	33.4±0.25	120.38±0.38	4.71±0.04	4.75±0.01	0.57±0.002
3F3R	SmF*(75°C)	11.72±0.03	6.76±0.017	33.42±0.58	116.9±1.52	5.6±0.03	5.4±0.07	0.47±0.01
	SmG*(71°C)	11.98±0.02	6.91±0.004	33.43±0.15	116.99±0.54	5.80±0.01	5.92±0.05	0.45±0.02

It was further noticed, clearly revealed in **figure 4.6** and **4.7**, that features of SmF* phase, observed both in low and high angles, started developing in the low temperature regime of SmC* phase, at 100°C in 2F3R and at 83°C in 3F3R. Even splitting of the inner maxima was observed (**figure 4.9**), more prominently in 3F3R. This had been identified as a signature of coexistence phase of (SmC*+SmF*).

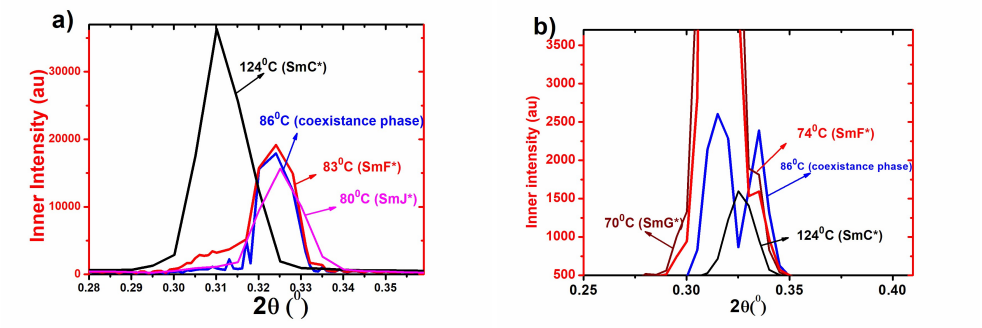

Figure 4.9: Intensity profile of inner maxima of a) 2F3R and b) 3F3R.

Similar splitting of inner maxima was reported by S. Krishna Prasad *et al.* [17] in a coexistence phase of (SmC*+SmI*). It had been argued that the coupling of molecular tilt may induce a weak bond orientation order even in SmC* phase since both the phases have same symmetry [12,16,17].

The correlation lengths (ξ) of the compounds, across and within the layer, were calculated to explore the range of molecular correlation using **equation 4.1**[18].

$$\xi = \frac{2\pi}{FWHM} \qquad [4.1]$$

The temperature variation of ξ are shown in **figure 4.10** and **4.11**.

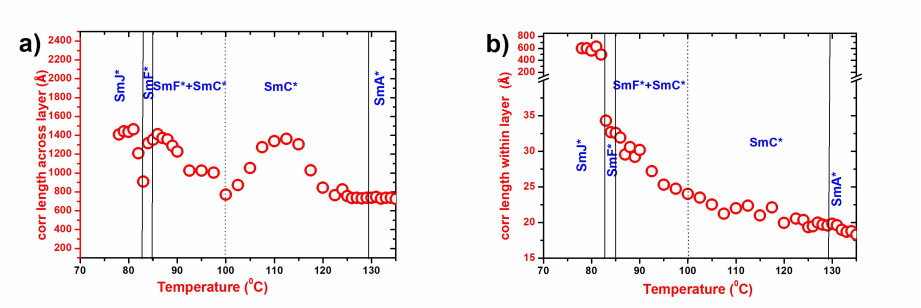

Figure 4.10: Temperature variation of correlation lengths of 2F3R a) across and b) within the layer.

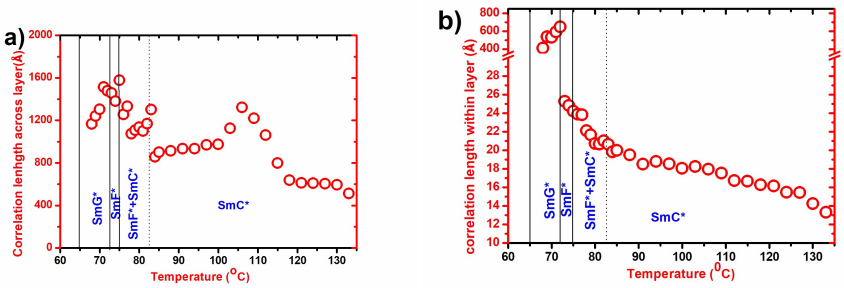

Figure 4.11: Temperature variation of correlation lengths of 3F3R a) across and b) within the layer.

Discontinuous changes of the correlation lengths across the layer ($\xi_{\parallel}$) can be observed at the phase boundaries whereas in plane correlation ($\xi_{\perp}$) was found to decrease continuously, except at SmJ*-SmF* and SmG*-SmF* transitions. $\xi_{\parallel}$ was found to be about 1400 Å and 1500 Å in SmJ* and SmG* phases of 2F3R and 3F3R respectively. Corresponding correlation lengths within the plane ($\xi_{\perp}$) was found to be about 700 Å and

600 Å, much less compared to $\xi_{\|}$. In SmF* phase $\xi_{\|}$ decreased to about 1300 Å and 1450 Å respectively in the two compounds which meant a correlation of more than 38 and 43 molecular lengths for 2F3R and 3F3R respectively. Similarly, the in plane correlation decreased to about 35 Å and 26 Å. Comparable values of correlation lengths were reported before in hexatic and soft crystal phases [18–20]. It was also noted that $\xi_{\|}$ showed an increasing trend with temperature within SmC* in both compounds, attained a maximum value and decreased thereafter. This might be due to the fact that correlation across the smectic planes is not fixed within SmC* but grows with temperature and becomes maximum at the middle.

The layer spacing (d_{001}) of the compounds in all phases were found to be less than the molecular length which further implied that even the hexagonal phases were tilted. The temperature variation of d_{001} is shown in **figure 4.12**. In the entire SmC* phase of 3F3R the layer spacing increased with temperature but in 2F3R it was found to decrease in the low temperature regime. Layer spacing in SmC* phase is expected to increase with temperature due to decrease of tile of the molecules. A possible explanation is discussed below. However, discontinuous changes in d values were observed in both the compounds at the transition from SmC* to the coexistence phase, Δd being 0.84 Å and 1.71 Å in 2F3R and 3F3R respectively. This sort of variation had been reported before at similar phase transitions [16]. However, in 3F3R the layer spacing of the coexistence phase was found to be higher than that in SmC*, while in 2F3R it was lower. Moreover, in 2F3R the layer spacing was found to increase as the coexistence phase was approached from above. This might be due to stretching of the chain and growth of the orientational order of long molecular axes [21,22]. This kind of pre-transitional effect had been reported at SmC* to the hexagonal smectic

phase transition point in other homologues and also in other chiral LCs [1,9,21,22]. Within SmF* phase layer spacings were observed to be independent of temperature. d values in SmF* phase of 2F3R and 3F3R were found to be nearly 29.0 Å and 29.8 Å respectively. In 2F3R it increased marginally in SmJ* phase but in 3F3R it remained almost same in SmG* phase. Within SmG* and SmJ* phases it showed a slightly decreasing trend with lowering of temperature, this type of behaviour had also been reported before [9].

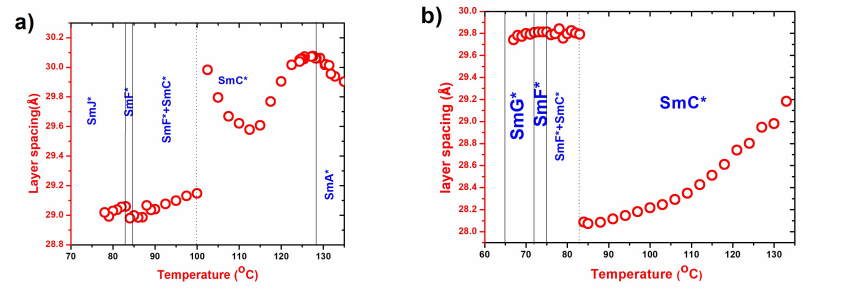

Figure 4.12: Temperature variation of layer spacing of a) 2F3R and b) 3F3R.

The ratio of layer spacing to molecular length was found to be nearly 0.90 in SmA* phase of 2F3R. This ratio for the homologues 5F6R, 4F6R, 1F4R and 1F3R was reported earlier as 0.50, 0.76, 0.97 and 1.01 respectively [1]. It is noticed that the ratio decreases with increasing fluorination. That the ratio is less than one in SmA* phase may occur due to the fact that the chains may not be totally extended [12] or the molecules may have tilts with azimuthal degeneracy as in a de Vries phase [23] . To inquire it further we revisited the temperature variation of 'd' in SmC* phase in 2F3R. The layers start contracting in SmC* phase at about 1° below SmA*-SmC* transition but after reaching a certain temperature (~112°C) it showed a negative layer thermal expansibility

and ultimately almost recovered the highest 'd' value observed at SmA*-SmC* transition. In SmA* phase also the overall expansibility of 'd' is negative. This kind of temperature dependence of the layer spacing is typically observed in de Vries type material [24,25]. Although the highest layer contraction in SmC* phase was found to be ~1.5%, effective layer contraction is only about 0.3%. This value is much less than in the mesogens having ordinary SmA phase [26], and very close to the value of ideal de Vries type material [24,27]. Thus the possibility of chevron defects in display will be reduced drastically in 2F3R.

Treating the molecules as rigid rods, the tilt of the molecules at different phases were calculated from the equation $\theta = cos^{-1}\frac{d}{l}$, where, '$l$' is the optimised molecular length. The temperature variation of tilt angles are shown in **figure 4.13**.

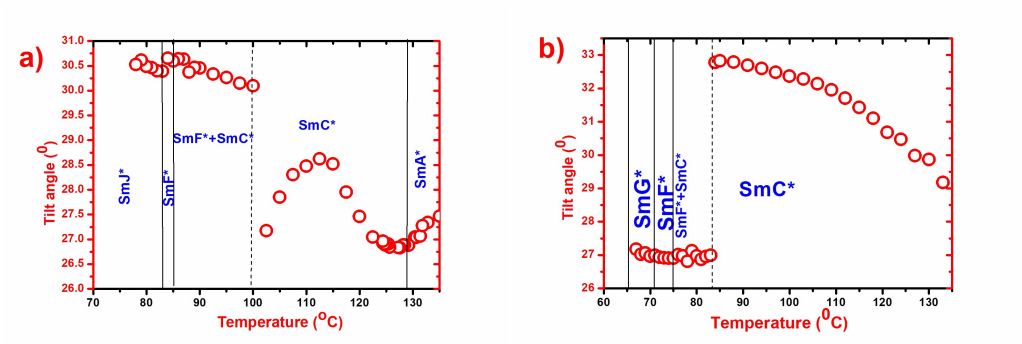

Figure 4.13: Temperature variation of X-ray tilt angle of a) 2F3R and b) 3F3R.

Quite high tilt was observed in both compounds, highest tilt in SmC* phase being 32.78° and 28.62° for 3F3R and 2F3R respectively. These are much higher than in 6F4R, 4F6R and 5F6R [1] but less than that of 4F3R [28]. Within the SmC* phase tilt angles decreased with temperature as expected except in the low temperature region in 2F3R. A discontinuous and anomalous change was observed in the coexistence phase like layer spacing. In SmF* phase tilt was found to be~ 30.5º and

27º in 2F3R and 3F3R respectively and remained almost constant throughout the phase. It is to be noted here that the absolute values of tilt has changed slightly here in comparison to what was reported in the paper, which is due to change in the optimised length. In some previous reports tilt angles were reported to decrease [21] or to have no change [29] or even to increase [9] after entering into SmF* phase. Tilt decreased slightly in SmJ* phase of 2F3R but not much change could be observed in SmG* phase of 3F3R.

Average intermolecular spacings (D) were calculated from the high angle diffraction ring in SmA* and SmC* phases and from (200) reflections in SmF* and SmG* phases, while in SmJ* phase from (020) reflections were used. D increased slightly with temperature in SmC* phase as shown in **figure 4.14**, no anomaly is observed in 2F3R as observed in d. In 3F3R discontinuous change was observed at SmF*-SmG* transitions and slight anomaly was noticed in the mixed phase.

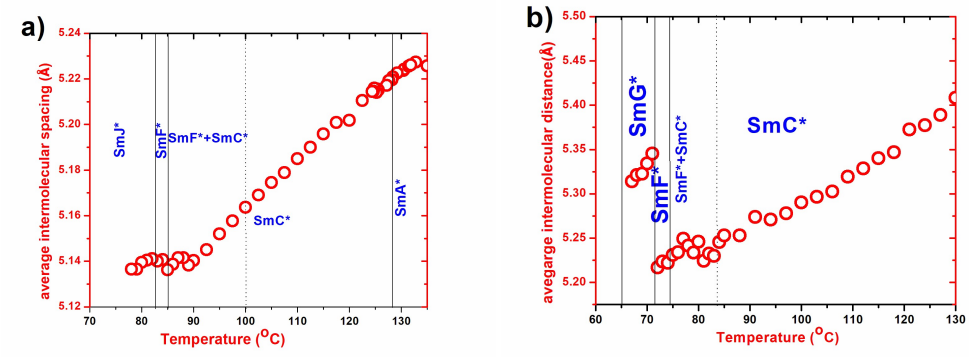

Figure 4.14: Temperature variation of average intermolecular spacings (D) of a) 2F3R and b) 3F3R.

4.3.5 Frequency dependent dielectric relaxation study

The dielectric relaxation study was conducted in cooling cycle for both compounds. One low frequency and one mid-frequency relaxation was

observed in SmC* phase. In fact the low frequency mode (in the range of 0.1 Hz to 10 Hz) was observed in all the phases including isotropic phase and critical frequency (f_C) of this mode was found to exhibit slight increasing trend with temperature. This mode has very high dielectric increment ($\Delta\varepsilon$ about 500 for 2F3R and 450 for 3F3R) and can be suppressed by applying DC bias. These characteristics indicate it to be the Maxwell Wagner mode (MW) which arises in heterogeneous materials having non-zero electrical conductivity due to the accumulation of charge at the interface [30], as described in detail in chapter 2. MW mode was observed also in 1F3R, described in chapter 3 and also in other compounds of the same homologous series 2F6R, 4F6R and 6F6R [31]. The other mode which was observed in SmC* phase at around ~10^3 Hz was assigned with Goldstone Mode relaxation (GM). It was mentioned in chapter 2 that GM mode is associated with the azimuthal fluctuations of directors in a smectic plane, is also known as phason mode. A DC bias suppressed this mode as well because of the unwinding of the helical structure. It showed moderately high dielectric increment (maximum $\Delta\varepsilon$ ~ 140 for 2F3R and ~135 in 3F3R). In 2F3R another high frequency mode (~480 kHz) appeared in SmC* phase near SmC* to SmA* transition which persisted throughout the SmA* phase also. This mode exhibited much smaller dielectric increment ($\Delta\varepsilon$ ~5) than that of GM or MW relaxation and did not get suppressed under bias. This relaxation was assigned with soft mode (SM) collective relaxation which arose due to tilt fluctuation of the molecules. However, just like in 1F3R, SM was not observed in 3F3R which did not have any SmA* phase. It is in consonance with our argument of chapter 3, related with the nonexistence of soft mode in absence of any orthogonal to tilt phase transition.

In the hexagonal SmF* phase three modes were observed. The low frequency mode was related to MW relaxation as stated before. The

second mode in the intermediate frequency range (~60Hz-100Hz) had the critical frequency (f_C) and dielectric increment comparable to that of GM relaxation in SmC* phase. However, a discontinuous drop in f_C and an increase in $\Delta\varepsilon$ were observed. In 2F3R the frequency decreased so much with the temperature that it could not be distinguished from MW relaxation in low temperature. The third mode was observed in the high frequency range (~200 kHz for 2F3R and ~50 kHz for 3F3R) with a very small dielectric increment (~5 for 2F3R and ~0.5 for 3F3R). As proposed by Rychetsky´ and Glogarova´[29], in tilted hexatic phases the dielectric relaxation is mainly contributed by tilt angle phason and bond orientation order (BOO) phason. Strong BOO phason softens the frequency in the vicinity of SmC* to SmF* transition resulting an increase in permittivity and decrease in f_C in SmF* phase. On the other hand, the tilt angle phason mode is accompanied with a decrease in permittivity and an increase in f_C. Thus both these phason modes are present in our compounds. The mid frequency relaxation is associated with BOO phason while the high frequency one is related to tilt angle phason. Two phason modes were also reported before but in SmI* phase [4]. As mentioned earlier, BOO phason was not observed in the lower temperature range of SmF* phase and hence in SmJ* phase of 2F3R due to its suppression by MW mode. In 3F3R also this mode along with MW mode went beyond the range of measurement in SmG* phase. However, in both compounds tilt phason relaxation was observed in SmJ* and SmG* phases in a range of 1-2°C near transition. As representative examples, two dielectric spectra, fitted to modified Cole-Cole relation, one showing SM relaxation in SmA* phase of 2F3R and the other showing MW, BOO and tilt phason relaxations in SmF* phase of 3F3R are presented in **figure 4.15**. As the $\varepsilon^{/}$ and $\varepsilon^{//}$ are related to each other by Kramers-Kronig relations, corresponding Cole-Cole plots are also

depicted in **figure 4.16** to show that the fitting was good. Temperature variations of dielectric increment and critical frequencies of all modes are shown in **figure 4.17** and **4.18** respectively.

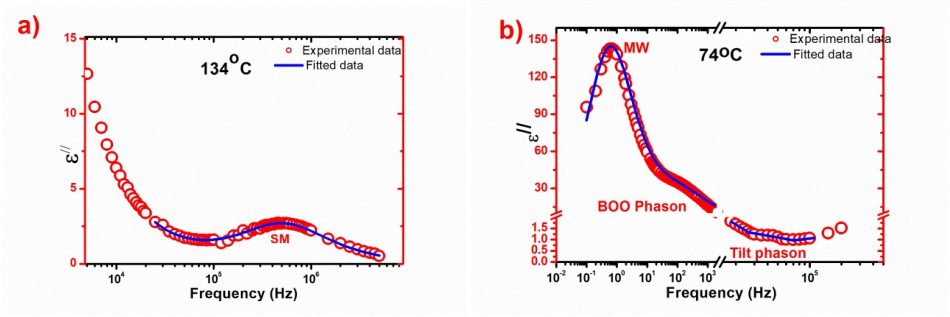

Figure 4.15: Fitted dielectric spectra showing a) SM relaxation in SmA* phase of 2F3R and b) MW, BOO and tilt phason relaxations in SmF* phase of 3F3R. Fitted parameters for a) are $\Delta\varepsilon_{SM}$: 5.25± 0.08, f_{CSM}: 520000± 234, α_{SM}: 0.01± 0.002, σ_{SM} : 2.4E-6 ±3.4E-8 and for b) are $\Delta\varepsilon_{MW}$: 465±1.3, f_{CMW}: 0.6 ±0.02, α_{MW}: 0.03± 0.005, $\Delta\varepsilon_{BOO}$: 108±13, f_{CBOO}: 130 ±5, α_{BOO}: 0.3± 0.004, $\Delta\varepsilon_{tilt\ phason}$: 0.5±0.02, $f_{Ctilt\ phason}$: 40000±102, $\alpha_{tilt\ phason}$: 0.3± 0.02, σ : 1.9E-12 ±2E-14.

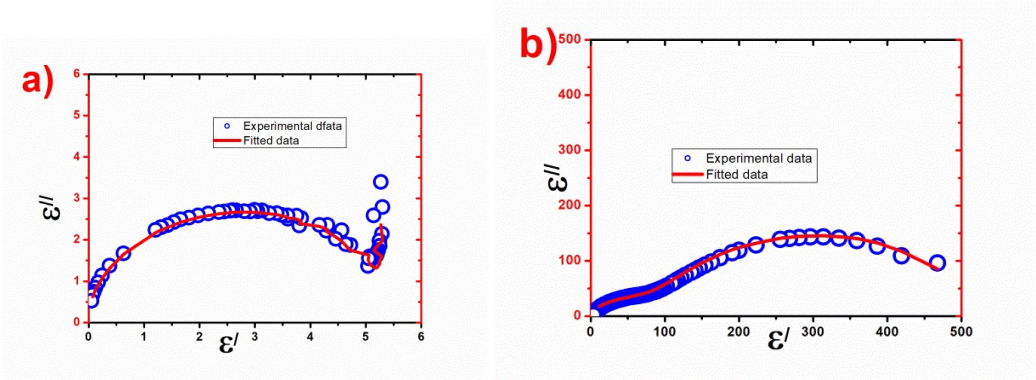

Figure 4.16: Cole-Cole plots of dielectric spectra of a) 2F3R at 134ºC and b) 3F3R at 74ºC

In 2F3R the soft mode dielectric increment and critical frequency showed respectively inverted 'V' shape and 'V' shape temperature variation in the vicinity of SmA*-SmC* transition as expected from generalized Landau model [32]. GM dielectric increments for both compounds were found to increase with temperature which can be

explained if in the expression of free energy density in the generalized Landau model stronger biquadratic coupling between tilt and polarization compared to bilinear one was assumed [32]. This has been discussed in chapter 2.

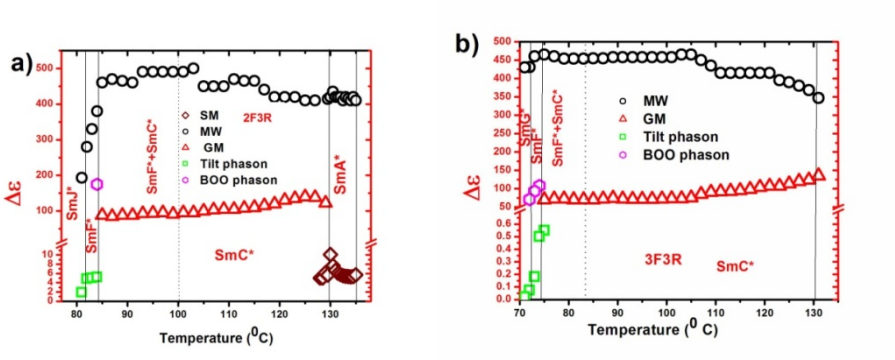

Figure 4.17: Temperature variation of dielectric increments of a) 2F3R and b) 3F3R in all phases.

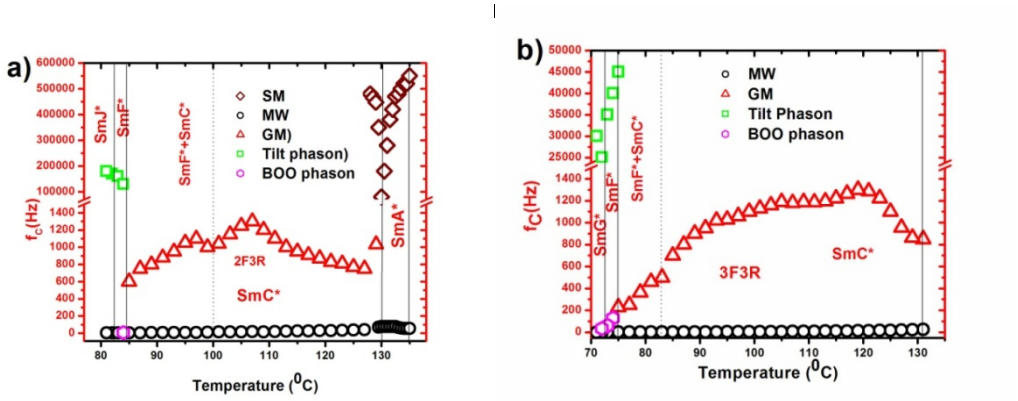

Figure 4.18: Temperature variation of critical frequencies of a) 2F3R and b) 3F3R in all phases.

Though the generalized Landau model does not predict any temperature dependence of GM critical frequency, but according to this theory f_C depends on rotational viscosity (γ_φ), elastic constant (k_φ) and helical pitch (p) as shown in **equation 4.2**:

$$f_c = \frac{k_\varphi q^2}{2\pi\gamma_\varphi} \qquad [4.2]$$

where, $q = \frac{2\pi}{p}$

Since the above parameters are temperature dependent, hence f_C should somehow depend on temperature. Similar temperature variation of GM critical frequency was reported before in 4F3R [28] , 4F5R and 7F3R [chapter 6 and 7].

4.3.6 Spontaneous polarization

The compounds are found to have moderate values of spontaneous polarization, maximum values being ~28 nC/cm^2 in 2F3R and ~35 nC/cm^2 in 3F3R. Temperature variations of the observed spontaneous polarizations (P_S) are shown in **figure 4.19**. The observed P_S data near the onset of ferroelectric phase were fitted to mean field model $\boldsymbol{P_S = P_0(1 - \frac{T}{T_C})^{\beta}}$, where T_C is the SmC*-SmA* or SmC*-Iso transition temperature for 2F3R and 3F3R respectively and β is the critical exponent of secondary order parameter P_S [33]. T_C values did not deviate more than 1° from the observed values and β value was found to be equal to the mean field value for 2nd order transition in 3F3R and 2F3R. In the inset of **figure 4.19** magnified view in the vicinity of SmC* to SmF* phase has been depicted. In both the compounds, P_S decreased in the SmF* phase. In 2F3R at lower temperatures inside SmF* phase, it was too small to measure. In the coexistence phase fluctuation in Ps was observed, more in 2F3R. The rate of change of P_S also increased in the coexistence phase. On cooling SmC*, the tilted hexagonal phase is formed because of coupling between tilt, polarization and bond orientation order. It was predicted theoretically that P_S may decrease or increase in SmF* phase if the coupling constant of the tilt, bond and polarization in the expression of free energy be positive or negative respectively [3,17,29]. Thus in the investigated compounds the coupling

constant is positive. Both increase [17,29] and decrease[21,29,34,35] of P_S in the tilted hexagonal phase had been reported earlier.

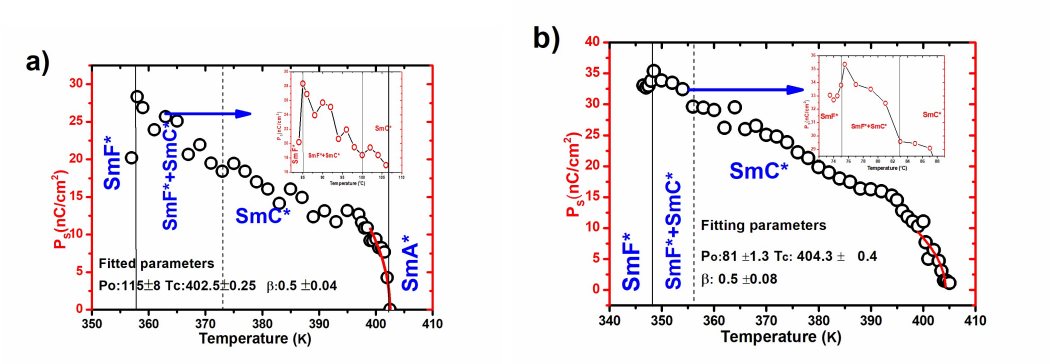

Figure 4.19: Temperature variations of spontaneous polarizations of a) 2F3R and b) 3F3R.

4.3.7 Rotational viscosity:

Rotational viscosity (γ_φ) related to the GM was calculated from the relation given by **equation 4.3**, which was derived from the generalized Landau model [32].

$$\gamma_\varphi = \frac{1}{4\pi\varepsilon_0}\frac{1}{\Delta\varepsilon f_C}\left(\frac{P_S}{\theta}\right)^2 \qquad [4.3]$$

The GM dielectric strength ($\Delta\varepsilon$) and relaxation frequency (f_C) were obtained from the dielectric relaxation study and tilt angles (θ) were obtained from the synchrotron diffraction study. This rotational viscosity can be realized as the hindrance against the azimuthal rotation of the tilted molecular directors about the cone. It greatly influences the electrical response time of the compounds. The temperature variation of γ_φ is shown in **figure 4.20**. It was found to increase very rapidly with decreasing temperature as expected. In SmF* phase highest observed value was nearly 0.92 Pa.s in 2F3R and 0.74 Pa.s in 3F3R. BOO phason mode dielectric data were used for this calculation. In SmC* phase, γ_φ

reduced drastically because of the absence of the BOO ordering, highest value was 0.05 Pa.s in 2F3R and 0.28 Pa.s in 3F3R. Thus γ_φ was found to increase with increasing number of carbons in the chain in SmC* phases.

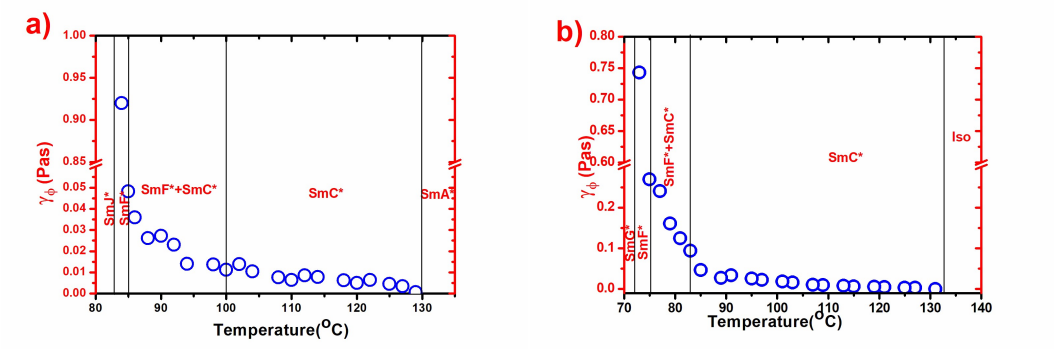

Figure 4.20: Temperature variation of rotational viscosities of a) 2F3R and b) 3F3R.

4.3.8 Electrical response time:

Observed electrical response times (τ) are shown in **figure 4.21**. In SmF* phase τ was found to be much higher than in SmC* phase for both systems which was expected due to the onset of BOO. The response was found be to about 10 times slower in 3F3R implying stronger BOO in it. This was consistent with higher in plane correlation observed from X-ray study. In SmC* phase also the response in 3F3R was much slower because of higher viscosity. In 2F3R highest τ value was 79.6 μs which was faster than any other compounds of the series reported so far - 4F3R (88μs) [28], 5F3R (112μs) and 6F3R (93μs) [chapter 6]. This makes 2F3R a promising material to be used as a dopant in the formulation of fast switching FLC mixtures.

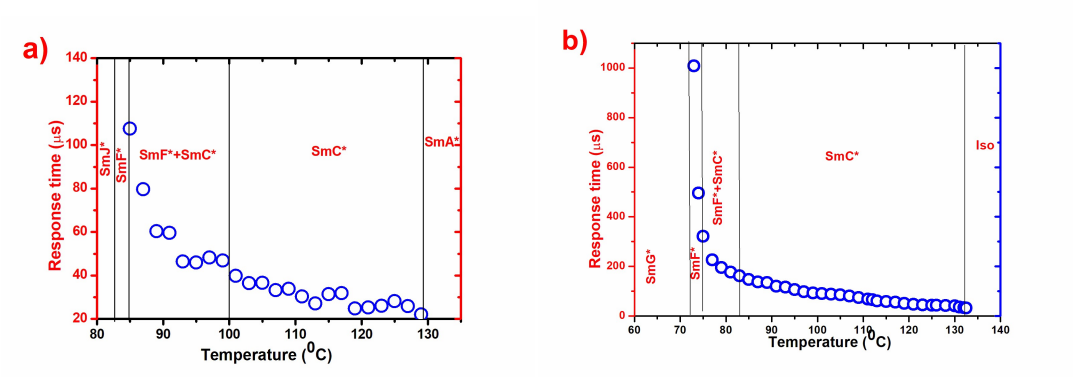

Figure 4.21: Temperature variation of response time of a) 2F3R and b) 3F3R.

4.3.9 Helical Pitch:

As mentioned before, in the optical textures of the tilted smectic phases equidistant parallel lines were observed as a signature of the helicoidal structure. The pitch length (p) of the helix was estimated from the spatial periodicity of the lines and is shown in **figure 4.22**. Of course, pitch determined from this type of measurement is not very accurate. Moreover, the determined pitch may be higher than those of the undisturbed bulk material because of the deformations of the helix due to elastic interactions with the substrate of the cell [7]. However, it was found to agree with theoretical predictions and reported data. Pitch of 3F3R was found to be higher (10μm in SmC*, 12.4μm in SmF*) than in 2F3R (8.5μm in SmC*, 5.8μm in SmF*). In fact, helical pitch lengths of these compounds in SmC* phase is found to be higher than most of the other reported compounds [36–39]. It is worth mentioning that for applicability of FLC in electro-optic devices, the perfect alignment of the compound inside a cell is still a major issue. In this regard compounds like 2F3R and 3F3R, having very long helical pitch, can be useful for SSFLC electro-optic effect [40]. The change in pitch (both increase and decrease) in the hexagonal phase was predicted theoretically [29]. In both

compounds, pitch lengths were found to decrease with temperature but just before the SmC*-SmA* or SmC*-Iso transition it started diverging as predicted in the generalized mean field theory [7,32,39].

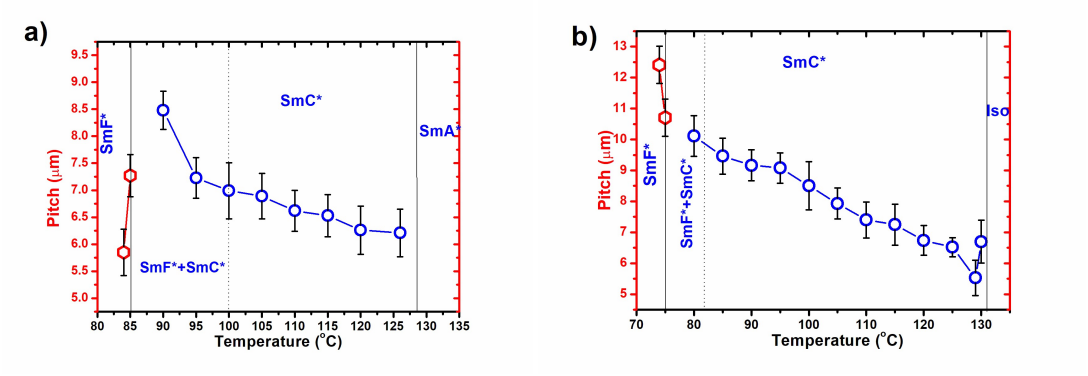

Figure 4.22: Temperature variation of helical pitch of a) 2F3R and b) 3F3R.

4.3.10 Elastic constant:

Modified elastic constant (K_ϕ) was calculated using **equation 4.2** which was derived from the generalized Landau model [28,32,39].
Temperature variation of K_ϕ is shown in **figure 4.23.**

In both compounds K_ϕ was found to be quite high in SmC* phase, ~ 480 pN in 3F3R and ~ 97 pN in 2F3R. In SmC* and SmC phases K_ϕ had been reported to be of the order of 10-20 pN [39,41,42]. However higher elastic constant (~70 pN) was reported even in a diphenylacetylene core nematic compound [43]. In both systems, K_ϕ increased in the coexistence phase, but in SmF* phase K_ϕ decreased in 2F3R (40 pN) while in 3F3R it increased (1957 pN). High pitch values might be responsible for higher K_ϕ.

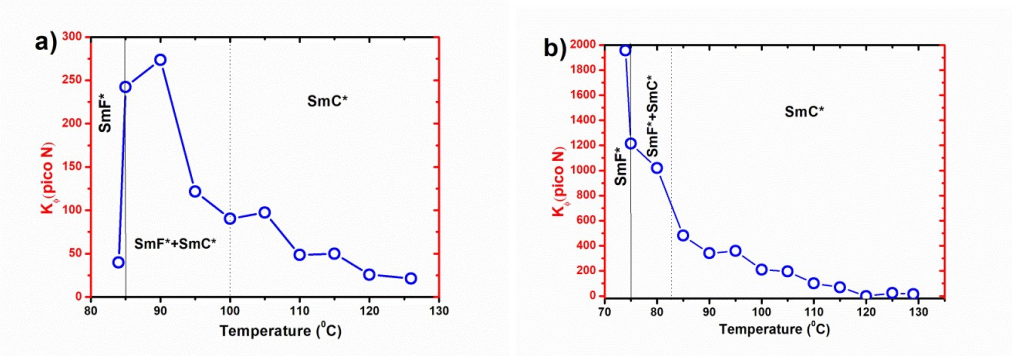

Figure 4.23: Temperature variations of elastic constants of a) 2F3R and b) 3F3R.

4.4 Conclusion

While the lower homologue 1F3R exhibits only orthogonal phases, addition of one or two carbon atoms in its fluorinated chain induces tilted phases in the compounds 2F3R and 3F3R. Unlike the lower variant 1F3R, both 2F3R and 3F3R show quite extended range of ferroelectric SmC* phase. While 2F3R forms a orthogonal SmA* from tilted SmC* on heating, 3F3R melts directly to the isotropic phase. From the chiral lines observed in the optical textures, indexing of satellites peaks found in the intensity profile of the outer diffraction ring, the measured tilt in synchrotron diffraction study, and from dielectric relaxation behaviour it is confirmed that both compounds undergo a transition to hexagonal SmF* phase below SmC* phase. On further cooling soft crystal like hexagonal SmJ* phase is formed in 2F3R, undergoing a change in the tilt direction, but in 3F3R, SmG* phase is formed with no change in tilt direction. A coexistence phase of (SmC*+SmF*) is also observed in a certain temperature range in both the compounds. From the optimisation of molecular structures it is revealed that the length and dipole moment of the higher member are slightly less than the lower member because introduction of additional carbon atom in the fluorinated chain results in

considerable change in the molecular conformation. This gives rise to subtle changes in the intermolecular interactions which play important role in the appearance of different phases in the two compounds. Within certain temperature range in SmC* phase, 2F3R shows negative thermal expansion and effective layer contraction is only around 0.3% as observed in a de Vries type material. Though present in 2F3R, no soft mode relaxation is observed in 3F3R due to the absence of SmA* phase. Both BOO phason and tilt angle phason modes are observed in SmF* phase for the first time. Cooperative relaxation behaviour is also observed in crystal like smectic phases. Long helical pitch and moderate value of spontaneous polarization, observed in both compounds, are expected to be useful in SSFLC based electro-optic devices. Around 80μs switching time in 2F3R, one order less than in 3F3R, makes it more suitable for display applications.

Reference

[1] Ziobro D, Dąbrowski R, Tykarska M, et al. Synthesis and properties of new ferroelectric and antiferroelectric liquid crystals with a biphenylyl benzoate rigid core. Liq. Cryst. 2012;39:1011–1032.

[2] Meyer RB, Liebert L, Strzelecki L, et al. Ferroelectric liquid crystals. Le J. Phys. 1975;36:69–71.

[3] Wróbel S, Mikułko A, Douali R, et al. Ferroelectric behaviour of hexatic phases. Phase Transitions. 2005;78:905–913.

[4] Pandey MB, Dhar R, Dabrowski R. Temperature and bias electric field dependence of dielectric parameters of (S)-(+)-4-(1-methylheptyloxycarbonyl) phenyl-4'-(3-butanoiloxyprop-1-oxy) biphenyl-4'-carboxylate. Philos. Mag. 2008;88:101–119.

[5] Böttcher C, Belle O, Rip A, et al. Theory of Electric Polarization, Vol II. Amsterdam, New York: Elsevier, Scientific Publishing Co; 1973.

[6] Miyasato K, Abe S, Takezoe H, et al. Direct Method with Triangular Waves for Measuring Spontaneous Polarization in Ferroelectric Liquid Crystals. Jpn. J. Appl. Phys. 1983;22:L661–L663.

[7] Dierking I. Textures of Liquid Crystals. wiley-vch. Weinheim: WILEY-VCH; 2003.

[8] Gaussian 09, Revision D.01, M. J. Frisch *et al.* Gaussian, Inc., Wallingford CT, 2013.

[9] Sinha D, Debnath A, Mandal PK. Hexatic and blue phases in a

chiral liquid crystal: Optical polarizing microscopy, synchrotron radiation and dielectric study. Mater. Res. Express. 2014;1:035101.

[10] Gane PAC, Leadbetter AJ, Wrighton PG. Structure and Correlations in Smectic B, F and I Phases. Mol. Cryst. Liq. Cryst.. 1981;66:247–266.

[11] Benattar JJ, Moussa F, Lambert M, et al. Two kinds of two-dimensional order : the SmF and SmI phases. J. Phys. Lettres. 1981;42:67–70.

[12] Demus D, Goodby J, Gray GW, et al. Handbook of Liquid Crystals. New y: WILEY-VCH; 1998.

[13] Mandal P, Paul R, Paul S. Studies on the Mesophases of OOBPD by X-Ray Diffraction Method. Mol. Cryst. Liq. Cryst. 1986;131:299–314.

[14] Urban S, Czub J, Przedmojski J, et al. Dielectric and X-ray Studies of Substances with the Smectic B phase. Mol. Cryst. Liq. Cryst.. 2007;477:87–100.

[15] Osiecka N, Budziak A, Galewski Z, et al. X-ray studies of the smectic B phase of the 4-bromobenzylidene-4′-alkoxyanilines. Phase Transitions. 2012;85:314–321.

[16] Prasad SK, Rao DSS, Chandrasekhar S, et al. Observation of the smectic-C-smectic-I critical point. Phys. Rev. Lett. 1995;74:270–273.

[17] Rychetský I, Pociecha D, Dvořák V, et al. Dielectric behavior of ferroelectric liquid crystals in the vicinity of the transition into the hexatic phase. J. Chem. Phys. 1999;111:1541–1550.

[18] Sirota EB, Pershan PS, Sorensen LB, et al. X-Ray Studies of Tilted Hexatic Phases in Thin Liquid-Crystal Films. Phys. Rev. Lett. 1985;55:2039–2042.

[19] Dierker SB, Pindak R. Dynamics of thin tilted hexatic liquid crystal films. Phys. Rev. Lett. 1987;59:1002–1005.

[20] LEADBETTER AJ, GAUGHAN JP, KELLY B, et al. CHARACTERISATION AND STRUCTURE OF SOME NEW SMECTIC F PHASES. Le J. Phys. Colloq. 1979;40:C3-178-C3-184.

[21] Novotná V, Kašpar M, Hamplová V, et al. Direct transition from the SmA phase to the tilted hexatic phase in liquid crystals with several lactate units. Liq. Cryst. 2004;31:1131–1141.

[22] Szydłowska J, Pociecha D, Górecka E, et al. New series of 4-(4'-octyloxybiphenyl-4-yloxymethyl)benzoic acid derivatives with mesogenic properties. J. Mater. Chem. 1999;9:361–369.

[23] Agra-Kooijman DM, Yoon H, Dey S, et al. Origin of weak layer contraction in de Vries smectic liquid crystals. Phys. Rev. E. 2014;89:032506.

[24] Singh HK, Singh SK, Nandi R, et al. Observation of exceptional 'de Vries-like' properties in a conventional aroylhydrazone based liquid crystal. RSC Adv. 2016;6:57799–57802.

[25] Sreenilayam SP, Rodriguez-Lojo D, Agra-Kooijiman D, et al. De Vries liquid crystals based on a chiral 5-phenylpyrimidine benzoate core with a tri- and tetra-carbosilane backbone tetra-carbosilane backbone. Phys. Rev. Mater. 2018;2:025603-1-025603–025612.

[26] Kumar S. High-resolution x-ray measurements ofthe smectic phases ofterephthal-bis-(4n)-alkylanilines. Phys. Rev. A. 1981;23:3207–3214.

[27] Roberts JC, Kapemaum N, Giesselmann F, et al. Design of liquid crystals with “de Vries-like” properties: Organosiloxane mesogen with a 5-phenylpyrimidine core. J. Am. Chem. Soc. 2008;130:13842–13843.

[28] Goswami D, Sinha D, Debnath A, et al. Molecular and dynamical properties of a perfluorinated liquid crystal with direct transition from ferroelectric SmC* phase to isotropic phase. J. Mol. Liq.. 2013;182:95–101.

[29] I. Rychetsky´, M. Glogarova´ VN. Competition between the chiral smectic-C* and hexatic phases . Phys. Rev. E. 2003;67:021704.

[30] Hasse W, Wróbel S. Relaxation Phenomena: Liquid Crystals, Magnetic Systems, Polymers, High-Tc Superconductors, Metallic Glasses. Berlin: Springer; 2003.

[31] Czerwiec JM, Dąbrowski R, Żurowska M, et al. Dielectric Properties of Ferroelectric Liquid Crystals with Diversified Molecular Structure - ERRATUM. Acta Phys. Pol. A. 2010;117:553–556.

[32] Carlsson T, Žekš B, Filipič C, et al. Theoretical model of the frequency and temperature dependence of the complex dielectric constant of ferroelectric liquid crystals near the smectic-C* — smectic- A phase transition. Phys. Rev. A. 1990;42:877–889.

[33] Lagerwall ST. Ferroelectric and antiferroelectric liquid crystals. Newyork: WILEY-VCH; 1999.

[34] Kolek Ł, Massalska-Arodź M, Paluch M, et al. Dynamics in ferro- and antiferroelectric phases of a liquid crystal with fluorinated molecules as studied by dielectric spectroscopy. Liq. Cryst. 2013;40:1082–1088.

[35] Kašpar M, Hamplová V, Novotná V, et al. New series of ferroelectric liquid crystals with two or three chiral centres exhibiting antiferroelectric and hexatic phases. Liq. Cryst. 2001;28:1203–1209.

[36] Bahr C, Heppke G. Infiuence of electric field on a first-order smectic-A —ferroelectric-smectic-C liquid-crystal phase transition: A field-induced critical point. Phys. Rev. A. 1990;41:4335–4342.

[37] Dey KC, Mandal PK. Effect of multi-walled carbon nanotubes on dielectric and electro-optic properties of a high tilt antiferroelectric liquid crystal. Phase Transitions. 2019;92:302–315.

[38] Zurowska M, Dbrowski R, Dziaduszek J, et al. Influence of alkoxy chain length and fluorosubstitution on mesogenic and spectral properties of high tilted antiferroelectric esters. J. Mater. Chem. 2011;21:2144–2153.

[39] Singh A, Singh S. Application of a generalised thermodynamic model to study of the ferroelectric properties of DOBAMBC and DOBA-1-MPC. Liq. Cryst. 2008;35:727–736.

[40] Kaznacheev A, Pozhidaev E, Rudyak V, et al. Biaxial potential of surface-stabilized ferroelectric liquid crystals. Phys. Rev. E. 2018;97:042703.

[41] Dunn PE, Brown C V, Jones JC. Measurement of the Elastic Constants and Effective Surface Anchoring Energy for a Smectic C

Liquid Crystal. Mol. Cryst. Liq. Cryst. Sci. Technol. Sect. A. Mol. Cryst. Liq. Cryst. 1997;304:371–376.

[42] Boussoualem Y, Ismaili M, Buisine JM, et al. Dielectric and electro-optical properties of a photosensitive liquid crystal. Liq. Cryst. 2009;36:899–905.

[43] Le K V, Aya S, Ogino S, et al. Large Twist Elastic Constant in Diphenylacetylene- Core-Based Liquid Crystals. Mol. Cryst. Liq. Cryst. 2015;614:124–127.

CHAPTER-5

Dielectric and electro-optic properties of two compounds of the biphenyl benzoate cored chiral mesogenic series having only ferroelectric SmC phase*

Part of this work has been published in AIP Conf. Proc.: 1731, 040012-1–040012-3,2016; and in AIP Conf. Proc. 1953, 050012-1–050012-4,2018

5.1 Introduction

In the last two chapters we have discussed about three compounds of the selected series, all having three oligomethylene spacers but different number of carbons in the fluorinated chain. The shortest member 1F3R, having only one fluorine in the chain was found to have only orthogonal phases, with two hexagonal higher order smectic phases SmE* and SmB* along with SmA* phase. As a result of adding more carbon atoms in the fluorinated chain, in the next two higher members, 2F3R and 3F3R, tilted phase were introduced – SmJ*/G*, SmF*, SmC* - along with SmA*. However in the low temperature regime the compounds retained the hexagonal phase structure. In this chapter we report properties of two higher derivatives of the series, with same number of oligomethylene spacers but having more number of carbons in the fluorinated chain, namely (*S*)-(+)-4′-[(3-undecafluoro-hexanoyloxy)prop-1-oxy]biphenyl-4-yl 4-(1-methylheptyloxy)- benzoate (5F3R) and ((S)-(+)-4′-[(3-tridecafluoro-heptanoyloxy) prop-1-oxy]biphenyl-4-yl 4-(1-methylheptyloxy)-benzoate (6F3R) [1]. As an effect of adding fluorine in the chains all the hexagonal or orthogonal phases are eliminated from these compounds. They are found to exhibit only the tilted SmC* phase albeit within a wide temperature range and directly melt into isotropic phase which is not common in FLC compounds. The intermediate member of this series having 4 carbon atoms in its fluorinated chain viz., 4F3R has also been studied by us but not included in this dissertation and is also found to have similar phase behaviour [2]. For displaying only ferroelectric SmC* phase over a wide span of temperature make them promising material to be used as dopant in the preparation of long range ferroelectric liquid crystal mixture. Besides, for having such a typical

phase behaviour, the study of the different dielectric and electro-optic properties of these compounds might be proved to be revealing. Keeping these in mind we discuss detailed dielectric and electro-optic characterisation of these two compounds in this chapter. The molecular structure of 5F3R and 6F3R are shown in **figure 5.1**.

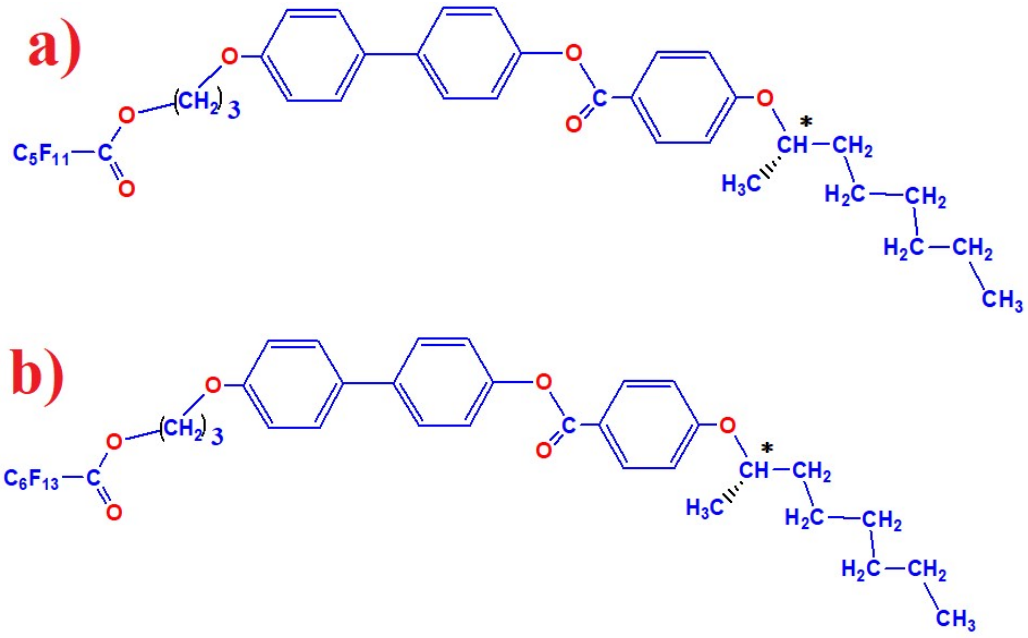

Figure 5.1: Molecular structure of a) 5F3R and b) 6F3R.

5.2 Experimental methods

The phase transition temperatures of the compounds were identified by polarising optical microscopy, using Olympus BX41 polarizing microscope equipped with a CCD camera. A Hioki 3532 50 impedance analyzer was used to perform the frequency dependent dielectric study in the frequency range from 40 Hz to 5 MHz. The dielectric spectra were fitted to the Cole-Cole function [3], modified for the low frequency parasitic effect. Spontaneous polarization was measured by reversal current method [4]. An Agilent 33220A function generator and a Tektronix TDS 2012B storage oscilloscope were used for electro–optic measurements. The response time was measured by measuring the time delay of the occurrence of polarization bump from the applied square

pulse (of frequency 60Hz) edge while monitoring the voltage across a resistor R in series with the cell. Optical tilt of the molecules was determined by electrically switching the sample under a low frequency (10 mHz) square wave and simultaneously observing it under polarizing microscope. The angle of rotation of the sample between two dark states was considered as a measure of double the tilt angle.

To control the temperature, in all experiments a Metller FP90 temperature controller with FP82 hot-stage was used. The detailed procedures of each experiment have been discussed in chapter 2.

5.3 Results and Discussions

5.3.1 The phase behaviour of the compounds

Both the compounds directly melt into SmC* phase from crystalline state and maintain that phase for a wide range of temperature and finally reach the isotropic phase. The phase sequence and the transition temperatures, as observed by POM, dielectric and electro-optic study, are summarised in **table 5.1**.

Table 5.1: Transition temperatures of the compounds. Figures within parentheses denote cooling data.

Compounds	Transition temperatures	ΔT_{SmC^*}
5F3R	Crystal (75ºC) 83°C SmC* 139.5°C isotropic	56.5ºC
6F3R	Crystal (80ºC) 83°C SmC* 146.2°C isotropic	63.2ºC

Both the compounds melt from the crystalline state at the same temperature, although at much higher temperature compared to the two lower homologues. But 6F3R has a wider span of SmC* phase than that of 5F3R. Thermal ranges of both compounds are much higher than its

lower derivatives 2F3R and 3F3R, as discussed in chapter 4. In both compounds super-cooling effect was observed. In 5F3R the SmC* phase extended up to 75ºC and in 6F3R it extended up to 80ºC.

5.3.2 Optimised geometry

To investigate the structural-property relationship, the molecular structures of the compounds were optimised, applying Hartree-Fock method and using 3-21G basis set in a commercial package [5]. The optimised structures are shown in **figure 5.2**. The optimised length of 5F3R and 6F3R were found to be 35.19Å and 36.46 Å respectively. This is larger than the lower derivatives 1F3R, 2F3R and 3F3R as expected. Dipole moments (μ) of 5F3R and 6F3R are respectively found to be 6.53 D (-5.05, 0.39, 4.12) and 6.52D (-5.04, 0.65, 4.08) where the components of dipole moments along the three coordinate axes are shown within brackets.

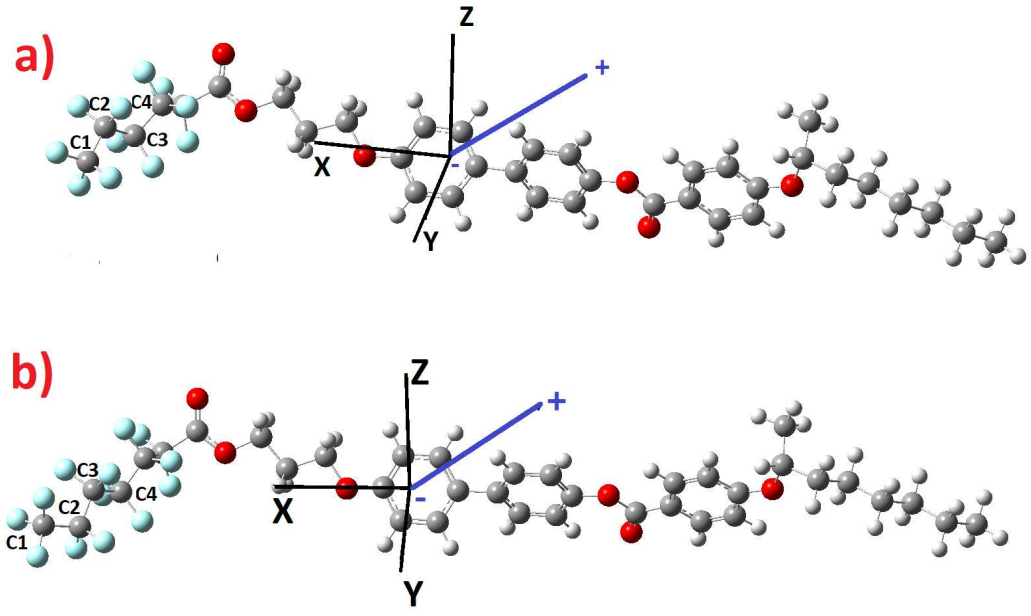

Figure 5.2: Optimised geometry of a) 5F3R and b) 6F3R.

The dipole moments of these molecules are found to be larger than 3F3R, probably for the presence of extra fluorine in the chain. However,

μ is still smaller than that of 2F3R, which may be due to the twist of the fluorinated chain at the carboxylic group by an angle ~85⁰ after the addition of extra fluorine. Same effect was observed in 3F3R, as discussed in chapter 4. It is worth noticing that the direction of dipole moment of 5F3R and 6F3R had rotated almost by 90⁰ along Y axis, in comparison to that of 2F3R and 3F3R. The absolute values of the dipole moments remain almost same for 5F3R and 6F3R, but the component of μ along x axis (parallel to the molecular director) is found to increase for 6F3R, most likely for the presence of extra fluorine in the chain. Conformation of the fluorinated chains of the two molecules has also changed slightly. For example the torsion angle, between the last four carbons in the chain (denoted as C1,C2, C3 and C4 in **figure 5.2**) of 6F3R is found to be larger by a fraction of a degree than that of 5F3R.

5.3.3 Polarized optical microscopy (POM) study

The optical textures of 5F3R are shown in **figure 5.3**, similar textures were observed in 6F3R. The parallel lines associated with the chirality of the molecules [6] are observed in the texture but more prominently in 5F3R. However no major domains can be seen in the textures of both the compounds, rather a poorly developed trace of broken fan shape texture is displayed. This type of textures were reported before in the SmC* phase of other members of same series having direct transition from SmC* to isotropic phase [1].

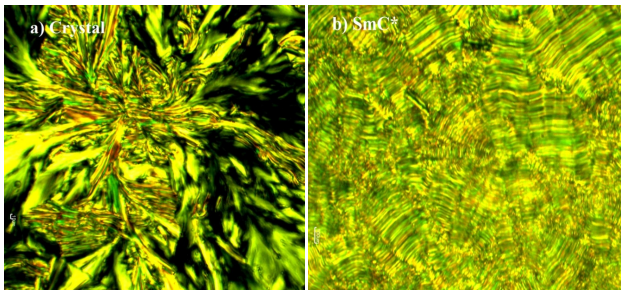

Figure 5.3: Optical texture of 5F3R at a) Crystalline state b) SmC* phase.

5.3.4 Frequency dependent dielectric study

The dielectric data were taken in cooling cycle in homogeneous cells. It has already been discussed in chapter 2 that the dielectric relaxation in SmC* phase is usually dominated by two collective modes. One is Goldstone Mode (GM) which is originated due to phase fluctuation of the azimuthal orientation of the directors and the other is soft mode (SM) which is related with the amplitude fluctuation of the tilt of the molecular directors [7,8]. But in 5F3R only one mode of relaxation was observed throughout SmC* phase. This mode could be suppressed by applying a suitable DC bias perpendicular to the smectic layer. The critical frequency (f_C) and dielectric increment ($\Delta\varepsilon$) of this relaxation was found to increase with temperature. The highest value of f_C and $\Delta\varepsilon$ was recorded to be 1600Hz and 143.5 respectively. From the bias dependency and range of critical frequency and high dielectric increment it can be inferred that this mode is due to GM relaxation. On the other hand, in 6F3R two modes of relaxations were observed throughout the SmC* phase. The lower frequency mode, whose critical frequency and dielectric increment varied with temperature from 1.4-44 Hz and 470-570 respectively, was observed even in the crystalline and isotropic phase. This mode was also observed to be suppressed under DC bias. Thus it is related with Maxwell-Wagner (MW) relaxation. The mechanism of this relaxation has been discussed in detail in chapter 2. This mode was also observed in 1F3R, 2F3R and 3F3R (chapter 1 and 2) and also in some other compounds (2F6R, 4F6R, 6F6R) of same homologous series [9]. However, MW mode was not observed in 5F3R. As, this mode arises due to accumulation of charge in between liquid crystal layer and polymer layer inside the dielectric cell [7], hence the absence of this mode in 5F3R may be related with the purity or the conductivity of the

compound, since same type of cell was used in measurement. The critical frequency (172 Hz-1850 Hz) and dielectric increment (65-166) of the second mode of relaxation were observed to increase with temperature. It was also got suppressed by DC bias. This mode was identified as the GM mode of relaxation. Two representative fitted spectra of both the compounds are shown in **figure 5.4** and. Corresponding Cole-Cole plots are shown in **figure 5.5**. The variation of critical frequency and dielectric increment with temperature are shown in **figure 5.6** and **5.7** respectively. Values of α signify that GM of both compounds deviate significantly from ideal Debye type process.

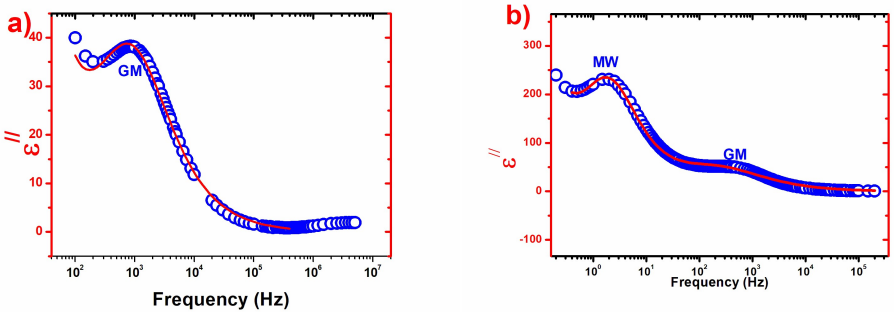

Figure 5.4: Fitted dielectric spectra showing a) GM in 5F3R (95ºC) and b) both MW and GM in 6F3R (86ºC). Fitted parameters for a) are $\Delta\varepsilon_{GM}$: 94± 3.2 , f_{CGM}: 870± 13, α_{GM}: 0.19± 0.003, σ_{GM} : 1.2E-7 ±1.4E-9 and for b) are $\Delta\varepsilon_{MW}$: 495±5, f_{CMW}: 1.9 ±0.5, α_{MW}: 0.1± 0.02, $\Delta\varepsilon_{GM}$: 165±4, f_{CGM}: 230 ±1, α_{GM}: 0.3± 0.01, σ_{GM}: 2.2E-9 ±1E-10.

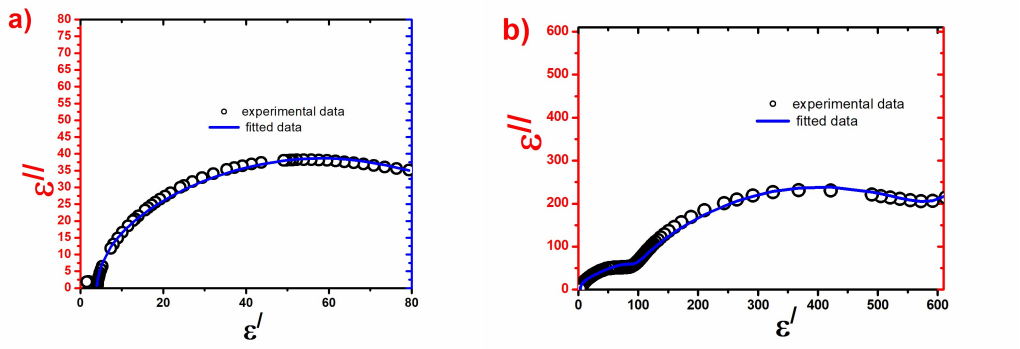

Figure 5.5: Fitted Cole-Cole plot of 5F3R (95ºC) and b) 6F3R (86ºC)

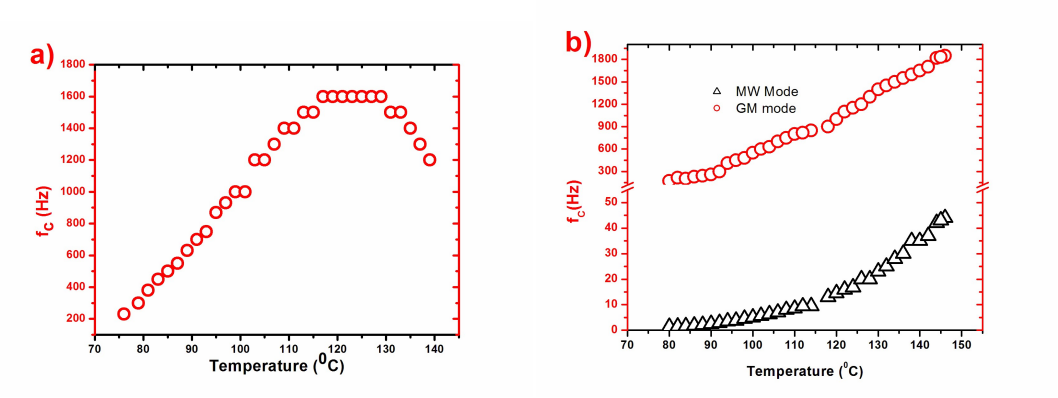

Figure 5.6: temperature dependence of critical frequency of a) 5F3R and b) 6F3R.

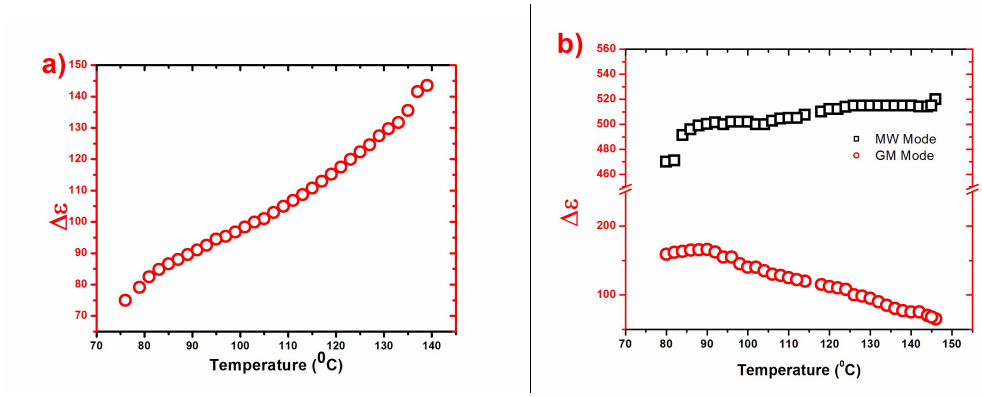

Figure 5.7: Temperature variation of dielectric increment of a) 5F3R and b) 6F3R.

In both compounds the dielectric increment of GM relaxation increased with temperature. As discussed in chapter 2 and 4, from **figure 5.7** it is evident that both compounds have strong biquadratic coupling between the tilt and the polarization in the expression of Landau free energy over the bilinear one, but for 5F3R it is stronger. Highest value of Δε of 5F3R (~143.7) is found to increase slightly from that of 2F3R (~140) and 3F3R (~135). For 6F3R it increases quite significantly (~166). Thus, it can be hypothesized that GM mode Δε of this homologous series is found to increase with number of fluorines in the chain, except for 3F3R.

The GM critical frequency of both the compounds also found to increase with temperature. It was shown in chapter 4 that the critical frequency of GM relaxation depends on the modified elastic constant, helical pitch, rotational viscosity of azimuthal motion and wave vector of the compound [2]. As these parameters are temperature dependent, so it can be deduced that f_C should also somehow depend on temperature. These type of temperature dependency of f_C was also observed in 2F3R and 3F3R as discussed in chapter 4, in some other compounds of the same homologous series [2] and also in some FLCs with different structures[10]. The highest value of GM f_C in SmC* phase of 6F3R (1850Hz) is found to be higher than that of 5F3R (1600Hz), which is again higher than that of 2F3R (1300Hz) and 3F3R (1285 Hz). Thus GM mode f_C also found to increase with increasing number of fluorine in the chain of this homologous series, except for 3F3R.

Soft mode was not observed in any of the compounds. As discussed in chapter 3, SM was not observed previously in absence of any orthogonal to tilted phase transition and the possible reason was discussed there. The present compounds (5F3R and 6F3R) exhibit only tilted SmC* phase and directly melt into isotropic phase, without any orthogonal phase in between. Thus absence of soft mode relaxation is in conformity with our previous results.

Using Landau model, Blinc and Zeks [11] for the first time proposed the idea of soft mode at the SmA*−SmC* phase transition for the case of a modulated structure. It was later modified by Carlsson et al. [12].They described the phase transition with reference to two order parameters, namely, one primary order parameter (two-component tilt vector) and one secondary order parameter (two-component in-plane polarization). SmA* to SmC* transition is a second order phase transition. During this

transition the continuous symmetry group D_∞ of SmA* breaks loose into C_2 symmetry of SmC*. Two characteristic modes are observed during this transition. The soft mode is a symmetry breaking mode. When the transition is attained from a higher temperature it slows down (softens).On the other hand the Goldstone mode attempts to re-establish the broken symmetry. Consequently near SmA* to SmC* transition the soft mode splits into the phase (GM) and amplitude (SM) modes. As shown by Clark and Lagerwall [13], in most of the cases SmA* to SmC* phase transition is a second order phase transition. However, during N* to SmC* or istropic to SmC* transition, the tilted smectic layers have to form directly at the transition. So, theoretically no soft mode is expected which is confirmed by experiment. These kinds of transitions in most cases are of first order. In the present compounds as well, SmC* phase is achieved directly from isotropic phase, and it can be seen from the clearing point enthalpy [1] and temperature dependence of both the primary and secondary order parameters discussed below that the phase transition is first order.

Sometimes a residual higher frequency mode termed as domain mode can be observed under a strong bias field [14,15]. Usually compounds having Ps > 50 nC/cm^2 are found to exhibit this mode. No such mode is observed in the present compounds. This may be due to less Ps of the present compounds (see below). It is also not apparent whether presence of SM in SmC* and SmA* phases is a precondition for observing the domain mode, because in all the above referred compounds SM was present in both the phases.

5.3.5 Spontaneous polarization (P_S)

Both 5F3R and 6F3R showed moderate value of spontaneous polarization. The super-cooling effect was observed even in P_S measurement. The highest P_S value in SmC* phase were found to be around 39 nC/cm^2 and 40.5 nC/cm^2 in 5F3R and 6F3R respectively which are higher than what was found for 2F3R (28 nC/cm^2) and 3F3R (35 nC/cm^2) in SmC* phase. This is probably an effect of additional fluorine atoms in the chain which results in the increase of molecular dipole moment (only exception is 2F3R as discussed before) and hence the spontaneous polarization. The temperature variations of spontaneous polarization (P_S) of the compounds are shown in **figure 5.8**. The observed data were fitted to mean field model equation $P_S = P_0(1 - \frac{T}{T_C})^{\beta}$, near SmC* to isotropic transition (T_C) [16]. In the expression β is the critical exponent of secondary order parameter P_S. The fitted values of T_C matched nicely with the observed values, it deviated only by 1°C. However, unlike the compounds discussed in chapter four, here β values are found to deviate significantly from the mean field value (0.5) for 2nd order transition for both compounds. However this nature was observed in another compound (4F3R) of the same homologous series [2]. It can be noted here that for 5F3R the fitted parameters presented here differ from the published paper, as here we have fitted the data only near T_C. It is worth noticing that the change in enthalpy values at SmC* to isotropic transition of 5F3R and 6F3R was quoted as 7.47 and 7.92 kJ/mole respectively in the reference [1]. This also indicates that the corresponding transition is not second order rather points to first order.

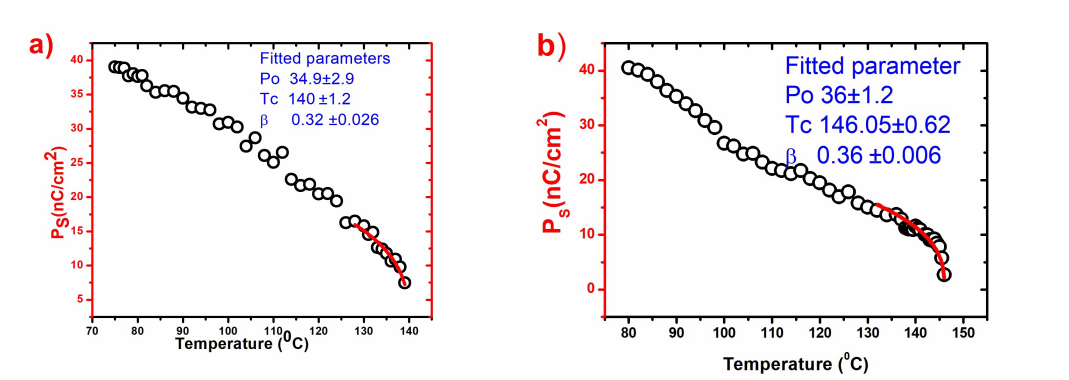

Figure 5.8: Temperature variation of spontaneous polarization of a) 5F3R and b) 6F3R. Fitted curves are also shown as discussed in text.

5.3.6 Electrical response time (τ)

As discussed in the preceding chapters, the electrical response time (τ) is a significant parameter for FLCs. The response time of FLCs are typically found to be smaller than that of nematics by a few orders, which make FLCs more useful for high-speed display applications.

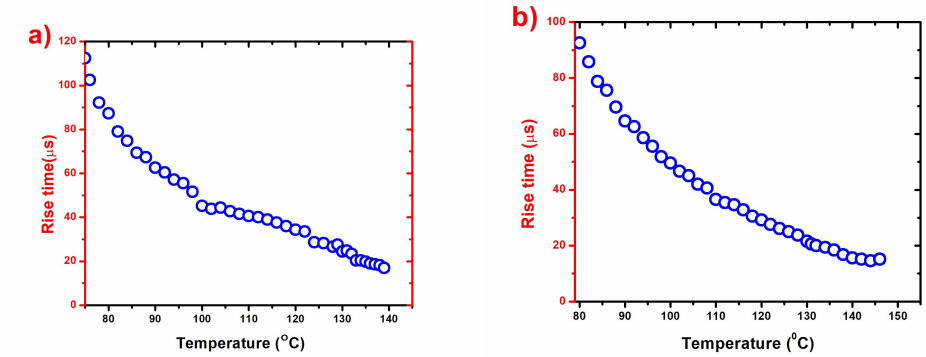

Figure 5.9: Temperature variation of response time of a) 5F3R and b) 6F3R.

The compounds show very fast switching, highest value of response time τ under a square pulse is found to be around 112 and 93 μs in 5F3R and 6F3R respectively. These are expected since the compounds possess

moderately large Ps and low rotational viscosity, described below. These values are marginally larger than what was observed in 2F3R (79.6 μs) [Chapter 4] and 4F3R (88μs) [2], but smaller than that of 3F3R (~200 μs) [Chapter 4]. However, τ value at the melting point (83ºC) was found to be ~ 79 μs for both the compounds. Response time in lower micro second range makes the compounds promising to be used in fabrication of sharp response FLC mixtures.

Both compounds show super-cooling effect also in response time measurement which signify that SmC* phase really extends to lower temperature region while cooling. The temperature variations of τ are shown in **figure 5.9**. It is found to decrease monotonically with increasing temperature which is a result of faster decrease of rotational viscosity compared to spontaneous polarization which makes the rotation of the molecules easier around the tilt cone in smectic plane.

It may be of interest to see the variation of response time with molecular cores and fluorination. In a biphenyl cored non-fluorinated FLC with ester group on both sides of core response time was reported to be of the order of a few millisecond [17], response time was found to vary between 150 and 600 μs for the compound obtained by adding of one more mono-fluorinated phenyl group in the above core structure [18], in a terphenyl based non-fluorinated compound with similar core structure as of 5F3R reported response time was around 3 μs [19].

5.3.7 Optical tilt angle

The tilt angle describes the angle between the core of the molecule and the smectic layer normal [1]. Moreover, as discussed in chapter 2, tilt angle of the molecules is the primary order parameter of the SmC* phase while the spontaneous polarization is the secondary parameter [20–22].

Tilt angles (θ) of the compounds were measured optically and are represented in **figure 5.10**.

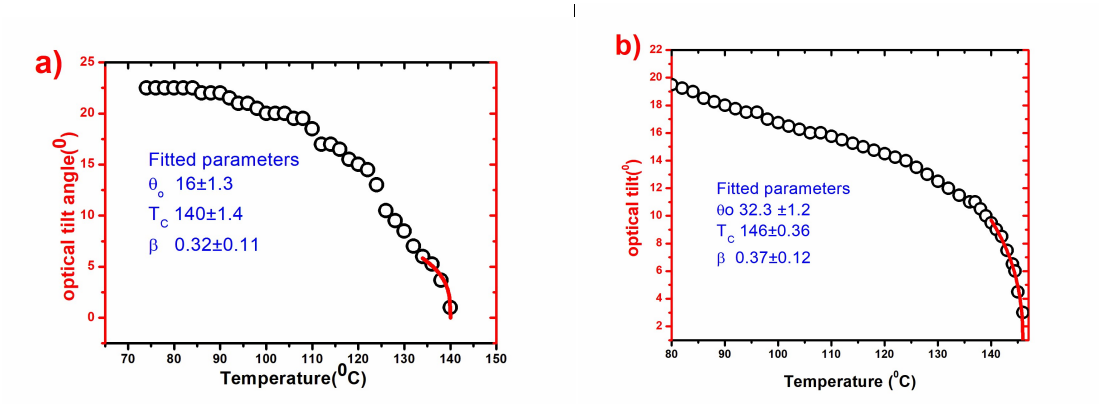

Figure 5.10: Temperature variation of optical tilt angle of a) 5F3R and b) 6F3R.

To investigate the nature of phase transition, the tilt angle data was fitted with the mean field model equation $\theta = \theta_0(1 - \frac{T}{T_C})^{\beta}$, near SmC* to isotropic transition. Fitted T_C values are found to match with measured data. The β values are found to deviate again from its ideal 2nd order phase transition value and matched with the values obtained from P_S data. Highest value of the tilt angle of 5F3R is found to be exactly equal to the ideal value of tilt (22.5º) required for surface stabilised ferroelectric liquid crystal display (SSFLCD) [23–25]. Though this tilt is marginally less in 6F3R (19.5º), yet it is quite close to the ideal value.

5.3.8 Rotational viscosity (γ_φ)

The Rotational viscosity in SmC* phase which is associated with the rotation of the molecular director around the SmC* cone has been calculated by the following equation obtained from generalized Landau model [12]

$$\gamma_\varphi = \frac{1}{4\pi\varepsilon_0}\frac{1}{\Delta\varepsilon f_C}\left(\frac{P_S}{\theta}\right)^2 \qquad [5.1]$$

Here, $\Delta\varepsilon$ and f_C were taken from the dielectric data; P_S and θ were obtained from electro-optic measurements as described before. γ_φ of 6F3R is found to be larger than that of 5F3R , 2F3R and 3F3R which might be because of higher spontaneous polarisation of the compound. Temperature variations of γ_φ for both compounds are shown in **figure 5.11**. Rotational viscosity is found to decrease with temperature in both compounds as expected. It is observed that the rotational viscosity falls to one eighth of its value near Cr-SmC* transition within a span of 20°C. However, in 5F3R it shows an increasing trend just before the transition to isotropic phase which may be due to pre-transitional effect. Similar diverging trend has been reported in some other members of this series such as in 4F4R, 4F5R and 7F3R described in chapter 6 and 7, and also in some other systems[26]. Further, highest values of γ_Φ found in these compounds are almost one-fourth the value observed in the ferroelectric phase of a partially fluorinated terphenyl based AFLC compound [27]. Thus rotational viscosity may be reduced substantially by introducing flexibility in the molecular structure. Moreover, it is found to conform the Arrhenius relationship: $\gamma_\varphi \propto \exp(E_a/k_\beta T)$, where E_a is the activation energy for the molecular rotation on the cone under the application of the AC field on the FLC material, and k_β is the Boltzmann constant. Activation energy was calculated from a linear least squares fit of the plot of ln γ_Φ versus inverse temperature, using only those data upto which γ_Φ followed the decreasing trend. Activation energy is found to be 4.71 kJ mol^{-1} and 4.68 kj mol^{-1} for 5F3R and 6F3R respectively.

The rotational viscosity in SmC* may also be measured only with the electro-optic parameters using **equation 5.1** [28].

$$\gamma_\varphi = \tau P_S E \qquad \textbf{[5.1]}$$

where, τ is the response time P_S is spontaneous polarization and E is the applied field. To compare the value obtained both from dielectric and electro-optic data we have plotted them together in **figure 5.12**. At lowest temperature the value matched perfectly. At higher temperature, γ_φ calculated by electro-optic parameters were found to be marginally larger (effect is more in 5F3R) than that calculated by dielectric parameters.

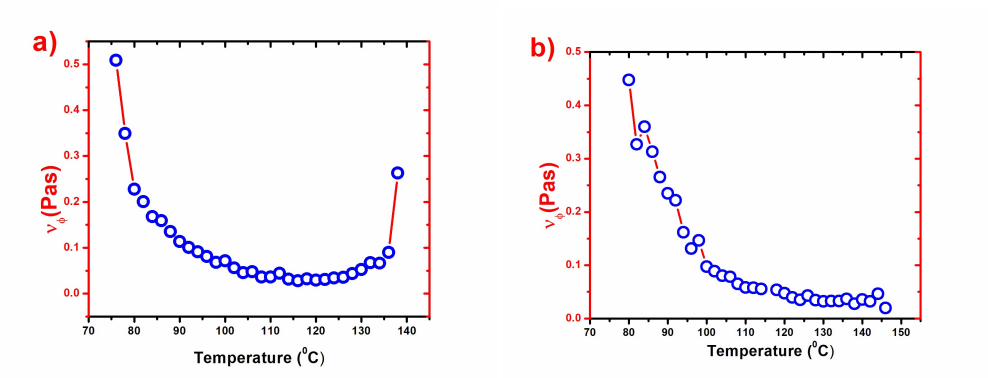

Figure 5.11: Temperature variation of rotational viscosity of a) 5F3R and b) 6F3R.

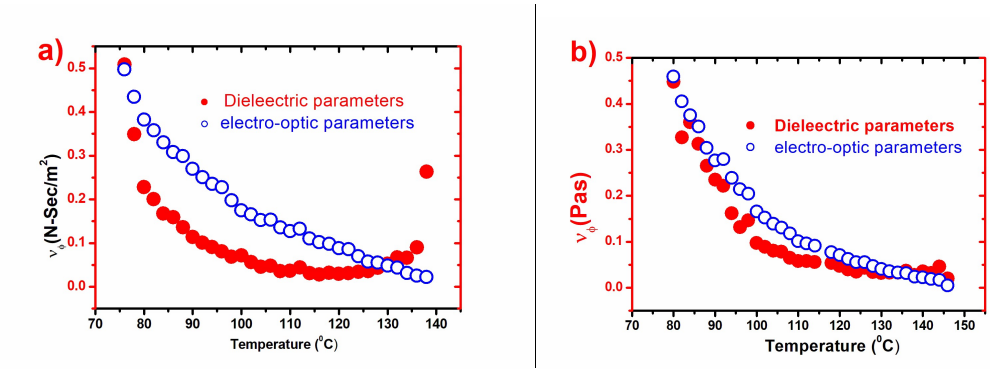

Figure 5.12: Temperature variation of rotational viscosity measured both by electro-optic and dielectric methods of a) 5F3R and b) 6F3R.

5.4 Conclusion

Unlike their lower derivatives, the compounds 5F3R and 6F3R are found to have only SmC* phase over a wide range of temperature and then melt into isotropic phase without going through the orthogonal

SmA* phase. Temperature dependences of both primary (tilt) and secondary order parameter (spontaneous polarization) near SmC* to isotropic phase transition suggest that the transition deviate significantly from second order. Goldstone mode relaxation is observed in both the compounds with quite high dielectric increments. Maxwell Wagner mode of relaxation is observed only in 6F3R. Moreover, soft mode relaxation is not observed in any of the compounds as a consequence of the absence of any tilted to orthogonal phase transition. It is thus concluded that soft mode is possible to observe only when SmA*-SmC* transition is present in a compound. The compounds exhibit moderate values of spontaneous polarisation. Maximum value of the optical tilt angle of the molecules is exactly 22.5^{o} in 5F3R and close to that in 6F3R. Response time is found to be around 100 micro second. Important display parameters of the materials are thus close to their optimum values required for SSFLC display devices. The two compounds are therefore expected to be useful for formulation of FLC mixtures suitable for display and other applications.

Reference

[1] Ziobro D, Dąbrowski R, Tykarska M, et al. Synthesis and properties of new ferroelectric and antiferroelectric liquid crystals with a biphenylyl benzoate rigid core. Liq. Cryst. 2012;39:1011–1032.

[2] Goswami D, Sinha D, Debnath A, et al. Molecular and dynamical properties of a perfluorinated liquid crystal with direct transition from ferroelectric SmC* phase to isotropic phase. J. Mol. Liq. 2013;182:95–101.

[3] Böttcher C, Belle O, Rip A, et al. Theory of Electric Polarization, Vol II. Amsterdam, New York: Elsevier, Scientific Publishing Co; 1973.

[4] Miyasato K, Abe S, Takezoe H, et al. Direct Method with Triangular Waves for Measuring Spontaneous Polarization in Ferroelectric Liquid Crystals. Jpn. J. Appl. Phys. 1983;22:L661–L663.

[5] Gaussian 09, Revision D.01, M. J. Frisch *et al.* Gaussian, Inc., Wallingford CT, 2013.

[6] Dierking I. Textures of Liquid Crystals. wiley-vch. Weinheim: WILEY-VCH; 2003.

[7] Hasse W, Wróbel S. Relaxation Phenomena: Liquid Crystals, Magnetic Systems, Polymers, High-Tc Superconductors, Metallic Glasses Berlin: Springer; 2003.

[8] Gouda F. Dielectric relaxation spectroscopy of chiral smectic liquid crystals. Chalmers University of Technology,Goteberg; 1992.

[9] Czerwiec JM, Dąbrowski R, Żurowska M, et al. Dielectric Properties of Ferroelectric Liquid Crystals with Diversified Molecular Structure - ERRATUM. Acta Phys. Pol. A 2010;117:553–556.

[10] Mikułko A, Arora P, Glushchenko A, et al. Complementary studies of BaTiO 3 nanoparticles suspended in a ferroelectric liquid-crystalline mixture. Europhys. Lett. 2009;87:27009.

[11] Blinc R, Zekes B. Dynamics of helicoidal ferroelectric smectic-C liquid crystals. Phys. Rev. A. 1978;18:740–745.

[12] Carlsson T, Žekš B, Filipič C, et al. Theoretical model of the frequency and temperature dependence of the complex dielectric constant of ferroelectric liquid crystals near the smectic-C* — smectic- A phase transition. Phys. Rev. A 1990;42:877–889.

[13] Clark NA, Lagerwall S. Introduction to ferroelectric liquid crystals, Ferroelectric Liquid Crystals Principles, Properties and Applications. Goodby J, Blinc R, Clark NA, et al., editors. Philadelphia: Gordon and Breach; 1991.

[14] Marzec M, Haase W, Jakob E, et al. The existence of four dielectric modes in the planar oriented S* c phase of a fluorinated substance. Liq. Cryst. 1993;14:1967–1976.

[15] Wróbel S, Cohen G, Davidov D, et al. Dielectric, electro optic and X-ray studies of a room temperature ferroelectric mixture. Ferroelectrics 1995;166:211–222.

[16] Lagerwall ST. Ferroelectric and antiferroelectric liquid crystals. Newyork: WILEY-VCH; 1999.

[17] Eidenschink R, Geelhaar T, Merck E, et al. Parameter characteristics of a ferroelectric liquid crystal with polarization sign reversal. Ferroelectrics 1988;84:167–181.

[18] Nayek P, Ghosh S, Roy S, et al. Electro-optic and dielectric investigations of a perfluorinated compound showing orthoconic antiferroelectric liquid crystal. J. Mol. Liq. 2012;175:91–96.

[19] Srivastava AK, Dhar R, Agrawal VK, et al. Switching and electrical properties of ferro- and antiferroelectric phases of MOPB(H)PBC. Liq. Cryst. 2008;35:1101–1108.

[20] Collings P, Hird M. Introduction to liquid crystals Chemistry and Physics. Gray G, Goodby J, Fakuda A, editors. London: Taylor & Francis; 1997.

[21] Priestley E., Wojtowicz PJ, Sheng P. INTRODUCTION TO LIQUID CRYSTALS. London: Plenum Press; 1974.

[22] Demus D, Goodby J, Gray GW, et al. Handbook of Liquid Crystals. New y: WILEY-VCH; 1998.

[23] Węgłowska D, Perkowski P, Piecek W, et al. The effect of the octan-3-yloxy and the octan-2-yloxy chiral moieties on the mesomorphic properties of ferroelectric liquid crystals. RSC Adv. 2015;5:81003–81012.

[24] Debnath A, Mandal PK, Węglowska D, et al. Induction of a room temperature ferroelectric SmC* phase in binary mixtures with moderate spontaneous polarization and sub-millisecond switching time. RSC Adv. 2016;6:84369–84378.

[25] Hird M. Ferroelectricity in Liquid Crystals and Its Applications.

Liq. Cryst. 2011;38:1467–1493.

[26] Pirkl S, Glogarová M. Ferroelectric liquid crystals with high spontaneous polarization. In: Lallart M, editor. Ferroelectr. - Phys. Eff. Croatia: InTech; 2011. p. 407–428.

[27] Haldar S, Dey KC, Sinha D, et al. X-ray diffraction and dielectric spectroscopy studies on a partially fluorinated ferroelectric liquid crystal from the family of terphenyl esters. Liq. Cryst. 2012;39:1196–1203.

[28] Pozhidaev E, Osipov M, Chigrinov V, et al. Rotational viscosity of the smectic C* phase of ferroelectric liquid crystals. Sov Phys JETP. 1988;94:125–132.

CHAPTER-6

Effect of oligomethylene spacers on the dielectric and electro-optic properties of–two biphenyl benzoate cored chiral mesogens

Part of this work has been published in Liquid Crystals, Vol: 43, pp1548-1549,2016.

6.1 Introduction

The compounds of the chiral mesogenic series that have been discussed so far in this dissertation, all have three oligomethylene spacers in their fluorinated chain. In this chapter we are presenting the dielectric and electro-optic properties of two compounds of the same series, namely **(***S***)**-(+)- 4′ - [(4 – nonafluoro-pentanoyloxy)but-1-oxy] biphenyl-4-yl 4-(1-methylheptyloxy)-benzoate (4F4R), **(***S***)**-(+)-4′-[(5-nonafluoro-pentanoyloxy)pent-1-oxy]biphenyl-4-yl 4-(1-methyl-heptyloxy)benzoate (4F5R) [1]. Both compounds have four carbons in their fluorinated chain and unlike the other compounds included in this thesis, 4F4R and 4F5R have four and five numbers of oligomethylene spacers in their chains respectively. Hence, along with fluorination, the effect of additional oligomethylene spacers on the dielectric and electro-optic properties of the compounds of this homologous series can also be explored by investigating the properties of these two compounds. Like the compounds discussed in the last two chapters, 4F4R and 4F5R also exhibit ferroelectric SmC* phase for a quite extended temperature range and following the trend of 3F3R (discussed in chapter 4), 5F3R and 6F3R (discussed in chapter 5), these two compounds also directly melt in to isotropic phase from SmC* phase. Thus their dielectric and electro-optic parameters can be useful from application perspective. The molecular structures of the compounds are shown in **figure 6.1**.

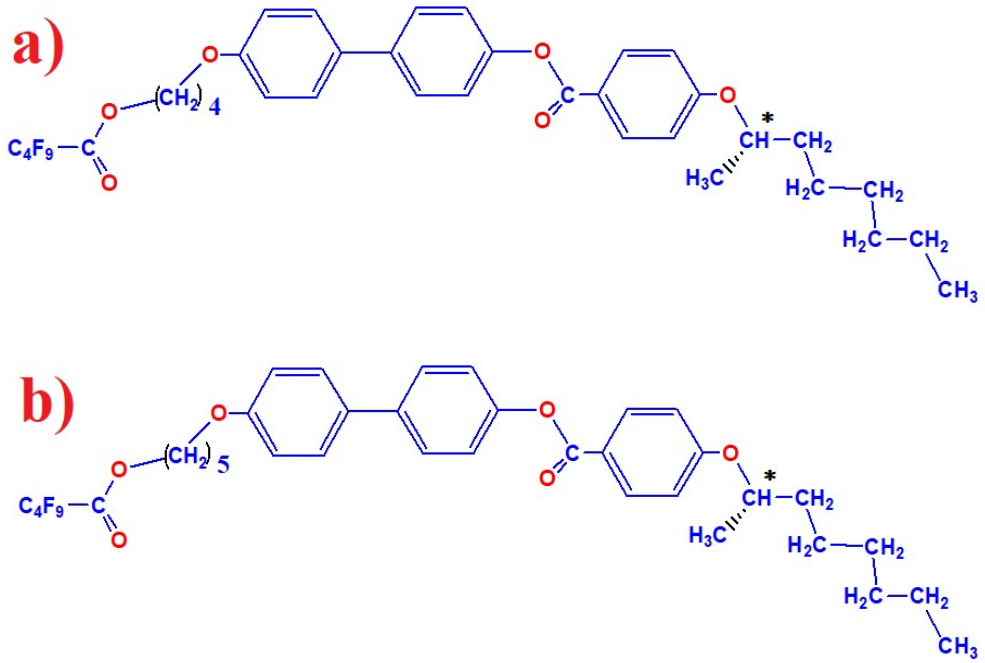

Figure 6.1: the molecular structures of a) 4F4R and b) 4F5R.

6.2 Experimental methods

Dielectric and electro-optic measurements were performed by taking the compounds inside a dielectric cell with low resistivity (about 20 Ω/□) indium tin oxide (ITO) coated electrodes and 8μm cell gap. The transition temperatures of the compounds were identified by polarising optical microscopy, using Olympus BX41 polarizing microscope equipped with a CCD camera. Complex dielectric permittivity was measured using a Hioki 3532 50 LCR meter in the frequency range from 40 Hz to 5 MHz. Observed dielectric spectra were fitted to the modified Cole–Cole function [2,3]. Spontaneous polarizations (P_S) were measured by reversal current method [4] for which an ac triangular voltage of 30V amplitude was applied as input from an Agilent 33220A function generator. The voltage drop across a resistor was measured with the help of an storage oscilloscope (Tektronix TDS 2012B) as a function of time. The electrical response time was measured by measuring the time delay of occurrence of polarization bump from the applied square pulse (of

frequency 60Hz) edge while monitoring the voltage across the same resistor in series with the cell. Optical tilt of molecules in smectic layers was determined by electrically switching the sample under a low frequency (10 mHz) square wave and simultaneously observing it under polarizing microscope. The angle of rotation of the sample between two dark states was considered as a measure of double the tilt angle. Mettller FP90 temperature controller along with FP82 hot stage was used to regulate temperature in all experiments. The procedures in detail have been discussed in chapter 2.

6.3 Results and discussions

6.3.1 Observed phases

The observed transition temperatures and thermal range or stability of SmC^* phase (ΔT_{SmC*}) of the compounds are presented in **table 6.1**. Though antiferroelectric SmC^*_A phase was reported in 4F4R below SmC* phase in the synthesis paper [1], but presence of that phase could not be confirmed in the present study. Rather below SmC* phase, within the temperature range of 98^0C to 86^0C, a *subphase* (SmX^*) has been detected in this compound. Both the compounds show SmC^* phase over a considerable temperature range (32.9º in 4F4R and 54.5º in 4F5R) and melts directly to isotropic phase.

Table 6.1. Transition temperatures and thermal stability of SmC^* phase of the compounds

Compounds	**Transition temperatures**	**Stability of SmC^* phase (ΔT_{SmC^*})**
4F4R	Crystal: 86.5^0C: SmX^*: 98^0C : SmC^*: 130.9^0C: Iso	32.9°
4F5R	Crystal: 78.0° C : SmC*:132.5° C: Iso	54.5°

The thermal stability or range ΔT_{SmC*} of SmC* phase in 4F4R is found to be less (32.9º) than all the compounds discussed so far viz. 3F3R, 5F3R and 6F3R, except 2F3R. In 4F5R also ΔT_{SmC*} was less (54.5º) than the other compounds except 2F3R and 3F3R. However, in 2F3R and 3F3R there was a mixed phase of SmF* and SmC*. Thus, the stability of SmC* phase decreased significantly after addition of the fourth oligomethylene spacer in the chain. However, after adding yet another oligomethylene spacer, ΔT_{SmC}^{*} increased slightly.

6.3.2 Optimised geometry

To elucidate the structure property relationship geometries of the molecules were optimised, as done for other compounds, applying Hartree-Fock method and using 3-21G basis set in a commercial package [5]. The optimised structures are shown in **figure 6.2**. The molecular length of 4F4R and 4F5R were found to be 33.83Å and 36.72Å respectively, thus the optimised molecular length (*l*) increased after adding additional oligomethylene spacers, as expected. Optimised molecular lengths (*l*) of the two compounds are greater than 1F3R, 2F3R and 3F3R (chapter 3 and 4), which is again expected as both the number of carbon in fluorinated chain and the number of oligomethylene spacer are less in those compounds, compared to that of 4F4R and 4F5R. However in 5F3R and 6F3R (chapter 5) '*l*' was found to be higher than 4F4R and 4F5R due to additional carbons in the fluorinated chain. The dipole moments of 4F4R and 4F5R are 6.12 D (5.31, 2.70, 1.4) and 5.65 D (-4.94, -2.67, 0.65) respectively where the components of dipole moments along the three coordinate axes are shown within parentheses. Dipole moments of these two compounds are less than all other compounds with three oligomethylene spacers. Thus dipole moment is observed to decrease with increasing oligomethylene spacers. This might

be attributed to the fact that, with addition of oligomethylene spacer, the distance between the fluorine part of the chain and the core of the molecule is increased and thus the dipole moment is decreased.

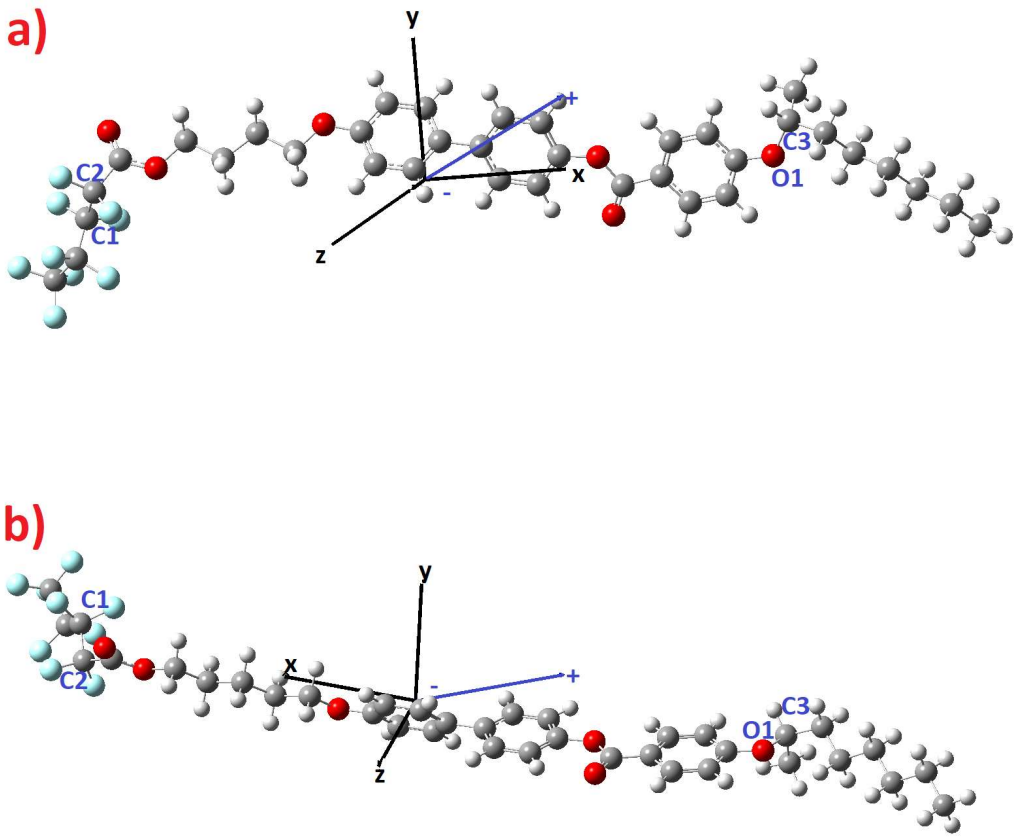

Figure 6.2: Optimised geometry of a) 4F4R and b) 4F5R.

It is noticed that the changes in the optimised parameters, compared to the other homologues, are much higher for 4F5R than 4F4R. That is due to a substantial change in the conformity of the optimised structure after the addition of the fifth oligomethylene spacer. For 3F3R, 5F3R, 6F3R [chapter 4 and 5] and even 4F4R the chiral chain and the fluorinated chain of the optimised geometry were observed to be bend in the same direction. But for 4F5R they are bent in the opposite direction. For quantitative description, the torsion angle of the molecules involving atoms C1, C2, O1, C3 (**figure 6.2**) were measured. For 4F4R and 4F5R it

was found to be 150.9º and -35.27º respectively. This change in molecular conformation might affect the phase sequence of the compounds.

It is worth mentioning that the optimised results published in the paper for these compounds differ from what has been reported in this dissertation. This is because of the fact that previously we used molecular mechanics method in a different program package, but here we have used Hartree Fock method of another program package which is considered to be more accurate. Moreover, we wanted optimised structures of all the compounds discussed in this dissertation are on same footing to make comparison more realistic.

6.3.3 Polarized optical microscopy (POM) study

Observed optical textures of the compounds are displayed in **figure 6.3** and **6.4**.

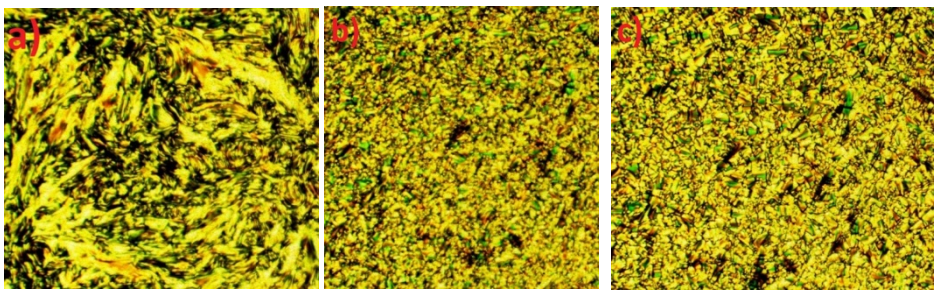

Figure 6.3: Optical textures of 4F4R in a) crystal b) SmX* and c) SmC* phases.

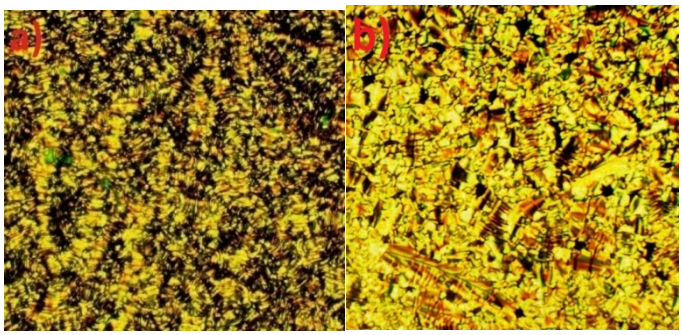

Figure 6.4: Optical textures of 4F5R in a) crystal and b) SmC* phase.

In SmC* phase of 4F4R the texture resembles to that of 6F3R (chapter 5), where just like other compounds of the series with direct transition from SmC* to isotropic phase, no significant domains can be observed [1], but a few poorly developed broken fan region can be observed with parallel lines due to helical structure. After entering into SmX* phase, the chiral lines become fainter and the broken fan structure broke even further. For 4F5R in SmC* phase, the broken fan texture was much more prominent, and chiral lines were also much more clearly visible.

6.3.4 Frequency dependent dielectric relaxation study

Only one strong dielectric relaxation mode was observed in SmX* and SmC* phases of 4F4R and in SmC* phase of 4F5R. As discussed in previous chapters, the collective dielectric behaviour of the SmC^* phase is dominated by two relaxation processes: the Goldstone mode (GM) and the soft mode (SM). Looking at the fact that the observed peak was suppressed after the application of a DC bias of 13V and 15V in 4F4R and 4F5R respectively and considering the range of critical frequencies (f_C) (159– 420 Hz in 4F4R and 400 – 1100 Hz in 4F5R) and values of dielectric increments ($\Delta\varepsilon$) (277 – 280 in 4F4R and 43 - 123 in 4F5R), this relaxation mode was identified as GM relaxation for both the compounds. No SM process was observed in any of these two compounds, even when a DC bias field is applied. As both compounds melt to isotropic phase directly from SmC* phase, the absence of SM relaxation is in conformity with our previous observations, where soft mode was not observed in absence of any orthogonal to tilted phase transition [chapter 3,5] . Reason for this has been discussed in detail in last chapter.

To probe the existence of SmX* phase in 4F4R from dielectric study, the perpendicular components of the real parts of dielectric permittivity

have been plotted as a function of temperature at 1 kHz and 10kHz (**figure 6.5**). When the data are fitted linearly, at both frequencies, a distinct change of slope has been observed at 98^0C. At 1 kHz the slope changes from 1.461 to 0.95, while at 10 kHz it changes from 0.12 to 0.06. This clearly indicates the existence of a new phase in 4F4R below SmC* (98^0C).

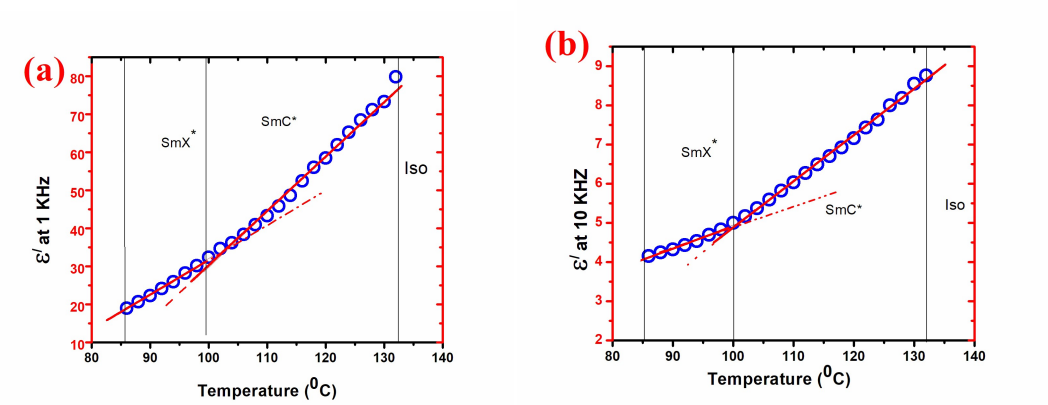

Figure 6.5: Variation of real part of dielectric permittivity of 4F4R with temperature (a) at 1kHz, (b) at 10 kHz.

Representative dielectric spectra, fitted to modified Cole–Cole function, showing the presence of GM both in SmC* and SmX* phases of 4F4R and in SmC* phase of 4F5R, are shown in **Figures 6.6** and **6.7** respectively. As the $\varepsilon^{/}$ and $\varepsilon^{//}$ are related to each other by Kramers-Kronig relation, Cole-Cole plots are shown in **figures 6.8** to show that the fitting is good. It has been observed that, in 4F4R, the average value of distribution parameter (α) in SmC* phase is ~ 0.17, while that in the SmX* *subphase* it is ~ 0.21, which signifies broadening of spectra in this phase and further points to the presence of a different phase below SmC*. It is also inferred that in these compounds also the GM process in SmC* phase is found to be non-Debye type as revealed from the values

of symmetric distribution parameter α. In SmX* phase it deviates further from the Debye type behaviour.

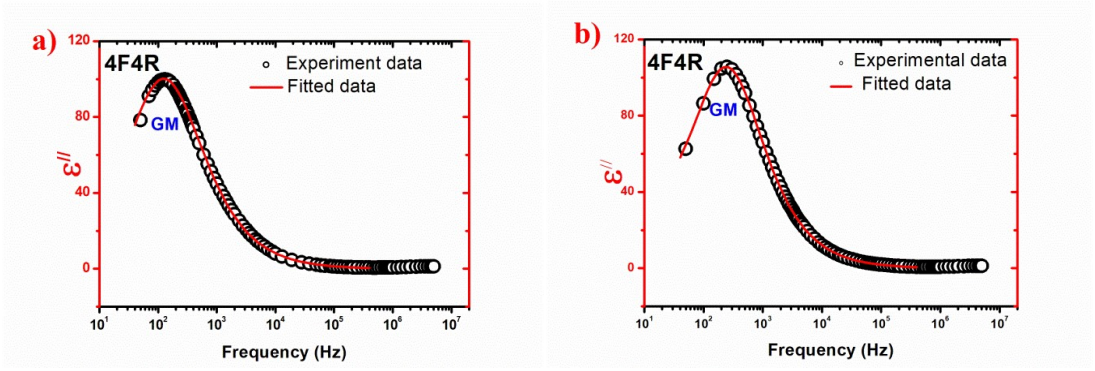

Figure 6.6: Fitted dielectric spectra for 4F4R showing GM: (a) SmX^* phase (96°C), (b) SmC^* phase (110°C) Fitted parameters for a) are $\Delta\varepsilon_{GM}$: 282± 0.87, f_{GM}: 125± 2.7, α_{GM}: 0.21± 0.004, σ_{GM} : 7E-12 ±1E-15 and for b) are $\Delta\varepsilon_{GM}$: 276± 0.94, f_{GM}: 247± 1.2, α_{GM}: 0.17± 0.002, σ_{GM} : 1.1E-8 ±1E-12

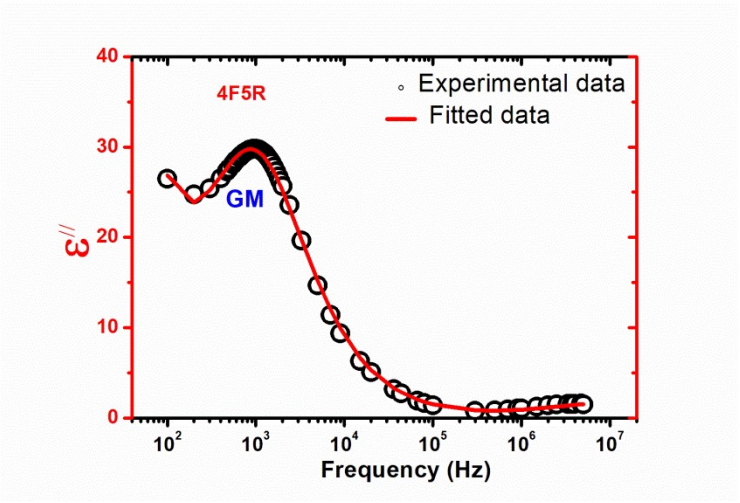

Figure 6.7: Fitted dielectric spectra in SmC* phase at 115ºC for 4F5R showing GM. Fitted parameters for are $\Delta\varepsilon_{GM}$: 71± 1.31, f_{GM}: 988± 6.3, α_{GM}: 0.15± 0.002, σ_{GM} : 9.8E-8 ±1.4E-10

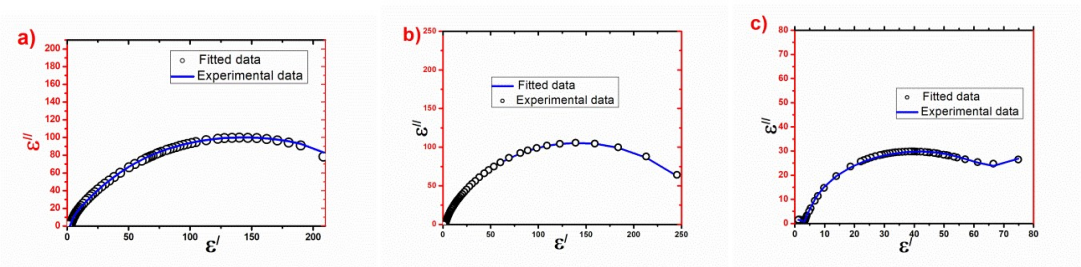

Figure 6.8: Fitted Cole-Cole plots in a) SmX* phase (96°C) and b) SmC* phase (110°C) of 4F4R and c) SmC* phase (115ºC) of 4F5R.

Relaxation frequency and dielectric increment observed from the fitted data are shown in **figures 6.9-6.10** as functions of temperature. Increasing dielectric increment and critical frequency with temperature, at least in low temperature region, may be explained from generalised Landau theory [6] as discussed in previous chapter.

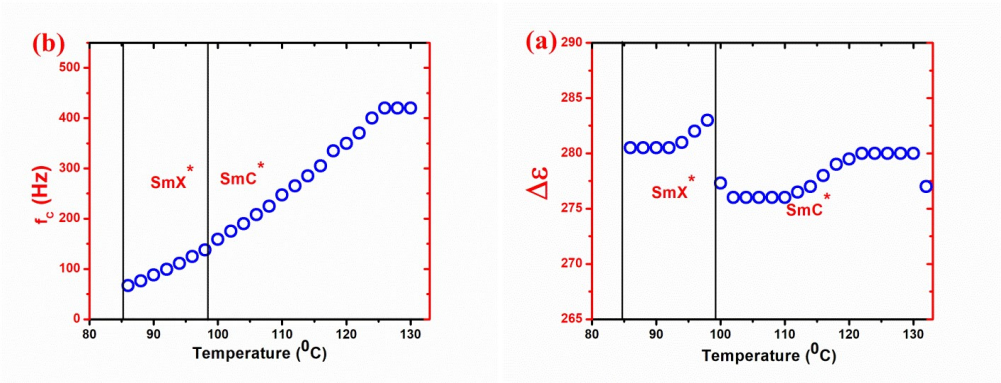

Figure 6.9: Temperature variations of (a) critical frequency and (b) dielectric increment of 4F4R.

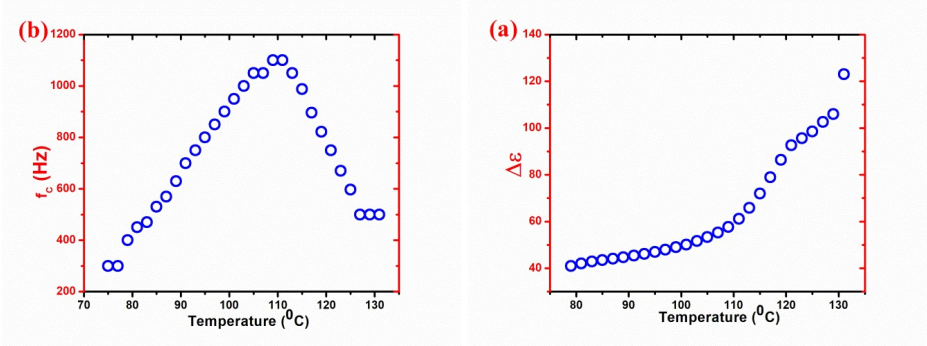

Figure 6.10: Temperature variations of (a) critical frequency and (b) dielectric increment of 4F5R.

It is seen that in 4F5R, having an extra oligomethylene spacer, dielectric increment is less but the critical frequency is more than that of 4F4R. In SmX^* phase of 4F4R critical frequency increases from 67 Hz (86ºC) to 138 Hz (98ºC) and in SmC^* phase it increases from 159 Hz (100°C) to 420 Hz (130°C), while in 4F5R it initially increases from 300 Hz (79ºC) to 1100 Hz (109ºC), then decreases to 500 Hz (131ºC). Thus the critical frequency increased considerably in 4F5R due to the addition of an extra oligomethylene spacer. Although f_C increased in 4F5R compared to 4F4R, but still it remains less than that of 2F3R, 3F3R, 5F3R and 6F3R as discussed in previous chapters. The dielectric increment of 4F4R increases from 280 (86°C) to 283 (98°C) in SmX^* phase and in SmC^* phase it increases from 277 (100°C) to 280 (130°C), hence while moving from SmC^* to SmX^* phase there is a discontinuous increase of dielectric increment justifying our identification of the new phase (SmX*) below SmC*. $\Delta\varepsilon$ is found to be highest and f_C to be the lowest in 4F4R out of all the compounds, discussed so far in this dissertation. In 4F5R the dielectric increment increases from 43 (78°C) to 123 (131°C).

Although a discontinuity in dielectric increment ($\Delta\varepsilon$) has been observed at SmX*-SmC* transition, but there is no such discontinuity in the critical frequency (**figure 6.9**). Discontinuous decrease in dielectric increment [7–9] and continuous variation of critical frequency [9,10] (**figure 6.9**) have been reported earlier in a three layer ferrielectric SmC_γ^* *subphase*. The broadening of dielectric spectra is also an inherent property of SmC_γ^* *subphase* [7], which was also observed in SmX* phase. Moreover, this only one low frequency relaxation process has already been identified as Goldstone mode, and ferrielectric Goldstone mode relaxation is often observed in SmC_γ^* phase [7,9,10]. Although in

SmC_γ^* *subphase*, dielectric increment higher than SmC^* [10–12], broadening of dielectric spectra [7] and higher tilt [13] were reported before as observed in 4F4R (higher tilt are discussed below), however, it is unusual that dielectric increment in three layer ferrielctric SmC_γ^* phase will be more than the ferroelectric SmC^* phase. We, therefore, designate the new phase as SmX* phase instead of SmC_γ^* *subphase*.

6.3.5 Spontaneous polarization (P_S)

The temperature variation of the spontaneous polarization is shown in **figure 6.11**. P_S is found to increase with decreasing temperature as expected. However, no anomaly at SmC*-SmX^* transition is observed may be due to application of strong electric field during P_S measurement. P_S is found to decrease from 57.3 nC/cm^2 (86°C) to 47.3 nC/cm^2 (98ºC) within SmX^* phase and in SmC^* phase it decreases from 46.9 nC/cm^2 (100°C) to 11.2 nC/cm^2(131°C), while in 4F5R it decreases from 50.7nC/cm^2 (79ºC) to 5.8 nC/cm^2 (133ºC). This values are within the acceptable range of polarization for different applications [14]. The measured value of P_S were found to be greater than that of 2F3R, 3F3R [chapter 4], 5F3R and 6F3R [chapter 5]. Thus spontaneous polarization is found to increase with increasing oligomethylene spacers.

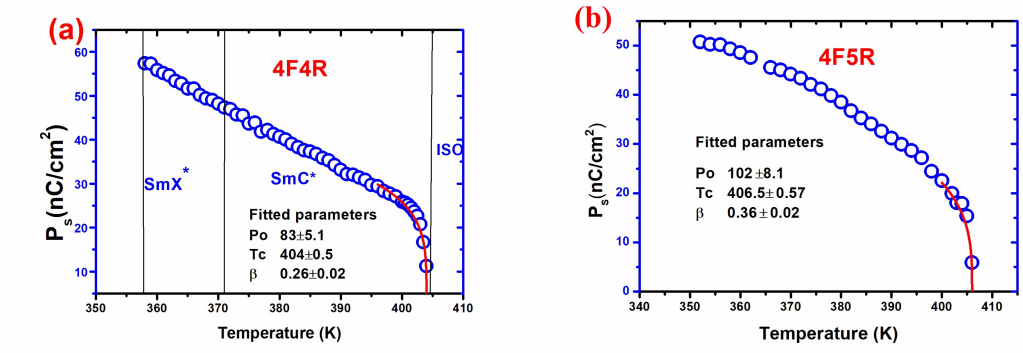

Figure 6.11: Dependence of Ps on temperature (a) 4F4R, (b) 4F5R.

The P_S data were fitted to the mean-field model, $P_S = P_0(1 - \frac{T}{T_C})^{\beta}$ [15] where T_C is the SmC* to isotropic transition temperature and β is critical exponent for the secondary order parameter P_S. In all cases β deviates significantly from the mean field value for a second order phase transition, however, fitted T_C matches nicely with observed T_C. It is worth mentioning that the change in enthalpy values at SmC* to isotropic transition of 4F4R and 4F5R was quoted as 8.39 and 6.79 kJ/mole respectively in the reference [1]. This also indicates that the corresponding transition is not second order rather points to first order.

6.3.6 Rotational viscosity (γ_Φ)

The rotational viscosity (γ_φ) associated with the GM fluctuations is another important parameter for ferroelectric liquid crystals as it strongly influences the switching time between the field-induced states of FLCs. γ_φ has been calculated from **equation 6.1**, which was derived from the generalized Landau model [6].

$$\gamma_\varphi = \frac{1}{4\pi\varepsilon_0}\frac{1}{\Delta\varepsilon f_C}\left(\frac{P_S}{\theta}\right)^2 \qquad [6.1]$$

Here Goldstone mode dielectric strength (Δε) and relaxation frequency (f_C) were obtained from dielectric relaxation study and tilt angle (θ) was obtained from electro optic measurement (discussed latter). The temperature variation of rotational viscosity is shown in **figure 6.12**.

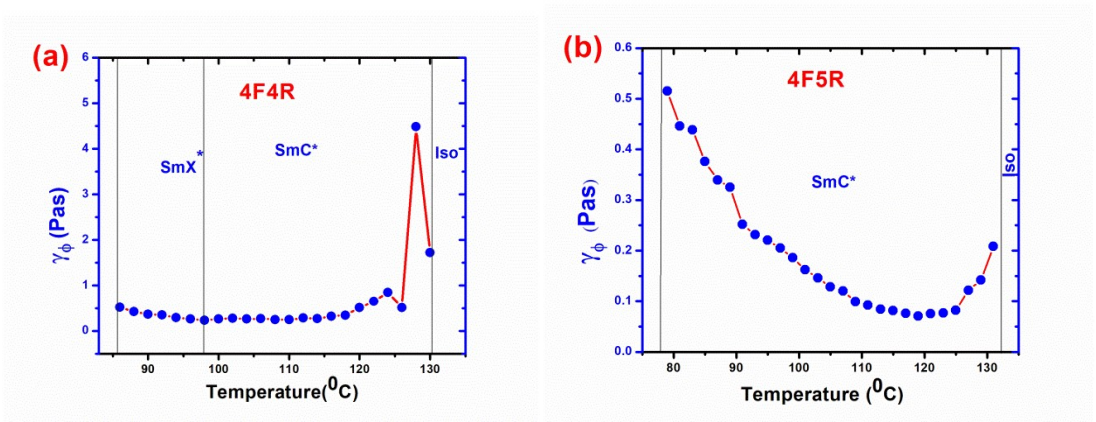

Figure 6.12: Rotational viscosity (γ_φ) of a) 4F4R and b) 4F5R.

The rotational viscosity first decreases with temperature, then near the SmC* to isotropic transition it diverges which may be due to pre-transitional effect. In most of FLC materials the rotational viscosity has been reported to decrease with temperature [4]. However, for certain FLC materials it has been reported to increase near the transition [16], as has been observed in the present compounds. The initial value of γ_φ in SmC* phase was found to be smaller in 4F4R (0.26 Pa.s) compared to that of 4F5R (0.51Pa.s). In fact the rotational viscosity of 4F4R was found to be smaller than all the other compounds discussed so far, except that of 2F3R. As mentioned in chapter 5, the rotational viscosity can be calculated also from electro-optic data. However, since two formulae give almost same values we have not repeated that in these compounds.

6.3.7 Optical tilt angle (θ)

Tilt angles for the compounds were determined optically. Optical tilt reflects the angle between the direction of molecular core and the layer normal, since the principal axis of indicatrix coincides with the core direction. As can be seen from **figure 6.13** the optical tilt in both cases is found to increase with decreasing temperature as expected. In 4F4R, it shows a clear jump at 98^0 C [**figure 6.13 (a)**], as previously reported in SmC_γ^* phase [17]. Dolganov and Kats [18] have argued that in 3 layer

ferrielectric SmC_{γ}^{*} phase, both quadratic and biquadratic interactions between nearest layers and the frustrating interaction between nearest and next nearest layers have negative energy contribution in the expression of Landau free energy, which favors the increase of tilt angle. Both compounds showed higher optical tilt angle at the onset of SmC* phase than 5F3R and 6F3R [chapter 5]. In fact initial value of θ in SmC* phase is higher in 4F5R than in 4F4R. Hence, it appears that optical tilt does increase with increasing number of oligomethylene spacer.

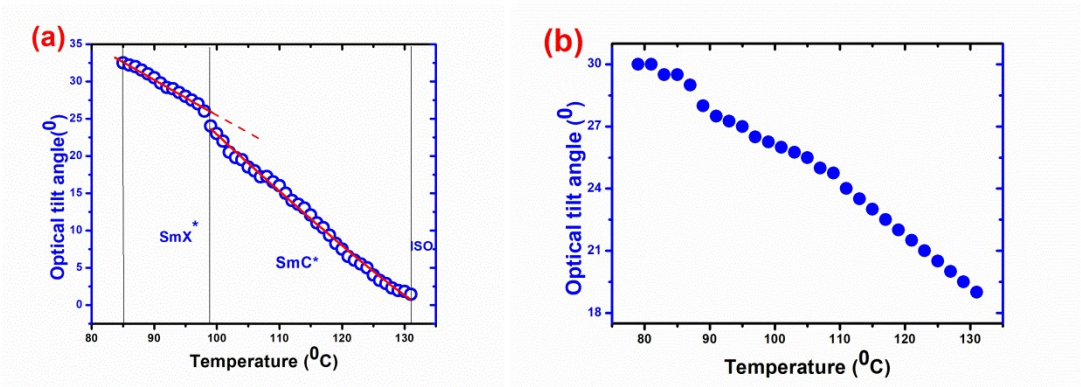

Figure 6.13: Optical tilt angles of a) 4F4R and b) 4F5R.

6.3.8 Response Time (τ):

The temperature variation of observed electric response time is depicted in **figure 6.14**. Response time was found to decrease with temperature as expected. In SmX* phase of 4F4R the compound exhibited much slower electrical response (1500 μs). Response became two times faster after entering into SmC* phase (810 μs). The highest response time in SmC* phase of 4F5R (214 μs) was found to be much smaller than that of 4F4R. Both compounds showed much slower response than the other compounds with three oligomethylene spacers (2F3R, 3F3R, 5F3R, 6F3R) [chapter 4 and 5]. Thus addition of one oligomethylene spacer resulted in increasing the response time at least by an order. However, τ decreased a bit after addition of a further spacer.

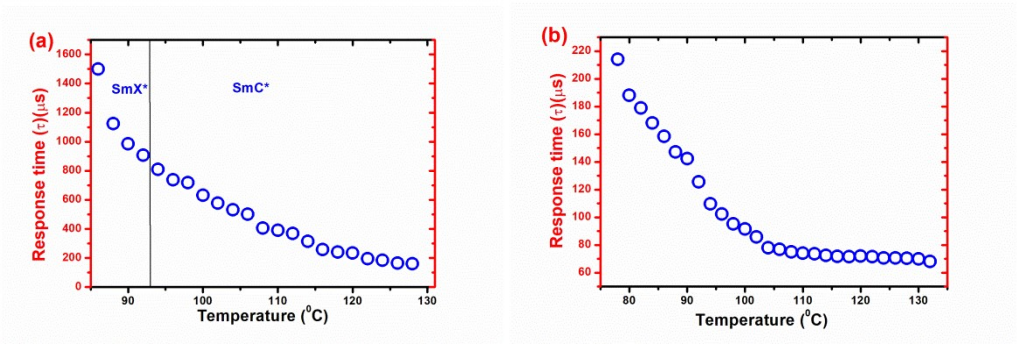

Figure 6.14: Response time of a) 4F4R and b) 4F5R.

6.4 Conclusion

Both compounds 4F4R and 4F5R exhibit SmC* phase over a broad temperature range and melt directly into isotropic phase without displaying an intermediate orthogonal phase. However, stability of this phase is less in 4F4R than in 4F5R, in fact less than in most other pure compounds studied in this dissertation, which might be attributed to the presence of a smectic *subphase* (SmX*) in this compound. Although existence of only one Goldstone mode like relaxation, broadening of the dielectric spectra and discontinuous increase in the dielectric increment and tilt angle indicate this newly detected *subphase* to be a 3 layer ferrielectric SmC_{γ}^{*} phase, but the higher dielectric increment than that of the ferroelectric SmC^{*} phase restrains us to conclusively assign it as SmC_{γ}^{*} phase, rather we prefer to designate it as SmX* phase. No soft mode relaxation is observed in these two compounds which melted directly into isotropic phase from SmC* phase, which is in conformity with our previous observations. GM critical frequency of these compounds is found to be less than any other compounds discussed so far. Compounds exhibit moderate spontaneous polarization and rotational viscosity. Optical tilt was found to increase with increasing oligomethylene spacer. They showed much slower response than other

compounds included in this thesis indicating addition of more oligomethylene specers results in slower response of the molecules.

Reference

[1] Ziobro D, Dąbrowski R, Tykarska M, et al. Synthesis and properties of new ferroelectric and antiferroelectric liquid crystals with a biphenylyl benzoate rigid core. Liq. Cryst. 2012;39:1011–1032.

[2] CJF B, P B. Theory of electric polarization. Vol 1. Amsterdam: Elsevier; 1978.

[3] Hasse W, Wróbel S. Relaxation Phenomena: Liquid Crystals, Magnetic Systems, Polymers, High-Tc Superconductors, Metallic Glasses. Berlin: Springer; 2003.

[4] Miyasato K, Abe S, Takezoe H, et al. Direct Method with Triangular Waves for Measuring Spontaneous Polarization in Ferroelectric Liquid Crystals. Jpn. J. Appl. Phys. 1983;22:L661–L663.

[5] Gaussian 09, Revision D.01, M. J. Frisch *et al.* Gaussian, Inc., Wallingford CT, 2013.

[6] Carlsson T, Žekš B, Filipič C, et al. Theoretical model of the frequency and temperature dependence of the complex dielectric constant of ferroelectric liquid crystals near the smectic-C* — smectic- A phase transition. Phys. Rev. A. 1990;42:877–889.

[7] Gorecka E, Pociecha D, Čepič M, et al. Enantiomeric excess dependence of the phase diagram of antiferroelectric liquid crystals. Phys. Rev. E. 2002;65:061703.

[8] Lagerwall JPF, Rudquist P, Lagerwall ST, et al. On the phase sequence of antiferroelectric liquid crystals and its relation to

orientational and translational order. Liq. Cryst. 2003;30:399–414.

[9] Pandey MB, Dhar R, Agrawal VK, et al. Dielectric relaxation studies in ferro-, ferri- and antiferro-electric phases of (S)-4′-octyloxybiphenyl-4-carboxylic acid 3-chloro-4-(1-methylheptyloxycarbonyl)phenyl ester. Phase Transitions 2005;78:457–470.

[10] Ghosh S, Nayek P, Roy SK, et al. Dielectric relaxation spectroscopy and electro-optical studies of a new, partially fluorinated orthoconic antiferroelectric liquid crystal material exhibiting V-shaped switching. Liq. Cryst. 2010;37:369–375.

[11] Lagerwall JPF, Dabrowski R, Scalia G. Antiferroelectric liquid crystals with induced intermediate polar phases and the effects of doping with carbon nanotubes. J. Non. Cryst. Solids 2007;353:4411–4417.

[12] Uehara H, Hanakai Y, Hatano J, et al. Dielectric Relaxation Modes in the Phases of Antiferroelectric Liquid Crystals. Jpn. J. Appl. Phys. 1995;34:5424–5428.

[13] Soltani T, Chmingui M, Marcerou JP, et al. Dielectric and thermodynamic studies of Smectic-A–Smectic-C* phase transition in antiferroelectric liquid crystal: thermal hysteresis. Liq. Cryst. 2014;41:222–227.

[14] Mandal PK, Haldar S, Lapanik A, et al. Induction and Enhancement of Ferroelectric Smectic C * Phase in Multi-Component Room Temperature Mixtures. Jpn. J. Appl. Phys. 2009;48:011501.

[15] Lagerwall ST. Ferroelectric and antiferroelectric liquid crystals. Newyork: WILEY-VCH; 1999.

[16] Pirkl S, Glogarová M. Ferroelectric liquid crystals with high spontaneous polarization. In: Lallart M, editor. Ferroelectr. - Phys. Eff. Croatia: InTech; 2011. p. 407–428.

[17] Škarabot M, Čepič M, Žekš B, et al. Birefringence and tilt angle in the antiferroelectric, ferroelectric, and intermediate phases of chiral smectic liquid crystals. Phys. Rev. E 1998;58:575–584.

[18] Dolganov P V., Kats EI. Landau theory description of polar smectic structures. Liq. Cryst. Rev. 2013;1:127–149.

CHAPTER-7

Structural, dielectric and electro-optic properties of a long chain biphenyl benzoate cored chiral mesogen and formulation of a room temperature ferroelectric liquid crystal mixture.

Part of this work has been published in Liquid crystal, Vol:43, pp1548-1549, 2016.

7.1 Introduction

The compound (*S*) - (+) -4′-[(3-pentadecafluorooctanoyloxy) prop-1-oxy]biphenyl-4-yl 4-(1-methylheptyl oxy)benzoate(7F3R) [1] has the highest number of fluorine atoms in its chain and is the longest member of the selected compounds. The molecular structure of the compound is shown in **figure 7.1**.

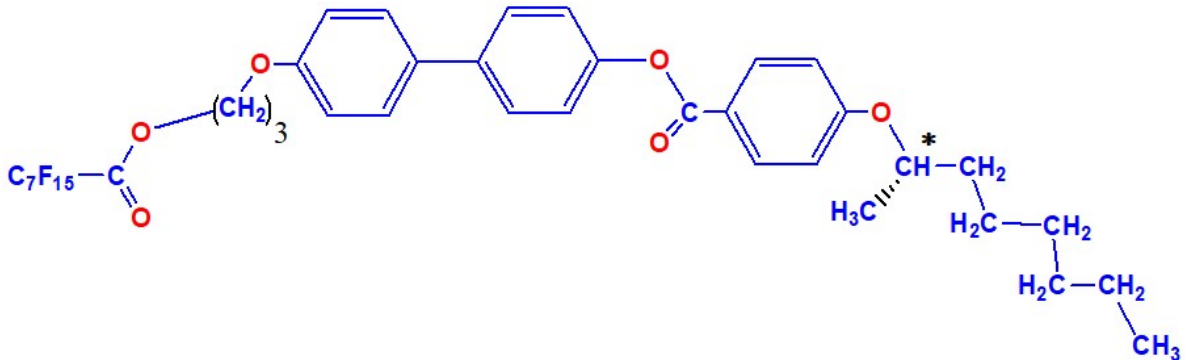

Figure 7.1: Molecular structure of 7F3R.

The compound has three oligomethylene spacers and seven carbons in its fluorinated chain. This compound exhibits largest range or highest stability of ferroelectric phase out of all the compounds included in this dissertation. It also gives rise to a paraelectric phase (SmA*) when heated beyond the ferroelectric phase, unlike the four compounds described in the last two chapters which melted directly to isotropic phase.

Main objective of studying the properties of different FLC systems is to find their comparative efficacy to FLC mixture formulation useful predominantly for display applications considering their microsecond order in-plane switching. It is well known that no single compound can satisfy all the properties required for such application like temperature range, switching time, optical birefringence, polarization, tilt angle, pitch, viscosity and above all thermal and UV stability [2–5]. Therefore, a mixture of achiral host molecules is normally doped with an appropriate

chiral molecule to formulate a useful FLC mixture. The host mixture is again usually a mixture of several achiral compounds with a reasonably wide range of SmC phase which controls the overall temperature range and tilt angle of the final mixture. Dopant is a compound with one or two chiral centres which controls the spontaneous polarization, viscosity, switching speed and helical pitch of the final mixture [6–10]. It might be noted that every component influences the properties of the resulting mixture, a particular property will depend not only on the type and proportion of chiral dopants, but also on the host materials used. However, the dopants are used to optimise the final properties to the desired level more effectively. Since 7F3R has the highest range of SmC* phase, therefore, we have chosen this compound to formulate a ferroelectric liquid crystal mixture.

In this chapter, we first present the structural, dielectric and electro-optic properties of the pure compound 7F3R. In the latter half we describe the formulation of the FLC mixture and results of the characterization of its properties.

7.2 Experimental procedure

For the Polarized optical microscopy (POM), small angle X-ray scattering (SAXS), dielectric and electro-optic studies, the material was fed into a polyimide coated planar dielectric glass cell of low resistivity and with transparent indium tin oxide electrodes of 8μm cell gap. The transition temperatures of the mixture were measured by differential scanning calorimeter (DSC), using a Mettler FP90 temperature controller, within an accuracy of ±0.1°C, along with FP84HT hot stage, in a heating cycle of rate 2°C/min. Phase transitions were also determined by investigating the optical textures of the compound by Olympus BX41

polarizing microscope equipped with a CCD camera using the same temperature controller.

Temperature dependent SAXS experiment was performed using PETRA III synchrotron beamline at P07 Physics Hutch station at Deutsches Elektronen- Synchrotron (DESY), Hamburg. An angular range (2θ) of ~ 5° was scanned using a beam of weave length 0.164 Å. Temperature in this experiment was controlled using a Lakeshore 340 temperature controller. For the mixture, SAXS experiment was done without applying any field as well as with field (12V/μm) across the cell. For the pure compound no field was applied.

Hioki 3532-50 impedance analyzer was used to measure the complex dielectric permittivity within the range 50Hz to 5MHz. The dielectric spectra were fitted using following modified Cole–Cole function[11]. Spontaneous polarization (P_S) was measured by time reversal method [12], using Agilent 33220A function generator by applying an triangular signal. Tektronix TDS 2012B digital storage oscilloscope was used to measure the voltage drop across a 100 kΩ resistance in series with the sample cell.

The details of all these experiments are discussed in chapter 2.

7.3 Characterisation of the pure compound

7.3.1 Observed phases

The phase sequence of the compound 7F3R was determined by combining the results of POM, SAXS and dielectric studies and is shown in **table 7.1**. Paraelectric SmA* phase is found to exist along with SmC* phase as mentioned before. It is worth noticing that SmA* phase was observed in the two short chain compounds of the series, namely, 1F3R

and 2F3R (discussed in chapter 3 and 4), but not in the intermediate derivatives studied in this dissertation. Thus this phase is found to reappear in the phase sequence with higher number of fluorine in its chain. Apart from that 7F3R shows the largest temperature span of SmC* phase (ΔT_{SmC*}): 72.5ºC out of all the compounds included in this dissertation.

Table 7.1. Transition temperatures and thermal stability of SmC^* phase of 7F3R

Compound	**Transition temperatures**	**stability of SmC^* phase (ΔT_{SmC*})**
7F3R	Crystal: 75.5 ^{0}C: SmC^* : 148.0 ^{0}C: SmA^* : 150.1 ^{0}C : Iso	72.5°

7.3.2 Polarized optical microscopy (POM) study

Optical textures of the compound in homogeneous geometry were recorded during cooling cycle. The textures of 7F3R at different phases are shown in **figure 7.2.**

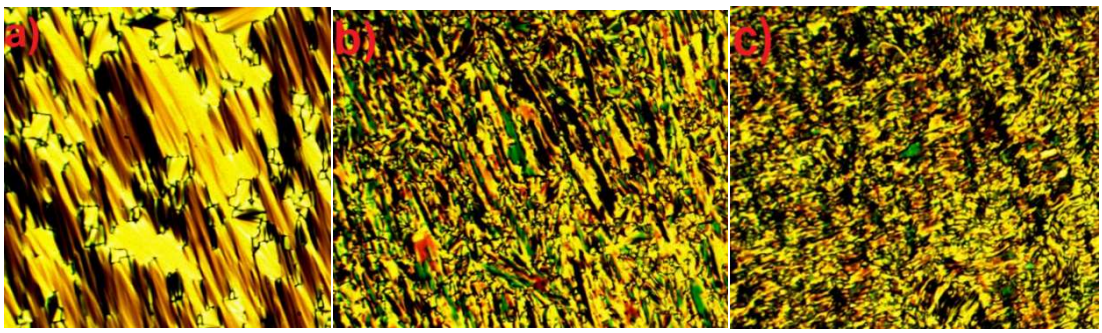

Figure 7.2: Optical texture of 7F3R at a) SmA* (149ºC) b) SmC* (114ºC) and c) crystal (74ºC) phases.

The signature fan shape texture [13] was observed in SmA* phase. After entering into SmC* phase the broken fan shape texture was observed with a little change in birefringence quite similar to what was observed in 2F3R (discussed in chapter 4). But unlike other compounds

the chiral lines were not distinctly visible even in SmC* phase. Absence of chiral lines are sometimes attributed to the smaller pitch of the compounds [13]. It can be mentioned here that for compounds with similar structures the pitch was reported to decrease with increasing number of fluorine atoms [1]. Since among the selected compounds, 7F3R has highest number of fluorine atoms so we can expect its pitch to be the lowest.

7.3.3 Optimised geometry

The molecular geometry of the compound was optimised applying Hartree-Fock method and using 3-21G basis set in a commercial package [14]. The optimised structure along with the direction of the dipole moment is shown in **figure 7.3**.

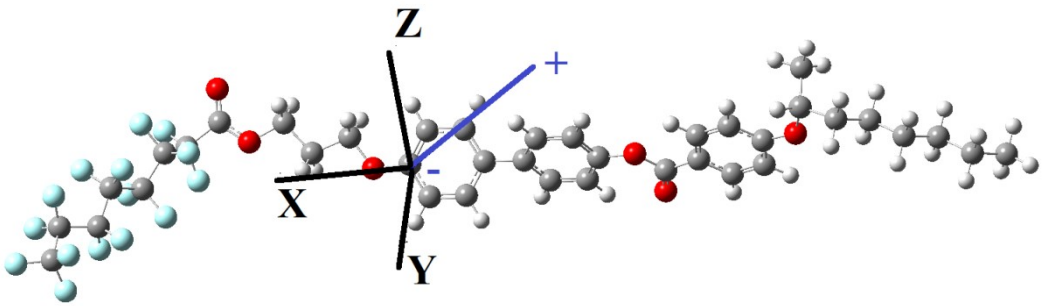

Figure 7.3: Optimised geometry of 7F3R.

The optimised length (*l*) of the compound is found to be 37.01Å, which is longer, as expected, than all the other compounds discussed in this dissertation. The dipole moment (μ) of 7F3R is found to be 6.55 D (-5.06, 0.4784, 4.14) where the components of dipole moments along the three coordinate axes are shown within parentheses as in other chapters. The dipole moment is found to be larger than all the other compounds since it is found to increase with increasing number of fluorines in the chain, except that of 1F3R and 2F3R, whose μ is still higher than 7F3R. This may be due to the twist of the fluorinated chain at the carboxylic group

by an angle ~85º which was observed in 3F3R and increased in all other higher derivatives including 7F3R. Thus 1F3R, 2F3R and 7F3R have larger dipole moments than the other compounds. This fact may have some relation with the presence of SmA* phase in these three compound and absence of the same in others.

7.3.4 Synchrotron diffraction study

Synchrotron diffraction studies were carried out in cooling cycle. In all the phases one sharp inner ring and one diffused outer ring were observed which correspond to smectic layer spacing and ordering within the layers respectively. Representative diffraction photographs of each phase are shown in **figure 7.4**.

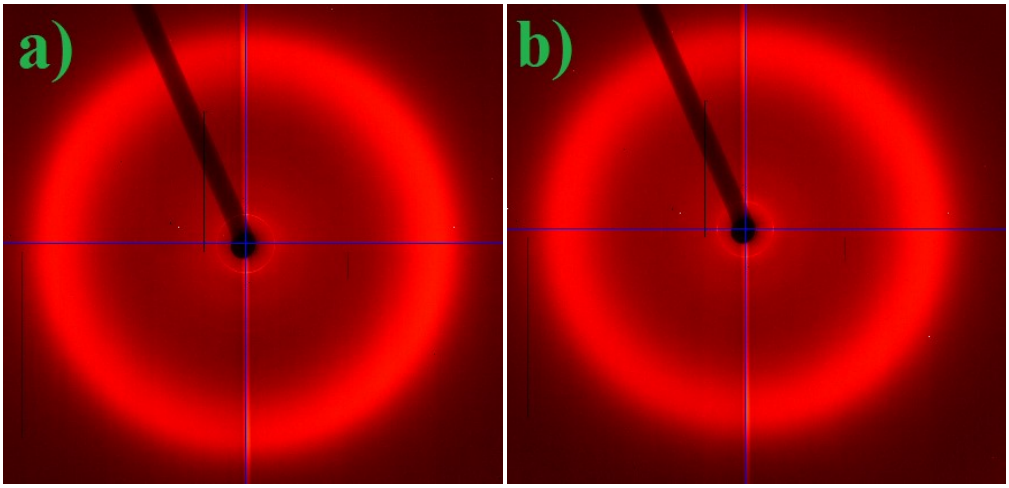

Figure 7.4: Diffraction photographs of 7F3R in a) SmC* (122ºC) and b) SmA* (149ºC) phases.

The layer spacings (d) were calculated from the low angle diffraction feature and the average intermolecular spacing (D) were calculated from the outer ring and these are depicted in **figure 7.5** as a function of temperature.

The layer spacing (d) is found to decrease with decreasing temperature in both the phases but a slight increase was observed near SmA*-SmC* transition. The layer spacing, however, is found to be less than the optimised molecular length (*l*) in both the phases, just like 2F3R as discussed in chapter 4.

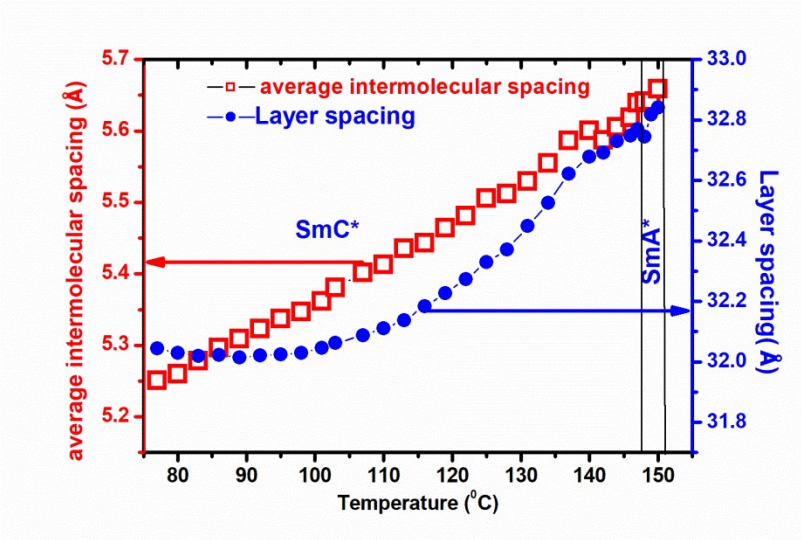

Figure 7.5: Temperature variation of layer spacing and average intermolecular spacing of 7F3R.

The ratio of layer spacing to molecular length (d/*l*) in SmA* phase was found to be nearly 0.88, which is less than 1F3R (1.07) and 2F3R (0.90). Thus d/*l* ratio is found to decrease with increasing chain fluorination. Moreover, this ratio was reported to be 0.50, 0.76, 0.97 for 5F6R, 4F6R and 1F4R respectively [1]. Hence it can be inferred that d/*l* ratio decreases even with increasing number of oligomethylene spacers. As the d/*l* ratio of 7F3R is less than one even in SmA* phase therefore SmA* phase may be de Vries type [15], as observed in 2F3R. To probe it further we have calculated the layer contraction in SmC* phase. The effective layer contraction was found to be 2.3% at 77ºC. Though this is higher

than that of 2F3R, but much less than ordinary SmA phase [16] and closer to de Vries type material [16,17].

In SmC* phase the temperature dependence of the layer spacing appeared to be parabolic. In accordance to the generalised mean field theory the tilt (θ) is $\theta \propto (T - T_C)^{\beta}$, where the value of the critical exponent β is expected to be (1/2) for a pure second order transition and (1/4) in case of second order transition approaching triclinic point. Following Hartley et al. [18] but keeping up to forth term in the expansion of cos(θ) it can be shown that near T_C

$$\frac{d_C}{d_A} \approx 1 - a|T - T_C|^{1/2} + b|T - T_C| \qquad [7.1]$$

when β is taken (1/4). Observed data fitted quite nicely to **equation 7.1**, signifying the SmC* to SmA* transition is probably tricritical type.

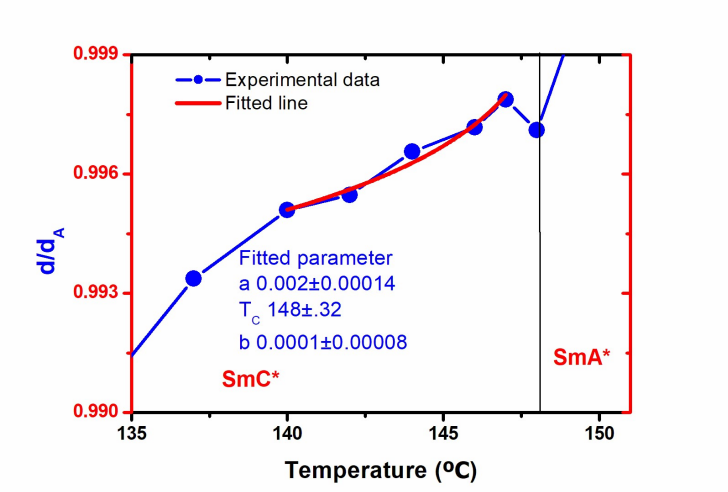

Figure 7.6: Temperature variation of d_C/d_A near transition.

The inter-molecular spacing is also found to increase with temperature as expected and it is (5.25 to 5.65 Å) of the same order as in 1F3R, 2F3R and 3F3R.

The molecular tilt angle was calculated from the relation, $= cos^{-1}\frac{d}{d_A}$, where d is the layer spacing at a particular temperature and d_A is the highest 'd' value at SmA phase. The temperature variation of the tilt angle is shown in **figure 7.7**.

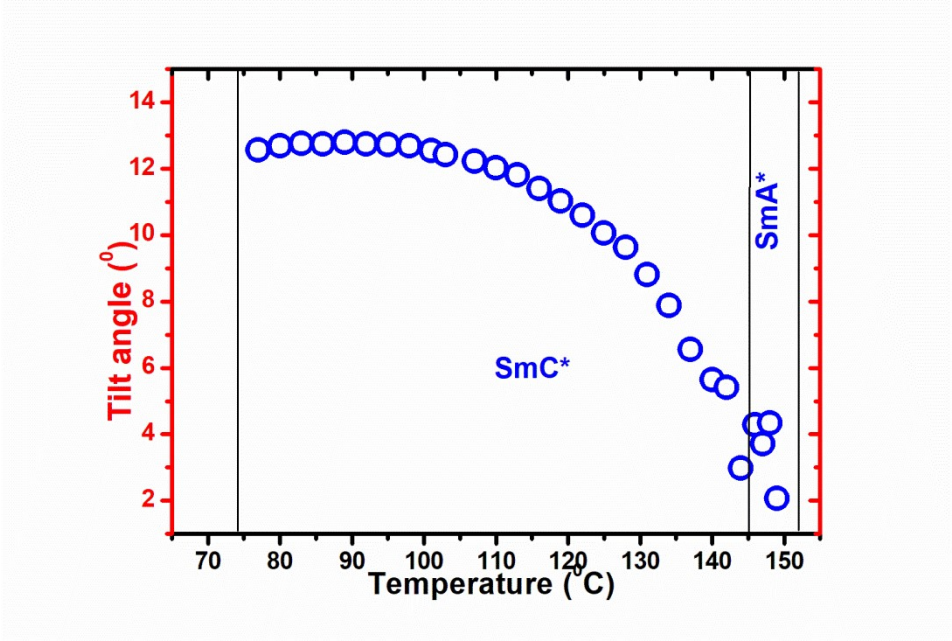

Figure 7.7: Temperature variation of X-ray tilt angle of 7F3R.

The tilt angle was much less than that of 2F3R (28.6º) and 3F3R (32.8º), but as discussed in chapter 2, in those cases the tilt was measured by dividing the layer spacing by the optimised molecular length to compare the values with other compounds having direct transition from SmC* to isotropic phase. However, as for the mixture we cannot have an exact value of the optimised length, so for the mixture and the dopant (7F3R) the tilt was calculated using the layer spacing in SmA* phase.

The correlation length (ξ) across and within the smectic layers was calculated using, $\xi = \frac{2\pi}{FWHM}$, where FWHM is the full width at half maxima in the scattering vector (Q) of the relevant Bragg's peak [19] and is shown in **figure 7.8**.

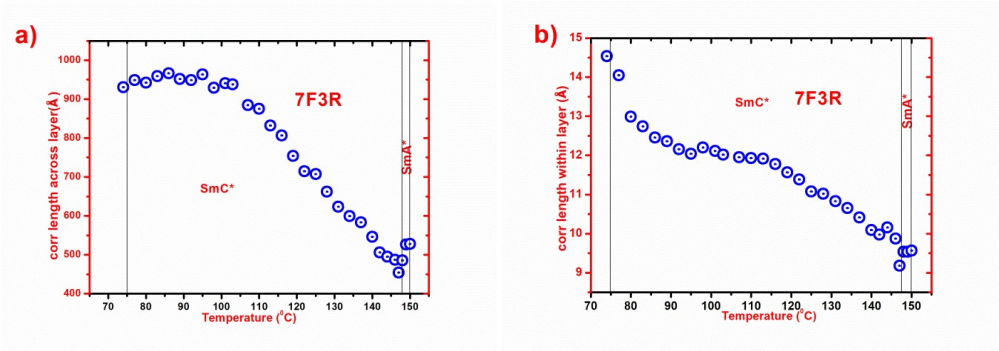

Figure 7.8: Correlation lengths of 7F3R a) across the layer and b) within layer.

The highest value of correlation length across and within layer in SmC* phase was found to be ~966Å and ~ 14Å respectively, which is slightly less than that of 2F3R and 3F3R. The correlation length across the layer was found to be approximately 26 times and 12 times of the optimised molecular length in SmC* and SmA* phases respectively. Surprisingly the correlation length across the plane, showed a little increasing trend after entering into SmA* phase.

7.3.5 Frequency dependent dielectric relaxation study

As discussed in chapter 2 the collective relaxation of SmC* phase is mainly dominated by Goldstone mode (GM) and soft mode (SM) relaxation. The Goldstone mode (GM) occurring at a lower frequency is associated with the azimuthal angle fluctuations of the directors in smectic planes and the soft mode (SM) is connected with the softening of the polar part of the tilt fluctuations which is seen throughout the SmA* phase and also in SmC* phase, but only near the transition temperature (T_C) [20]. Both these modes are observed. As a representative example, fitted dielectric spectra showing the presence of both the GM and SM in 7F3R is shown in **figure 7.9**. Fitted to Cole–Cole plot is shown in **figure**

7.10 Since the $\varepsilon^{/}$ and $\varepsilon^{//}$ are related to each other by Kramers- Kronig relation, Cole-Cole plot is to show that the fitting is good.

Goldstone mode relaxation is observed throughout the SmC* phase. This mode could be suppressed by applying proper DC bias. Near T_C another peak is seen at higher frequency range which sustained throughout the SmA* phase and did not vanish even under DC bias. This peak is associated with the soft mode relaxation. But as in 2F3R, here soft mode dielectric increment and critical frequency did not show respectively reverse 'V' shape and 'V' shape temperature variation in the vicinity of SmA*-SmC* transition as can be seen in **figure 7.11**. It is to be noted here, soft mode was observed before in 2F3R which also had both SmC* and SmA* phases, but not in other compounds which didn't have any orthogonal to tilted phase transition.

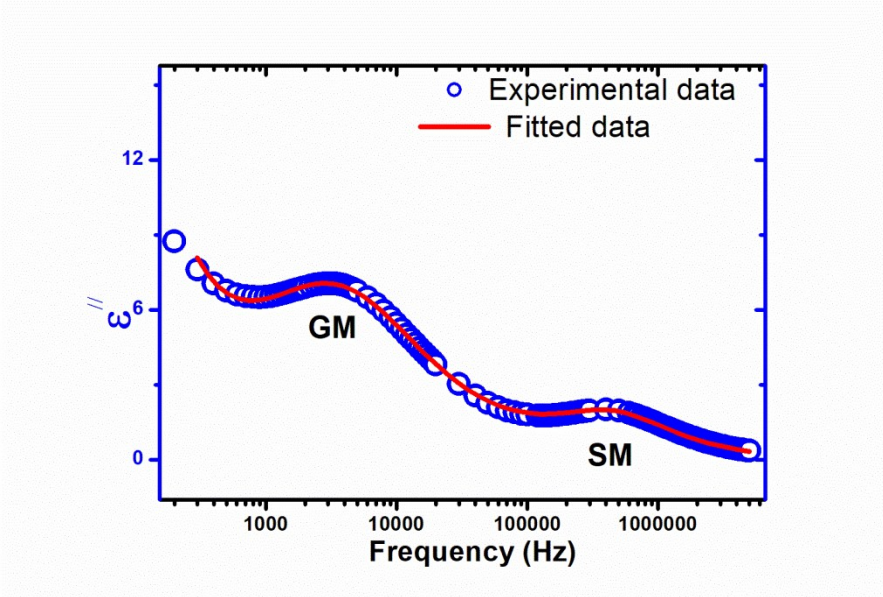

Figure 7.9: Fitted dielectric spectra in SmC* phase at 147.7ºC showing both GM and SM. Fitted parameters are $\Delta\varepsilon_{GM}$: 34.8±0.1, f_{CGM}: 3009 ±91.3, α_{GM}: 0.22± 0.003, $\Delta\varepsilon_{SM}$: 4.5±0.2, f_{CSM}: 365007±392, α_{SM}: 0.01± 0.003, σ :9.6E-8 ±1E-9.

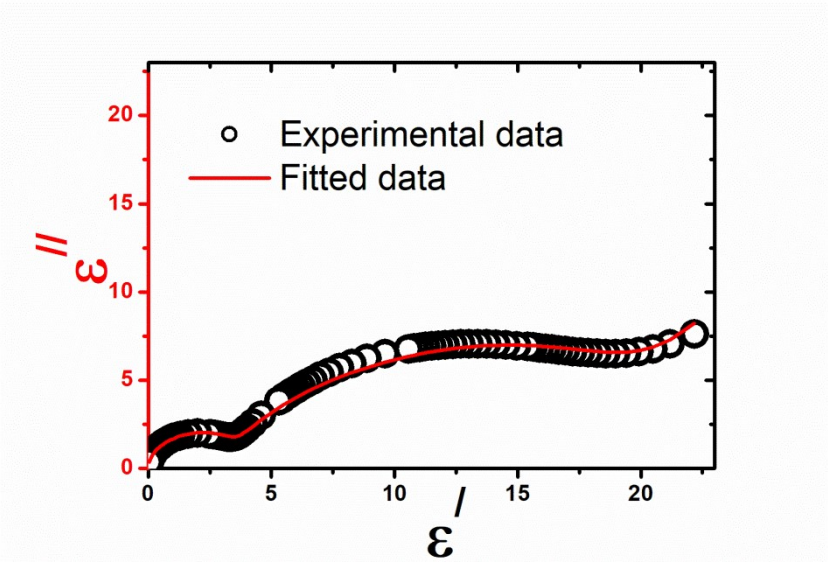

Figure 7.10: Fitted cole-cole plot at 147.7ºC

Relaxation frequency and dielectric increment observed from the fitted data are shown in **figures 7.11**, as functions of temperature.

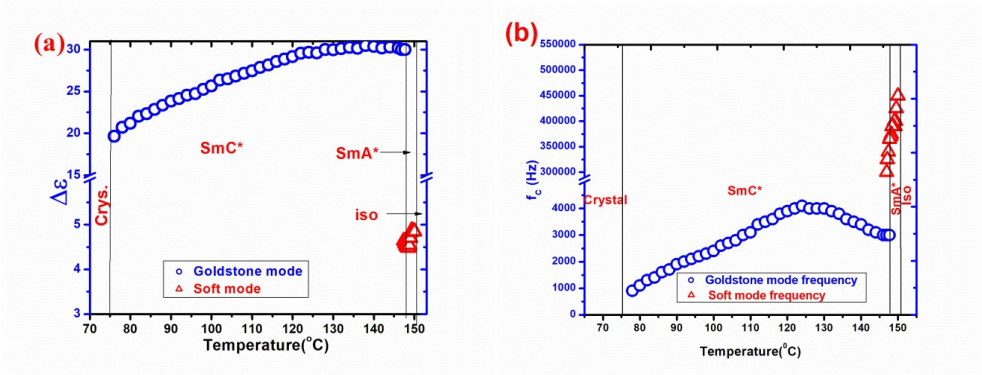

Figure 7.11: Temperature variation of a) dielectric increment and b) critical frequency of 7F3R.

The highest value of dielectric increment of Goldstone mode was found to be 30, much less than the other compounds discussed in this dissertation. GM critical frequency increased from 600 Hz (76°C) to 4100 Hz (124°C) and then decreased to 3000 Hz (146°C). Similar temperature variation was observed in 2F3R, 3F3R and 4F5R. However, the GM critical frequency of 7F3R was found to be much higher than all other compounds. For soft mode relaxation the critical frequency was

much higher than the GM critical frequency and it showed much stronger dependency with temperature as expected from generalized Landau model [21]. It increased from 300 kHz (147°C, SmC* phase) to 475 kHz (151°C, SmA* phase). The dielectric increment of soft mode was much smaller as noted, in comparison to its Goldstone mode counterpart which remained more or less constant with temperature.

7.3.6 Spontaneous polarization (P_S)

Temperature dependence of spontaneous polarization (P_S) is shown in **figure 7.12**.

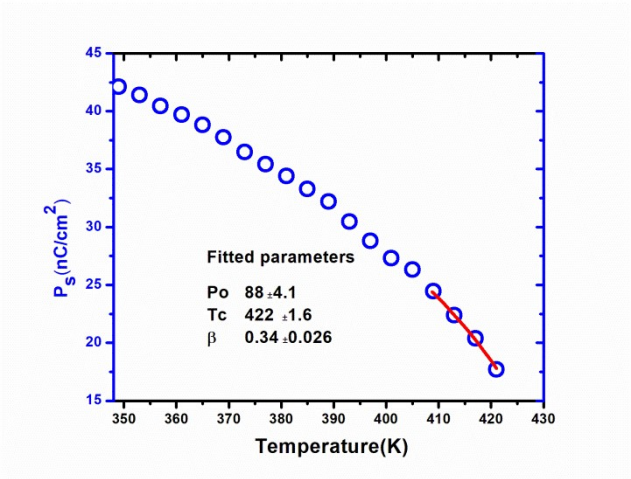

Figure 7.12: Temperature variation of spontaneous polarisation of 7F3R.

The spontaneous polarization (P_S) of the compound was found to increase with decreasing temperature as expected. The measured P_S data were fitted to the mean-field model, $P_S = P_0(1 - \frac{T}{T_C})^{\beta}$ [22] where T_C is the SmC* to SmA* transition temperature and β is critical exponent for the secondary order parameter P_S. β deviates significantly from the mean field value for a second order phase transition, however, fitted T_C matches nicely with observed T_C. It is worth mentioning that the change in enthalpy values at SmC* to SmA* transition was quoted as 1.61

kJ/mole in the reference [1]. This also indicates that the corresponding transition is not second order rather points to first order.

Maximum P_S value was found to be 42.1 nC/cm^2, which is higher than all other compounds with three oligomethylene spacers (2F3R, 3F3R, 5F3R and 6F3R). Thus P_S increases with fluorination for those compounds. However, P_S value of 7F3R is less than that of 4F4R and 4F5R. P_S strongly varies with the orientational order parameter (S) of the molecules, which depends on molecular length. It was reported previously that there is an optimal length of the molecule, for which P_S is maximum and any further increase in length results in decreased P_S [23]. Thus larger molecular length of 7F3R may cause its smaller P_S.

7.3.7 Rotational viscosity (γ_φ) and Response time (τ)

The temperature variation of rotational viscosity and response time is shown in **figure 7.13**.

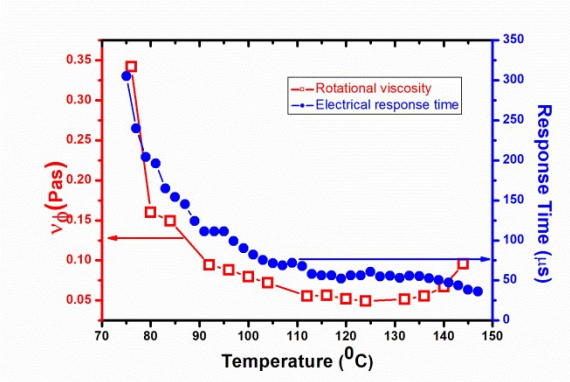

Figure 7.13: Temperature variation of rotational viscosity and response time.

The rotational viscosity in Goldstone mode was determined using the following relation $\gamma_\varphi = \frac{1}{4\pi\varepsilon_0}\frac{1}{\Delta\varepsilon f_C}(\frac{P_S}{\theta})^2$ derived from generalized Landau model [21], where Goldstone mode dielectric strength ($\Delta\varepsilon$) and relaxation frequency (f_C) were obtained from dielectric relaxation study and tilt

angle (θ) was obtained from electro optic measurement (described in section **7.3.8**). Highest value of rotational viscosity was found to be 0.34 Pas. Rotational viscosity first decreases with temperature, then near the SmC* to SmA* transition it diverges which may be due to pre-transitional effect.

The highest value of response time was found to be ~ 300 μs which is larger than all other nF3R compounds. However, it decreased rapidly with temperature and near SmC*-SmA* transition reduced to below 50 μs.

7.3.8 Optical tilt angle

Tilt angles for the compound was also determined optically and have been depicted in **figure 7.14**.

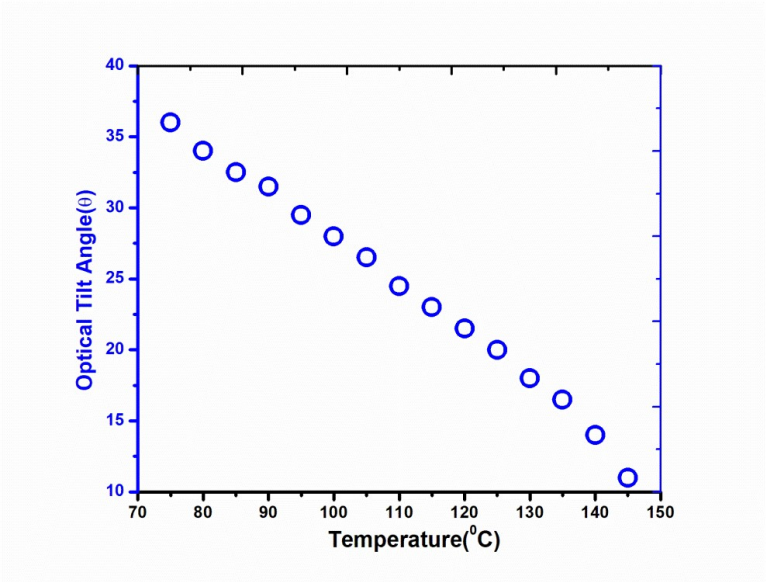

Figure 7.14: Temperature variation of optical tilt angle.

Optical tilt reflects the angle between the direction of molecular core and the layer normal. The highest value of optical tilt was found to be ~36º which is higher than all other compounds whose tilt has been

measured optically in this dissertation. The X-ray tilt, shown in **figure 7.7**, was observed to be much less than optical tilt. X-ray tilt arises from the tilt of electron-density function of the whole molecule, on the other hand optical tilt is a result of tilt of only the rigid polarisable group of the molecule, thus the two tilts may differ. This difference depends on the zig-zag shape of the molecules[24]. The zig-zag molecular shape coming out of the rigid core may tilt independently whereas the melted end chains are on the average closer to the layer normal. The X-ray tilt was observed to be less than optical tilt when the chain of a zig-zag molecule are in trans position [1].

7.4 Formulation and characterisation of a room temperature ferroelectric liquid crystal mixture using 7F3R as dopant

7.4.1 Formulation of the mixture

As discussed in the introduction section, ferroelectric liquid crystals (FLC) can be promising in display application for their high speed switching. However most of the FLCs exhibit ferroelectric behaviour at higher temperatures, a fact also observed in all the compounds studied in this dissertation. Thus there has been constant effort to formulate multi-component ferroelectric liquid crystal mixtures, which would show ferroelectric phase even at and below room temperature. We have successfully formulated a FLC mixture, which showed ferroelectric SmC* phase at room temperature and beyond, by doping 7F3R into an achiral host mixture (HM) having smectic C phase. The host matrix was formulated by mixing four pyrimidine based achiral compounds (H1, H2, H3 and H4). The molecular structures and phase sequences with

transition temperatures of these compounds and that of the host matrix are shown in **table 7.2**. The mixture was formulated following similar procedure reported previously by our group [25].

To prepare the mixtures, weights of the individual pure compounds were measured by a weighing balance (Sartorius-CPA225D, Germany) having accuracy of ±0.01mg and then were mixed (in various wt% as required) in a cleaned glass bottle. Chloroform was added to make the mixtures homogeneous and was ultrasonicated (GT Sonic Professional, Apex, India) at 65°C for four hours to evaporate chloroform completely. The complete evaporation of chloroform was confirmed by regaining the weight of the mixture. The FLC mixture was produced by mixing 30 wt% of 7F3R with 70 wt% of HM.

7.4.2 Observed phases of the mixture

Initially we mixed 10 wt% and 20 wt% of 7F3R in the host matrix, but in these mixtures no polarity was induced. But when 30 wt% of 7F3R was mixed in the host matrix, polarity could be induced and the ferroelectric SmC* phase continued far below room temperature, to around 15°C beyond which we couldn't investigate. It is relevant to note here that 4F3R was also found to induce polarity only at a minimum of 40 wt% [26], thus 7F3R induced polarity at lower concentration. Moreover, it was found to retain the SmA* phase of the dopant albeit over a larger temperature range. The phase sequence and transition temperatures of the mixture are given in **table 7.3**. The range of the SmC* phase (ΔT_{SmC*}) was found to be at least 59°, which is moderately high but less than that of the dopant (72°). However, unlike the dopant, the mixture exhibits SmC* phase even below room temperature whereas the dopant formed SmC* phase at as high as 75.5°C.

Table 7.2 Molecular structure and transition temperatures of host molecules and host mixture

H1	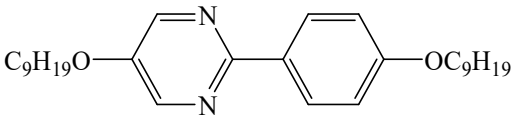
	Cr 61.8ºC SmC 95.6ºC SmA 99.1ºC I
H2	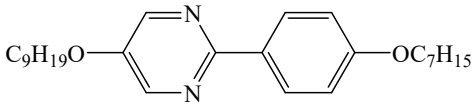
	Cr 57.4ºC SmC 95.1ºC SmA 98.4ºC I
H3	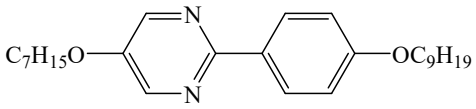
	Cr 57.2ºC SmC 79.1ºC SmA 91.2ºC N 94.7ºC I
H4	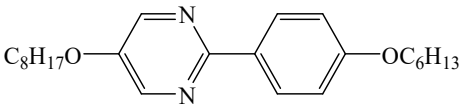
	Cr 27.5ºC SmC 46.3ºC SmA 57.5ºC N 65.6ºC I
HM	H1 20wt% + H2 20wt% + H3 20wt% + H4 40wt%
	Cr 19ºC SmC 69.4ºC SmA 78.7ºC N 81.2ºC I

Table 7.3: Phase sequence and transition temperature of the mixture

Composition:	HM (70 wt%) + 7F3R (30 wt%)
	~15°C < SmC* 74.3°C SmA* 101.4°C Isotropic

7.4.3 Polarised optical microscopy (POM) and Differential Scanning Calorimetry (DSC) study

The transition temperatures and the phase behaviour of the mixture were investigated both by POM and DSC studies. The transition temperatures matched more or less in both the processes. The DSC theromogram, showing the variation of heat flow with temperature in a cooling cycle is shown in **figure 7.15**. Peaks in the thermogram were observed at temperatures 74.3°C and at 101.4°C. It is noted that the clearing point peak is much flatter than the other one. Clearing started from a temperature ~ 96°C and continued till ~ 105°C which indicates that the transition from SmA* to the isotropic phase is not a sharp one.

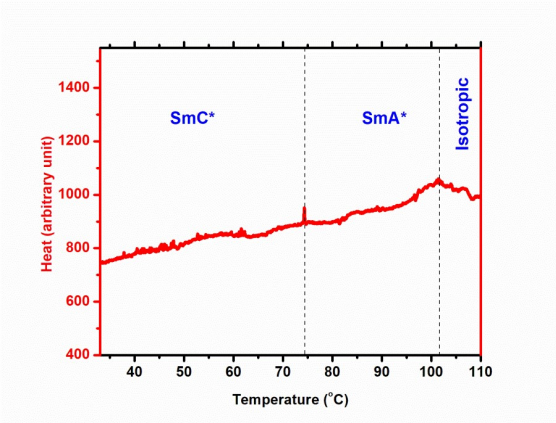

Figure 7.15: DSC thermogram of the mixture during cooling.

Observed textures are shown in **figure 7.16**. Within the temperature range 74-101°C the mixture showed clear fan shaped texture, typically observed in SmA* phase [13]. Below 74°C the texture changed to broken fan shape. A change in birefringence was also noticed. However, no chiral lines were observed, as is usually seen in SmC* phase. As noted before, even in the optical texture of pure 7F3R the chiral lines were not visible and this might be due to short pitch. Change in colour may be due to change in tilt and birefringence with temperature[13]. From about 90°C, domains of isotropic phase could be observed within the SmA* texture. This seems to be in conformity with the DSC observation that asserted a continuous transition to isotropic phase rather than a sharp one.

Although no chiral lines could be observed in SmC* phase, switching of the molecules was observed under an ac field of strength 0.12 V/µm which confirmed the ferroelectric nature of the phase. Switching could also be observed at 2.0 V/µm field in SmA* indicating the presence of electroclinic effect.

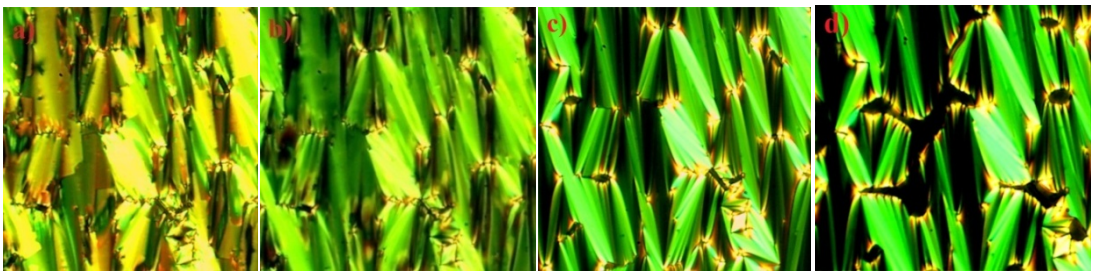

Figure 7.16: Textures of the mixture at temperature a) 33°C (SmC*) b) 63°C (SmC* with changed birefringence) c) 85°C (SmA*) and d) 93°C (SmA* with isotropic domain).

7.4.4 Synchrotron diffraction study

Synchrotron diffraction studies were carried out on the mixture and also on the constituent compounds to compare their structural properties.

In all the phases one sharp inner ring and one diffused outer ring were observed. Representative diffraction photographs of the host compound in SmC phase and of the mixture in SmC* and SmA* phase are shown in **figure 7.17** and **7.18** and intensity profiles of inner and outer maximum of the mixture are shown in **figures 7.19** and **7.20.** The layer spacing (d), average intermolecular spacing (D) and X-ray tilt angle were calculated by the same procedure described before.

To inculcate the structural properties, temperature variation of layer spacing and X-ray tilt of the host matrix (HM) are plotted along with those of the host matrix components (H1,H2, H3 and H4) and are shown in **figure 7.21**.

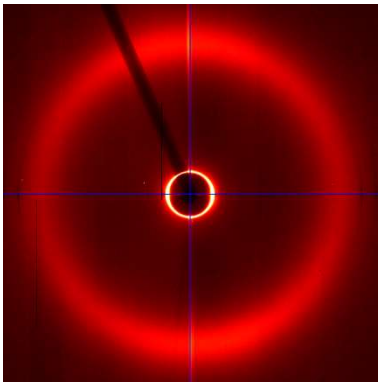

Figure7.17: Diffraction photograph of HM in SmC phase (60ºC)

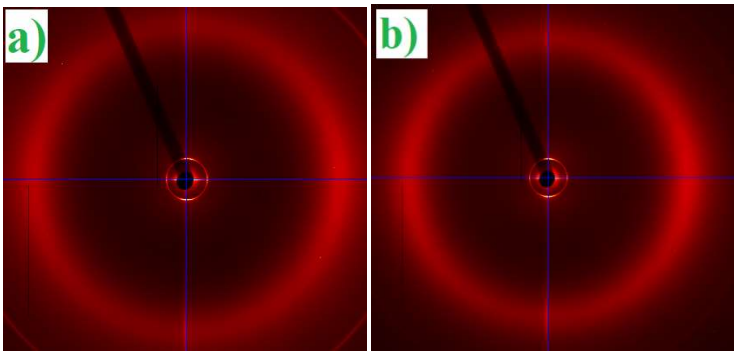

Figure 7.18: Diffraction photograph of the mixture in a) SmC* (66ºC) and b) SmA* (84ºC) phases.

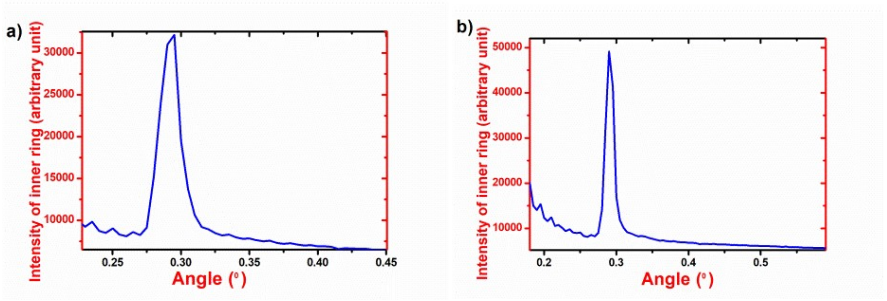

Figure 7.19: The intensity profile of the inner maxima of X- ray photograph in a) SmC* (66ºC) and b) SmA* (84ºC) phases of the mixture.

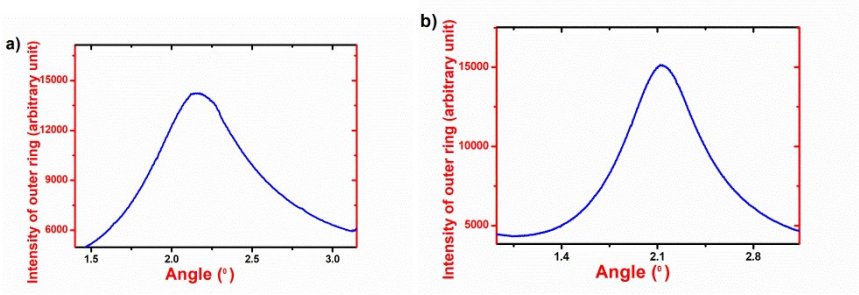

Figure 7.20: The intensity profile of the outer maxima of X- ray photograph in a) SmC* (66ºC) and b) SmA* (84ºC) phases of the mixture.

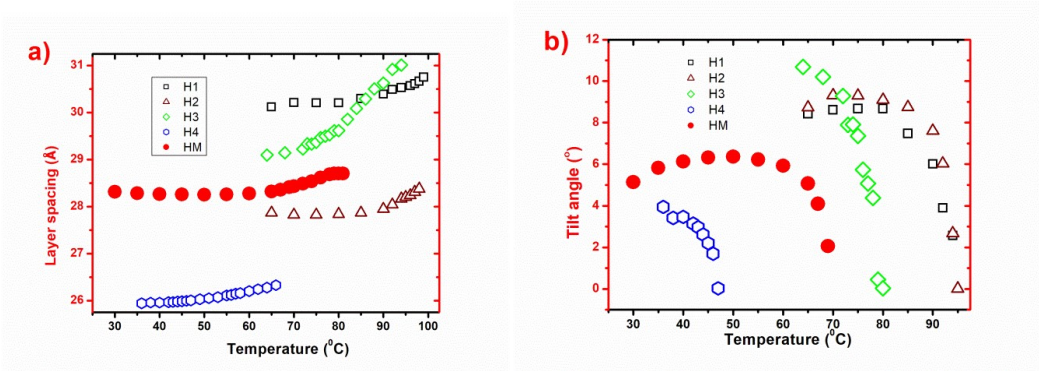

Figure 7.21: Temperature variation of a) layer spacing and b) tilt angle of H1, H2, H3, H4 and HM.

For all the compounds the layer spacing increased and tilt angle decreased with temperature as expected. The rate of increase of 'd' with temperature was found to be highest for the constituent H3. In HM layer spacing was found to have a marginal increasing trend with temperature even within SmA phase and became constant after entering into the nematic phase. Layer spacing of the host matrix is found to be almost equal to the weighted average layer spacing of the constituents, but the tilt is lower. The minimum and maximum 'd' values of the mixture diverged only by 0.52 Å and 0.2Å from the respective weighted average 'd' values of the constituents. But for tilt these differences are higher, respectively being 1.5° and 1.6º.

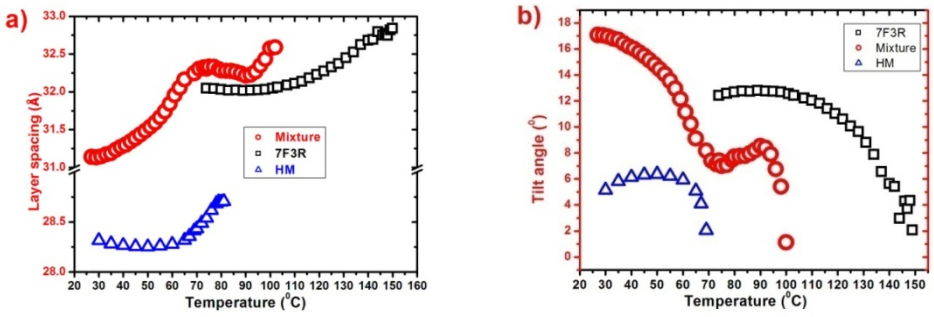

Figure 7.22: Temperature variation of a) layer spacing and b) tilt angle of the mixture, HM and 7F3R.

Temperature evolutions of layer spacing and tilt angle compared to the host matrix and the dopant have been presented in **figure 7.22**. In the low temperature region of SmC* phase the layer spacing of the mixture is in between the host and the dopant (if we extrapolate the values of dopant to low temperature). However, the maximum value of the layer spacing of the mixture in SmC* phase (32.3 Å) is found to be closer to that of the dopant (32.8Å) rather than in the host matrix (28.7Å). On the other hand, in the low temperature region of SmC* phase the tilt is much higher in the mixture than in the host and the dopant. The maximum tilt of the

mixture in SmC* phase is found to be moderate (~17°) and it decreased with temperature as expected. Thus the mixture had more suitable tilt than the dopant 7F3R, to use in SSFLD, where ideally a tilt of 22.5° is preferred [27].

To analyse further the temperature evolution of layer spacing in the mixture in different phase it has been shown separately in **figure 7.23**. It is noted here that temperature scan could be carried out till only 27°C in the diffraction experiment.

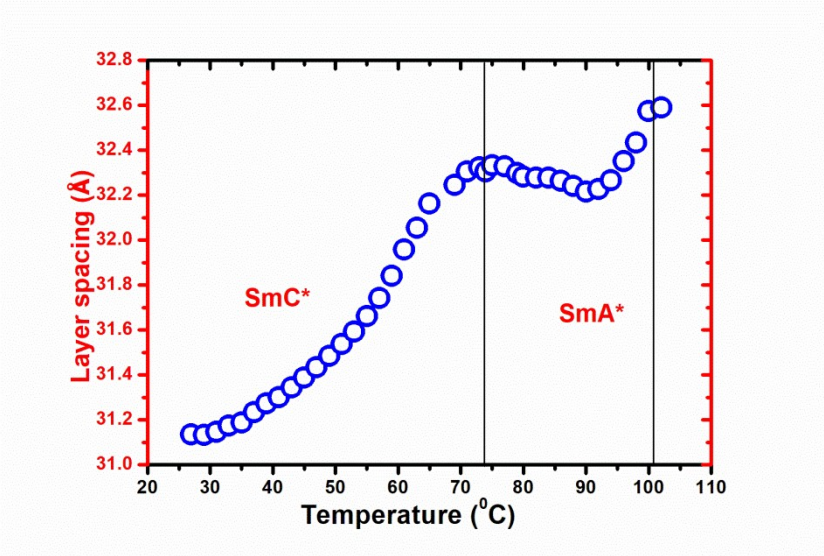

Figure 7.23: Temperature variation of layer spacing of the mixture.

The minimum value of layer spacing in SmC* phase was found to be 31.13Å which increased with temperature as expected. But in SmA* phase 'd' value first decreased and then increased with temperature. However, its maximum value (~32.6Å) was found to be less than the weighted average of the optimised molecular lengths of the constituent molecules (32.75Å), just like in the dopant 7F3R. It indicates that the mixture may exhibit de vries type SmA* phase. The increasing trend of 'd' with temperature within SmA* phase from a temperature ~92°C may be due to pre-transition effect. It can be recalled that from DSC and POM

data it was inferred that isotropic domains seem to form within SmA* phase from that temperature range. Below that temperature d value showed a negative thermal expansivity which is seen in a de veries like SmA* phase [16,28]. The highest layer shrinkage in SmC* phase was found to be only 3% which is still much less than normal SmA* phases [29,30]. However, the layer shrinkage is more than that of pure 7F3R (2.3%). To probe this further we have calculated, using **equations 7.2** and **7.3**, the figures of merits 'R' and 'f' defined by Radcliffe *et al.* [16,31] to gauge the capability of a de veries type material to achieve defect free book shelf geometry.

$$R = cos^{-1}\left[\frac{d_c(T)}{d(T_{AC})}\right]/\theta_{OPT}(T) \qquad [7.2]$$

$$f = cos^{-1}\left[\frac{d_c(T)}{d_A(T)}\right]/\theta_{OPT}(T) \qquad [7.3]$$

Here, $d_C(T)$ is smectic layer spacing at T, d (T_{AC}) is layer spacing at SmC* to SmA* transition, $d_A(T)$ is the layer contraction relative to SmA* layer spacing extrapolated to SmC* phase, and $\theta_{OPT}(T)$ is the optical tile angle (optical tilt of the mixture will be reported in section **7.4.5**).

R and f are found to be 0.34 and 0.36 respectively in 7F3R which are in excellent agreement with the de Veries like compounds capable of having defect free bookshelf geometry [16,32]. However, in the mixture these values are found to be 0.71 and 0.79. Though 'de veries like character' has been compromised to some extent in the mixture, but comparing the 'R' and 'f' values (~0.8) of other reported partially de veries like compounds [32,33], it can be concluded that there is partial de veries like characteristics even in the mixture.

To see the effect of electric filed on the mixture property, tilt angles had been measured both without and with application of a dc field of 12V/µm across the measuring cell. These results are shown in **figure 7.24**. In the mixture in SmA* phase a tilt of ~8° was observed even without external field, which might be related with its de Vries like character. After application of field, tilt angle increased in both phases and electroclinic effect was observed in SmA* phase where the tilt increased by ~ 2.5°.

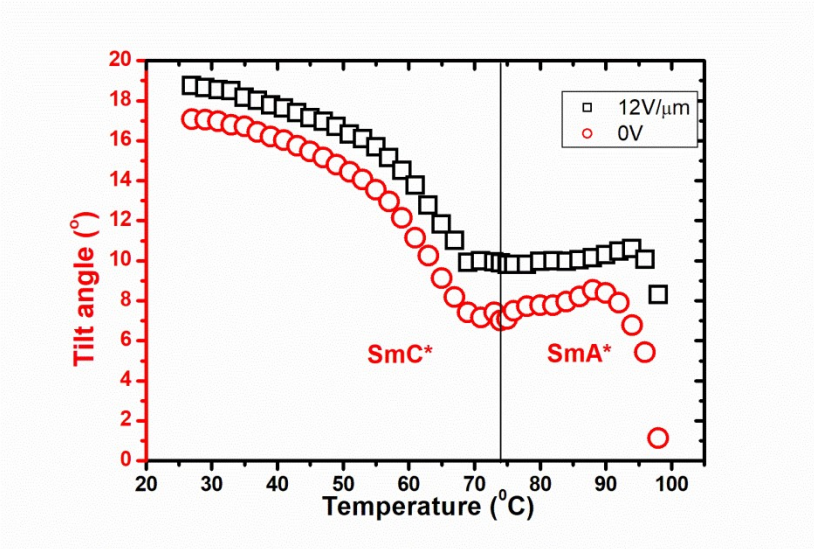

Figure 7.24: Temperature variation of X-ray tilt of mixture with and without bias.

To explore the positional correlation of the molecules in different phases of the mixture, the correlation lengths across and within the layers were measured from the full width at half maxima of the scattering vector of corresponding Bragg's peak. The temperature variations of the correlation lengths in the mixture are shown in **figure 7.25**, variations in the dopant are also shown for ease of comparison.

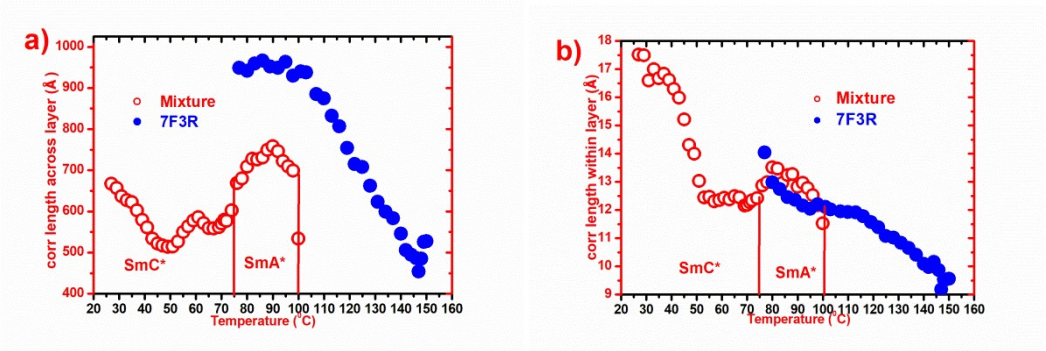

Figure 7.25: Correlation lengths of the mixture and the dopant a) across the layers and b) within the layers.

It is observed that the correlation length across the layer ($\xi_{\parallel}$) in the mixture decrease slightly from that of dopant 7F3R. In 7F3R it is found to be about 26 times of its molecular length, while in the mixture it is about 23 times of the weighted average of the molecular lengths of the constituent compounds. Surprisingly this correlation length is found to increase by ~ 100Å in SmA* phase than in SmC* phase following the same trend as was observed even in 7F3R. The correlation length of the mixture within the layers ($\xi_{\perp}$) is found to be maximum in SmC* (17.5Å), then it decreases with temperature. However after entering into SmA* phase it increased marginally. In the common temperature range correlation lengths ($\xi_{\perp}$) of the dopant and the mixture are found to be comparable for 7F3R and the mixture, with a minor increase in the mixture. No appreciable change in correlation lengths were observed under the influence of electric field.

7.4.5 Spontaneous and induced polarization (P_S)

The temperature variation of P_S of the mixture is shown in **figure 7.26**. The P_S was measured with a voltage 19V/μm which was the saturation field (discussed below). In SmC* phase the spontaneous polarization

initially increased with temperature and reached its highest value (31.7 nC/cm^2) at 46ºC and then was found to decreased with temperature as expected. The highest value of spontaneous polarization in SmC* phase (31.7 nC/cm^2) was found to be less than that of 7F3R (42.1 nC/cm^2) (discussed in section **7.3.6**). In electroclinic SmA* phase the total polarization (P_S) consists of two parts: one part represents the orientation and electronic polarization and the second part is due to P-θ coupling [34]. It is difficult to separate these two parts, so, in SmA* phase by P_S we represent the total induced polarization. Moderate value of P_S (24.6 nC/cm^2) was observed in the electroclinic SmA* phase. Such moderate values of induced polarization in electroclinic SmA* phase were reported previously in other chiral compounds [35,36] as well. P_S changed almost continuously at SmC* to SmA* transition. In de Vries type SmA* phase such continuous change in Ps was reported before and this is expected as in addition to usual electroclinic effect, here the induced polarization is also a result of "the biasing of the molecular azimuthal distribution perpendicular to the electric field"[35].

Near the SmA* to isotropic transition the measured data was fitted to the mean field model $P_S = P_0(1 - \frac{T}{T_C})^{\beta}$, [24] where T_C is the SmA* to isotropic phase transition temperature and β is the critical exponent of second order parameter. T_C is not found to deviate more than 1°C from the observed data in the mixture. β is also found to be 0.21which is comparable to the value (0.25) predicted by Landau theory at the cross over (triclinic) point from 2nd order to 1st order transition [33,37].

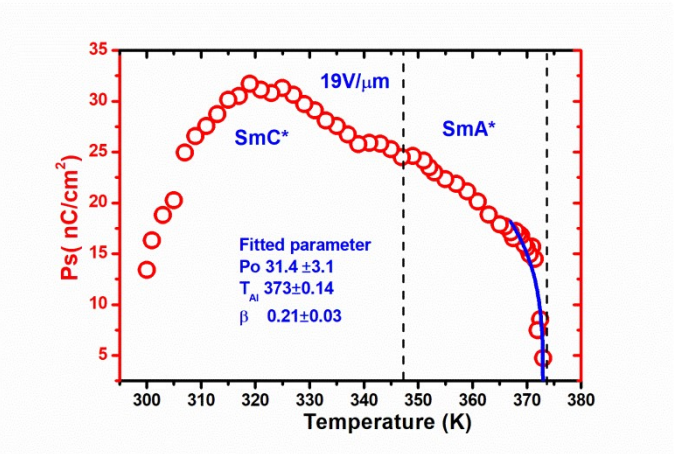

Figure 7.26: Temperature variation of P_S of the mixture.

To explore the bias dependence of P_S, spontaneous polarization was measured as a function of voltage at two particular temperatures in two different phases as shown in **figure 7.27**. In SmC* phase switching was observed at a minimum field of 0.12V/μm, however, in SmA* phase about twenty times more field was required (2V/μm) to observe the switching. But due to noise in signal at low voltage, P_S could be reported only at a minimum voltage of 4V/μm. In both phases P_S was found to increase with applied voltage and ultimately reached saturated polarization at a field of ~19 V/μm. P_S was also measured with decreasing voltage to see the hysteresis effect. In SmC* phase appreciable hysteresis was observed, which might be useful in terms of memory effects in FLC [38]. In SmA* phase also hysteresis could be observed, but the effect is less than that in SmC* phase.

Similar increase of induced polarization with applied electric field in electroclinic de Vries type SmA* phase was reported before [35]. For de Vries like SmA* phase, this variation can be explained if we consider the reorientation of the molecular dipoles in presence of electric field is of Langevin type and assume that the effective dipole moment (μ_{eff}) will also increase with the applied field [35]. μ_{eff} can be calculated from the

relation $\mu_{eff} = \pi d(\frac{\xi_\perp}{2})^2 P_s$ derived from Langevin formula [35], where $\xi_\perp$ is the correlation length within a layer, d is the layer spacing and P_S is induced polarization. The effective dipole moment has been calculated for the mixture in SmA* phase (77ºC) as a function of applied voltage and is shown in **figure 7.28**.

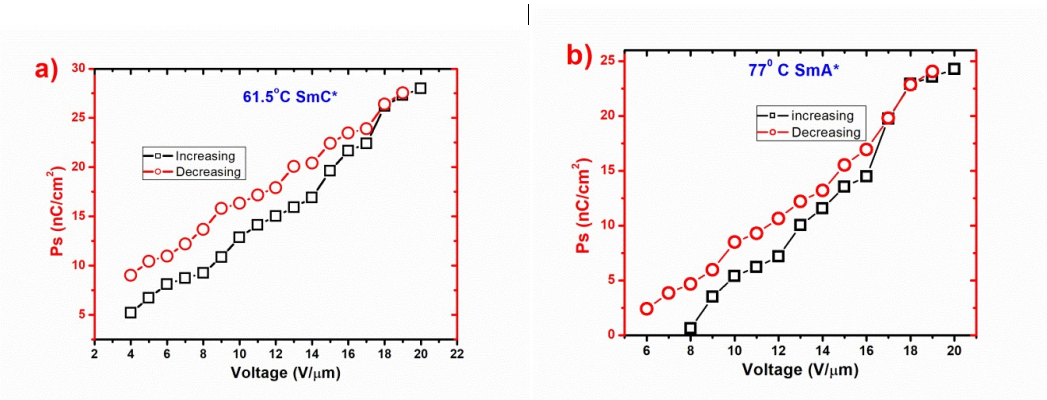

Figure 7.27: Field variation of P_S in a) SmC* and b) SmA* phases.

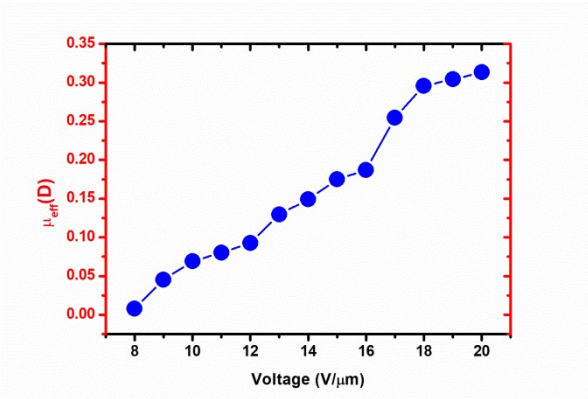

Figure 7.28: Dependence of effective dipole moment on applied field in SmA* phase (77ºC).

μ_{eff} increases with applied voltage as expected and reached a saturation value of ~ 0.32 D near 19V/μm. The saturated value of the dipole moment is comparable with the perpendicular component of molecular dipole moment of 7F3R (0.47D), obtained by optimising the molecular structure as discussed in section 7.3.3.

7.4.5 Optical tilt angle (θ)

The optical tilt angle of the mixture was measured in both SmC* and SmA* phases with an applied voltage of 16V/µm as shown in **figure 7.29**. The θ was found to decrease with temperature as expected. Highest tilt in SmC* phase was 20.6°. Even in SmA* phase it was as high as 17°, which established the electroclinic behaviour of the compound once again. For the ease of comparison the X-ray and optical tilt of the mixture and 7F3R are shown together in **figure 7.30**. The optical tilt of the mixture was found to be much less compared to the dopant 7F3R but it was found to be comparable but marginally higher than X-ray tilt. In the mixture tilt angle was also measured at a particular temperature in SmA* phase as a function of applied voltage and is shown in **figure 7.30**. This clearly shows that induced tilt is linear function of applied field at low field region and at higher field it saturates.

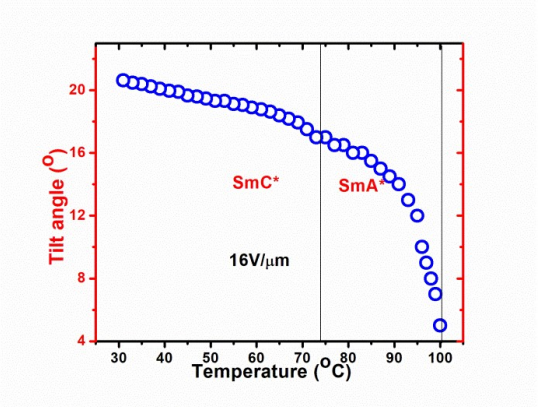

Figure 7.29: Temperature variation of optical tilt of the mixture.

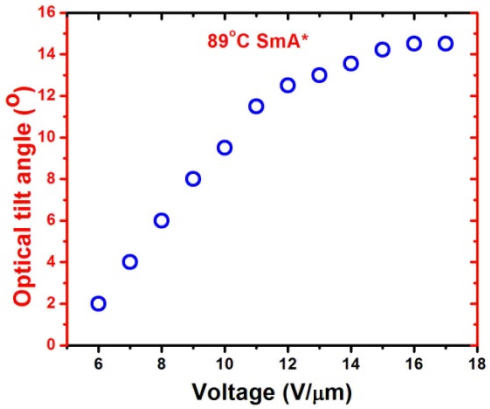

Figure 7.30: Bias dependence of optical tilt of the mixture at temperature 89°C (SmA*).

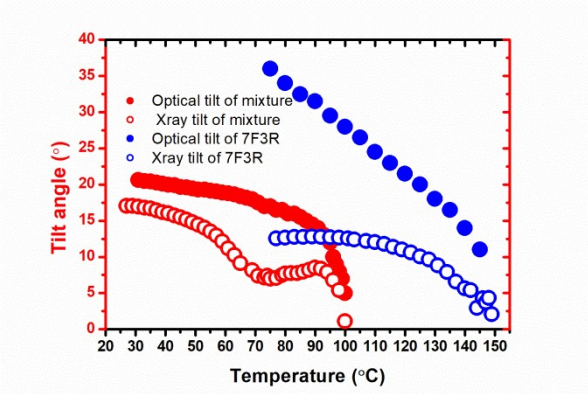

Figure 7.31: The X-ray and optical tilt of mixture and 7F3R.

7.4.6 Response time (τ)

Response time is one of the most important parameter from application perspective. In pure 7F3R the highest rise time in SmC* phase was found to be 300μs. In the mixture the response time decreased significantly probably because of lower viscosity which makes the mixture more suitable for fast display applications. Temperature dependence of τ, measured at a voltage 11V/μm for the mixture is shown in **figure 7.32**. In SmC* phase τ was found to be ~ 215 μs. In SmA* phase it decreased

again. The maximum value of response time in SmA* phase was found to be ~190μs. Though this value is higher than in many electroclinic compounds [36], but response time in order of few hundred microsecond had also been reported before for electroclinic de Vries type compounds [35,39].

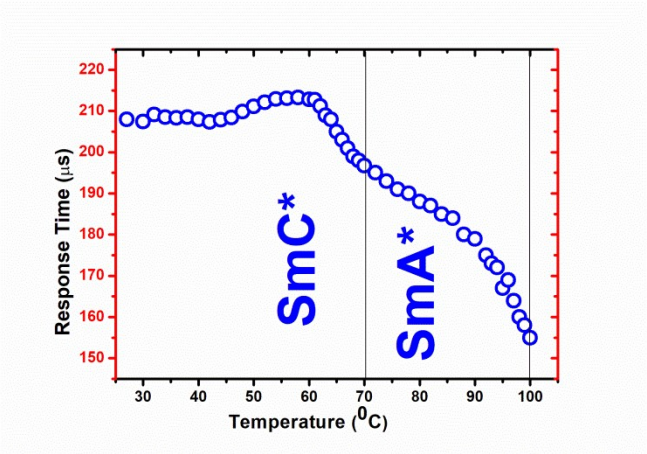

Figure 7.32: Temperature variation of rise time of the mixture.

7.5 Conclusion

The compound 7F3R, having highest number of fluorine atoms in the chain, exhibits SmC* phase for the widest span of temperature among the selected compounds. The compound is also found to have de Vries type SmA* phase. It showed both GM and SM relaxation modes. It showed high optical tilt and sharp electrical response time. An FLC mixture is obtained by doping 30% 7F3R in an achiral pyrimidine based host mixture, for the lower homologue 4R3R minimum 40% doping was necessary for inducing polarity. While the dopant produce ferroelectric phase from 75.5^{o}C, the mixture is found to exhibit ferroelectric SmC* phase from below room temperature and the phase is found to exist over a wide temperature range. It also shows SmA* phase before melting into isotropic phase. Further, the SmA* phase is found to exhibit partial de

Vries type property and electroclinic effect. In the low temperature region of SmC* phase the layer spacing of the mixture is in between the host and the dopant while the tilt is found to be much higher in the mixture than in the host and the dopant. It was found to have moderate spontaneous polarization. Optical tilt of around 20° at room temperature and a response time of a few hundred microseconds make the mixture suitable to use in SSFLCDs. It is expected that problem of chevron defect and hence reduced contrast ratio will be minimum since highest layer shrinkage of in SmC* phase is 3%. Further, the mixture in SmC* phase shows appreciable hysteresis which might be useful in terms of memory effects in FLC.

Reference

[1] Ziobro D, Dąbrowski R, Tykarska M, et al. Synthesis and properties of new ferroelectric and antiferroelectric liquid crystals with a biphenylyl benzoate rigid core. Liq. Cryst. 2012;39:1011–1032.

[2] Maltese P. Advances and problems in the development of ferroelectric liquid crystal displays. Mol. Cryst. Liq. Cryst. Sci. 1992;215:57–72.

[3] Rudquist P. Orthoconic antiferroelectric liquid crystals. Liq. Cryst. 2013;40:1678–1697.

[4] Takezoe H, Gorecka E, Čepič M. Antiferroelectric liquid crystals: Interplay of simplicity and complexity. Rev. Mod. Phys. 2010;82:897–937.

[5] Hird M. Ferroelectricity in Liquid Crystals and Its Applications. Liq. Cryst. 2011;38:1467–1493.

[6] Bennis N, Dąbrowski R, Spadlo A, et al. Non-conventional alignment surfaces for antiferroelectric liquid crystals. Mol. Cryst. Liq. Cryst. 2004;422:307–316.

[7] Kuczyński W, Stegemeyer H. Ferroelectric properties of smectic C liquid crystals with induced helical structure. Chem. Phys. Lett. 1980;70:123–126.

[8] Thurmes WN, Wand MD, Vohra RT, et al. FLC materials for microdisplay applications. Proc. Spie. 1997;3015:1–6.

[9] Wand MD, Vobra R, Thurmes W, et al. NEW FERROELECTRIC LIQUID CRYSTAL HOST MATERIALS FOR USE IN

OPTOELECTRONIC APPLICATIONS. Proc. Spie. 1994;2175:2–7.

[10] Wand M, Thurmes W, Meadows M, et al. FLC Displays for High Resolution Magnified View and Projection Applications. Proc. Spie. 1999;3635:2–7.

[11] Böttcher C, Belle O, Rip A, et al. Theory of Electric Polarization, Vol II. Amsterdam, New York: Elsevier, Scientific Publishing Co; 1973.

[12] Miyasato K, Abe S, Takezoe H, et al. Direct Method with Triangular Waves for Measuring Spontaneous Polarization in Ferroelectric Liquid Crystals. Jpn. J. Appl. Phys. 1983;22:L661–L663.

[13] Dierking I. Textures of Liquid Crystals. wiley-vch. Weinheim: WILEY-VCH; 2003.

[14] Gaussian 09, Revision D.01, M. J. Frisch *et al.* Gaussian, Inc., Wallingford CT, 2013.

[15] Agra-Kooijman DM, Yoon H, Dey S, et al. Origin of weak layer contraction in de Vries smectic liquid crystals. Phys. Rev. E 2014;89:032506.

[16] Singh HK, Singh SK, Nandi R, et al. Observation of exceptional 'de Vries-like' properties in a conventional aroylhydrazone based liquid crystal. RSC Adv. 2016;6:57799–57802.

[17] Sreenilayam SP, Rodriguez-Lojo D, Agra-Kooijiman D, et al. De Vries liquid crystals based on a chiral 5-phenylpyrimidine benzoate core with a tri- and tetra-carbosilane backbone tetra-carbosilane

backbone. Phys. Rev. Mater. 2018;2:025603-1-025603–025612.

[18] Hartley CS, Kapernaum N, Roberts JC, et al. Electroclinic effect in chiral SmA* liquid crystals induced by atropisomeric biphenyl dopants: Amplification of the electroclinic coefficient using achiral additives. J. Mater. Chem. 2006;16:2329–2337.

[19] Sirota EB, Pershan PS, Sorensen LB, et al. X-Ray Studies of Tilted Hexatic Phases in Thin Liquid-Crystal Films. Phys. Rev. Lett. 1985;55:2039–2042.

[20] Hasse W, Wróbel S. Relaxation Phenomena: Liquid Crystals, Magnetic Systems, Polymers, High-Tc Superconductors, Metallic Glasses. Berlin: Springer; 2003.

[21] Carlsson T, Žekš B, Filipič C, et al. Theoretical model of the frequency and temperature dependence of the complex dielectric constant of ferroelectric liquid crystals near the smectic-C* — smectic- A phase transition. Phys. Rev. A. 1990;42:877–889.

[22] Lagerwall ST. Ferroelectric and antiferroelectric liquid crystals. Newyork: WILEY-VCH; 1999.

[23] Mikułko A, Arora P, Glushchenko A, et al. Complementary studies of BaTiO 3 nanoparticles suspended in a ferroelectric liquid-crystalline mixture. Europhys. Lett. 2009;87:27009.

[24] Bartolino R, Doucet J, Durand G. Molecular tilt in the smectic C phase : a zigzag model. Ann. Phys. (Paris). 1978;3:389–395.

[25] Debnath A, Mandal PK. Dielectric properties of four room temperature ferroelectric and antiferroelectric multi- component liquid crystalline mixtures. Liq. Cryst. 2019;46:234–248.

[26] Debnath A, Mandal PK. Wide range room temperature ferroelectric liquid crystal mixture with microsecond order switching. J. Mol. Liq. 2016;221:287–291.

[27] Debnath A, Mandal PK, Węglowska D, et al. Induction of a room temperature ferroelectric SmC* phase in binary mixtures with moderate spontaneous polarization and sub-millisecond switching time. RSC Adv. 2016;6:84369–84378.

[28] Gorkunov M V., Giesselmann F, Lagerwall JPF, et al. Molecular model for de Vries type smectic A - smectic C phase transition in liquid crystals. Phys. Rev. E. 2007;75:060701.

[29] Kumar S. High-resolution x-ray measurements ofthe smectic phases ofterephthal-bis-(4n)-alkylanilines. Phys. Rev. A. 1981;23:3207–3214.

[30] Lagerwall JPF, Giesselmann F. Current Topics in Smectic Liquid Crystal Research. ChemPhysChem. 2006;7:20–45.

[31] Radcliffe MD, Brostrom ML, Epstein KA, et al. Smectic A and C materials with novel director tilt and layer thickness behaviour. Liq. Cryst. 1999;26:789–794.

[32] Roberts JC, Kapemaum N, Giesselmann F, et al. Design of liquid crystals with “de Vries-like” properties: Organosiloxane mesogen with a 5-phenylpyrimidine core. J. Am. Chem. Soc. 2008;130:13842–13843.

[33] Roberts JC, Song Q, Ayub K, et al. Design of liquid crystals with “de Vries-like” properties: Frustration between SmA- and SmC-promoting elements. J. Am. Chem. Soc. 2010;132:364–370.

[34] Kitzerow H, Bahr C, editors. Chirality in Liquid Crystals. New York: Springer; 2001.

[35] Manna U, Song J-K, Vij JK, et al. Anomalous dependence of response time on the electric field in an electroclinic liquid crystal with large induced tilt and polarization. Appl. Phys. Lett. 2009;94:012901.

[36] Bahr C, Heppke G. Infiuence of electric field on a first-order smectic-A —ferroelectric-smectic-C liquid-crystal phase transition: A field-induced critical point. Phys. Rev. A. 1990;41:4335–4342.

[37] Birgeneau RJ, Garland C, Kortan A, et al. Smectic-A —smectic-C transition: Mean field or critical. Phys. Rev. A. 1983;27:1251–1254.

[38] Prakash J, Chandran A, Biradar AM. Scientific developments of liquid crystal-based optical memory: a review. Reports Prog. Phys. 2017;80:016601.

[39] Naciri J, Ruth J, Crawford G, et al. Novel Ferroelectric and Electroclinic Organosiloxane Liquid Crystals. Chem. Mater. 1995;7:1397–1402.

CHAPTER-8

Summary and conclusion

The main objective of this dissertation was to characterise the phase behaviour and study the dielectric, electro-optic, structural properties of a few selected chiral liquid crystal compounds of the same homologous series (1F3R, 2F3R, 3F3R, 4F4R, 4F5R, 5F3R, 6F3R, 7F3R), with biphenyl benzoate core and fluorinated chains, whose molecular structure differ only by the number of carbon atoms and the number of oligomethylene spacers in the fluorinated chain. It was also proposed to explore a relationship of their physical properties with change in their molecular structures. Finally, it was proposed to formulate one multi-component mixture using one of the above compounds as a dopant.

In the last five chapters we have discussed in detail the characterisation of phases present in all these compounds and their structural, dielectric and electro-optic properties. In the last chapter we have also presented method of formulation and characterization of a room temperature ferroelectric liquid crystal mixture by doping the longest chain compound 7F3R in an achiral multi-component host matrix. In this chapter the major observations made in this dissertation and few insights on the structure-property correlations will be highlighted.

Analysis of the optimised molecular structures reveals:

- In three oligomithylene spacer containing compounds (nF3R), both dipole moment and optimised length are found to increase with increasing number of fluorinated carbons, except at the transition from 2F3R to 3F3R, where trend is opposite. This has been depicted schematically in the **figure 8.1**. This is because after addition of the third carbon, the fluorinated chain gets twisted in the z direction (perpendicular to the plane of molecule) by almost 87º. Although in the remaining compounds it persists, but the dipole moment and molecular length continue to increase due to the addition of further carbon atoms.

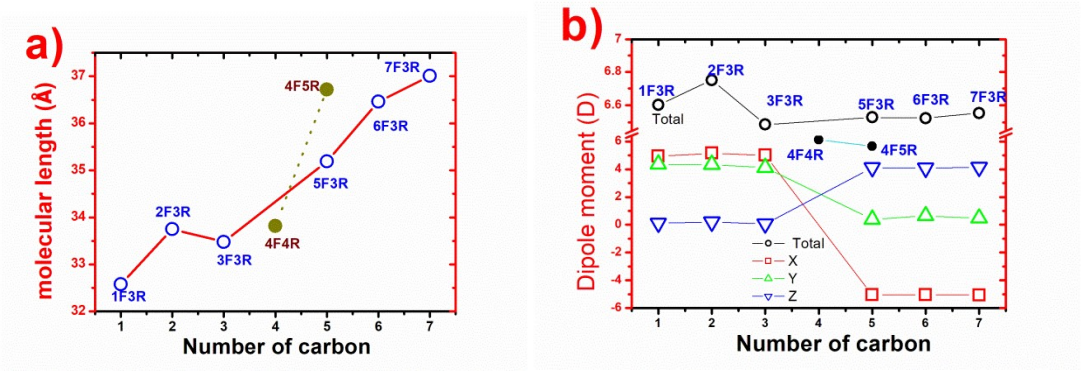

Figure 8.1: a) Optimised molecular length and b) Dipole moments of compounds nFmR. For 4F4R and 4F5R, number of oligomethylene spacers is plotted along x-axis.

- In all molecules dipole moments are found to be transverse.
- X and Y components of dipole moments change orientation with respect to the Z component from 5F3R. This might be due to a combined effect of the twist in the chain and the addition of extra 4 fluorinated carbon atoms. However, only change in sign of the Y component dipole moment of 4F5R is observed compared to 4F4R.
- The molecular length increases after addition of oligomethylene spacers (4F4R, 4F5R) as expected. However dipole moment decreases compared to nF3R series.
- Conformation of 4F5R is substantially different from other molecules. In 3F3R, 5F3R, 6F3R and even in 4F4R both the chiral chain and the fluorinated chain are bent in the same direction of the core while in 4F5R they are bent in the opposite directions.

A wide variety of orthogonal and tilted phases have been observed, at-a-glance-view of which is presented in **table 8.1**. From studying the phase sequence of the compounds it is observed:

- The compound 1F3R, having just one carbon atom in the fluorinated chain, exhibits three orthogonal smectic phases - SmE*, SmB* and SmA*. When just one extra carbon atom is added in the fluorinated chain, in 2F3R along with SmA* phase three tilted phases are induced – SmJ*, SmF* and SmC*. In the next higher homologue (3F3R) phase sequence remain same, but SmA* phase disappeared and tilting of the molecules only in the soft crystalline phase (SmJ*) changes from edge towards an apex in the pseudo-hexagonal cell giving rise to SmG* phase. Therefore, change of tilt occurs within two consecutive phases in 2F3R whereas no such change takes place in 3F3R.

Table 8.1: Phase sequence of the compounds.

Compound	Phase sequence with transition temperatures (^{o}C)
1F3R	Crystal 80 SmE* 103 $SmB_{hex}^{*\,mo}$ 121^{o}C $SmB_{hex}^{*\,lo}$ 127.5 SmA* 151 Iso
2F3R	Crystal 68 SmJ* 83 SmF* 85 (SmF*+SmC*) 100 SmC* 129 SmA*135 Iso
3F3R	Crystal 65 SmG* 73.5 SmF* 75 (SmF*+SmC*) 83 SmC* 131 Iso
5F3R	Crystal 83 SmC* 139.5 Iso
6F3R	Crystal 83 SmC* 146.2 Iso
4F4R	Crystal 86.5 SmX* 98 SmC* 130.9 Iso
4F5R	Crystal 78 SmC* 132.5 Iso
7F3R	Crystal: 75.5 SmC* 148.0 SmA* 150.1 Iso
Mixture	15 < SmC* 74.3 SmA* 101.4 Iso

- Hexagonal phases are observed only in 1F3R (orthogonal), 2F3R (tilted) and 3F3R (tilted), but not in higher homologous.

- Ferroelectric SmC* phase is observed in all except in 1F3R. Stability or thermal range of SmC* phase increases with fluorinated chain length and also with increasing oligomethylene spacers. Lower stability in 4F4R compared to 3F3R is may be due to the presence of a *subphase* (SmX*). This is depicted graphically in **figure 8.2**.

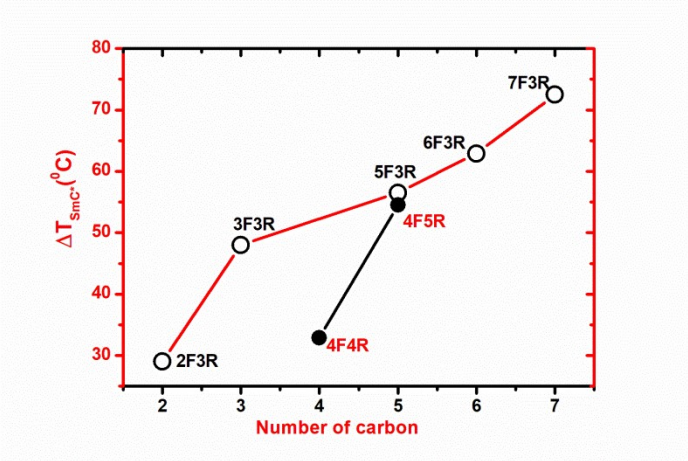

Figure 8.2: Span of SmC* phase of different compounds. For 4F4R and 4F5R, number of oligomethylene spacers is plotted along x-axis.

- In 4F4R one *subphase* is observed below SmC*. Although this phase shows many characteristics of ferrielectric SmC*$_\gamma$ phase, but since the GM dielectric increment is found to be higher than in SmC* phase, the new phase is termed as SmX* phase.
- Paraelectric SmA* phase is observed in 1F3R and 2F3R, then it is found to be absent in the higher homologous. However, it reappears in the phase sequence in the longest chain compound 7F3R. A major change in the conformations of the optimised molecular structures and thus in the dipole moments is observed from 3F3R. This results in a change in the intermolecular interactions and probably plays an important role in the

disappearance of SmA* phase. This effect is neutralized when chain length increases substantially (7F3R) and reappearance of SmA* takes place. It may further be added that even a subtle change in the intermolecular interactions produces a significant change in the phase behaviour of these kinds of self organized soft materials.

Temperature evolution of frequency domain dielectric spectroscopy gives considerable insight into the dynamics of the molecules within different phases.

- Only in the SmB* phase of 1F3R short axis flip-flop mode of molecular relaxation is observed.
- Both bond orientation order (BOO) phason and tilt phason relaxation modes are observed in the SmF* phase. This is observed in both 2F3R and 3F3R which exhibit this phase. To the best of our knowledge for the first time both (BOO) phason and tilt phason are observed in a single compound.
- Maxwell-Wagner mode of relaxation is observed only in 1F3R, 2F3R, 3F3R and 6F3R. Since MW mode is related with the accumulation of charge in the interface of heterogeneous materials, thus its presence in certain compounds and absence in others might be related with the purity of the samples.
- Goldstone mode is observed in SmC* phase of all compounds. Temperature dependences of its critical frequency and dielectric increment are explained in the light of generalized Landau theory.
- Soft mode relaxation is observed only compounds having both SmA* and SmC* phases. Thus SM is observed only in 2F3R and 7F3R (also in the mixture) throughout the SmA* phase and also in SmC* phase but in the vicinity of SmC*-SmA* transition.

- Soft mode relaxation is not observed in any other compounds, neither in SmC* phase (3F3R, 4F4R, 4F5R, 5F3R and 6F3R) nor in SmA* phase (1F3R). When a material is cooled down from orthogonal SmA* phase to the tilted SmC* phase, the elastic constant, responsible for keeping the molecules perpendicular to the smectic layer, softens considerably. Due to softening of the restoring force, when an AC signal is applied, the molecules vibrate by making their tilt angles fluctuate. This gives rise to the soft mode relaxation. Thus it is hypothesized that soft mode relaxation cannot be observed in any substance where SmA*-SmC* phase transition is absent.
- In nF3R series of compounds Goldstone mode critical frequency is found to increase with fluorinated chain length. Thus it shows a direct correlation with the dipole moments of the molecules. GM critical frequency also found to increase with increasing oligomethylene spacers. Dielectric increment also increases with chain length in these compounds with two exceptions. Δε of 3F3R is found to be marginally less than that of 2F3R, which may be due to smaller moment of 3F3R. Δε decreases sharply in the longest chain compound 7F3R becoming the least of all the compounds. Δε is the highest in 4F4R but decreasing once again in 4F5R. However, dipole moment of 4F5R is less than 4F4R. Thus there is also a direct correlation between the dielectric increments and dipole moments of the molecules, only exception being 7F3R These correlations are shown in **figure 8.3**.

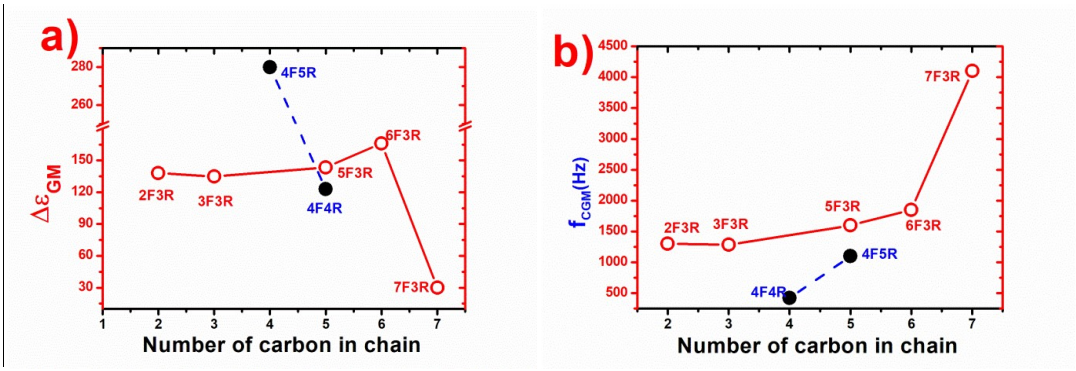

Figure 8.3: Variation of Goldstone mode a) dielectric increment (Δε) and b) critical frequency (f_C) of nFmR. For 4F4R and 4F5R, number of oligomethylene spacers is plotted along x-axis.

Structures of several higher order smectic phases of 1F3R, 2F3R, 3F3R are confirmed by synchrotron X-ray diffraction studies. Notable observations are as follows:

- The existence of two variants of SmB* phase has been confirmed in 1F3R. Cell parameters of these two phases along with of SmE* phase have been determined. Existence of a pseudo-hexagonal lattice with herringbone structure is confirmed in these phases.
- All the orthogonal phases of 1F3R are found to be partially bilayer type, which is observed, to the best of our knowledge, first time in a chiral system.
- The existence of tilted hexagonal SmF* phase has been confirmed in 2F3R and 3F3R. On further cooling soft crystal like hexagonal SmJ* phase is formed in 2F3R, undergoing a change in the tilt direction, but in 3F3R, SmG* phase is formed without any change in tilt direction. A coexistence phase of (SmC*+SmF*) is also observed in a certain temperature range in both the compounds. Cell parameters of SmF*, SmJ* and SmG* phases in 2F3R and 3F3R have also been determined.

- The SmA* phase of 2F3R and 7F3R is found to have de Vries type characteristics. Negative thermal expansion is also observed in these compounds in SmC* phase which signify possibility of reduced chevron defects in display.
- The ratio of the layer spacing (d) to the optimised molecular length (*l*) in SmA* phase is found to be the highest in the shortest chain compound 1F3R (1.07) and lowest in the longest chain one 7F3R (0.88) indicating a clear decreasing trend with increasing fluorinated chain length.

From the electro-optic response of the compounds the following observations are worth noting:

- In compounds with three oligomethylene spacers (nF3R) the highest value of spontaneous polarisation (P_S) in SmC* phase is found to increase with increasing fluorinated chain length, schematically shown in **figure 8.4**. With the addition of another oligomethylene spacer also it is found to increase and it attains the highest value in 4F5R.

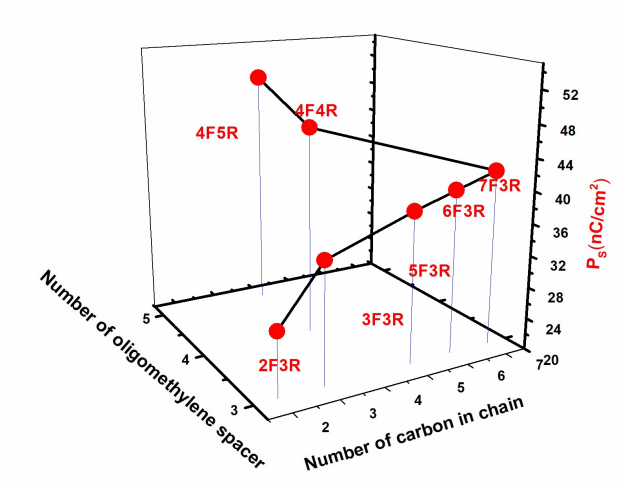

Figure 8.4: Highest value of spontaneous polarization of all compounds having SmC* phase.

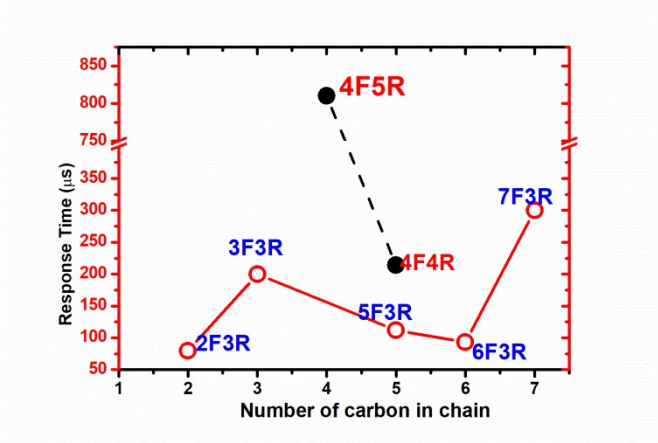

Figure 8.5: Highest value of response time of compounds nFmR. For 4F4R and 4F5R, number of oligomethylene spacers is plotted along x-axis.

- Response time (τ), the most significant parameter for display applications, is found to be the minimum in 2F3R meaning it shows fastest response to a square pulse. It is highest in 7F3R but increases further in compounds with more oligomethylene spacers which is schematically shown in **figure 8.5**. Rotational viscosity is also found to vary in a similar fashion. From these observations it may be inferred that both flexibility and dipole moment of the molecules play important role in their response to electric field

A few important selected parameters of the compounds have been gathered in **table 8.2** for ease of comparison.

Table 8.2: Few selected parameters of the compounds.

Compound	ΔT_C* (°C)	Dipole moment (D)	Optimised molecular length (Å)	$\Delta\varepsilon_{GM}$	f_{CGM} (Hz)	Rotational viscosity (Pas)	P_S (nC/cm^2)	Response time (µs)
1F3R	.....	6.60	32.58	…..	…..	…..	…..	…..
2F3R	29.0	6.75	33.75	140	1300	0.05	28.0	80
3F3R	48.0	6.48	33.48	135	1285	0.28	35.0	200
4F4R	32.9	6.12	33.82	280	420	0.26	46.5	810
4F5R	54.5	5.65	36.72	123	1100	0.51	50.7	214
5F3R	56.5	6.53	35.19	143	1600	0.50	39.0	112
6F3R	62.9	6.52	36.46	166	1850	0.44	40.5	93
7F3R	72.5	6.55	37.01	30	4100	0.34	42.1	300

Finally by doping 7F3R, having highest thermal range of SmC* phase, in a four-component achiral pyrimidine based host matrix a ferroelectric liquid crystal mixture has been formulated, the following characteristics of which are worth mentioning:

- While the dopant exhibits ferroelectric SmC* phase at as high as 75.5°C, in the mixture it is induced from below room temperature and the phase is found to exist over a wide temperature range.
- The mixture also shows SmA* phase which is found to exhibit partial de Vries type characteristics and electroclinic effect.
- In the low temperature region of SmC* phase the layer spacing of the mixture is in between the host and the dopant while the tilt is found to be much higher in the mixture than in the host and the dopant.
- At room temperature moderate value of spontaneous polarization, tilt of around 20° and a response time of a few hundred microseconds make the mixture suitable to use in SSFLCDs. It is expected that problem of chevron defect and hence reduced contrast ratio problem will be minimum since the highest layer shrinkage in the SmC* phase is 3%.

APPENDIX A

LIST OF SELECTED BOOKS AND MONOGRAPHS ON LIQUID CRYSTALS

[1] Textures of Liquid Crystals. Dierking I. Weinheim: WILEY-VCH; 2003.

[2] Ferroelectric Liquid Crystals: Principles, Properties and applications. Goodby J, Blinc R, Clark N, et al. Philadelphia: Gordon & Breach; 1991.

[3] Ferroelectric and antiferroelectric liquid crystals. Lagerwall ST. New York: WILEY-VCH; 1999.

[4] Relaxation Phenomena: Liquid Crystals, Magnetic Systems, Polymers, High-Tc Superconductors, Metallic Glasses. Editors Hasse W, Wróbel S. Berlin: Springer; 2003.

[5] Chirality in Liquid Crystals. Editors Kitzerow H, Bahr C. New York: Springer; 2001.

[6] Structure of Liquid Crystal Phases. Pershan PS. Singapore: World Scientific Publishing Co. Pte. Ltd.; 1988.

[7] Smectic and columnar Liquid Crystals. Oswald P, Pieranski P. London: Taylor & Francis; 2006.

[8] Molecular Structure and Physical Properties of Liquid Crystals. G.W. Gray. Academic Press; 1962.

[9] The Physics of Liquid Crystals. Editor: P. G. de Gennes. London : Oxford University Press; 1974.

[10] Liquid Crystals & Plastic Crystals. Vols 1 and 2. G. W. Gray and P.A. Winsor. Ellis Horwood Ltd; 1974.

[11] Introduction to Liquid Crystals. E. B. Priestley, P. J. Wojtowicz and P. Sheng. Plennum Press; 1975.

[12] Applications of Liquid Crystals. G. Meier, E. Sackmann and J. G.Grabmaier. Verlag: Springer; 1975.

[13] Liquid Crystals. S. Chandrasekhar. Cambrige University Press; 1977.

[14] Liquid Crystals. Solid State Physics Suppl. 14. Editor: L. Liebert. Academic Press; 1978.

[15] Textures of Liquid Crystals. Editors: D. Demus and L. Richter. Verlag:Chemie; 1978.

[16] The Molecular Physics of Liquid Crystals. Editors: G. R. Lukhurst and G.W. Gray. New York : Academic Press; 1979.

[17] Liquid Crystals and Biological Structure. G. H. Brown and J. J.Wolken. Academic Press; 1979.

[18] Liquid Crystals. Proceedings of the International Conference held at Bangalore, in 1979. Editor: S. Chandrasekhar. HEYDEN, London; 1980.

[19] Handbook of Liquid Crystals. Vol. 1 "Fundamentals", 2A "Low MolecularWeight Liquid Crystals I", 2B "Low Molecular Weight Liquid Crystals II", 3 "High Molecular Weight Liquid Crystals", Editors: D. Demus, J. Goodby, G.W. Gray, H. W. Spiess and V. Vill, WILEY-VCH, Verlag GmbH, Weinheim,FRG; 1998.

[20] Physical Properties of Liquid Crystalline Materials. Editor: W. H. de Jeu. Gordon and Breach Science Publishers; 1980.

[21] Polymeric Liquid Crystals. Editors: A. Ciferri, W. R. Krigbaum and Robert B. Meyer. Academic Press; 1982.

[22] Smectic Liquid Crystals. G. W. Gray and J. W. Goodby. Glasgow, Leonard Hill; 1984.

[23] Thermotropic liquid crystals. G. W. Gray. Wiley, Chichester; 1987.

[24] Thermotropic Liquid Crystals, Fundamentals. G. Vertogen and W.H. de Jeu. Springer-Verlag; 1988.

[25] Crystals That Flow : Classic Papers From the History of Liquid Crystals Liquid Crystals Book Series. Editors Sluckin T, Dunmur D, Stegemeyer H. London: Taylor & Francis; 2004

[26] Introduction to Liquid Crystals Chemistry and Physics. P. J. Coolings and M. Hird. Taylor & Francis (1998)

[27] Advances in Liquid Crystals. Vol. 1-6. Glenn H. Brown. Academic Press; 1978-1983.

[28] Liquid Crystals: Nature's Delicate Phase of Matter. P. J. Collings, Princeton Press, Princeton; 1990.

[29] Liquid Crystals Application and Uses. Vol. 1-3. Editor: B. Bahadur. World Scientific; 1990- 1992.

[30] Liquid Crystals in the Nineties and Beyond. Editor: S. Kumar. World Scientific; 1995.

[31] The Surface Physics of Liquid Crystals. A. A. Sonin. Gordon and Breach Science Publishers; 1995.

[32] The Physics of Ferroelectric and Antiferroelectric Liquid Crystals. I. Musevic, R. Blinc and B. Zeks. World Scientific, Singapore; 2000.

[33] Electrooptic Effects in Liquid Crystal Materials. L.M. Blinov V.G. Chigrinov Springer. Newyork; 1996.

[34] Liquid Crystals. Iam Choon Khoo. Neew Jersey: Wiley Intersciencea Jhon Wiley & Sons, INC; 2007.

[35] The Molecular Dynamics of Liquid Crystals. Proceedings of the NATO Advanced Study Institute. Editors G. R. Luckhurst, C. A. Veracini. Barga: Springer Science+Business Media;1989.

[36] The Physics and Chemistry of liquid crystal devices.IM research symposium series. Editor. Gerald J. Sprokel. Califoria: Springer Science+Business Media, LLC; 1980.

APPENDIX B

LIST OF PUBLICATIONS

[1] Haldar S, Sinha D, **Goswami D**, et al. Smectic layer spacing, Average intermolecular distance and spontaneous polarization of room temperature FLC mixtures. Mol. Cryst. Liq. Cryst. 2011;547:25–32. (work not presented in this thesis)

[2] Sinha D, **Goswami D**, Mandal PK, et al. On the nature of molecular associations, static permittivity and dielectric relaxation in a uniaxial nematic liquid crystal. Mol. Cryst. Liq. Cryst. 2012;562:156–165. (work not presented in this thesis)

[3] **Goswami D**, Sinha D, Debnath A, et al. Molecular and dynamical properties of a perfluorinated liquid crystal with direct transition from ferroelectric SmC* phase to isotropic phase. J. Mol. Liq. 2013;182:95–101. (work not presented in this thesis)

[4] **Goswami D**, Debnath A, Mandal PK, et al. Effect of chain length and fluorination on the dielectric and electro-optic properties of three partially fluorinated biphenylyl benzoate rigid core based ferroelectric liquid crystals. Liq. Cryst. 2016;43:1548–1559.

[5] **Goswami D**, Mandal PK, Debnath A, et al. Maxwell Wagner and Goldstone mode relaxations in a oligomethylene spacer based ferroelectric liquid crystal. AIP Conf. Proc. 2016; 1731: 040012

[6] Debnath A, **Goswami D**, Sinha D, et al. Study of electroclinic effect in the chiral Smectic A* phase by dielectric spectroscopy. AIP Conf. Proc.1832; 2017. (work not presented in this thesis)

[7] **Goswami D**, Debnath A, Mandal PK, et al. Orthogonal smectic phases in a biphenylyl chiral mesogen: Polarizing microscopy, synchrotron diffraction and dielectric spectroscopy studies. J. Mol. Liq. 2018;256:29–38.

[8] **Goswami D**, Sinha D, Mandal PK. Dielectric and electro-optic characterization of a partially fluorinated ferroelectric liquid crystal. AIP Conf. proceeding 2018;1953:050012.

[9] Debnath A, **Goswami D**, Mandal PK. Formulation of electroclinic, ferroelectric and antiferroelectric liquid crystal mixtures suitable for display devices. AIP Conf. Proc. 2018. p. 020001. (work not presented in this thesis)

[10] **Goswami D**, Mandal PK, Gutowski O, et al. Phase behaviour and structural properties of two members of biphenylyl benzoate chiral mesogenic series. Liq. Cryst. 2019; 46: 2115-2126.

[11] **Goswami D**, Mandal PK, Węgłowska D. Dielectric and electro-optic properties of two biphenylyl benzoate-based ferroelectric mesogens with tilted hexagonal phases. 2019 published online ; doi: https://doi.org/10.1080/02678292.2019.1686776

LIST OF PAPERS PRESENTED IN SEMINARS AND CONFERENCES

1. Presented a paper in the national conference on Nonlinear Dynamics and its applications at Dept of Physics, Darjeeling Govt College, 26th-28th November 2013.
   Title: Dielectric spectroscopy and electro optic studies of a partially fluorinated ferroelectric liquid crystal
   Author: D. Goswami, P. K. Mandal
2. Presented paper in the ***International conference on non linear dynamics and its application*** at Dept of Physics, Darjeeling Govt College,1st – 3rd November 2014
   Title: Change in the different properties of 6CHBT liquid crystal, doped with CNT particles at different Concentration
   Author: D. Goswami, P. K. Mandal
3. Presented paper in the national conference on the ***Modern Trends in Materials Science*** at Dept of Physics, University of North Bengal, 5th -6th February 2015.
   Title: Effect of multi walled carbon nano tubes on display parameters of room temperature liquid crystal 6CHBT.
   Author: D. Goswami, P. K. Mandal

4. Presented paper in the ***National conference on new approaches of basic science towards the development of engineering and technology*** at Dept of Physics Don Bosco college of engineering and technology, Assam, 27th – 28th February 2015
   Title: Dielectric and electro-optic characterization of To newly synthesized fluorinated ferroelectric liquid crystal

Author: D. Goswami, P. K. Mandal

5. Presented paper in the regional conference titled 22nd West Bengal State Science and Technology Congress-28th February-1st march 2015 at university of northbengal.
   Title: Properties of a fluorinated ferroelectric liquid crystal
   Author: D. Goswami, P. K. Mandal
6. Presented paper in the national conference on ***Indian workshop and Symposium on Modelling, Experimentation and Simulation on complex systems***, at Haldia Institute of Technology, 5th – 07th August 2015
   Title: Investigation on electro-optic properties of three newly synthesized ferroelectric liquid crystals
   Author: D. Goswami, P. K. Mandal
7. Presented a paper in the national conference at DAESSPS, Amity university, Noida, 21st -25th December 2015
   Title: Maxwell Wagner and Goldstone mode relaxations in a oligomethylene spacer based ferroelectric liquid crystal.
   Author: D. Goswami, A. Debnath, P. K. Mandal
8. Presented a paper in the national conference at DAESSPS KIT university, Bhubaneswar, 26th – 30th Decamber 2016,
   Title: Structural and electro optic properties of a Biphenyl Benzoate based chiral liquid crystal.
   Author: D. Goswami, A. Debnath, P. K. Mandal

9. Presented a paper in the ***2ND*** ICC2017, 24th-25th November2017 at Govt. Engineering College, Bikaner.
   Title: Dielectric and electro-optic characterization of a partially fluorinated ferroelectric liquid crystal.
   Author: D. Goswami, D. Sinha, P. K. Mandal

10. Presented a paper in the national conference Optical photonics and synchrotron radiation for technological application at RRCAT Bhopal on 29th April- 7th May 2018.

    Title: Identifying a new phase and revealing the structural properties of a biphenilyl chiral liquid crystal by synchrotron diffraction study

    Author: D. Goswami, A. Debnath, P. K. Mandal

11. Presented a paper in the international conference at IEMPHYS-19 at Institute of Engeneering and Management, Kolkata,14th -16th November 2019.

    Title: Optical polarizing microscopy and electrical response time of three ferroelectric liquid crystals having biphenyl benzoate core.

    Author: D. Goswami, A. Debnath, P. K. Mandal

INDEX

Journal of Molecular Liquids 256 (2018) 29–38

Contents lists available at ScienceDirect

Journal of Molecular Liquids

journal homepage: www.elsevier.com/locate/molliq

Orthogonal smectic phases in a biphenylyl chiral mesogen: Polarizing microscopy, synchrotron diffraction and dielectric spectroscopy studies

Debarghya Goswami [a], Asim Debnath [b], Pradip Kumar Mandal [b,*], Dorota Weglowska [c]

[a] Department of Physics, St. Joseph's College, Darjeeling 734104, India
[b] Department of Physics, University of North Bengal, Siliguri 734013, India
[c] Institute of Chemistry, Military University of Technology, Warsaw, Poland

ARTICLE INFO

Article history:
Received 12 July 2017
Received in revised form 7 January 2018
Accepted 4 February 2018
Available online 05 February 2018

Keywords:
Orthogonal smectic phases
Phase transition
Synchrotron X-ray diffraction
Dielectric relaxation property
Correlation length

ABSTRACT

Three orthogonal smectic phases (SmE*, SmB*$_{hex}$ and SmA*) have been identified in a biphenylyl chiral compound from optical polarizing microscopy, synchrotron X-ray diffraction and dielectric spectroscopy studies. SmB*$_{hex}$ phase exhibits two variants – the lower temperature one is more ordered. All the phases are found to be partially bi-layer type, observed first time in a chiral system without any cyano terminal group. Long range ordering is revealed in both the in-plane and across the plane correlations. Cell parameters of the herringbone like structures of higher ordered smectic phases have been determined and are found to be densely packed. Transitions from SmE* to SmB*$_{hex}$ and within the two SmB*$_{hex}$ variants are of displacive type. Dielectric spectroscopy reveals Maxwell Wagner relaxation in all the phases, however, flip-flop mode relaxation about molecular short axis has been observed in the higher ordered smectic phases only. Absence of short axis relaxation mode as well as soft mode in SmA* phase has been explained.

© 2018 Elsevier B.V. All rights reserved.

1. Introduction

Liquid crystals (LC) have been a matter of intense interest in fundamental research for exhibiting different unique phases along with their specific structural, orientational, dielectric, electro optic and other properties. Introduction of chirality in LC molecules has profound impact on their phase behavior and on various physical properties. Chirality in LCs not only leads to phases with helical structure (like N*, SmC* etc.), but also other novel and frustrated phases like blue phase, twist grain boundary phase etc. From the last few decades, many of these chiral phases have attracted the attention of researchers for their unique structural properties and their superior electro optic or display properties from application point of view, than their non-chiral counter parts [1,2]. In the present study we have investigated the phase behavior as well as structural and dielectric relaxation properties of a fluorinated biphenylyl benzoate rigid cored chiral liquid crystal viz.: (*S*)-(+)-4-[(3-trifluoroetanoyloxy)prop-1-oxy] biphenyl-4-yl 4-(1-methylheptyloxy) benzoate (1F3R) (where in the code nFmR, n and m respectively denote the number of C atoms in the fluorinated unit and in the oligomethylene spacer) [3] whose molecular structure is given in Fig. 1.

We have recently published the phase behavior and electro optic properties of five LCs viz. 4F3R, 4F4R, 4F5R, 6F3R and 7F3R of the same homologous series as of the present sample [4–6]. Phase sequence and dielectric properties of these homologues have been compared with those of the present compound.

2. Experimental method

The transition temperatures of 1F3R were investigated by observing the optical textures under an Olympus BX41 polarizing microscope equipped with a CCD camera. Temperature was regulated by Metller FP90 temperature controller with FP82 hot stage with an accuracy of ±0.1 °C. Phase transition temperatures and enthalpies of compounds were also investigated by differential scanning calorimetry (DSC) using the DSC SETARAM 141 instrument with a scanning rate of 2 °C/min. Measurements were made both at the heating and cooling cycles.

To elucidate the mesophase structures small angle X-ray scattering (SAXS) experiments were performed using PETRA III synchrotron beam line at P07 Physics Hutch station at Deutsches Elektronen-Synchrotron (DESY), Hamburg, Germany. Angular range (2θ) of nearly 5° was explored using a beam of wavelength 0.2483 Å. Sample was taken in a capillary tube of diameter 0.1 mm and for alignment it was cooled down slowly from isotropic phase to the desired temperature. 10 images with exposure time 0.1 s were captured and averaged to achieve the final diffraction image. Three such images were taken at a particular temperature. All the physical parameters were averaged over these three image data. A Perkin Elmer 2D detector of size 400 × 400 mm with individual pixel size of 200 × 200 μm was used to capture the images. It was placed 3.3 m away from the sample. Standard

* Corresponding author.
E-mail address: mandal_pradip@yahoo.com (P.K. Mandal).

https://doi.org/10.1016/j.molliq.2018.02.023
0167-7322/© 2018 Elsevier B.V. All rights reserved.

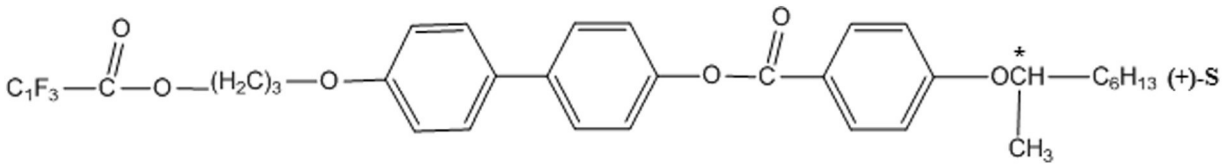

Fig. 1. Molecular structure of 1F3R.

program was used for data acquisition and also for analyzing the images [7]. To get intensity versus Bragg angle (2θ) distribution, images were integrated using a step size of 0.001.

Experimental setup and detail process of the dielectric measurements had been discussed elsewhere [8]. To measure the complex permittivity, the sample was fed into a polyimide coated planar glass cell with low resistivity (about 20 Ω/□) indium tin oxide (ITO) electrodes having 8 μm cell gap. To align the sample, it was cooled down very slowly from the isotropic phase. Complex permittivity was measured using a Hioki Impedance analyzer (3532–50) in the frequency range 100 Hz to 5 MHz while in the frequency range 0.1 mHz to 270 kHz a HIOKI IM3533 analyzer was used. A Mettler FP90 temperature controller along with FP82HT hot stage was used to control the temperature of the cell with an accuracy of ±0.1 °C. Observed dielectric spectra were fitted to the following complex permittivity function proposed by Cole–Cole [9] which was modified to take into account the low frequency parasitic effect.

$$\varepsilon^* = \varepsilon' - i\varepsilon'' = \varepsilon_\infty + \sum \frac{\Delta\varepsilon_k}{1 + (i\omega\tau_k)^{1-\alpha_k}} - i\frac{\sigma}{\omega\epsilon_0}$$

where $\Delta\varepsilon_k = \varepsilon_0 - \varepsilon_\infty$ is the dielectric increment, ε_0 and ε_∞ are the real part of the low and high frequency limit dielectric permittivity, τ_k is the relaxation time ($2\pi f_c\tau_k = 1$, f_c being the critical frequency) and α_k is the asymmetry parameter which indicates the deviation from Debye type behavior of k^{th} mode relaxation process. σ is the conductivity of the cell due to charge impurities which contributes mainly in low frequency region andϵ_0 is the free space dielectric permittivity.

3. Results and discussions

3.1. Observed phases

Although in the earlier publication [3] it was stated that with increasing temperature SmE*, SmB* and SmA* phases evolve in 1F3R before it melts into isotropic phase at 151 °C, no confirmatory structural evidence could be provided there and the nature of the SmB* phase was also not identified. In the present study we have confirmed the presence of all those orthogonal phases, characterized their structures by SAXS and have detected a new phase in between SmB* and SmA* phases and initially designated it as SmX* phase as enumerated in Table 1. Characters of the previous SmB* phase and the new SmX* phase have finally been established as more ordered SmB^{*mo}_{hex} and less ordered SmB^{*lo}_{hex} combining the results of the optical microscopy, synchrotron diffraction and dielectric study.

While comparing the properties of the compounds – 4F4R, 4F5R, 6F3R and 7F3R – it was concluded that the stability of ferroelectric SmC* phase increases with increasing chain length and fluorination of the molecule [4,6]. Although SmC* was first introduced in this homologous series for the member 1F2R for a very short span of temperature (2.9 °C) [3], 1F3R which is much smaller in length and having less fluorine than those members, does not exhibit SmC* phase at all rather it self-assemble in three higher order orthogonal smectic phases.

Table 1
Phase sequence with transition temperatures of 1F3R.

From texture: Cr 80 °C SmE* 99 °C SmB* 119 °C SmX* 127.5 °C SmA* 151 °C Iso.
From dielectric and XRD: Cr 80 °C SmE* 103 °C SmB^{*mo}_{hex} 121 °C SmB^{*lo}_{hex} 127.5 °C SmA* 151 °C Iso.

mo: more ordered; lo: less ordered.

3.2. Differential scanning calorimetry (DSC) and optical polarizing microscopy (OPM) studies

DSC thermograms, both for heating and cooling cycles, are shown in Fig. 2. Almost same transition temperatures were observed from OPM study in heating and cooling cycles, however, these differed slightly from those reported earlier [3]. This might be due to the fact that present investigation was made on homogeneously aligned sample taken in a 8 μm dielectric cell whereas the previous study was made on an unaligned sample taken within a glass slide and cover slip. Absence of SmX* phase in DSC data may be due to very small enthalpy change at this transition. Lack of such thermal signature at transitions involving higher ordered smectic phases is not uncommon in LC systems as discussed by Budai et al. [10].

Fan shaped textures were observed in SmE*, SmB*, SmX* and SmA* phases. Representative textures, observed during cooling, are shown in Fig. 3. While cooling from SmA* to SmX* phase, transition bars occurred at the transition temperature (127 °C) which entering into SmX* phase vanished quickly, leaving a clear fan shaped texture once again. In the heating cycle no such transition bar appeared in the transition from SmX* to SmA* phase, but the fan shaped texture of SmA* phase displayed parabolic focal conic defects. These phenomena were reported before for SmA to hexatic B or crystal B transition [11]. Thus from texture study it appears that the SmX* phase must be some kind of SmB* phase. There is not much difference in the textures of SmE* and SmB* phase. In both the phases there are parallel lines across the fan shaped texture, however, in SmE* phase these lines are slightly stronger than in SmB* phase.

3.3. Optimized geometry using Hartree-Fock method

To explore the structure property correlation, the molecular structure of the sample was optimized applying Hartree-Fock method using 3-21G basis set in a commercial package [12]. The optimized structure of the molecule, along with the directions of the coordinate axes and the dipole moment are shown in Fig. 4. The optimized length of the molecule is found to be 32.34 Å, which is less than the lengths of the molecules of same homologous series but with longer chains (4F3R,4F4R, 4F5R, 6F3R and 7F3R) [4–6] as expected. It has a strong dipole moment 7.06 D with components of −5.54, 4.38 and −0.19 D along the three coordinate axes respectively.

3.4. Synchrotron diffraction study

Temperature evaluation of different phases of 1F3R can be very distinguishably observed by synchrotron radiation study, though the transition temperatures are shifted to higher temperatures by a few degrees, than what are observed in dielectric, DSC and texture studies. This is probably due to the fact that the temperature baths were different in different studies and also due to different thermal history in different studies. Although no magnetic or electric fields were applied to align the sample, due to surface interaction the sample got aligned in the

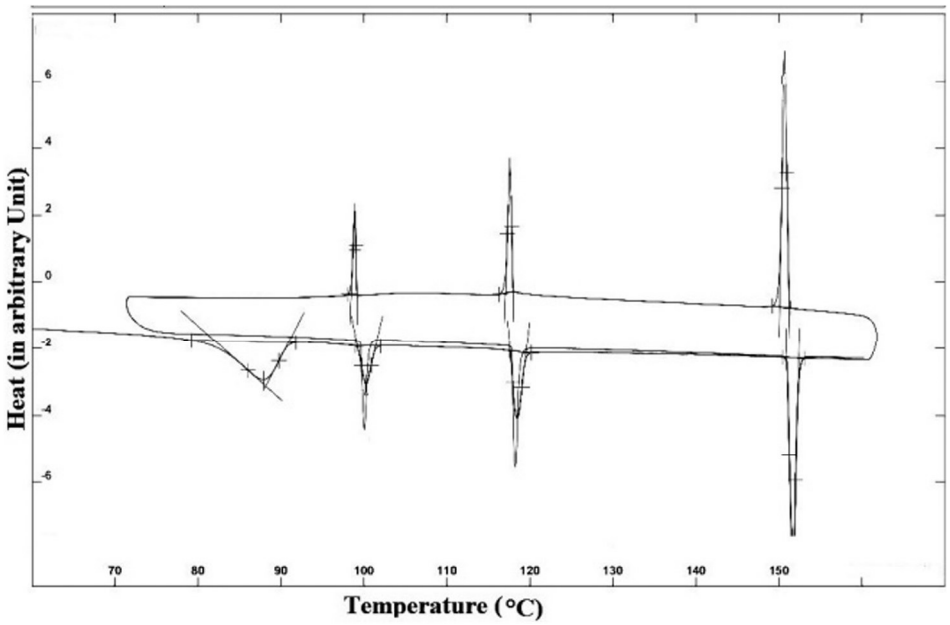

Fig. 2. DSC thermogram of 1F3R.

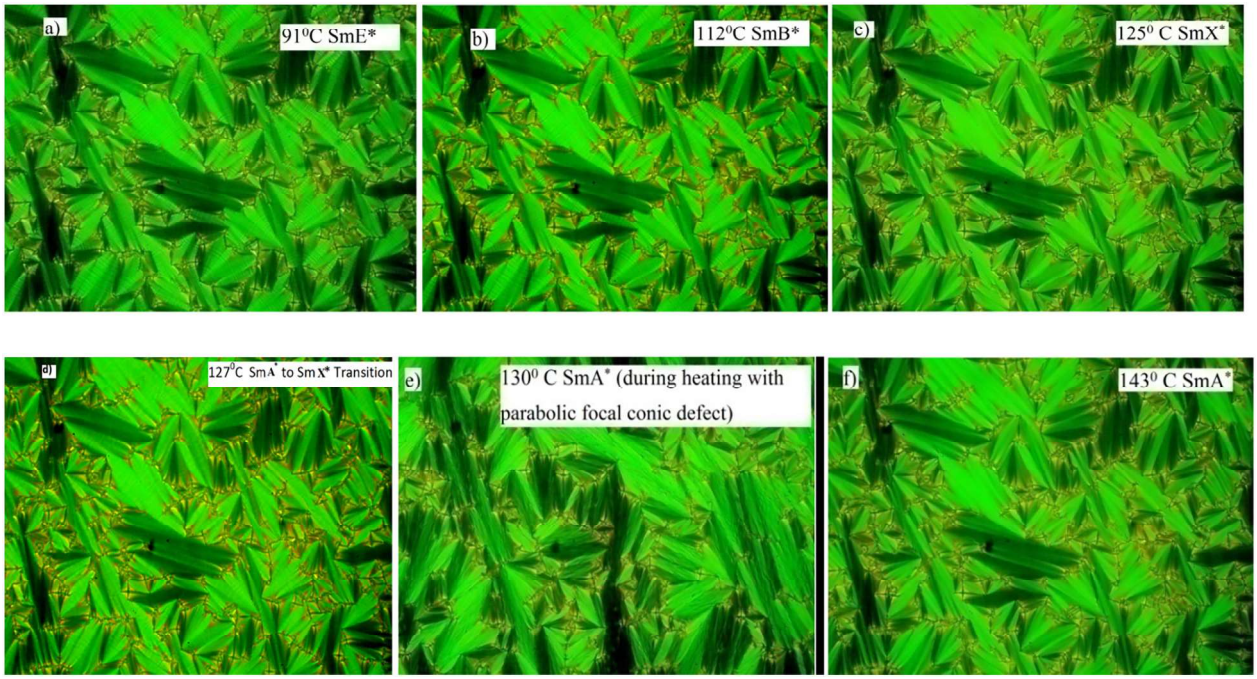

Fig. 3. Observed textures of 1F3R in different phases during cooling cycle.

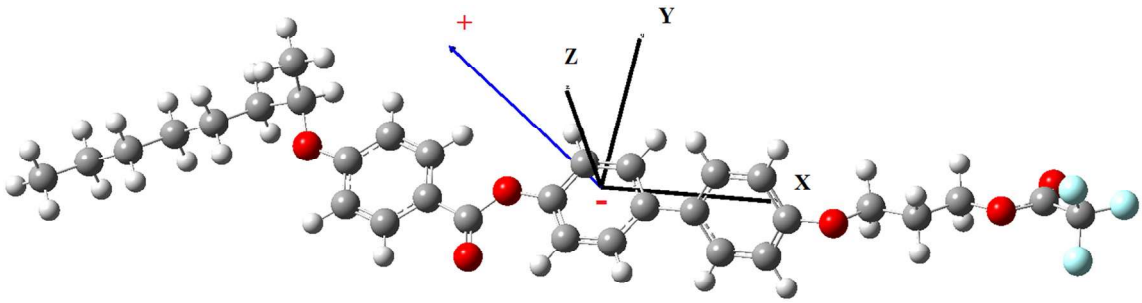

Fig. 4. Optimized geometry of 1F3R.

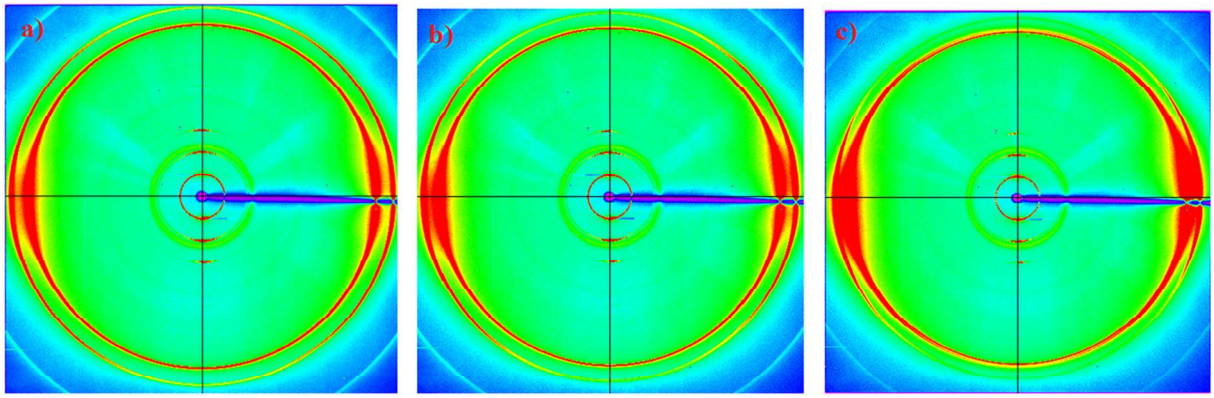

Fig. 5. Diffraction photographs of higher ordered smectic phases (a) SmE* (89.5 °C) (b) SmB* $^{mo}_{hex}$ (107°) (c) SmB* $^{lo}_{hex}$ (125 °C). Faint greenish inner ring is due to Kapton window of the hot stage.

capillary with molecular axis perpendicular to the beam direction. Observed diffraction photographs for only the higher ordered smectic phases are shown in Fig. 5 while the intensity profiles for all the phases are shown in Figs. 6 and 7. In all the higher order smectic phases strong low and high angle diffraction features are present. Low angle features correspond to smectic layer spacings and high angle features arise due to ordering within the layers. The fact that the maxima of the low and high angle diffraction features are at 90° apart signifies unambiguously that all the phases are orthogonal in nature. Presence of a quite strong second and a weak third order diffraction features at low angles signifies long range ordering across the smectic layers in all the phases, though its intensity decreases with temperature as expected. On the other hand, appearance of two outer rings at higher angles, except in SmA* phase, signifies presence of positional ordering or bond orientational ordering within the smectic layers. More ordering within the layers in the SmX* phase is revealed by the appearance of satellite feature in higher angle outer ring. In SmA* phase presence of only one diffuse outer ring suggests the absence of any ordering within the layers.

Moreover not much change is observed in the inner ring (001) profiles of SmE*, SmB* and SmX* phases, except in SmA* phase where a clear broadening can be seen. When we move from SmE* to SmX* through SmB* phase, in the peak profiles of both the outer rings broadening is observed. Satellite peak in the SmX* phase may arise from a local herringbone packing structure as observed for hexatic B phase by

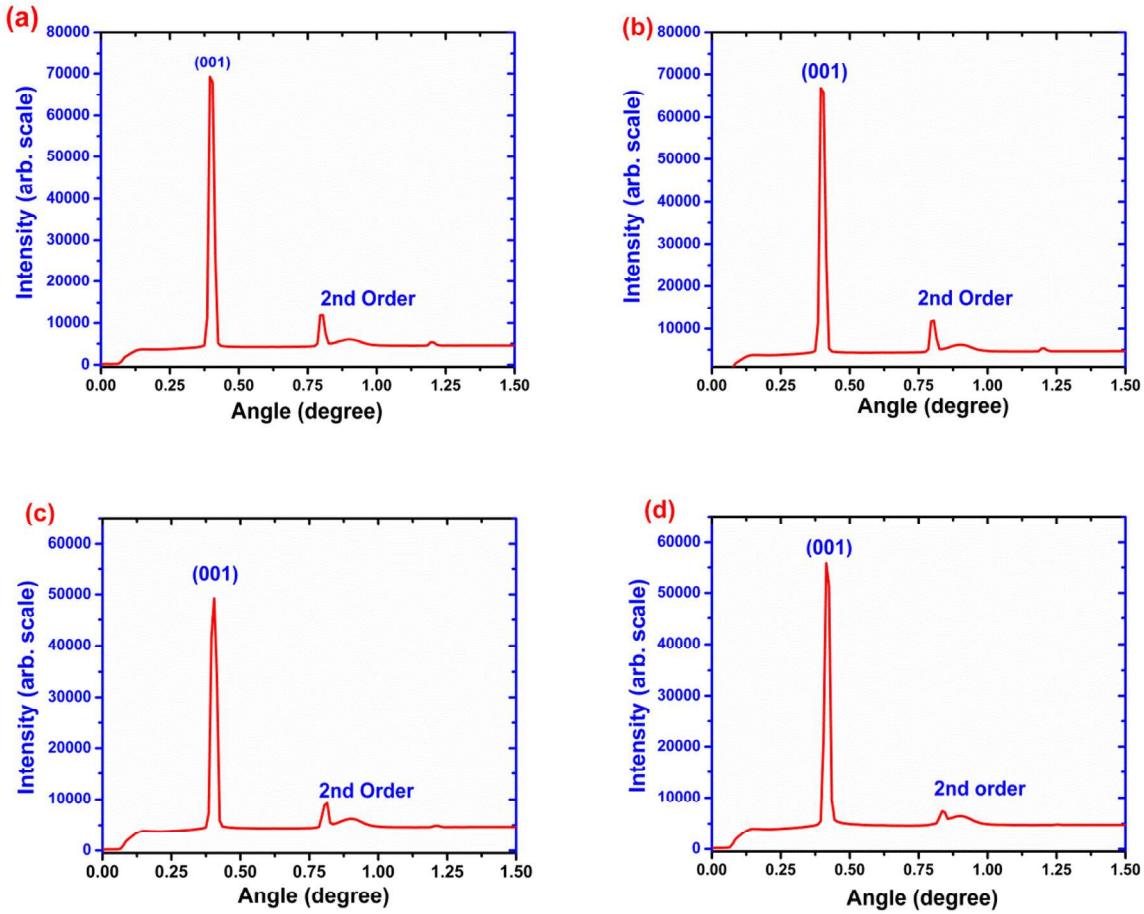

Fig. 6. Intensity profile of inner rings; (a) SmE*, (b) SmB* $^{mo}_{hex}$ (c) SmB* $^{lo}_{hex}$ and (d) SmA*.

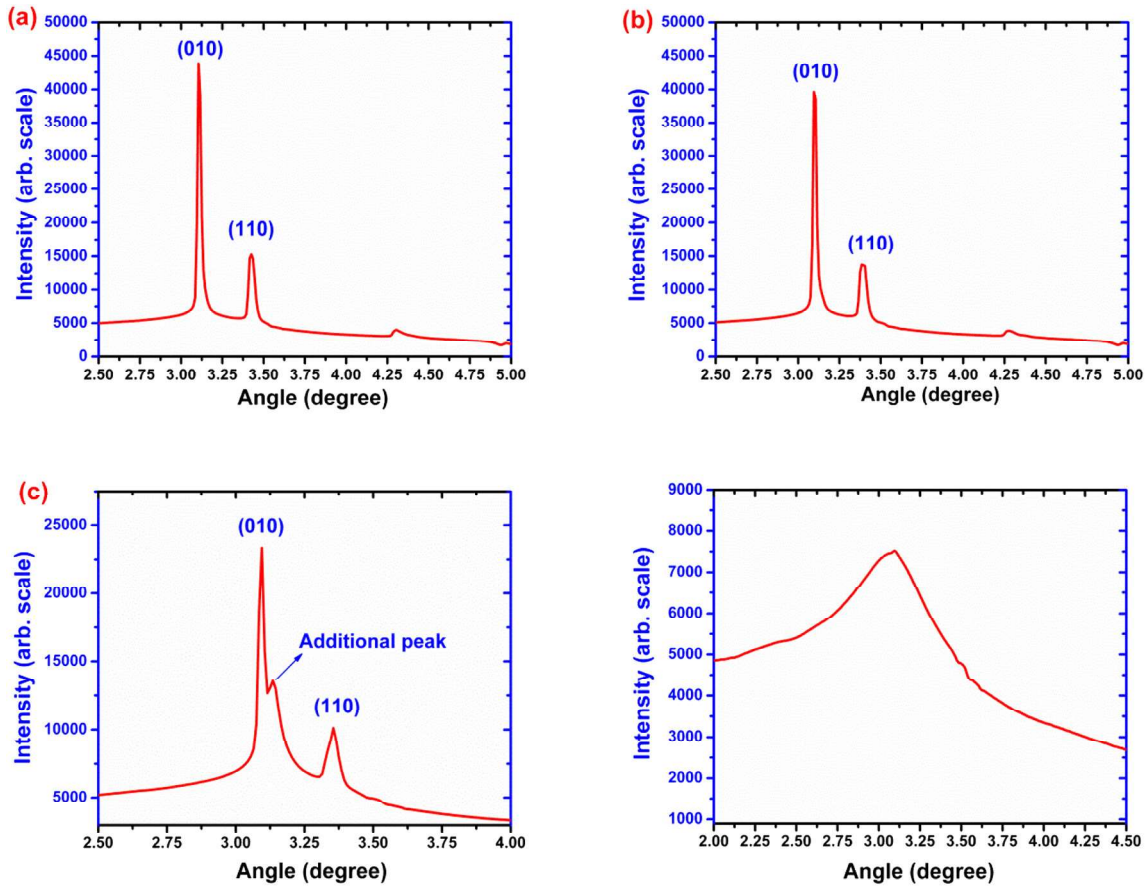

Fig. 7. Intensity profile of outer rings; (a) SmE*, (b) SmB^{*mo}_{hex} (c) SmB^{*lo}_{hex} and (d) SmA*.

Pindak et al. [13]. So the SmX* phase is satisfying the criteria of hexatic B phase. It has also been reported before that this kind of double peak sometimes arises because of chain packing or partial ordering of the long alkyl tail of the LC molecules [14]. To make sure whether SmX* is actually a new phase or not, we have plotted, in Fig. 8, the intensity of the Bragg scattering (both small angle and wide angle), as a function of temperature, which is a direct method of studying the translational order parameter [15].

In the intensity plot of the first order inner ring a slight discontinuity can be observed in the vicinity of SmE* to SmB* transition (103 °C). When we move from SmB* to SmX* (121 °C) a sharp fall in the intensity is observed, which increases again once we enter in SmA* phase (127 °C). The different phases can be distinguished even more prominently in the intensity plot of the first order outer ring. Thus the temperature variation of Bragg diffraction intensity further indicates a new phase (SmX*) in the temperature range 121 °C to 127 °C as has been discussed before.

The layer spacings, calculated from the (001) peaks and depicted in Fig. 9, are found to be larger than the molecular length ($l = 32.34$ Å) in all the phases, which again implies that the phases are orthogonal, with no tilt involved. In SmE* and SmB* phases the layer spacing 'd' remains almost constant at ~35.5 Å. Near SmB* to SmX* transition, it starts to decrease with temperature. Entering into SmA* phase, the rate of decrease of d with temperature increases and saturates at 33.83 Å. Within the smectic phases the d/l ratio varies from 1.10 to 1.05. This ratio for the

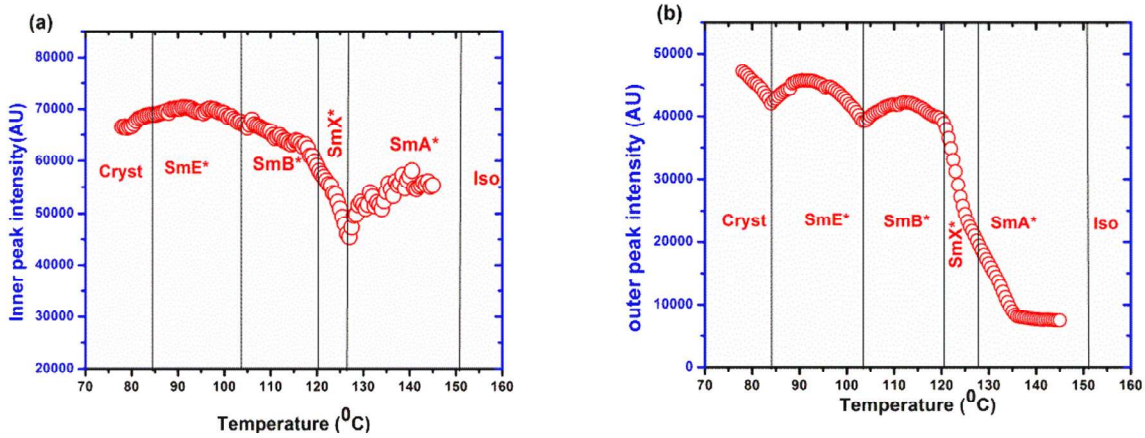

Fig. 8. Intensity of the first order (a) inner and (b) outer diffraction peaks with temperature.

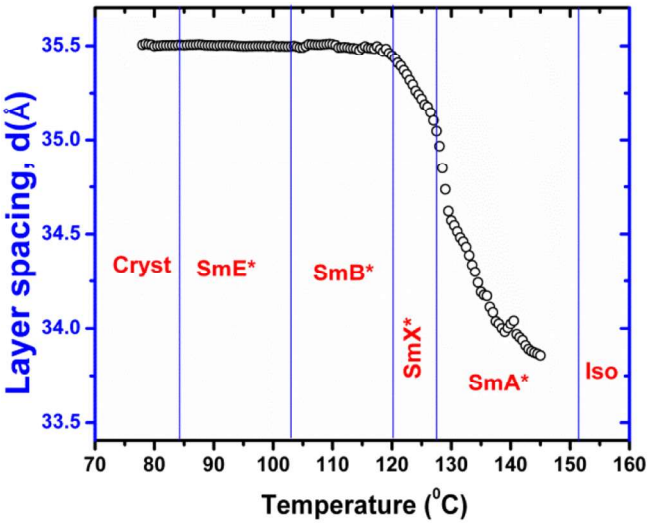

Fig. 9. Variation of layer spacing with temperature.

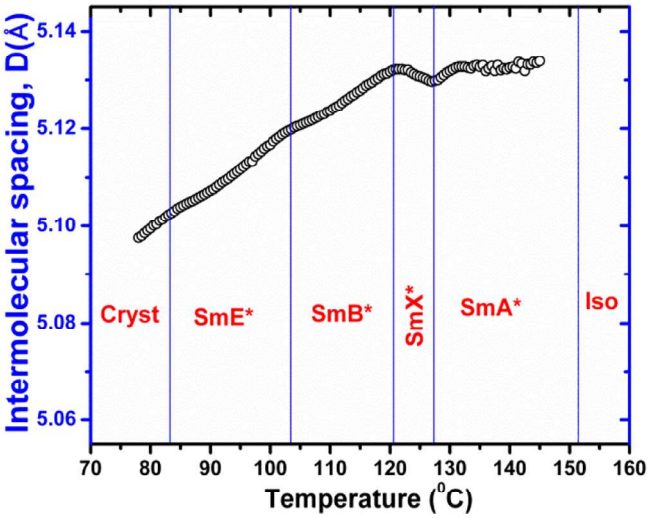

Fig. 10. Variation of intermolecular spacing with temperature.

homologues 5F6R, 4F6R and 1F4R was reported earlier as ~0.5, 0.76 and 0.97 respectively [3]. Thus the ratio was found to increases with decreased fluorination and chain length and the present observation is consistent with the previous trend. Similar observation was reported before in SmA* and SmB* phases of a Schiff base compound containing azomethin [16]. Thus all the smectic phases of 1F3R are partial bilayer type [17,18], to the best of our knowledge there is no such report so far for any chiral compound without any cyano terminal group. N. V. Madhusudan [17] suggested that achiral SmA liquid crystals with high longitudinal dipole moment (~4 D), should favour anti parallel arrangement to minimize the interaction energy which lead to polymorphism of SmA phase. The present 1F3R system possesses strong longitudinal component of dipole moment (5.54 D), which is in conformity of the observed partial bilayer smectics although other chiral systems did not show such behavior.

The intermolecular spacing (D) has been calculated for all the phases from the (010) peak and has been presented in Fig. 10. Although D increases with temperature in SmE* and SmB* phases but it decreases in SmX* phase, clear anomalies are observed at the transition points of the phases. Near clearing point the peak became too diffuse to measure D accurately.

In terms of the full width at half maxima (FWHM) in the scattering vector (Q) of the relevant Bragg's peak it is possible to define a correlation length (ξ), as $\xi = \frac{2\pi}{FWHM}$, to find the extent of correlation of the molecular order. It can be realized physically as the length scale at which the lack of the translational order within or across the smectic layer becomes prominent [19,20]. Calculated correlation lengths (ξ) across and within the layer have been presented in Fig. 11.

With temperature the correlation length (Fig. 11(a)) across the layer is found to vary differently in different phases. An overall increasing trend is observed in the SmE* phase (from about 371 Å to 375 Å). Moving into SmB* phase it falls down sharply to ~333 Å while in SmX* phase it decreases strongly with temperature and reaches a minimum value of 236 Å .The same trend is continued in SmA* phase leading to the lowest value of 180 Å. In SmE* phase ξ is found to be 11.5 times of the optimized molecular length meaning that the correlation extends to about 11 molecular lengths. While in SmB*, SmX* and SmA* phases it is found to be 9.9, 7 and 5.37 times respectively.

Correlation within the layers (Fig. 11(b)), in higher order smectics, is observed to be much higher. In SmE phase ξ is found to be ~656 Å, that in SmB* phase is ~600 Å and in SmX* phase the lowest value is found to be 534 Å. During the phase transition from HexB to CryB phase this kind of discontinuity in the correlation length had been reported before [21]. It reaches to a lowest value of 11 Å in SmA* phase, much smaller than across the plane. Clear anomalies are observed at SmB*-SmX* and SmX*-SmA* transitions in both the correlation lengths signifying again the presence of the new phase SmX*. It had been explained before theoretically that smectic structure with dislocation type imperfections might lead to local displacements of the layers resulting in a much larger broadening of Bragg peaks in the direction $Q_{\perp}$, which is related with

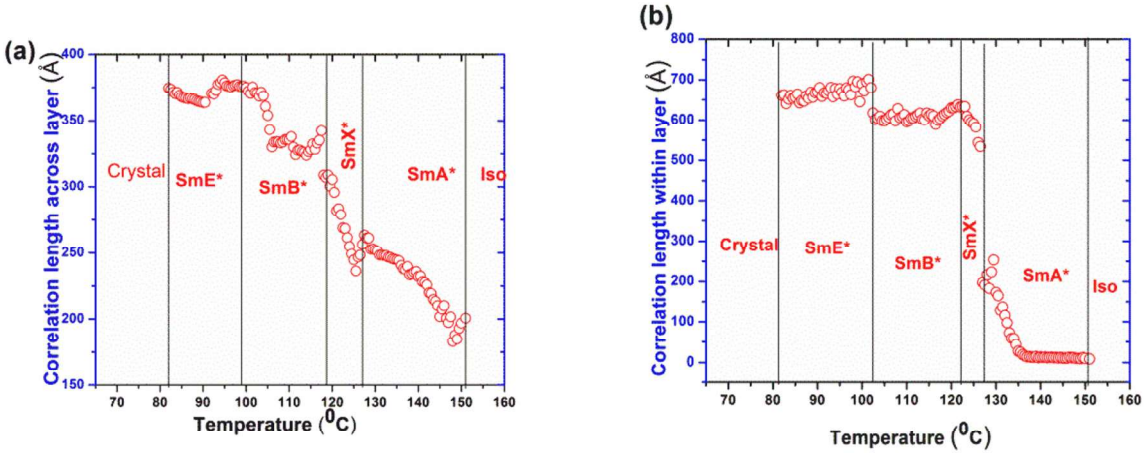

Fig. 11. Temperature variation of correlation length (a) across the layer and (b) within the layer.

Table 2
X-ray data in SmE*(90 °C), SmB*(110 °C) and SmX*(123 °C) phases.

Phase	a (Å) [calculated]	b (Å) [d_{010} observed]	c (Å) [d_{001} observed]	d_{110} (Å) [calculated]	d_{110} (Å) [observed]	*p*
SmE*	8.85 ± 0.02	5.11 ± 0.002	35.50 ± 0.15	4.43 ± 0.008	4.63 ± 0.010	0.62 ± 0.006
SmB*	8.87 ± 0.03	5.12 ± 0.009	35.50 ± 0.15	4.44 ± 0.02	4.69 ± 0.004	0.62 ± 0.010
SmX*	8.88 ± 0.01	5.13 ± 0.0035	35.31 ± 0.2	4.44 ± 0.01	4.73 ± 0.003	0.62 ± 0.010

interlayer correlation, than in $Q_{//}$, which is related with the in plane correlation [22], as observed in our sample.

Following the method used for indexing the SmB* phase diffraction photograph [16,23], we have estimated the cell parameters a, b and c, shown in Table 2, in SmE*, SmB* and SmX* phases, where the parameters a, b and c represent the distance between the centre of mass of the adjacent molecules, the molecular diameter and smectic layer thickness 'd' respectively. The values of c and b have been calculated directly from d_{001} and d_{010}, then a is calculated from the relation $a = 2b\cos 30°$ which can be derived for a orthorhombic unit cell resulting from a hexagonal lattice with herringbone structure as shown in Fig. 12. Using these cell parameters we have calculated d_{110} spacings and in no case the calculated values deviate >0.3 Å from the observed values. Both the SmE* and SmB* phases are believed to exhibit herringbone crystal structure (in SmB* phase herringbone structure is observed locally) [13,24,25], as has been observed by us. Even entering into SmX* phase we observe no structural change of the unit cell although the crystal parameters have changed a bit in different phases. So we can conclude that both the SmB* and SmX* phases are hexagonal type and displacive kind of phase transition is involved rather than reconstitutive type [26,27].

We have also calculated the volume of the molecule (502.4 $Å^3$) in its optimized geometry and have calculated the packing fraction (p) in each phase, excluding SmA*, which are shown in Table 2. The packing fraction is found to be ~0.62, signifying a close packed hexagonal structure. Packing fraction of this order for hexatic B phase has been reported earlier [16]. Furthermore, it was reported earlier that the molecular flip flop rotation around short axis is possible for $p \leq 0.65$ [16,28], which have indeed been observed in dielectric spectroscopic study, described in the next section.

3.5. Dielectric spectroscopy study

Dielectric spectroscopic measurements were done during the cooling cycle. Temperature dependence of the transverse component of the real part of the dielectric permittivity ($\varepsilon'_{\perp}$) at 100 Hz is shown in Fig. 13. $\varepsilon'_{\perp}$ increases with temperature and reaches from about 2 in SmE* phase to a value of 486 in SmA* phase. When the data are fitted with polynomial equation of order 2 in different phases, clear change in curvatures is observed at each transition. Such changes at transition points were also observed in three higher members of the series [4].

In this compound, only one distinct low frequency relaxation mode, whose critical frequency increases with temperature (100 Hz–950 Hz), is observed in SmA* phase. Usually collective mode relaxation is seen in SmA* phase and it is designated as soft mode which arises due to the softening of polar part of the tilt fluctuations [4]. But the soft mode relaxation frequency is two orders higher than the observed frequency. The observed value of dielectric increment is also much higher than the values reported for soft mode. Moreover, soft mode relaxation cannot be suppressed by applying DC bias voltage along with the measuring ac voltage. But the observed mode gets suppressed by a DC bias. These facts suggest that the observed peak is not due to soft mode relaxation. Moreover, the mode sustains in all the phases, including crystal and isotropic phases. Noting the low relaxation frequency, bias dependence and presence of the mode even in isotropic phase, it has been identified as Maxwell Wagner (MW) mode of relaxation which arises due to accumulation of charge in the interface of heterogeneous materials having non-zero electrical conductivity [6]. Distinct MW mode was also observed in all the phases in the higher homologue 6F3R [6]. For a few other homologues (2F6R, 4F6R, 6F6R) of the present series MW mode was also reported earlier, but in those cases the mode was not observed as distinctly, since MW mode was overlapped by the conductivity contribution [29]. However, in few other members of the same homologous series (4F3R, 4F4R, 4F5R and 7F3R) MW mode was not observed [4,5]. Moreover, no soft mode in SmC* phase had been reported earlier for the members 4F3R, 4F4R, 4F5R and 6F3R [4,6], which directly melts to isotropic phase from SmC* phase. It is argued that the elastic constant, that keeps the molecules perpendicular in smectic layers, softens when the sample is cooled down from SmA* to SmC* phase. This softening of restoring force causes the tilt fluctuation, due to which soft mode relaxation arises. Thus in absence of SmA* phase soft mode cannot be observed in SmC* phase. We can extend the same argument here, keeping in mind the fact that, all phases of 1F3R are

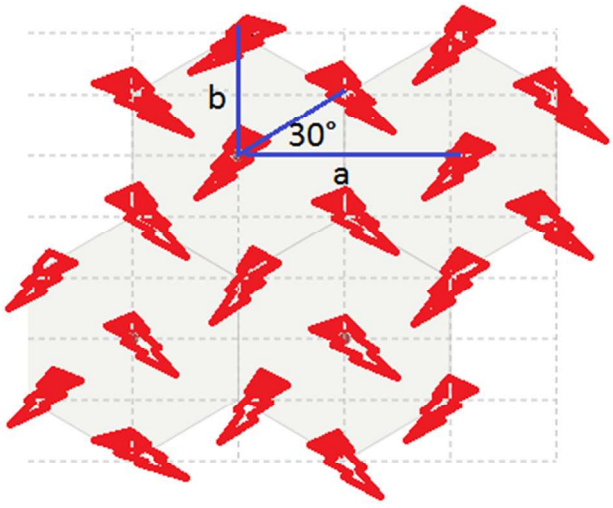

Fig. 12. Hexagonal lattice with herringbone structure.

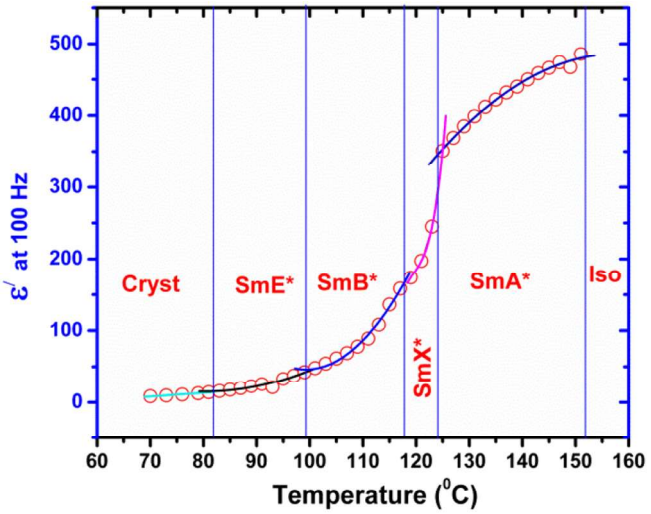

Fig. 13. Temperature variation of real part of dielectric permittivity $\varepsilon'_{\perp}$ at 100 Hz.

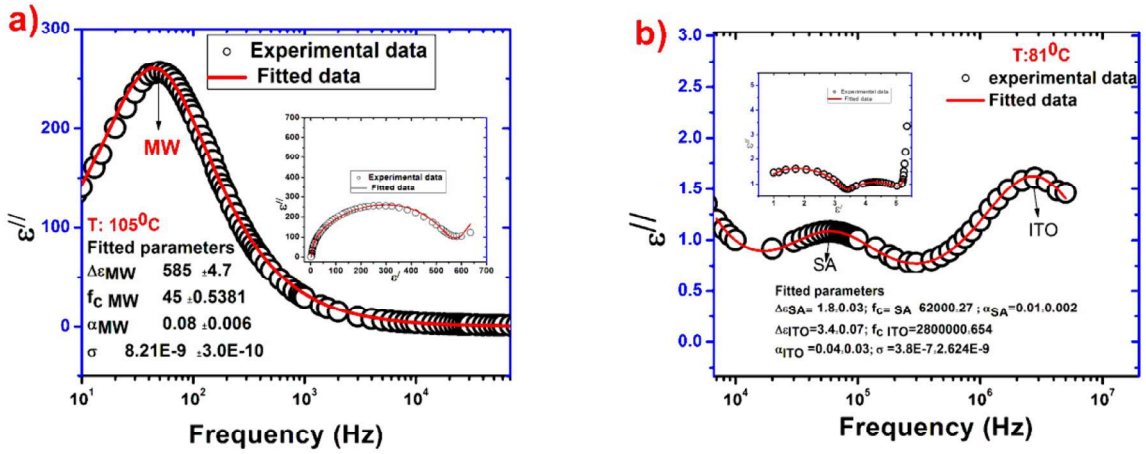

Fig. 14. Fitted spectra of (a) MW mode in SmB* phase at 105 °C and of (b) SA mode in SmE* phase at 81 °C. Cole-Cole plots are shown in the inset.

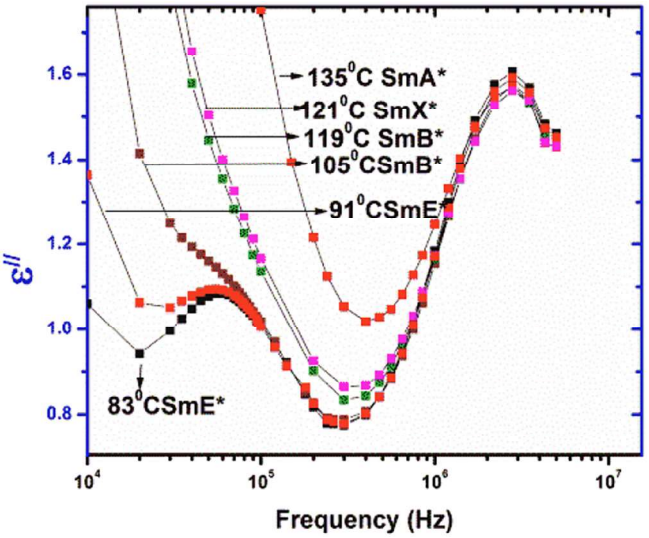

Fig. 15. Imaginary parts of the dielectric spectra in different phases.

orthogonal phases. Thus in absence of any orthogonal to tilt phase transition, no soft mode is observed in SmA*, as the molecules always remain parallel to the layer normal.

A second relaxation peak at higher frequency is observed in SmE*, SmB* and SmX* phases and has been identified as short axis (SA) flip flop mode. Representative dielectric spectra, fitted to the Cole-Cole function, showing MW mode and short axis relaxation are shown in Fig. 14. The relaxation frequency of this mode also increases with temperature in SmX* (85 kHz to 86.5 kHz) and in SmB* (70 kHz to 85 kHz) phase, while the dielectric increment decreases in both the phases (SmX*: 1.3–1.1, SmB*: 1.6–1.3). On the basis of temperature dependence of critical frequency (f_C) and dielectric increment ($\Delta\varepsilon$) and looking at their typical values, it can be concluded that, this mode is due to fluctuation of molecules about their short axis [30]. When the sample is cooled down to SmE* phase from SmB*, the relaxation frequency of this mode drops discontinuously to 50 kHz from 71 kHz. Within SmE* phase, however, f_C increases slightly with decreasing temperature. A similar discontinuous decrease in $\Delta\varepsilon$ is also observed. This high frequency SA mode of relaxation has not been observed in SmA* phase, may be because of the well planar alignment of the molecules in this phase. Besides that, the value of dielectric increment decreases sharply with temperature, becoming very small in SmA* phase. Imaginary part of the dielectric permittivity in different phases (Fig. 15) clearly depicts how the short axis mode become absent in SmA* phase. The critical frequency and dielectric increment of all the modes in all the phases have been shown in Fig. 16 for comparison which again confirms presence of the SmX* phase.

Critical frequencies of the SA mode obey Arrhenius law in SmB* and SmX* phases but not in SmE* phase as shown in Fig. 17. It was reported before that in some compounds both the long and short axis rotation modes in the SmE* phase did not follow Arrhenius law [31]. Activation energy in SmB* phase is found to be 14.2 kJ mol^{-1} which substantially decreased to a value of 3.78 kJ mol^{-1} in SmX* phase. Sharp change in the activation energy again confirms the presence of the new phase. It

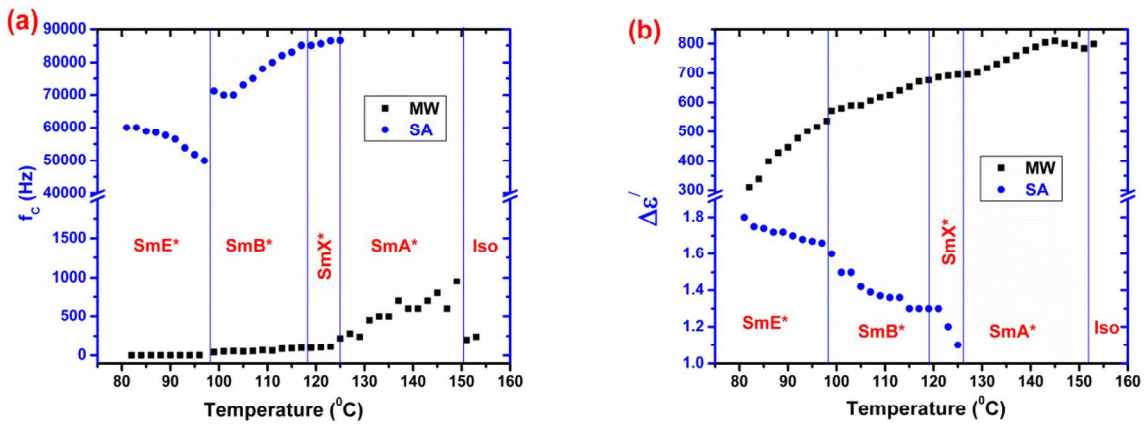

Fig. 16. Temperature variation of (a) critical frequency and (b) dielectric increment.

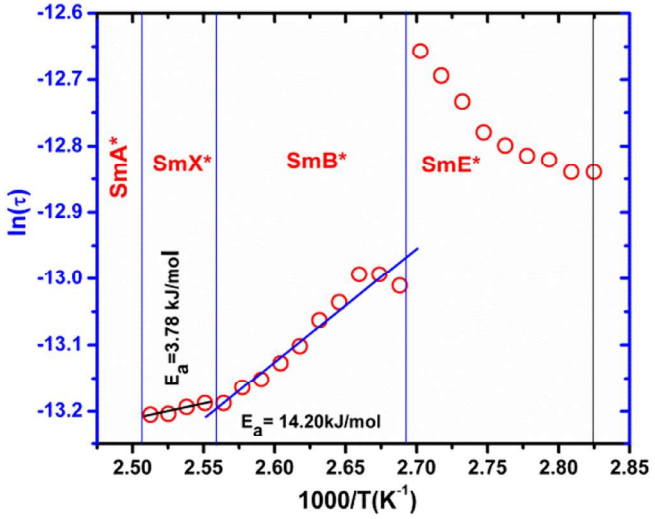

Fig. 17. Arrhenius plot for 1F3R.

was also reported earlier that in the crystal B phase the short axis relaxation is frozen whereas the long axis relaxation sustains [23,31,32]. Therefore SmB* and SmX* phases cannot be of crystal SmB* type.

Moreover, it was reported before that two variants of hexatic B phases -one more ordered and another less ordered- could persist in some compounds and those were differentiated on the basis of the change in activation energy [23]. Thus it is concluded that the phase which was simply identified as SmB* in previous report [3] is a more ordered hexatic SmB* phase while the new phase, which initially we designated as SmX* phase, is a low ordered hexatic SmB* phase.

4. Conclusions

From different features observed in optical polarizing microscopy, synchrotron X-ray diffraction and dielectric studies it is concluded that three orthogonal smectic phases (SmE*, SmB^*_{hex} and SmA*) are present in the biphenylyl chiral compound 1F3R, SmB^*_{hex} phase exhibits two variants – the lower temperature phase is more ordered. The proper phase sequence of 1F3R is, therefore, finally written as: Crystal – SmE* – SmB^{*mo}_{hex} – SmB^{*lo}_{hex} – SmA* – Isotropic. All the phases are partially bilayer type, observed first time in a chiral system without any cyano terminal group. Transition from SmE* to SmB^*_{hex} and within the two SmB^*_{hex} variants are of displacive type.

Acknowledgement

DG acknowledges financial support under the University Grants Commission Minor Research Project in Science [F. No. PSW-121/14-15 (ERO)]. Authors thank Department of Science and Technology, India (SR/NM/Z-07/2015) for the financial support and Jawaharlal Nehru Centre for Advanced Scientific Research (JNCASR) for managing the project under India@DESY program (Project No.·I-20140026). Authors also thankfully acknowledge the technical assistance provided by P07 beam line scientists at DESY and Professor Anirban Misra, Department of Chemistry, North Bengal University for assistance in DFT geometry optimization.

References

[1] I. Dierking, Chiral liquid crystals: structures, phases, effects, Symmetry (Basel). 6 (2014) 444–472, https://doi.org/10.3390/sym6020444.
[2] D. Catalano, V. Domenici, A. Marini, C.A. Veracini, A. Bubnov, M. Glogarová, Structural and orientational properties of the ferro, antiferroelectric, and re-entrant Smectic C* phases of ZLL7/* by deuterium NMR and other experimental techniques, J. Phys. Chem. B 110 (2006) 16459–16470, https://doi.org/10.1021/jp0621777.
[3] D. Ziobro, R. Dąbrowski, M. Tykarska, W. Drzewiński, M. Filipowicz, W. Rejmer, K. Kuśmierek, P. Morawiak, W. Piecek, Synthesis and properties of new ferroelectric and antiferroelectric liquid crystals with a biphenylyl benzoate rigid core, Liq. Cryst. 39 (2012) 1011–1032, https://doi.org/10.1080/02678292.2012.691560.
[4] D. Goswami, A. Debnath, P.K. Mandal, D. Węgłowska, R. Dabrowski, K. Czupryński, Effect of chain length and fluorination on the dielectric and electro-optic properties of three partially fluorinated biphenylyl benzoate rigid core based ferroelectric liquid crystals, Liq. Cryst. 43 (2016) 1548–1559, https://doi.org/10.1080/02678292.2016.1186755.
[5] D. Goswami, D. Sinha, A. Debnath, P.K. Mandal, S.K. Gupta, W. Haase, D. Ziobro, R. Dabrowski, Molecular and dynamical properties of a perfluorinated liquid crystal with direct transition from ferroelectric SmC* phase to isotropic phase, J. Mol. Liq. 182 (2013) 95–101, https://doi.org/10.1016/j.molliq.2013.03.002.
[6] D. Goswami, P.K. Mandal, A. Debnath, R. Dabrowski, Maxwell Wagner and Goldstone mode relaxations in a oligomethylene spacer based ferroelectric liquid crystal, AIP Conf. Proc, 1713, 2016 040012-1-040012-3 https://doi.org/10.1063/1.4947648.
[7] G. Jennings, QXRD program: for acquisition and analysis of X-ray data with Perkin Elmer flat panel detector, version 0.9.8 (64bit), Naperville, United States, https://git.code.sf.net/p/qxrd/code qxrd-code.
[8] S. Haldar, K.C. Dey, D. Sinha, P.K. Mandal, W. Haase, P. Kula, X-ray diffraction and dielectric spectroscopy studies on a partially fluorinated ferroelectric liquid crystal from the family of terphenyl esters, Liq. Cryst. 39 (2012) 37–41, https://doi.org/10.1080/02678292.2012.706322.
[9] C.J.F. Botcher, P. Bordewijk, Theory of Electric Polarization, vol. I, Elsevier, Amsterdam, 1978.
[10] J. Budai, R. Pindak, S.C. Davey, J.W. Goodby, A structural investigation of the liquid crystal phases of 4-(2′-methylbutyl)phenyl 4′-n-octylbiphenyl-4-carboxylate, J. Physique Lett. 45 (1984) L-1053–L-1062, https://doi.org/10.1051/jphyslet:0198400450210105300.
[11] J.W. Goodby, R. Pindak, Characterization of the hexatic B and crystal B phases by optical microscopy, Mol. Cryst. Liq. Cryst. 75 (1981) 233–247https://doi.org/10.1080/00268948108073618.
[12] M.J. Frisch, G.W. Trucks, H.B. Schlegel, G.E. Scuseria, M.A. Robb, J.R. Cheeseman, V.G. Zakrzewski, J.A. Montgomery Jr., R.E. Stratmann, J.C. Burant, S. Dapprich, J.M. Millam, A.D. Daniels, K.N. Kudin, M.C. Strain, O. Farkas, J. Tomasi, V. Barone, M. Cossi, R. Cammi, B. Mennucci, C. Pomelli, C. Adamo, S. Clifford, J. Ochterski, G.A. Petersson, P.Y. Ayala, Q. Cui, K. Morokuma, N. Rega, P. Salvador, J.J. Dannenberg, D.K. Malick, A.D. Rabuck, K. Raghavachari, J.B. Foresman, J. Cioslowski, J.V. Ortiz, A.G. Baboul, B.B. Stefanov, G. Liu, A. Liashenko, P. Piskorz, I. Komaromi, R. Gomperts, R.L. Martin, D.J. Fox, T. Keith, M.A. Al-Laham, C.Y. Peng, A. Nanayakkara, M. Challacombe, P.M.W. Gill, B. Johnson, W. Chen, M.W. Wong, J.L. Andres, C. Gonzalez, M. Head-Gordon, E.S. Replogle, J.A. Pople, Gaussian 98, Revision A.11.4, Gaussian, Inc., Pittsburgh PA, 2002.
[13] R. Pindak, D.E. Moncton, S.C. Davey, J.W. Goodby, X-ray observation of a stacked hexatic liquid-crystal B phase, Phys. Rev. Lett. 46 (1981) 1135–1138, https://doi.org/10.1103/PhysRevLett.46.1135.
[14] M.R. Schenkel, J.B. Hooper, M.J. Moran, L.A. Robertson, D. Bedrov, D.L. Gin, Effect of counter-ion on the thermotropic liquid crystal behaviour of bis(alkyl)-tris(imidazolium salt) compounds, Liq. Cryst. 41 (2014) 1668–1685, https://doi.org/10.1080/02678292.2014.948087.
[15] S. Chandrasekhar, Liquid Crystals, 2nd ed. Cambridge University Press, New York, 1977.
[16] N. Osiecka, A. Budziak, Z. Galewski, M. Massalska-Arodź, X-ray studies of the smectic B phase of the 4-bromobenzylidene-4′-alkoxyanilines, Phase Transit. 85 (2012) https://doi.org/10.1080/01411594.2011.646268.
[17] N.V. Madhusudan, On the polymorphism of SmA phase of highly polar compounds, Proc. - Indian Acad. Sci., Chem. Sci. 92 (1983) 509–525.
[18] B.R. Ratna, R. Shashidhar, V.N. Raja, Smectic-A phase with two collinear incommensurate density modulations, Phys. Rev. Lett. 55 (1985) 1476–1478https://doi.org/10.1103/PhysRevLett.55.1476.
[19] K.A.L. Guermaia, M. Ayadi, K.A.L. Boussiri, Correlation length in PBnA liquid crystal family, Acta Phys. Pol., A 94 (1998) 779–784, https://doi.org/10.12693/APhysPolA.94.779.
[20] A. Debnath, P.K. Mandal, D. Węglowska, R. Dąbrowski, Induction of a room temperature ferroelectric SmC* phase in binary mixtures with moderate spontaneous polarization and sub-millisecond switching time, RSC Adv. 6 (2016) 84369–84378, https://doi.org/10.1039/C6RA11238B.
[21] E. Górecka, L. Chen, W. Pyżuk, A. Krówczyński, S. Kumar, X-ray studies of the hexatic phase in liquid crystals with a crystal- B –hexatic- B –smectic- A phase sequence, Phys. Rev. E 50 (1994) 2863–2867, https://doi.org/10.1103/PhysRevE.50.2863.
[22] V.M. Kaganer, B.I. Ostrovskii, W.H. De Jeu, X-ray scattering in smectic liquid crystals: from ideal- to real-structure effects, Phys. Rev. A 44 (1991) 8158–8166, https://doi.org/10.1103/PhysRevA.44.8158.
[23] S. Urban, J. Czub, J. Przedmojski, R. Dąbrowski, M. Geppi, Dielectric and X-ray studies of substances with the Smectic B phase, Mol. Cryst. Liq. Cryst. 477 (2007) 87–100, https://doi.org/10.1080/15421400701732340.
[24] I. Dierking, Textures of Liquid Crystal, Wiley-VCH, Dramstadt, 2003.
[25] D. Demus, J. Goodby, G.W. Gray, H.W. Spiess, V. Vill, Hand book of liquid crystal, vol. 2A, Wiley-VCH, New York, 1998 447–449.
[26] B.R. Jaishi, P.K. Mandal, K. Goubitz, H. Schenk, R. Dabrowski, K. Czuprynski, The molecular and crystal structure of a polar mesogen 4-cyanobiphenyl-4′-hexylbiphenyl carboxylate, Liq. Cryst. 30 (2003) 1327–1333, https://doi.org/10.1080/0267829031000161193 1.
[27] R.F. Bryan, P.G. Forcier, Contrasting solid-state structures for two nematogenic benzylideneanilines. Crystal structures of *p* [(*p*'-ethoxybenzylidene)amino]-benzonitrile and *p*-[(*p*'-methoxybenzylidene)amino]-phenyl acetate, Mol. Cryst. Liq. Cryst. 60 (1980) 133–152https://doi.org/10.1080/00268948008072429.

[28] S. Urban, J. Przedmojski, J. Czub, X-ray studies of the layer thickness in smectic phases, Liq. Cryst. 32 (2005) 619–624https://doi.org/10.1080/02678290500116920.
[29] J.M. Czerwiec, R. Dąbrowski, M. Żurowska, D. Ziobro, S. Wróbel, Dielectric properties of ferroelectric liquid crystals with diversified molecular structure, Acta Physica Polonica A in Conf. Proc, 117, 2010, pp. 553–556http://przyrbwn.icm.edu.pl/APP/PDF/117/a117z405.pdf.
[30] A. Mishra, D. Węgłowska, R. Dabrowski, R. Dhar, Relaxation phenomena of a highly tilted ferroelectric liquid crystalline material (S)-(+)-4′-(3-pentanoyloxy prop-1-oxy)biphenyl-4-yl-4-(1-methylheptyloxy)benzoates, Liq. Cryst. 42 (2015) 1543–1549, https://doi.org/10.1080/02678292.2015.1066893.
[31] J. Schacht, M. Buivydas, F. Gouda, L. Komitov, B. Stebler, S.T. Lagerwall, P. Zugenmaier, F. Horii, Broad band dielectric relaxation spectroscopy of molecular reorientation in smectic liquid crystalline phases (SmA, SmB, and CrE), Liq. Cryst. 26 (1999) 835–847, https://doi.org/10.1080/026782999204525.
[32] F. Gouda, S.T. Lagarwall, K. Skarp, B. Stebler, F. Kremer, S.U. Vallerien, Broad band dielectric relaxation spectroscopy of a chiral smectic B-crystal phase, Liq. Cryst. 17 (1994) 367–379, https://doi.org/10.1080/02678299408036577.